

OPTIMAL CONTROL IN FLUID FLOW PROBLEMS WITH POD
APPLICATIONS TO FEM SOLUTIONS

A THESIS SUBMITTED TO
THE GRADUATE SCHOOL OF APPLIED MATHEMATICS
OF
MIDDLE EAST TECHNICAL UNIVERSITY

BY

CANSU EVCİN

IN PARTIAL FULFILLMENT OF THE REQUIREMENTS
FOR
THE DEGREE OF DOCTOR OF PHILOSOPHY
IN
SCIENTIFIC COMPUTING

SEPTEMBER 2018

Approval of the thesis:

**OPTIMAL CONTROL IN FLUID FLOW PROBLEMS WITH POD
APPLICATIONS TO FEM SOLUTIONS**

submitted by **CANSU EVCİN** in partial fulfillment of the requirements for the degree of **Doctor of Philosophy in Scientific Computing Department, Middle East Technical University** by,

Prof. Dr. Ömür Uğur
Director, Graduate School of **Applied Mathematics**

Assist. Prof. Dr. Hamdullah Yücel
Head of Department, **Scientific Computing**

Prof. Dr. Ömür Uğur
Supervisor, **Scientific Computing, METU**

Examining Committee Members:

Prof. Dr. Münevver Tezer-Sezgin
Department of Mathematics, METU

Prof. Dr. Ömür Uğur
Institute of Applied Mathematics, METU

Prof. Dr. Ayhan Aydın
Department of Mathematics, Atılım University

Assoc. Prof. Dr. Murat Uzunca
Department of Mathematics, Sinop University

Assist. Prof. Dr. Hamdullah Yücel
Institute of Applied Mathematics, METU

Date:

I hereby declare that all information in this document has been obtained and presented in accordance with academic rules and ethical conduct. I also declare that, as required by these rules and conduct, I have fully cited and referenced all material and results that are not original to this work.

Name, Last Name: CANSU EVCİN

Signature :

ABSTRACT

OPTIMAL CONTROL IN FLUID FLOW PROBLEMS WITH POD APPLICATIONS TO FEM SOLUTIONS

Evcin, Cansu

Ph.D., Department of Scientific Computing

Supervisor : Prof. Dr. Ömür Uğur

September 2018, 155 pages

This study investigates the numerical solutions of optimal control problems constrained by the partial differential equations (PDEs) of laminar fluid flows and heat transfer with the model order reduction (MOR). This is achieved by the three objectives of the thesis: obtaining accurate solutions, controlling the dynamics of the fluid and reducing the computational cost.

Fluids exposed to an external magnetic field and the heat transfer are governed by the magnetohydrodynamics (MHD) and energy equations. Considering an advanced physical systems with a temperature dependent viscosity such as chemical reactors, their control has significant importance and becomes one of the major subject of this thesis. Furthermore, power-law fluid flow, which describes the dynamics for non-Newtonian fluids such as polymer solutions, is considered as an optimal control problem for the characterization of these fluids as shear-thinning or shear-thickening.

Simulations of solutions of the fluid flows and heat transfer equations are carried out by the finite element method (FEM). First of all, FEM solution of the Navier-Stokes (N-S) equations with an exact solution is obtained for the validation of the method using quadratic-linear elements for the velocity-pressure formulation. On the other hand, considering the coupled non-linearity of the MHD flow and heat transfer equations with temperature dependent viscosity, quadratic elements are used for both

velocity and temperature. Moreover, for the power-law fluid flows, due to the fact that equations are decoupled and the temperature equation is linear, quadratic elements for the velocity and the linear elements for the temperature are considered.

Solutions of the optimal control problems are attained by employing the adjoint method within the *discretize-then-optimize* approach. While the control of N-S equations are studied with a distributed force function, control of the MHD flow and power-law fluid flow is attained by using the problem parameters as control variables.

Computational cost and data storage problems arise with implementation of the optimal control strategies. Thus, computing resources are optimized by performing MOR using the proper orthogonal decomposition (POD) method to obtain a reduced order model (ROM). The system dynamics is transferred by POD bases using the sample solutions (snapshots) for various values of the parameters. Setting up a user-friendly framework for the development of the ROM is also provided to help reduce the discretization procedure of the system of equations.

Consequently, the dynamics of the fluid flows and heat transfer are well identified by applying FEM and their control are successfully achieved by the optimal control using the parameters of the problems as control variables. Besides, providing a user-friendly framework, computational costs are minimized.

Keywords: optimal control, finite element method, proper orthogonal decomposition, magnetohydrodynamics

ÖZ

SONLU ELEMANLAR ÇÖZÜMLERİNE ÖZ DİK AYRIŞIM UYGULANMASI İLE AKIŞKAN AKIŞI PROBLEMLERİNDE EN İYİLEMELİ KONTROL

Evcin, Cansu

Doktora, Bilimsel Hesaplama Bölümü

Tez Yöneticisi : Prof. Dr. Ömür Uğur

Eylül 2018, 155 sayfa

Bu çalışmada, düzgün akışkan akışı ve ısı transferinin kısmi diferansiyel denklemleri ile kısıtlanmış en iyilemeli kontrol problemlerinin nümerik çözümleri model indirgeme yöntemi ile araştırılmaktadır. Bu, tezin üç hedefi ile elde edilmektedir: doğru çözümler elde etmek, akışkanın dinamiklerini kontrol etmek ve hesaplama maliyetini düşürmek.

Harici bir manyetik alana maruz kalan akışkanlar ve ısı transferi manyetohidrodinamik ve enerji denklemleri tarafından yönetilmektedir. Kimyasal reaktörler gibi sıcaklığa bağlı viskoziteye sahip gelişmiş bir fiziksel sistem göz önüne alındığında, bunların kontrolü büyük önem taşımaktadır ve bu tezin ana konusu haline gelmektedir. Dahası, polimer çözeltileri gibi Newtonian olmayan akışkanların dinamiklerini tanımlayan kuvvet-kanunu akışkan akışı, bu akışkanların kesme ile incelen veya kesme ile kalınlaşan olarak ikiye ayrılan karakterizasyonu için bir en iyilemeli kontrol problemi olarak ele alınmaktadır.

Akışkan akışları ve ısı transfer denklemlerinin çözümlerinin simülasyonları sonlu elemanlar yöntemi ile gerçekleştirilmektedir. İlk olarak, tam çözümleri olan Navier-Stokes denklemlerinin sonlu elemanlar çözümü metodun doğrulanması için hız-basınç formülasyonunda ikinci dereceden-doğrusal elemanlar kullanılarak elde edilmektedir. Öte yandan, sıcaklığa bağlı viskozite ile manyetohidrodinamik akış ve ısı trans-

fer denklemlerinin birleştirilmiş doğrusal olmayanlığı göz önüne alındığında, ikinci dereceden elemanlar hem hız hem de sıcaklık için kullanılmaktadır. Dahası, kuvvet-kanunu akışları için denklemler ayrık olup sıcaklık denklemi doğrusal olduğundan, hız için ikinci dereceden elemanlar ve sıcaklık için doğrusal elemanlar ele alınmaktadır.

En iyilemeli kontrol problemlerinin çözümlerine, ayrıklaştır-sonra-en iyile yaklaşımı ile adjoint metodu kullanılarak ulaşılmaktadır. N-S denklemlerinin kontrolü dağıtılmış bir kuvvet fonksiyonu ile çalışılırken, kontrol değişkenleri olarak problem parametreleri kullanılarak manyetohidrodinamik akışın ve kuvvet-kanunu akışkan akışının kontrolü sağlanmaktadır.

En iyilemeli kontrol stratejilerinin uygulanması ile hesaplama maliyeti ve veri depolama problemleri ortaya çıkmaktadır. Bu nedenle, hesaplama kaynakları, öz dik ayrışım yöntemini kullanarak model indirgeme ile optimize edilmektedir. Sistem dinamikleri, parametrelerin çeşitli değerleri için alınan çözümleri kullanarak öz dik ayrışım bazları ile aktarılmaktadır. Derecesi indirgenmiş modeldeki denklem sistemlerinin ayrıklaştırma prosedürünü ortadan kaldırmak için bu modelin geliştirilmesinde kullanıcı dostu bir çerçevenin oluşturulması sağlanmaktadır.

Sonuç olarak, akışkan akışları ve ısı transferinin dinamikleri sonlu elemanlar yöntemi uygulanarak hesaplanmaktadır ve kontrolleri, problem parametrelerinin kontrol değişkenleri olarak kullanılmasıyla en iyilemeli kontrol uygulanarak başarılı olarak sağlanmaktadır. Kullanıcı dostu bir çerçeve sağlayarak, hesaplama maliyetleri en aza indirgenmektedir.

Anahtar Kelimeler: en iyilemeli kontrol, sonlu elemanlar yöntemi, öz dik ayrışım, manyetohidrodinamik

To my son, Teoman

ACKNOWLEDGMENTS

It is a great pleasure to thank all the people who helped and supported me during the preparation of this thesis.

First and foremost, I would like to express my sincere gratitudes to my supervisor Prof. Dr. Ömür Uğur, whose expertise and enthusiasm for research had set an excellent example for me. I am grateful for his valuable advices, ideas and great research atmosphere that he provided me. I appreciate all his inspiration, understanding and patience throughout my graduate study.

I also would like to thank Prof. Dr. Münevver Tezer for her invaluable contributions which greatly influenced the outcome of this thesis. It has been an excellent opportunity to work with her and to benefit from her expert guidance.

I would like to thank my examining committee members, Prof. Dr. Ayhan Aydın, Assoc. Prof. Dr. Murat Uzunca and Assist. Prof. Dr. Hamdullah Yücel for their valuable comments and suggestions.

I would also like to express my gratitudes to TÜBİTAK (The Scientific and Technological Research Council of Turkey) for partially supporting me by National Ph.D. Fellowship Programme under the grant number 2211-E.

Many thanks go to my colleagues at the Institute of Applied Mathematics for providing me such a pleasant and lovely working environment. I would like to thank Özge Tekin for careful proofreading parts of this thesis, her valuable suggestions and also endless support. Thanks also to Sinem Kozpınar, Meral Şimşek, Hasan Bartu Yünüak and Ahmet Sınak for offering me enjoyable office hours together.

My special thanks go to my husband, Mustafa Evcin, it would not be possible to complete this thesis without his love and encouragement. I cannot thank him enough for standing by me in stressful times and enduring my long working hours.

Last but not the least, my lovely thanks to Teo, who taught me not only how to work after sleepless nights but also to handle all problems owing to his huggings and beautiful smiles.

TABLE OF CONTENTS

ABSTRACT	vii
ÖZ	ix
ACKNOWLEDGMENTS	xiii
TABLE OF CONTENTS	xv
LIST OF TABLES	xix
LIST OF FIGURES	xxii
CHAPTERS	
1 INTRODUCTION	1
2 OPTIMAL CONTROL PROBLEMS CONSTRAINED BY INCOM- PRESSIBLE FLUID FLOWS AND HEAT TRANSFER	7
2.1 Navier-Stokes Equations	7
2.2 MHD Flows and Heat Transfer with Temperature Dependent Viscosity and Hall effect	12
2.3 Power-Law Fluid Flow and Heat Transfer	18
3 FEM SOLUTION OF FLUID FLOW PROBLEMS	25
3.1 Introduction	25
3.2 FEM Applications to the Navier-Stokes Equations	29

3.3	FEM Applications to MHD Flows and Heat Transfer with Temperature Dependent Viscosity	33
3.4	FEM Applications to Power-Law Fluid Flow and Heat Transfer	37
3.5	Numerical Results	40
3.5.1	Navier-Stokes Equation with Exact Solutions . . .	41
3.5.2	The MHD Flows and Heat Transfer with Temperature Dependent Viscosity and Hall Effect	43
3.5.3	Power-Law Fluid Flow and Heat Transfer	50
4	OPTIMAL CONTROL IN FLUID FLOW PROBLEMS	61
4.1	Introduction to Optimal Control with PDE Constraints	61
4.2	Optimization Algorithm	65
4.3	Distributed Control of Navier-Stokes Equations with Exact Solution	68
4.4	Parameter Control of MHD Flows with Temperature Dependent Viscosity	70
4.5	Parameter Control of Power-Law Fluid Flow and Heat Transfer	72
4.6	Numerical Results	74
4.6.1	Control for Navier-Stokes Equations	75
4.6.2	Control for MHD Flow and Heat Transfer with Temperature Dependent Viscosity and Hall Effect .	76
4.6.3	Control for Power-Law Fluid Flow and Heat Transfer	82
5	MODEL ORDER REDUCTION OF OPTIMAL CONTROL PROBLEMS IN FLUID FLOWS	89
5.1	Introduction	89

5.2	Proper Orthogonal Decomposition (POD)	92
5.3	Reduced Model for Distributed Control of Navier-Stokes Equations	96
5.4	Reduced Model for Parameter Control of MHD Flow and Heat Transfer with Temperature Dependent Viscosity	99
5.5	Reduced Model for Parameter Control of Power-Law Fluid Flow and Heat Transfer	102
5.6	Numerical Results	104
5.6.1	POD Application to Navier-Stokes Equations	105
5.6.2	POD Application to Control of MHD Flow and Heat Transfer with Temperature Dependent Viscosity	107
5.6.3	POD Application to Control of Power-Law Fluid Flow and Heat Transfer	117
6	CONCLUSION	129
	REFERENCES	133
APPENDICES		
A	ALGORITHMS, COMPUTER CODES AND OPTIMALITY CONDITIONS	141
A.1	L-BFGS two loop recursion	141
A.2	Python Codes	141
A.3	First-order optimality conditions for the control of the MHD Flow and heat transfer equations with variable viscosity	142
	CURRICULUM VITAE	153

LIST OF TABLES

TABLES

Table 3.1	L^2 Errors and convergence rates for $\nu = 0.1$	43
Table 3.2	The effect of the viscosity parameter B and Ha on Nu ($m = 0$, $Br = 0$).	49
Table 3.3	The effect of the viscosity parameter B and Ha on fRe ($m = 0$, $Br = 0$)	49
Table 3.4	The effect of the Hall parameter m and Ha on Nu ($Br = 0$, $B = 1$) .	49
Table 3.5	The effect of the Hall parameter m and Ha on fRe ($Br = 0$, $B = 1$)	50
Table 3.6	The effect of the parameter n and Ha on fRe	52
Table 3.7	The effect of the parameter Br and Ha on Nu (when $n = 0.5$)	57
Table 3.8	The effect of the parameter Br and Ha on Nu (when $n = 1.0$)	57
Table 3.9	The effect of the parameter Br and Ha on Nu (when $n = 1.5$)	57
Table 4.1	Distributed control for regaining the desired states given below with the uncontrolled initial state of $\nu = 1.0$	75
Table 4.2	Control with Hartman number Ha , $m = 1$, $Br = 1$, $B = 1$, $\alpha_\omega = 10^3$, $\alpha_T = 10^0$, $\alpha_{Ha} = 10^{-5}$, $Ha^0 = 0.1$	79
Table 4.3	Control with Hall parameter m , $Ha = 1$, $Br = 1$, $B = 1$, $\alpha_\omega = 10^3$, $\alpha_T = 10^0$, $\alpha_m = 0.0$, $m^0 = 10.0$	79
Table 4.4	Control with Hall parameter m , $Ha = 1$, $Br = 1$, $B = 1$, $\alpha_\omega = 10^3$, $\alpha_T = 10^0$, $\alpha_m = 10^{-5}$, $m^0 = 10.0$	79
Table 4.5	Control with Brinkman number Br , $Ha = 1$, $m = 1$, $B = 1$, $\alpha_\omega = 10^0$, $\alpha_T = 10^3$, $\alpha_{Br} = 10^{-5}$, $Br^0 = 0.0$	80
Table 4.6	Control with B , $Ha = 1$, $m = 1$, $Br = 1$, $\alpha_\omega = 10^3$, $\alpha_T = 10^3$, $\alpha_B = 10^{-5}$, $B^0 = 0.0$	80

Table 4.7	Control with Hartmann number Ha and B , $m = 1$, $Br = 1$, $\alpha_\omega = 10^3$, $\alpha_T = 10^0$, $\alpha_{(Ha,B)} = 10^{-5}$, $(Ha^0, B^0) = (0.1, 0.0)$	81
Table 4.8	Control with Brinkman number Br and B , $m = 1$, $Ha = 1$, $\alpha_\omega = 10^3$, $\alpha_T = 10^3$, $\alpha_{(Br,B)} = 10^{-5}$, $(Br^0, B^0) = (0.0, 0.0)$	82
Table 4.9	Control with the Hall parameter m and Br , $B = 1$, $Ha = 1$, $\alpha_\omega = 10^0$, $\alpha_T = 10^3$, $\alpha_{(m,Br)} = 10^{-5}$, $(m^0, Br^0) = (10.0, 0.0)$	82
Table 4.10	Control with the Hall parameter m and B , $Br = 1$, $Ha = 1$, $\alpha_\omega = 10^3$, $\alpha_T = 10^3$, $\alpha_{(m,B)} = 10^{-5}$, $(m^0, B^0) = (10.0, 0.0)$	84
Table 4.11	Control with n , $Ha = 1.0$, $Br = 1.0$, $\alpha_\omega = 10^5$, $\alpha_T = 10^0$, $\alpha_n = 10^{-5}$, and $n_0 = 0.5$	85
Table 4.12	Control with Ha , $n = 1.5$, $Br = 1.0$, $\alpha_\omega = 10^3$, $\alpha_T = 10^0$, $\alpha_{Ha} = 10^{-5}$, and $Ha_0 = 0.1$	85
Table 4.13	Control with n and Ha , $Br = 1.0$, $\alpha_\omega = 10^5$, $\alpha_T = 10^0$, $\alpha_{Ha} = 10^{-5}$, $\alpha_n = 10^{-5}$, $Ha_0 = 0.1$ and $n_0 = 0.5$	86
Table 5.1	FOM-ROM Errors and CPU times for the solutions of N-S equations and speed-up with POD	109
Table 5.2	Distributed control for regaining the desired states given below with the uncontrolled initial state of $\nu = 1.0$ in ROM	109
Table 5.3	FOM-ROM Errors and CPU times for solutions of the MHD equations and heat transfer with temperature dependent viscosity and speed-up with POD	116
Table 5.4	Control with Hartman number Ha , $m = 1$, $Br = 1$, $B = 1$, $\alpha_\omega = 10^3$, $\alpha_T = 10^0$, $\alpha_{Ha} = 10^{-5}$, $Ha^0 = 0.1$	117
Table 5.5	Control with Brinkman number Br , $m = 1$, $Ha = 1$, $B = 1$, $\alpha_\omega = 10^0$, $\alpha_T = 10^3$, $\alpha_{Br} = 10^{-5}$, $Br^0 = 0.0$	117
Table 5.6	Control with B , $Ha = 1$, $m = 1$, $Br = 1$, $\alpha_\omega = 10^3$, $\alpha_T = 10^3$, $\alpha_B = 10^{-5}$, $B^0 = 0.0$	117
Table 5.7	Control with Hall parameter m , $Ha = 1$, $Br = 1$, $B = 1$, $\alpha_\omega = 10^3$, $\alpha_T = 10^0$, $\alpha_m = 0.0$, $m^0 = 10.0$	118
Table 5.8	Control with Hall parameter m , $Ha = 1$, $Br = 1$, $B = 1$, $\alpha_\omega = 10^3$, $\alpha_T = 10^0$, $\alpha_m = 10^{-5}$, $m^0 = 10.0$	118

Table 5.9 Control with Hartmann number Ha and B , $m = 1$, $Br = 1$, $\alpha_\omega = 10^3$, $\alpha_T = 10^0$, $\alpha_{(Ha,B)} = 10^{-5}$, $(Ha^0, B^0) = (0.1, 0.0)$	118
Table 5.10 Control with Brinkman number Br and B , $m = 1$, $Ha = 1$, $\alpha_\omega = 10^3$, $\alpha_T = 10^3$, $\alpha_{(Br,B)} = 10^{-5}$, $(Br^0, B^0) = (0.0, 0.0)$	118
Table 5.11 Control with the Hall parameter m and Br , $B = 1$, $Ha = 1$, $\alpha_\omega = 10^3$, $\alpha_T = 10^0$, $\alpha_{(m,Br)} = 10^{-5}$, $(m^0, Br^0) = (10.0, 0.0)$	118
Table 5.12 Control with the Hall parameter m and B , $Br = 1$, $Ha = 1$, $\alpha_\omega = 10^3$, $\alpha_T = 10^3$, $\alpha_{(m,B)} = 10^{-5}$, $(m^0, B^0) = (10.0, 0.0)$	118
Table 5.13 FOM-ROM Errors and CPU times for solutions of the power-law fluid flow and heat transfer and speed-up with POD	120
Table 5.14 Control with n , $Ha = 1.0$, $Br = 1.0$, $\alpha_\omega = 10^5$, $\alpha_T = 10^0$, $\alpha_n = 10^{-5}$, and $n_0 = 0.5$	121
Table 5.15 Control with Ha , $n = 1.5$, $Br = 1.0$, $\alpha_\omega = 10^3$, $\alpha_T = 10^0$, $\alpha_{Ha} = 10^{-5}$, and $Ha_0 = 0.1$	122
Table 5.16 Control with n and Ha , $Br = 1.0$, $\alpha_\omega = 10^5$, $\alpha_T = 10^0$, $\alpha_{Ha} = 10^{-5}$, $\alpha_n = 10^{-5}$, $Ha_0 = 0.1$ and $n_0 = 0.5$	123

LIST OF FIGURES

FIGURES

Figure 2.1	Physical Configuration of the MHD Problem.	13
Figure 3.1	Uniform mesh and linear basis on a square duct.	28
Figure 3.2	FEM nodes for linear and quadratic basis functions on a triangle. . .	28
Figure 3.3	Solutions v_1, v_2 and p of the Navier-Stokes equation, row 1: $\nu = 1$, row 2: $\nu = 10^{-1}$, row 3: $\nu = 10^{-2}$, row 4: $\nu = 10^{-3}$	42
Figure 3.4	Error and CPU time analysis of FEM solutions with increasing number of degrees of freedom (Dofs) for $Ha = 1.0$, $m = 1.0$, $Br =$ 1.0 , $B = 1.0$	44
Figure 3.5	Velocity contours for $m = 0$, $Br = 0$, $B = 1$ and for increasing values of Ha	44
Figure 3.6	Velocity contours for $Ha = 3$, $Br = 0$, $m = 0$ and for increasing values of B	45
Figure 3.7	Velocity contours for $Ha = 3$, $Br = 0$, $B = 1$ and for increasing values of m	45
Figure 3.8	Velocity contours for $Ha = 3$, $Br = 1$, $B = 1$ and for increasing values of m	45
Figure 3.9	Velocity profiles along the midline of the square duct.	46
Figure 3.10	Isolines for $m = 0$, $Br = 0$, $B = 1$ and for increasing values of Ha . .	47
Figure 3.11	Isolines for $Ha = 3$, $Br = 0$, $B = 1$ and for increasing values of m . .	47
Figure 3.12	Isolines for $Ha = 3$, $Br = 1$, $B = 1$ and for increasing values of m . .	48
Figure 3.13	Isolines for $Ha = 3$, $Br = 0$, $m = 0$ and for increasing values of B . .	48
Figure 3.14	Isolines for $Ha = 5$, $B = 2$, $m = 3$	48
Figure 3.15	Isolines for $Ha = 5$, $B = 2$, $m = 1$	48

Figure 3.16 Error and CPU time of FEM solutions for $Ha = 1.0$, $n = 1.5$, $Br = 1.0$	51
Figure 3.17 Velocity contours for $n = 0.5$ and increasing values of Ha	52
Figure 3.18 Velocity contours for $n = 1.5$ and increasing values of Ha	53
Figure 3.19 Velocity contours for $n = 2.0$ and increasing values of Ha	54
Figure 3.20 Midline velocity profiles for $Ha \leq 10$	55
Figure 3.21 Midline velocity profiles for $Ha = 30, 50, 100$	56
Figure 3.22 Isolines for $n = 0.5$ and increasing values of Ha	57
Figure 3.23 Isolines for $n = 1.5$ and increasing values of Ha	58
Figure 3.24 Isolines for $n = 0.5$, $Ha = 5.0$, $Br = 1.0$	58
Figure 3.25 Variation of the average Nusselt number with Ha for various values of Br	59
Figure 4.1 Norm of the gradient values versus number of function evaluations (Nofe) during optimization.	75
Figure 4.2 Uncontrolled ($\nu_0 = 1.0$), desired ($\nu_d = 0.005$) and controlled velocity profiles and control profile.	77
Figure 4.3 Velocity field and control field for the desired state of $\nu_d = 0.005$ and uncontrolled state $\nu_0 = 1.0$	78
Figure 4.4 Norm of the gradient versus the number of evaluations of the cost function (Nofe) for the control with single parameter.	81
Figure 4.5 Gradient of the objective function during the optimization iterations for the control with pairwise parameters.	83
Figure 4.6 Norm of the gradient versus the number of evaluations of the cost function (Nofe): (a) when n is the control parameter and $Ha = 1$; (b) when Ha is the control parameter and $n = 1.5$; (c) when both n and Ha are control parameters. For all cases $Br = 1$	87
Figure 5.1 Singular values of velocity and pressure.	105
Figure 5.2 POD basis functions of velocity vector field.	106
Figure 5.3 Contours of POD basis functions of velocity vector components. . .	107

Figure 5.4	POD basis functions of pressure.	108
Figure 5.5	Contours of POD basis functions of pressure.	108
Figure 5.6	Reduced controlled velocity	110
Figure 5.7	Components of the reduced control.	110
Figure 5.8	Reduced controlled velocity vector field and control vector field. . .	111
Figure 5.9	Singular values of velocity and temperature.	111
Figure 5.10	POD basis functions of velocity.	112
Figure 5.11	Contours of POD basis functions of velocity.	113
Figure 5.12	POD basis functions of temperature.	114
Figure 5.13	Isolines of POD basis functions of temperature.	115
Figure 5.14	POD Errors of Velocity and Temperature corresponding to the so- lution for $Ha = 1, Br = 1, B = 1, m = 1$	116
Figure 5.15	Singular values of velocity and temperature.	119
Figure 5.16	POD basis functions of velocity.	124
Figure 5.17	Contours of POD basis functions of velocity.	125
Figure 5.18	POD basis functions of temperature.	126
Figure 5.19	Isolines of POD basis functions of temperature.	127
Figure 5.20	POD Errors of Velocity and Temperature corresponding to the so- lution for $Ha = 1, n = 1.5, Br = 1$,	127

CHAPTER 1

INTRODUCTION

Computational fluid dynamics (CFD) has become a powerful tool serving as a sub-branch of fluid mechanics that uses scientific computing and data analysis to understand the physical characteristics of fluid flows. It has been introduced as a new third approach being equal partner with the theoretical and experimental approaches in the development of fluid dynamics. The arrival of the high performance computers and newly developed algorithms enables CFD to analyze and predict the results of theory and experiment by doing so-called ‘numerical experiments’. In this manner, CFD has appeared an attractive branch providing numerical experiments conducted by a computer program which has more favorable conditions in the implementation. For instance, unlike a wind-tunnel experiment, a code for a computer program can be carried in your disks and can be accessible remotely by people far away from it. Even it can simulate the extreme cases where real experiments are difficult or impossible to perform. Thus, CFD is an appealing research tool for science and engineering as well as applied mathematics.

CFD is based on providing solutions to the problems governed by the fundamental equations of fluid dynamics which are, in general, the triple of the following principles: conservation of mass, Newton’s second law, and conservation of energy. They give rise to the continuity, momentum and energy equations, respectively.

Moreover, they represent the ‘complete Navier-Stokes equations’ for the solution of a viscous flow where the thermal conduction and transport phenomena of viscosity are considered. If these principles are combined with the presence of a magnetic field and electrically conducting fluid, which brings the laws of electromagnetic, then the

subject is extended to the study of Magnetohydrodynamics (MHD). It is concerned with the interaction of magnetic fields and conducting fluids. Considering their vital importance in industry, in addition to the Navier-Stokes equations, these are primary interest of this thesis.

The equations corresponding to the fundamental principles of fluid dynamics are replaced by the integrals or partial derivatives. However, closed form solutions may not be available in general or may be difficult to evaluate. In such cases, CFD emerges as an efficient tool using numerical methods to express them as a discrete algebraic system of equations. Among many numerical approaches, finite difference, finite volume and finite element methods are mostly used and well-known by the CFD community. They provide solutions to the above problems at discrete points in space and/or time.

Because of their simplicity in the implementation, finite difference methods (FDMs) are the first and widely used approach in literature. FDMs obtain the discrete system of equations using the Taylor series expansions of the derivatives around the grid points in the domain. However, due to the need for a structured grid, FDMs are not directly applicable for complex geometries.

On the other hand, finite volume methods (FVMs) offer a discretization of the integral form of the equations. In FVMs, the discretization is carried out directly in the physical space, which is divided into a number of control volumes. However, an irregular mesh computation of fluxes leads to a huge amount of effort.

In finite element methods (FEMs), the weighted residual is used to integrate the partial differential equations over an element by multiplying the weight functions, so-called the shape functions. As an advantage, its application to any geometric shape does not cause an extra cost.

However, all well-interpreted results are achievable with a price of large computing sources and long computation time, which is the main obstacle of the CFD. As a result, many toolbox, packages and computing platforms have been developed to present efficient tools in terms of both accuracy and cost. Yet, the advance in high level technology in science demands for a more modest and enhanced programming environment everyday.

One of the major topics in CFD is the control of the fluid flow and the determination of the physical characteristic of the fluid. Besides obtaining numerical approximations to the fluid variables such as velocity, temperature and viscosity, it is also vital to drive the fluid to a predefined/desired state or to determine the physical parameters of the fluid for a desired state. So, the problem is designed as an optimization problem where the constraint equations are formed from the dynamics of the fluid. This is called a partial differential equation (PDE)-constrained optimal control problem and it has to be treated by the optimization tools. Furthermore, the solution to an optimal control problem can be reached iteratively by solving the constraint equations at each optimization step until the optimality conditions meet. But, this process requires repeated evaluations of the equations and increases the computational cost enormously. For example, the dimension of the systems to be solved in order to obtain a high-fidelity finite element method (FEM) solution of a flow problem may be hundred of thousands or even more and this reveals the possible costs in an optimization problem with the PDE constraints.

The key progress on the reduction of the costs in optimization algorithms has been obtained by the advancement of ‘model order reduction’ (MOR), which still is a hot topic in fluid dynamics and control problems. In this manner, MOR provides an alternative way to find both sufficient and low-dimensional approximations by using detailed information about the dynamics of the problem. The well-known technique used in this concept is proper orthogonal decomposition (POD) method. The main idea is to collect sample solutions which are obtained from the fine-scaled approximations via any numerical method such as FDMs, FEMs; and use them to get an overall view about the system. POD saves these solutions to the so called ‘snapshot matrix’ to which a singular value decomposition (SVD) is applied. So, the left singular vectors corresponding to the significant singular values constitutes the POD basis, which are only a few. Later on, the problem is projected to a low-dimensional space generated by the POD basis.

Despite the expense of obtaining fine-scaled solutions, which are named as offline work and performed only once, POD provides high profits in computational cost and time for the problems where repeated evaluations of the system’s equations are required. Thus, it becomes promising to use POD for the solution of the optimal control

problems for the fluid flows.

Inspired from the discussion above, this thesis deals with the optimal control problems in fluid flows and their reduced order modeling for the FEM solutions with the POD method.

Rest of the thesis is organized as follows.

In Chapter 2, we introduce the optimal control problems considered in this thesis. Starting with the main stone of the fluid dynamics problems, Navier-Stokes (N-S) equations are presented as coupling of the momentum and the continuity equations. Then, problems are extended with the energy and Maxwell equations as Magnetohydrodynamics (MHD) flow considering a temperature dependent viscosity. Next, the MHD equations are reformulated for the power-law fluids flow, where the underlying fluid can exhibit Newtonian and non-Newtonian characteristic. Transformations of the equations for a cross section of a rectangular duct and into non-dimensional forms are given.

Furthermore in Chapter 2, optimal control problem is modeled for the N-S equations by the control of distributed source force. On the other hand, control of the MHD flow and heat transfer and also the power-law fluid flows are designed for the control by the physical parameters of the systems in order to regain the desired states or determine the characteristics of the fluid flow.

In Chapter 3, the FEM solutions of the problems introduced in Chapter 2 are analyzed. The variational formulations and the fully discrete non-linear system of equations are derived. Following the ‘*discretize-then-linearize*’ approach, Newton’s method is applied to the solutions of the nonlinear problems. While the numerical solutions of the N-S equations are compared with the exact solution, the validity of the results for the MHD flow and power-law fluid flows are tested with the computation of the critical quantities, which reflect the capability of the method for obtaining solutions, such as the fanning friction factor and the Nusselt number. Also, midline velocity, contours and isolines of the solutions are depicted for various values of the problem parameters.

In Chapter 4, the solution of the optimal control of the fluid flow problems are studied

for control with a distributed force function and control with the physical parameter of the problem. Firstly, a gradient-based optimization algorithm, L-BFGS, is introduced. Then, pursuing a ‘*discretize-then-optimize*’ approach, problems are projected to the FEM spaces to obtain finite dimensional approximations. Furthermore, first-order optimality conditions are derived in the fully discrete setting and adjoint equations are formulated. Using the selected optimization algorithm, optimal states are attained for different simulations of the desired states.

In Chapter 5, the MOR idea is introduced with the POD method by using the SVD of the snapshot matrix. After giving the underlying algorithm, reduced order models are constructed with the ‘*reduce-then-discretize*’ approach for the control of steady parametrized problems.

In Chapter 6, a summary of the applications in this thesis and their numerical results are presented and possible future work and extensions are discussed.

CHAPTER 2

OPTIMAL CONTROL PROBLEMS CONSTRAINED BY INCOMPRESSIBLE FLUID FLOWS AND HEAT TRANSFER

This chapter presents equations of the fundamental principles of fluid dynamics and related optimal control problems. In the following, we begin with introducing these equations and then continue with forming the control problems. Firstly, coupling of the continuity and momentum equations are introduced in order to form the Navier-Stokes equations. Then, the momentum equation is coupled with the energy equation under the effect of an external magnetic field, which yields the MHD equations and heat transfer problem with a temperature dependent viscosity. Finally, momentum and energy equations are coupled in such a way that the fluid may exhibit Newtonian and non-Newtonian behavior according to the values of the parameter in the viscosity.

2.1 Navier-Stokes Equations

Many physical phenomena of science and engineering are described with the help of the well-known Navier-Stokes equations. They serve as a core design tool for various areas such as the simulation of air-conditioning, compressors, flow ducts and airplane. Mainly, they are originated by the mass conservation and Newton's second law, which yield to the continuity and momentum equations. For a model of an infinitesimally small element fixed in a space, the continuity equation of a viscous flow takes the

following form [5]

$$\frac{\partial \rho}{\partial t} + \nabla \cdot (\rho \vec{v}) = 0, \quad (2.1)$$

where ρ is the flow density and \vec{v} is the fluid velocity in vector form.

On the other hand, the mathematical formulation of Newton's second law has to consider the forces acting on the fluid; they are the body forces (gravitation, electromagnetic) and the surface forces (pressure, normal and shear stresses). Body forces are represented by the vector, $\rho \vec{f} = (\rho f_x, \rho f_y)$, assuming a two dimensional domain. Conventionally, for the surface forces from the viscosity, τ_{ij} denotes a stress in the j direction exerted on a plane perpendicular to the i axis. Hence, τ_{ii} represents the normal stress for each coordinate axis; and the shear stress, which is related to the time rate of change of the shearing deformation of the fluid element, is represented by τ_{ij} , $i \neq j$. The fact that the shear stresses can be used to classify the fluid as Newtonian or non-Newtonian, which was first stated by Isaac Newton, gives the vital importance of their presence in the dynamical system. So, if the shear stress has a linear relationship with the gradient of the velocity then the fluid is called Newtonian, otherwise non-Newtonian. Therefore, the momentum equations are obtained as the following system of equations

$$\frac{\partial(\rho v_1)}{\partial t} + \nabla \cdot (\rho v_1 \vec{v}) = -\frac{\partial p}{\partial x} + \frac{\partial \tau_{xx}}{\partial x} + \frac{\partial \tau_{yx}}{\partial y} + \rho f_x, \quad (2.2)$$

$$\frac{\partial(\rho v_2)}{\partial t} + \nabla \cdot (\rho v_2 \vec{v}) = -\frac{\partial p}{\partial y} + \frac{\partial \tau_{xy}}{\partial x} + \frac{\partial \tau_{yy}}{\partial y} + \rho f_y, \quad (2.3)$$

where p is the pressure and v_1, v_2 are the components of the velocity \vec{v} .

The Newtonian fluids are considered following the Stokes hypothesis; and normal and shear stresses are replaced with the forms given by

$$\tau_{xx} = -\frac{2}{3}\mu(\nabla \cdot \vec{v}) + 2\mu\frac{\partial v_1}{\partial x}, \quad (2.4)$$

$$\tau_{yy} = -\frac{2}{3}\mu(\nabla \cdot \vec{v}) + 2\mu\frac{\partial v_2}{\partial y}, \quad (2.5)$$

$$\tau_{xy} = \tau_{yx} = \mu \left[\frac{\partial v_1}{\partial x} + \frac{\partial v_2}{\partial y} \right], \quad (2.6)$$

where μ is the dynamic viscosity. For instance, substituting the (2.4)–(2.6) into the right hand side of (2.2) leads to

$$\frac{\partial(\rho v_1)}{\partial t} + \nabla \cdot (\rho v_1 \vec{v}) = -\frac{\partial p}{\partial x} - \frac{2}{3}\mu\frac{\partial^2 v_1}{\partial x^2} - \frac{2}{3}\mu\frac{\partial^2 v_2}{\partial x \partial y} + 2\mu\frac{\partial^2 v_1}{\partial x^2} + \mu\frac{\partial^2 v_1}{\partial y^2} + \mu\frac{\partial^2 v_2}{\partial x \partial y},$$

then, rearranging and using the property $\nabla \cdot \vec{v} = 0$ give

$$\frac{\partial(\rho v_1)}{\partial t} + \nabla \cdot (\rho v_1 \vec{v}) = \mu \left(\frac{\partial^2 v_1}{\partial x^2} + \frac{\partial^2 v_1}{\partial y^2} \right).$$

Meanwhile, for an incompressible flow, the momentum and continuity equations reduce to

$$\rho \left(\frac{\partial \vec{v}}{\partial t} + (\vec{v} \cdot \nabla) \vec{v} \right) = -\nabla p + \mu \Delta \vec{v} + \rho \vec{f}, \quad (2.7)$$

$$\nabla \cdot \vec{v} = 0. \quad (2.8)$$

In order to obtain a non-dimensional form of the Navier-Stokes equations for an incompressible fluid with a constant viscosity, the dimensionless quantities,

$$x' = \frac{x}{l}, \quad y' = \frac{y}{l}, \quad \vec{v}' = \frac{\vec{v}}{v_c}, \quad t' = \frac{t}{(l/v_c)}, \quad p' = \frac{p}{v_c^2 \rho}, \quad (2.9)$$

are introduced, where l denotes a characteristic length and v_c denotes a characteristic velocity. Substituting these quantities into (2.7)–(2.8) results in the dimensionless form of the N-S equations for a time-dependent, incompressible, viscous fluid flow:

$$\frac{\partial \vec{v}'}{\partial t'} + (\vec{v}' \cdot \nabla) \vec{v}' = -\nabla p' + \nu \Delta \vec{v}' + \vec{f}', \quad (2.10)$$

$$\nabla \cdot \vec{v}' = 0, \quad (2.11)$$

where ν is the reciprocal of the Reynolds number Re so that

$$\nu = \frac{1}{\text{Re}} = \frac{\mu}{\rho v_c l}.$$

Reynolds number is a dimensionless quantity that identifies the tendency of the fluid as laminar or turbulent. Values of $\text{Re} \leq 2000$ generally produces laminar regimes, and we will be interested in this case. Specifically, the main focus in this thesis will be to consider steady flows; thus the term for time derivative is dropped and also the prime notation is omitted from the variables for simplicity. Consequently, the N-S equations of a two-dimensional, steady, incompressible, viscous fluids are given in the vector form:

$$-\nu \Delta \vec{v} + (\vec{v} \cdot \nabla) \vec{v} + \nabla p = \vec{f}, \quad (2.12)$$

$$\nabla \cdot \vec{v} = 0. \quad (2.13)$$

Of course, the steady N-S equations are supplemented with the essential boundary condition for the velocity as $\vec{v} = \vec{v}_D$ with a specified vector function v_D on the boundary of the domain, say Ω . Since there is no boundary condition defined for the pressure, its unique solution can be achieved by imposing a constraint such as $\int_{\Omega} p \, d\Omega = 0$.

Instead of working in the vector form of the N-S equations, it is also possible to obtain a stream function-vorticity formulation where the pressure term is removed from the system. However, in this case the vorticity function fails to have a boundary condition; and the boundary values of the vorticity are calculated by using the derivative of the boundary conditions of stream function. Nevertheless, each case requires a special treatment of the boundary conditions and the choice between them can be made according to the demand of the underlying problem. In this respect, pressure is preserved and the N-S equations are preferred to work within the vector form as given in (2.12)–(2.13) in this section of the thesis.

Having mathematical formulation for the velocity and pressure of a fluid flow enables to determine the motion and behavior of the flow for different physical conditions. This information is of great importance in the design of many technological equipments where there is a fluid flow. Moreover, it might be necessary to specify the required forces to evolve the flow into a desired profile. At this point, the optimal control strategies enter the scene and optimization algorithms begin to play.

A control problem can be designed for the fluid flow to regain the velocity vector field for a desired flow behavior by applying, for instance, a distributed force function as the control. In this case, the N-S equations corresponding to the physical principles are participated as the constraints of the control process. Meanwhile, an objective functional having a velocity tracking profile is added to minimize the difference between the optimal and desired states. Furthermore, having a control function may need a cost and this may be introduced as the norm of the control function. Therefore a cost functional may be given as

$$J(\vec{v}, \vec{u}) = \frac{\alpha_v}{2} \int_{\Omega} (\vec{v} - \vec{v}_d)^T (\vec{v} - \vec{v}_d) \, d\Omega + \frac{\alpha_u}{2} \int_{\Omega} \vec{u}^T \vec{u} \, d\Omega,$$

where α_v and α_u are the regularization parameters of the velocity \vec{v} and the control function \vec{u} , respectively.

Consequently, the PDE-constrained optimal control problem for the distributed control of the N-S equations is formulated as follows:

$$\underset{\vec{u}}{\text{minimize}} \quad J(\vec{v}, \vec{u}) = \frac{\alpha_v}{2} \int_{\Omega} (\vec{v} - \vec{v}_d)^T (\vec{v} - \vec{v}_d) d\Omega + \frac{\alpha_u}{2} \int_{\Omega} \vec{u}^T \vec{u} d\Omega \quad (2.14)$$

$$\text{subject to} \quad -\nu \Delta \vec{v} + (\vec{v} \cdot \nabla) \vec{v} + \nabla p = \vec{f} + \vec{u} \quad \text{in } \Omega \quad (2.15)$$

$$\nabla \cdot \vec{v} = 0 \quad \text{in } \Omega \quad (2.16)$$

$$\vec{v} = 0 \quad \text{on } \partial\Omega. \quad (2.17)$$

Throughout the thesis, we shall investigate the solution of this problem by solving PDEs and the controlling the flow. Thus, numerical solutions are obtained by the FEM and the control problem is examined by the adjoint method. Since there have been many studies conducted before on the subject, a short literature survey is provided in the following.

Solutions of the Navier-Stokes equations have been studied extensively in literature since it serves as the fundamental tools of the fluid flow. The finite difference solutions have been introduced by Chorin in [16] for the time-dependent case by solving the velocity and pressure iteratively, which is also named as Chorin's projection method. Taylor and Hood in [91] have presented velocity-pressure and stream function-vorticity formulations using the finite element discretization technique, as founders of the Taylor-Hood finite element pairs. The existence and the uniqueness results and the regularity of solutions has been investigated by Temam in [92], Girault and Raviart in [32] and Thomasset in [93] using the finite element method. An upwind finite element scheme for the convective part of the N-S equations has been introduced by Heinrich in [46]. The discontinuous Galerkin approach has been used by Baumann and Oden [10]. Elman[23] has applied the preconditioning for the steady state case with low viscosity. On the other hand, the detailed finite volume analysis is provided by Jasak in [53]. A higher order approximation by the finite volume is given by Pereira et al. in [75].

Besides the numerical solutions, the optimal control of the N-S equations have also attracted many researchers. Abergel and Temam [1] have given the proof of an existence of solutions to control problems for various physical situations, such as distributed control, boundary control in a channel; and they have provided basic numerical algorithms, such as steepest descent and conjugate gradient methods. Ghattas

and Bark have investigated the optimal control of the stationary N-S equations in two and three dimensions by developing large scale optimization methods such as quasi-Newton and sequential quadratic programming in [31]. Considering an augmented Lagrangian method, optimality conditions are established for the control problems on the N-S equations by Desai and Ito in [21]. Further studies are provided by Gunzburger, Hou and Svobodny in [38, 40], by Málek and Roubíček in [69], by Heinkenschloss in [45] and by Kunisch in [57]. A comprehensive overview on control of N-S equations is given in [39, 86].

2.2 MHD Flows and Heat Transfer with Temperature Dependent Viscosity and Hall effect

As is clear from the previous section, the evolution of the fluid flow is based on the N-S equations. However, if applications with fluid flow are enlarged to the physical systems such as chemical reactor, cooling modules or heat exchangers for an electrically conducting fluid then it becomes necessary to take into account the magnetic effects as well as the heat transfer. This brings out the readjustment of the N-S equations with the addition of new terms, and hence, one needs to consider the third principle of the fluid dynamics: conservation of energy.

In order to implement such improvements, the model problem is investigated for a steady flow of a viscous, incompressible, electrically conducting fluid in a long channel of rectangular cross-section together with heat transfer: This is generally referred to the problem of MHD flow and heat transfer. The configuration of the problem is shown in Figure 2.1, where a uniform magnetic field of intensity B_0 is applied with an angle to the duct which is perpendicular to the axis of the channel (z -axis). Herewith, we assume a constant pressure gradient $-\frac{dp}{dz}$ applied in the z -direction and the induced magnetic field is neglected due to the assumption of small magnetic Reynolds number. Moreover, both the flow and the temperature are assumed to be steady and fully developed along the channel. Besides, the viscosity of the fluid is considered to vary exponentially with the temperature; however, the Joule and viscous dissipations are not neglected. Due to the strong effect of magnetic force, the Hall effect is necessarily taken into account as well. As a result, the flow is only in the channel axis

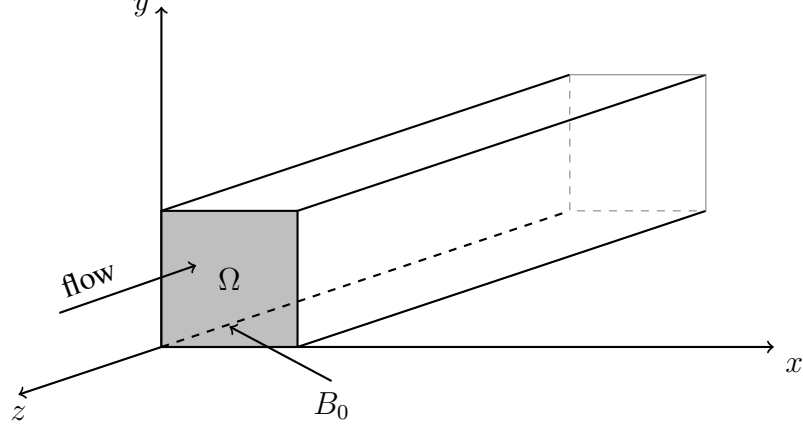


Figure 2.1: Physical Configuration of the MHD Problem.

direction with the velocity, $\vec{v} = \omega \hat{k}$, which varies in the duct, that is, $\omega = \omega(x, y)$ for $(x, y) \in \Omega = [0, a] \times [0, b]$.

According to the problem definition given above, the equations of the flow are obtained by adding the electromagnetic Lorentz force $\vec{J} \times \vec{B}$, as in [22], to the governing N-S equations so that (2.7) with a variable viscosity turns into

$$\rho \left(\frac{\partial \vec{v}}{\partial t} + (\vec{v} \cdot \nabla) \vec{v} \right) = -\nabla p + \nabla \cdot (\mu \nabla \vec{v}) + \vec{J} \times \vec{B}, \quad (2.18)$$

where $\vec{B} = (B_x, B_y, 0)$ with $B_0 = (B_x^2 + B_y^2)^{1/2}$ is the magnetic field perpendicular to the channel axis lying on the duct plane, and \vec{J} is the current density. Also, the effect of a variable viscosity is included to enhance the heat transfer; the viscosity μ is chosen such that it varies exponentially with temperature in the form

$$\mu = \mu_0 e^{-b_0(T-T_\omega)}, \quad (2.19)$$

as given in [7, 8, 81] where μ_0 is the coefficient of viscosity at temperature $T = T_\omega$, and b is a constant. Although the common expression for the temperature dependent viscosity in engineering literature is the Arrhenius equation [43], the choice of such a dynamic viscosity in (2.19) is considered to weaken the convection dominance of the flow due to the high temperature. Moreover, the physical properties of the system is flourished by the addition of the impact of the Hall current. Since it can affect the magnetic force term by altering the magnitude and the direction of the current density, the Ohm's law is included with the Hall effect having form [22]

$$\vec{J} = \sigma(\vec{v} \times \vec{B} - \beta(\vec{J} \times \vec{B})), \quad (2.20)$$

in which σ is the electrical conductivity of the fluid and β is the Hall factor. Solving (2.20) for \vec{J} yields to

$$\vec{J} \times \vec{B} = \frac{\sigma B_0^2}{1 + m^2} \omega(x, y) \hat{k},$$

where $m = \sigma \beta B_0$ is the Hall parameter; hence, $\vec{J} \times \vec{B}$ has only the z component to be added to (2.18). Consequently, for the steady fluid motion in z -direction, the terms multiplied by the flow density parameter ρ vanish; hence, the N-S equations reduce to [81]

$$\frac{\partial}{\partial x} \left(\mu \frac{\partial \omega}{\partial x} \right) + \frac{\partial}{\partial y} \left(\mu \frac{\partial \omega}{\partial y} \right) - \frac{\partial p}{\partial z} - \frac{\sigma B_0^2}{1 + m^2} \omega = 0. \quad (2.21)$$

We also assume a no-slip wall condition for the velocity that

$$\omega = 0 \quad \text{on} \quad \partial\Omega.$$

On the other hand, the law of conservation of energy is taken into consideration in a general form based on the temperature as

$$\rho c_p \left(\frac{\partial T}{\partial t} + \vec{v} \cdot \nabla T \right) = k \nabla^2 T + q''', \quad (2.22)$$

where ρ , c_p , k , and q''' are the density, the specific heat capacity, the thermal conductivity of the fluid and heat source, respectively. Assuming a steady problem and a velocity vector which has only the z component defines a energy equation with viscous and Joule dissipation in the following form

$$\rho c_p \omega \frac{\partial T}{\partial z} = k \nabla^2 T + \mu \left[\left(\frac{\partial \omega}{\partial x} \right)^2 + \left(\frac{\partial \omega}{\partial y} \right)^2 \right] + \frac{\sigma B_0^2}{1 + m^2} \omega^2, \quad (2.23)$$

where the second and the third terms on the right hand side of the equality represent the viscous and Joule dissipations, respectively. Furthermore, having a hydrodynamically and thermally developed flow, the H1 thermal boundary condition, which assumes constant heat flux axially and constant wall temperature peripherally, replaces the term $\frac{\partial T}{\partial z}$ by the following equation

$$\frac{\partial T}{\partial z} = \frac{dT_m}{dz},$$

for which the temperature equation is supplied with the boundary condition as $T = T_\omega$ on the duct walls. This condition is preferable in many applications such as resistance heating and heat exchanger [70].

In order to simplify the equations and to reduce the number of parameters, the non-dimensional quantities are introduced as follows

$$x' = \frac{x}{a}, \quad y' = \frac{y}{a}, \quad \omega' = \frac{\mu_0 \omega}{-\frac{dp}{dz} a^2}, \quad T' = \frac{k(T - T_\omega)}{\rho c_p \omega_m a^2 \frac{dT_m}{dz}}, \quad \bar{\mu} = \frac{\mu}{\mu_0},$$

where a is the characteristic length (i.e., major side of the rectangular cavity). Having left the prime notation in the new quantities, the dimensionless momentum and energy equations on the domain $\Omega = [0, 1] \times [0, b/a]$ become

$$\frac{\partial}{\partial x} \left(\bar{\mu} \frac{\partial \omega}{\partial x} \right) + \frac{\partial}{\partial y} \left(\bar{\mu} \frac{\partial \omega}{\partial y} \right) = -1 + \frac{\text{Ha}^2}{1 + m^2} \omega \quad (2.24)$$

and

$$\nabla^2 T + \text{Br} \bar{\mu} \left[\left(\frac{\partial \omega}{\partial x} \right)^2 + \left(\frac{\partial \omega}{\partial y} \right)^2 \right] + \frac{\text{Ha}^2 \text{Br}}{1 + m^2} \omega^2 = \frac{\omega}{\omega_m}, \quad (2.25)$$

where

$$\omega_m = \frac{1}{L} \int_{\Omega} \omega \, d\Omega, \quad \bar{\mu} = e^{-BT} \quad (2.26)$$

and $L = b/a$ is the aspect ratio; m , B , Br and Ha are the resulting dimensionless parameters: Hall parameter, viscosity parameter, Brinkman number, and the Hartmann number, respectively. These are defined as

$$m = \sigma \beta B_0, \quad B = \frac{b_0 \rho c_p \omega_m a^2 \frac{dT_m}{dz}}{k}, \quad \text{Br} = \frac{-\frac{dp}{dz}}{k \rho c_p \frac{dT_m}{dz} \omega_m}, \quad \text{and} \quad \text{Ha}^2 = \frac{\sigma B_0^2 a^2}{\mu_0}.$$

Regarding the physically significant parameters of the problem, the dynamics of the system can be altered by changing these specific constants. A reasonable way to take advantage of this fact is to use these parameters in order to manipulate the behavior of the flow or determine the properties of a given state of the flow. This is achieved by defining an optimal control problem by using the problem parameters as control variables. Hereby, the control problem is designed for the flow and the temperature equations (2.24)–(2.25) for regaining the problem parameters for a desired flow behavior.

Therefore, an objective function(al) is defined to track the difference between the optimal and desired fluid velocity as well as temperature, and possibly, the magnitude of the control variables as well. Such a cost function is

$$J(\omega, T, \mathbf{u}) = \frac{\alpha_\omega}{2} \int_{\Omega} (\omega - \omega_d)^2 d\Omega + \frac{\alpha_T}{2} \int_{\Omega} (T - T_d)^2 d\Omega + \frac{\alpha_{\mathbf{u}}}{2} \int_{\Omega} \|\mathbf{u}\|^2 d\Omega,$$

where the regularization parameters α_ω , α_T , and $\alpha_{\mathbf{u}}$, (respectively for the cost of achieving desired velocity ω_d , temperature T_d , and the control variable vector \mathbf{u}) may be regarded as penalty parameters. They may vary based on the effects of the control parameters as well as the accuracy required to achieve the desired state; and further, they also affect the number of iterations of the underlying optimization algorithm.

Consequently, the PDE-constrained optimal control problem of MHD flow and heat transfer with temperature dependent viscosity reads as follows:

$$\begin{aligned} \underset{\mathbf{u} \in \mathcal{U}}{\text{minimize}} \quad J(\omega, T, \mathbf{u}) &= \frac{\alpha_\omega}{2} \int_{\Omega} (\omega - \omega_d)^2 d\Omega + \frac{\alpha_T}{2} \int_{\Omega} (T - T_d)^2 d\Omega \\ &\quad + \frac{\alpha_{\mathbf{u}}}{2} \int_{\Omega} \|\mathbf{u}\|^2 d\Omega \end{aligned} \quad (2.27)$$

$$\text{subject to} \quad \frac{\partial}{\partial x} \left(\bar{\mu} \frac{\partial \omega}{\partial x} \right) + \frac{\partial}{\partial y} \left(\bar{\mu} \frac{\partial \omega}{\partial y} \right) = -1 + \frac{\text{Ha}^2}{1 + m^2} \omega \quad \text{in } \Omega \quad (2.28)$$

$$\nabla^2 T + \text{Br} \bar{\mu} \left[\left(\frac{\partial \omega}{\partial x} \right)^2 + \left(\frac{\partial \omega}{\partial y} \right)^2 \right] + \frac{\text{Ha}^2 \text{Br}}{1 + m^2} \omega^2 = \frac{\omega}{\omega_m} \quad \text{in } \Omega \quad (2.29)$$

$$\omega = 0, \quad T = 0 \quad \text{on } \partial\Omega. \quad (2.30)$$

The admissible set of controls is defined as the set of parameters of the problem, $\mathcal{U} = \{\text{Ha}, m, \text{Br}, B\}$. In the course of this study, this problem will be one of the main contributions of the thesis in terms of obtaining solutions by the FEM, applying optimization by using the physical parameters of the system and also constructing a ROM. A short overview on the literature is provided below.

Some researchers have studied the magnetic effects on the flow and heat transfer of electrically conducting fluids in rectangular ducts by using numerical methods. Turk and Tezer-Sezgin [97] have given a solution of natural convection flow in square enclosures under magnetic field using the finite element method (FEM). Akgün and Tezer [4] have solved natural convection MHD flow equations in a cavity by using both the dual reciprocity boundary element method (DRBEM) and the differential quadrature method (DQM) comparing the solutions from the two methods. DRBEM solution of MHD flow with magnetic induction and heat transfer has been shown in [74]. A finite difference (FD) solution has been provided for MHD flow free convection flow in a vertical rectangular duct considering the effects of Ohmic heating and viscous dissipation by Umavathi et al. [98]. Kishan and Shekar [56] have showed the combined effects of viscous and Ohmic dissipations on MHD flow by using the FEM.

When the viscosity of the fluid is temperature dependent, a significant heat transfer enhancement is achieved even neglecting the Hall effect, viscous and Joule dissipations. Under strong external magnetic field the Hall current is important and has an effect on the current density due to the influence of the electromagnetic force. Attia [7, 8] has employed FD solutions to transient MHD flow with heat transfer for dusty fluid with temperature dependent viscosity. The effects of variable viscosity and the magnetic field on the flow and heat transfer of both the fluid and dust particles are shown between parallel plates. The problem of MHD flow and heat transfer with variable viscosity for Newtonian fluids in a rectangular duct with the Hall effect has been investigated using finite difference method (FDM) by Ahmed and Attia [81]. Ahmed [80] has investigated numerically with FDM also the effect of Hall current on MHD flow and heat transfer for Bingham fluids in a rectangular duct. The solution to transient MHD flow and heat transfer of a dusty fluid between parallel plates has been given by Türk and Tezer-Sezgin [96] using Chebyshev spectral collocation when the fluid possesses time-dependent viscosity.

Many researchers have also studied and derived theoretical results on control problems in fluid mechanics. The boundary control of an electrically conducting fluid has been studied by Hou and Meir [48] using Lagrange multiplier technique for instance. Ito and Ravindran [51] have used the thermal convection on part of the boundary and provided a first-order necessary optimality condition for control of cavity and channel type flows. An analysis and discretization of an optimal control problem of tracking the velocity and the magnetic fields of viscous, incompressible, electrically conducting fluid for the time-periodic MHD equations has been studied by Gunzburger and Trencha [41]. Griesse and Kunisch [34] have considered the control mechanisms by external and injected currents and magnetic fields and provided optimality conditions for a stationary MHD system in a velocity-current formulation. A comprehensive study on the boundary control of the incompressible MHD equations has been conducted by Bornia [12], where a new boundary control approach is proposed based on lifting functions of the boundary condition. Optimal control problem of non-isothermal viscous fluid with a temperature dependent viscosity has been solved by Cox and Lee [19] using FEM for the state and adjoint equations and within the framework of the *optimize-then-discretize* approach. Recently, Ren et al. [77] have worked

on the control problem in 1D MHD flow by a *discretize-then-optimize* approach using SQP optimization algorithm.

The idea of controlling the dynamics by using parameters of the problem have been also considered in some studies in the literature. Kunisch and Sachs [58] have introduced the reduced SQP methods with BFGS update for parameter identification problems. An augmented Lagrangian method for the estimation of parameters in elliptic systems has been used by Ito et al.[49]. Ito and Kunisch [50] have also studied the augmented Lagrangian-SQP methods in parameter estimation problems. An application of the optimal control as a parameter identification problem to hyperthermia has been introduced by Ganzler et al. [28]. Tonn et al. [94] have studied optimal control of parameter dependent convection-diffusion problems. Parameter estimation via derivative-based optimization has been applied to fluid-structure interaction problems by Richter and Wick [78]. Stoll et al.[87] have used a Lagrange-Newton scheme to identify parameters of a reaction-diffusion type model in pattern formation. Optimal experimental design has been applied to Bingham fluids for parameter identification by Logashenko et al.[65]. Garvie and Trencha[29] have considered the Gierer-Meinhardt reaction diffusion system for identification of space-time distributed parameters. A trust-region Gauss–Newton approach has been proposed for the parameter identification of the Cahn–Hilliard-Chemotaxis system by Kahle and Lam [54].

2.3 Power-Law Fluid Flow and Heat Transfer

The viscosity of a fluid is defined as the ratio of the shear stress and the shear rate, or informally a fluid’s resistance to flow. Previously, assuming a Newtonian fluid, viscosity is a linear function of the shear rate: it is assumed to be constant in Section 2.1 and it varies exponentially with the temperature in Section 2.2. Although they may correspond to many physical phenomena, it is also important to consider a viscosity which is a non-linear function of the shear rate since it represents the non-Newtonian fluids. They are employed in many applications from industry to biotechnology such as polymer solutions [13] and biofluids [42].

Among various viscosity models of non-Newtonian fluids such as Powell-Eyring [73], Cross or Carreau [3], the power-law model is mostly preferred for which the apparent viscosity μ assumes the form

$$\mu = K\gamma^{n-1} \quad (2.31)$$

as in [11, 88], where K is the consistency index of the model, γ is the shear rate and n is the flow index. Particularly, subclasses are identified according to the value of n . If n is greater than one then the model represents *dilatant fluids* having shear-thickening behavior, for example, suspensions of starch and potassium silicate. On the other hand, if n is less than one, then the model introduces *pseudoplastic fluids* having shear-thinning behavior like solution of polymers. Thus, n plays a crucial role in the determination of the dynamics of the flow, which brings out the idea of the control by the parameters. As a result, the control problem of the power-law fluid flow and heat transfer becomes one of the primary interests of this thesis.

In the following, we consider the laminar, fully developed, steady MHD flow and heat transfer for an incompressible, electrically conducting non-Newtonian fluid within a power-law model in a cross section of a rectangular duct. The flow is only in the channel axis direction with the velocity, $\vec{v} = \omega\hat{k}$, so that $\omega = \omega(x, y)$ for $(x, y) \in \Omega = [0, a] \times [0, b]$. The configuration of the problem is again as depicted in Figure 2.1; however, the channel has a rectangular shape. Physical problem assumes similar conditions of Section 2.2 such as having an external magnetic field $\vec{B} = (B_x, B_y, 0)$ with $B_0 = (B_x^2 + B_y^2)^{1/2}$ and a constant pressure gradient $-\frac{dp}{dz}$ applied in the z -direction. However, Hall effect is not considered here; hence the term resulted from the Lorenz force turns into

$$\vec{J} \times \vec{B} = \sigma B_0^2 \omega(x, y)\hat{k}$$

and the apparent viscosity μ of the power-law fluid assumes the form [44]

$$\mu = K \left(\sqrt{\left(\frac{\partial\omega}{\partial x}\right)^2 + \left(\frac{\partial\omega}{\partial y}\right)^2} \right)^{n-1}, \quad (2.32)$$

where n represents the flow index. Under these specifications, following the similar procedure in Section 2.2 the Navier-Stokes equations integrated with the Lorenz force and Ohm's law reduce to

$$\frac{\partial}{\partial x} \left(\mu \frac{\partial\omega}{\partial x} \right) + \frac{\partial}{\partial y} \left(\mu \frac{\partial\omega}{\partial y} \right) - \frac{\partial p}{\partial z} - \sigma B_0^2 \omega = 0, \quad (2.33)$$

where σ is the electrical conductivity of the fluid. The no-slip wall condition is valid for the velocity on the whole boundary.

On the other side, similarly, the energy equation with viscous and Joule dissipation is given for the temperature T [80]:

$$\rho c_p \omega \frac{\partial T}{\partial z} = k \left(\frac{\partial^2 T}{\partial x^2} + \frac{\partial^2 T}{\partial y^2} \right) + \mu \left[\left(\frac{\partial \omega}{\partial x} \right)^2 + \left(\frac{\partial \omega}{\partial y} \right)^2 \right] + \sigma B_0^2 \omega^2. \quad (2.34)$$

Here, the temperature equation is accompanied with the H2 thermal boundary condition, which considers a constant heat flux, allowing the heat transfer through the walls where the flux q'' is constant. Thus, the term $\frac{\partial T}{\partial z}$ in the energy equation (3.17) can be represented as $\frac{\partial T}{\partial z} = \frac{dT_m}{dz}$, where T_m is the mean fluid temperature defined by

$$T_m = \frac{1}{L w_m} \int_{\Omega} \omega T \, d\Omega, \quad (2.35)$$

and w_m is the average velocity:

$$\omega_m = \frac{1}{L} \int_{\Omega} \omega \, d\Omega. \quad (2.36)$$

In order to express the equations in non-dimensional form, the dimensionless variables those which are different from the previous problem are introduced as follows:

$$\omega' = \frac{\omega}{\omega_r}, \quad w_r = \left[\frac{\left(-\frac{dp}{dz} \right) a^{n+1}}{K} \right]^{1/n}, \quad T' = \frac{kT}{aq''},$$

and

$$\bar{\mu} = \frac{\mu}{\mu_r}, \quad \mu_r = \left[\frac{K}{\left\{ \left(-\frac{dp}{dz} \right) a \right\}^{1-n}} \right]^{1/n}.$$

To summarize, the non-dimensional momentum and energy equations with dimensionless velocity ω and temperature T (leaving the prime notation in the new quantities) on the domain $\Omega = [0, 1] \times [0, b/a]$ become

$$\frac{\partial}{\partial x} \left(\bar{\mu} \frac{\partial \omega}{\partial x} \right) + \frac{\partial}{\partial y} \left(\bar{\mu} \frac{\partial \omega}{\partial y} \right) = -1 + \text{Ha}^2 \omega \quad (2.37)$$

and

$$\nabla^2 T + \text{Br} \bar{\mu} \left[\left(\frac{\partial \omega}{\partial x} \right)^2 + \left(\frac{\partial \omega}{\partial y} \right)^2 \right] + \text{Ha}^2 \text{Br} \omega^2 = \frac{4\omega}{\omega_m}, \quad (2.38)$$

where the viscosity of the power-law fluid is given as

$$\bar{\mu} = \left(\sqrt{\left(\frac{\partial \omega}{\partial x} \right)^2 + \left(\frac{\partial \omega}{\partial y} \right)^2} \right)^{n-1}.$$

The dimensionless boundary conditions are also given as

$$\omega = 0 \quad \text{on} \quad \partial\Omega$$

and

$$\frac{\partial T}{\partial y} \Big|_{(x,b/a)} = \frac{\partial T}{\partial x} \Big|_{(1,y)} = 1, \quad \frac{\partial T}{\partial y} \Big|_{(x,0)} = \frac{\partial T}{\partial x} \Big|_{(0,y)} = -1,$$

where we consider to have four heated walls; that is, $\frac{\partial T}{\partial \hat{n}} = 1$ on the walls. The resulting dimensionless parameters Br and Ha are the Brinkman number and the Hartmann number, respectively; these are

$$\text{Ha} = \frac{B_0 a \sqrt{\sigma}}{\sqrt{\mu_r}} \quad \text{and} \quad \text{Br} = \frac{1}{q''} \left(\frac{a}{K} \right)^{1/n} \left(-\frac{dp}{dz} \right)^{(n+1)/n},$$

where μ_r is the reference viscosity of the power-law fluid.

Although the idea of designing a control problem for parameter dependent fluid flow and heat transfer equations is well-interpreted in Section 2.2, the same idea has gained more importance for the power-law fluid flow since it enables to make a classification of the non-Newtonian fluids as shear-thinning or shear-thickening. Also, the determination of an optimal value for the desired state of the flow has a sound structure to drive the fluid viscosity to a required form. Therefore, the control problem is designed for the flow and the temperature equations (2.37)–(2.38) by using the problem parameters as control variables for regaining a desired flow behavior as in the Section 2.2 with the same cost functional in (2.27).

As a result, the PDE-constrained optimal control problem of power-law fluid flow and

heat transfer is formulated as follows:

$$\begin{aligned} \underset{\mathbf{u} \in \mathcal{U}}{\text{minimize}} \quad J(\omega, T, \mathbf{u}) = & \frac{\alpha_\omega}{2} \int_{\Omega} (\omega - \omega_d)^2 d\Omega + \frac{\alpha_T}{2} \int_{\Omega} (T - T_d)^2 d\Omega \\ & + \frac{\alpha_{\mathbf{u}}}{2} \int_{\Omega} \|\mathbf{u}\|^2 d\Omega \end{aligned} \quad (2.39)$$

$$\text{subject to} \quad \frac{\partial}{\partial x} \left(\bar{\mu} \frac{\partial \omega}{\partial x} \right) + \frac{\partial}{\partial y} \left(\bar{\mu} \frac{\partial \omega}{\partial y} \right) = -1 + \text{Ha}^2 \omega \quad \text{in } \Omega \quad (2.40)$$

$$\nabla^2 T + \text{Br} \bar{\mu} \left[\left(\frac{\partial \omega}{\partial x} \right)^2 + \left(\frac{\partial \omega}{\partial y} \right)^2 \right] + \text{Ha}^2 \text{Br} \omega^2 = \frac{4\omega}{\omega_m} \quad \text{in } \Omega \quad (2.41)$$

$$\omega = 0 \quad \text{on } \partial\Omega \quad (2.42)$$

$$\frac{\partial T}{\partial y} \Big|_{(x,1)} = \frac{\partial T}{\partial x} \Big|_{(1,y)} = 1, \quad \frac{\partial T}{\partial y} \Big|_{(x,0)} = \frac{\partial T}{\partial x} \Big|_{(0,y)} = -1. \quad (2.43)$$

The admissible set of controls is defined as the set of parameters of the problem, $\mathcal{U} = \{\text{Ha}, n\}$. The numerical solution of these flows is of great importance and has attracted many researchers. Hartnett and Kostic [44] have reported a comprehensive review of the flow and heat transfer for non-Newtonian fluids in a rectangular duct. The finite element solution of the laminar flow of power law fluid has been studied by Syrjala [89, 90]. A few researchers have introduced the presence of the external magnetic field on non-Newtonian fluids and heat transfer. In this respect, the finite difference solution of laminar flow and heat transfer of a viscous incompressible electrically conducting power law fluid flows has been provided by Ahmed [80].

The characterization and controlling of complex fluids are the main concerns of industry and engineering. Statistical models to investigate the physical characteristics of such fluids and optimal environmental setting for desired flows require large amount of data to examine. However, optimal control approach to such problems provides a more systematic way by coupling of a finite element model with an optimization framework to identify the best set of parameters. Thus, the determination of physical properties of the fluid by optimal control algorithms is of great importance. However, the studies in the optimal control of non-Newtonian fluids from the theoretical point of view are very few. Some researchers have studied the existence, uniqueness and optimality conditions of the distributed controls of such fluids [6, 35, 85, 100].

On the other hand, the studies from the numerical point of view have started with Gavrus and Massoni [30] by minimizing an objective function in the least-squares

sense using FEM for the identification of the parameters. Then, Kunisch and Mar-
duel [57] have studied the optimal control of the viscoelastic fluid to find the optimal
temperature on the boundary of the domain. The estimation of the physical parame-
ters by solving an inverse problem using conjugate gradient and finite volume meth-
ods has been investigated by Park and Hong [72]. The optimal control in blood flow
with shear thinning viscosity has been conducted by Guerra and Tiago [37] using
the discretize-then-optimize (DO) approach within the data assimilation technique.
Recently, they have also extended their results for 3D geometries in [36].

CHAPTER 3

FEM SOLUTION OF FLUID FLOW PROBLEMS

This chapter presents the finite element method (FEM) analysis of two-dimensional flows of laminar, incompressible viscous Newtonian and non-Newtonian fluids. As being the origin of FEM, the foundation of the method of weighted residuals is introduced first and then the basic steps of the FEM are presented. Starting with the derivation of the variational formulation, solutions of the problems are projected into the finite-dimensional spaces (so-called finite element spaces) by the Galerkin-type projection. That is, equations of the problem are multiplied by test functions which are same with the basis functions of the finite element spaces. Next, the Green formula is used to weaken the second-order derivatives to obtain the so-called weak formulation of the problem. Consequently, the discretized system of equations are obtained for the finite dimensional approximations.

3.1 Introduction

The method of weighted residuals [25] aims to find an approximate solution (trial solution) \hat{z} for the solution z of a boundary value problem; such a problem can be given in a compact form as

$$C(z(\vec{x})) = 0, \quad \vec{x} = (x^1, x^2, \dots, x^n) \in \Omega \subset \mathbb{R}^n. \quad (3.1)$$

Basically, \hat{z} is expanded in a set of trial functions, $\{\phi_i\}_{i=1}^N$, in the form

$$z \approx \hat{z} = \sum_{i=1}^N z_i \phi_i, \quad (3.2)$$

where the ϕ_i satisfy the homogeneous Dirichlet boundary conditions so that $\phi_i = 0$ on the boundary for every $i = 1, 2, \dots, N$. This trial solution is then used in the boundary value problem (3.1) and the residual R is defined by

$$R(\hat{z}(\vec{x})) = C(\hat{z}(\vec{x})). \quad (3.3)$$

The principal idea is to force the residual to vanish in an average sense so that the weighted integrals of the residual are set to zero:

$$\langle \psi_j, R \rangle = 0, \quad (3.4)$$

where ψ_j are the weight functions for $j = 1, 2, \dots, N$ and the inner product $\langle u, v \rangle$ on the space of square integrable functions over domain Ω is defined by

$$\langle u, v \rangle_{\Omega} = \int_{\Omega} uv \, d\Omega.$$

Combining (3.3) and (3.4) results in

$$\left\langle \psi_j, C \left(\sum_{i=1}^N z_i \phi_i \right) \right\rangle = 0 \quad (3.5)$$

which is to be solved for z_i to obtain the approximate solution in (3.2).

The choice of the weighting functions determines the type of the method of weighted residuals. For example, collocation method is derived when the weighting functions are chosen as the displaced Dirac delta function

$$\psi_j = \delta(\vec{x} - \vec{x}_j),$$

which corresponds to that

$$\int_{\Omega} \psi_j R \, d\Omega = R(\hat{z}(\vec{x}_j)).$$

Therefore, the residual becomes zero at the specified collocation points \vec{x}_j . Furthermore, the Galerkin method, which this thesis is interested in, is developed if the weighting functions are chosen to be the trial functions, $\phi_i = \psi_i$. Particularly, in the FEM, the domain is partitioned into elements (triangles, tetrahedrons, etc.) and the trial functions (for example, Lagrange type elements: piecewise polynomials) are defined on each element.

Basically, a typical construction of piecewise linear polynomials [62] on a mesh $\mathcal{K} = \{K\}$, where K is a triangle of a domain $\Omega \subset \mathbb{R}^2$, requires the space of all continuous piecewise linear polynomials Q_h given by

$$Q_h = \{q \in \mathcal{C}(\Omega) \mid q|_K \in \mathcal{P}_1(K), K \in \mathcal{K}\},$$

where h denotes the local mesh size, defined as the length of the longest edge on K , $\mathcal{P}_1(K)$ is the space of linear functions on K defined by

$$\mathcal{P}_1(K) = \{q = c_0 + c_1x + c_2y \mid (x, y) \in K \subset \mathbb{R}^2, c_0, c_1, c_2 \in \mathbb{R}\}.$$

A function q in Q_h can be determined uniquely by its nodal values

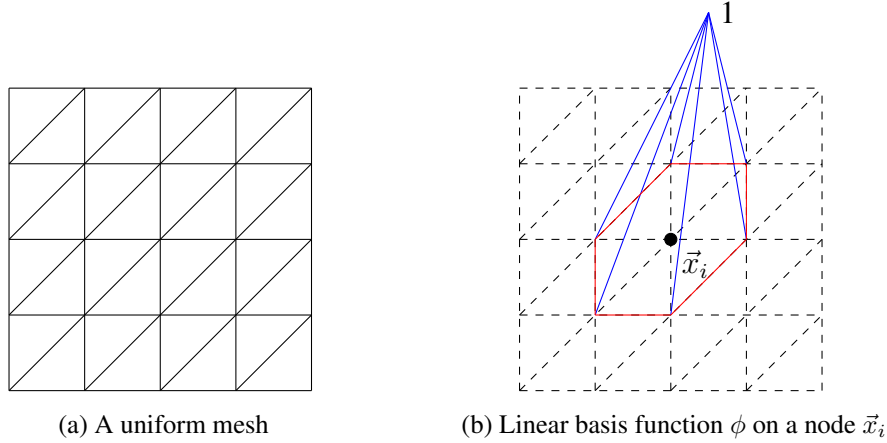
$$\{q(\vec{x}_j)\}_{j=1}^N$$

and conversely, for each set of nodal values there is a unique function q in Q_h with the given nodal values: the degrees of freedom. Hence, a basis $\{\phi_j\}_{j=1}^N \subset Q_h$ is defined such that

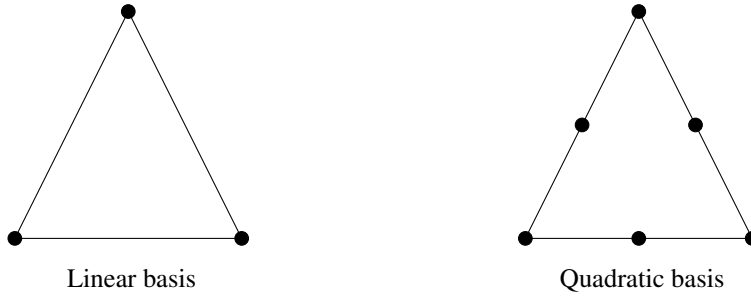
$$\phi_j(\vec{x}_i) = \begin{cases} 1, & i = j, \\ 0, & i \neq j \end{cases}$$

for $i, j = 1, \dots, N$. According to this construction of basis functions, their supports share a small set of triangles and this enables to have a sparse matrix equation in system (3.5). Although the structure is more complicated than matrices obtained by the finite differences, it becomes more advantageous for arbitrary complicated boundaries and provides systematic rules for the developments of numerical schemes. For the implementations in this thesis, uniform meshes are considered and an illustrative example is given in Figure 3.1(a). FEM basis functions are chosen linear or quadratic with respect to the type of the problems: linear or non-linear. A piecewise linear basis function is depicted in Figure 3.1(b) and nodes of the linear and quadratic basis functions are shown in Figure 3.2.

One of the computational efficiency of the FEM is the procedure for the treatment of the integrals in (3.5). These integrals are evaluated firstly on each element (triangle) then an efficient summation of the element-wise matrices into the global matrix, the so-called ‘assembling’, is conducted. Due to the structure of the basis functions and the need for an automated framework for the integral evaluations, numerical quadrature rules become highly appealing. In the finite element literature, Gaussian quadrature is preferred mostly among all quadratures because it requires fewer function



(a) A uniform mesh (b) Linear basis function ϕ on a node \vec{x}_i
Figure 3.1: Uniform mesh and linear basis on a square duct.



Linear basis Quadratic basis
Figure 3.2: FEM nodes for linear and quadratic basis functions on a triangle.

evaluations for a given order of accuracy. Basic cases such as first and second order Gaussian quadrature nodes and weights for the integral of a function g on a standard triangle in $\Omega \subset \mathbb{R}^2$ can be given as follows:

$$\begin{aligned} \text{1st-order : } \int\int_K g(\vec{x}) d\vec{x} &= \frac{1}{2} g(1/3, 1/3), \\ \text{2nd-order : } \int\int_K g(\vec{x}) d\vec{x} &= \frac{1}{6} [g(1/6, 1/6) + g(2/3, 1/6) + g(1/6, 2/3)], \end{aligned}$$

where $\vec{x} = (x, y)$ and K is the standard triangle defined by the vertexes $(0, 0)$, $(1, 0)$, and $(0, 1)$.

In the following, the analysis of the Navier-Stokes equations, which consist of the momentum and continuity equations, is introduced in Section 3.2. Section 3.3 presents the analysis for the MHD flow and heat transfer equations with temperature dependent viscosity and Hall effect. The analysis is conducted for the power-law fluid flow and heat transfer equations where the momentum and energy equations are combined with a flow dependent viscosity in Section 3.4. The FEM approximations in this chapter constitute a basis for the solution of the optimal control problems in Chapter 4 and

the model order reduction applications in Chapter 5.

3.2 FEM Applications to the Navier-Stokes Equations

The FEM approximation of the Navier-Stokes equations are formulated for steady, laminar flow of an incompressible fluid in a domain $\Omega \subset \mathbb{R}^2$ in terms of velocity and pressure which are introduced in Section 2.1 as

$$-\nu \Delta \vec{v} + (\vec{v} \cdot \nabla) \vec{v} + \nabla p = \vec{f} \quad \text{in } \Omega, \quad (3.6)$$

$$\nabla \cdot \vec{v} = 0 \quad \text{in } \Omega, \quad (3.7)$$

where the homogeneous Dirichlet type boundary condition $\vec{v} = 0$ on the boundary $\partial\Omega$ is considered for the velocity.

The first attempt to derive a finite element method is to reconstruct the system of equations (3.6)–(3.7) in the weak form. The Sobolev spaces used in this context are standard; for a general domain Ω , with the inner product $\langle u, v \rangle_\Omega = \int_\Omega uv \, d\Omega$ and $\|u\|_{L^2(\Omega)} = \sqrt{\langle u, u \rangle}$, we define

$$H^1(\Omega) = \{v \mid \|v\|_{L^2(\Omega)} + \|\nabla v\|_{L^2(\Omega)} < \infty\}$$

$$H_0^1(\Omega) = \{v \mid v \in H^1(\Omega) \text{ and } v = 0 \text{ on } \partial\Omega\}.$$

Multiplying (3.6) and (3.7) by the test functions $(\vec{v}, q) \in (H_0^1(\Omega))^2 \times L^2(\Omega)$ and integrating over the domain Ω , respectively, the Green formula corresponds to that

$$-\nu \int_\Omega \Delta \vec{v} \cdot \vec{w} \, d\Omega = -\nu \int_{\partial\Omega} (\nabla \vec{v} \cdot \hat{n}) \vec{w} \, dS + \nu \int_\Omega \nabla \vec{v} : \nabla \vec{w} \, d\Omega,$$

where $\hat{n} = (n_1, n_2)$ is the unit normal vector pointing out of $\partial\Omega$ and

$$\int_\Omega \nabla \vec{v} : \nabla \vec{w} \, d\Omega = \sum_{i,j=1}^2 \int_\Omega \frac{\partial v_i}{\partial x_j} \frac{\partial w_i}{\partial x_j} \, d\Omega.$$

Accordingly, we have

$$\begin{aligned} \nu \int_\Omega \nabla \vec{v} : \nabla \vec{w} \, d\Omega - \int_{\partial\Omega} (\nu \nabla \vec{v} \cdot \hat{n}) \vec{w} \, dS + \int_\Omega (\vec{v} \cdot \nabla) \vec{v} \cdot \vec{w} \, d\Omega - \int_\Omega p (\nabla \cdot \vec{v}) \, d\Omega \\ + \int_{\partial\Omega} p \hat{n} \cdot \vec{w} \, dS - \int_\Omega \vec{f} \cdot \vec{w} \, d\Omega = 0 \end{aligned}$$

and from (3.7),

$$\int_{\Omega} (\nabla \cdot \vec{v}) q \, d\Omega = 0.$$

Thus, the variational formulation of the problem (3.6)–(3.7) yields: find $(\vec{v}, p) \in (H_0^1(\Omega))^2 \times L_0^2(\Omega)$ such that

$$\begin{aligned} \nu \int_{\Omega} \nabla \vec{v} : \nabla \vec{w} \, d\Omega + \int_{\Omega} (\vec{v} \cdot \nabla) \vec{v} \cdot \vec{w} \, d\Omega - \int_{\Omega} p (\nabla \cdot \vec{w}) \, d\Omega - \int_{\Omega} \vec{f} \cdot \vec{w} \, d\Omega &= 0, \\ \int_{\Omega} (\nabla \cdot \vec{v}) q \, d\Omega &= 0 \end{aligned}$$

for $\vec{w} \in (H_0^1(\Omega))^2$ and $q \in L_0^2(\Omega)$, where introduction of the trilinear form is necessary; namely,

$$(\vec{u} \cdot \nabla) \vec{v} \cdot \vec{w} = \sum_{i,j=1}^2 u_j \frac{\partial v_i}{\partial x_j} w_i$$

so that

$$(\vec{v} \cdot \nabla) \vec{v} \cdot \vec{w} = \sum_{i,j=1}^2 v_j \frac{\partial v_i}{\partial x_j} w_i.$$

Next, the finite dimensional approximations for the governing equations are introduced by employing quadratic and linear finite elements for velocity and pressure, respectively. Let \mathcal{K}_h be a triangulation of Ω with size $h > 0$ and let $V_{h,0}$ and Q_h be the space of quadratic and linear polynomials on \mathcal{K}_h and $V_{h,0} \subset H_0^1(\Omega)$, $Q_h \subset L_0^2(\Omega)$, where

$$L_0^2(\Omega) = \left\{ q \in L^2(\Omega) \mid \int_{\Omega} q \, d\Omega = 0 \right\}.$$

Replacing $H_0^1(\Omega)$ with $V_{h,0}$ and $L_0^2(\Omega)$ with Q_h in the variational formulation, the following finite element formulation is obtained: find $(\vec{v}, p) \in V_{h,0}^2 \times Q_h$ such that

$$\langle \nu \nabla \vec{v}, \nabla \vec{w} \rangle_{\Omega} + \langle (\vec{v} \cdot \nabla) \vec{v}, \vec{w} \rangle_{\Omega} - \langle p, \nabla \cdot \vec{w} \rangle_{\Omega} - \langle \vec{f}, \vec{w} \rangle_{\Omega} = 0, \quad (3.8)$$

$$\langle \nabla \cdot \vec{v}, q \rangle_{\Omega} = 0 \quad (3.9)$$

for $\vec{w} \in V_{h,0}^2$ and $q \in Q_h$. Therefore, letting $\{\vec{\phi}_i\}_{i=1}^{\beta_v}$ and $\{\psi_k\}_{k=1}^{\beta_p}$, being the basis functions respectively for $V_{h,0}^2$ and Q_h , it is obtained that

$$\vec{v} \approx \sum_{j=1}^{\beta_v} \mathbf{v}_j \vec{\phi}_j \quad \text{and} \quad p \approx \sum_{l=1}^{\beta_p} p_l \psi_l,$$

where \mathbf{v}_j and p_l are the components of the vectors \mathbf{v} and \mathbf{p} .

Accordingly, the vector $\mathbf{f} = (f_i)$ for the finite element approximation of \vec{f} is introduced so that

$$\vec{f} \approx \sum_{i=1}^{\beta_v} f_i \vec{\phi}_i \quad \text{with} \quad f_i = \int_{\Omega} \vec{f} \cdot \vec{\phi}_i \, d\Omega,$$

and the matrices $\mathbf{M} = (M_{ij})$, $\mathbf{K} = (K_{ij})$ and $\mathbf{D} = (D_{ik})$ with entries

$$\begin{aligned} M_{ij} &= \int_{\Omega} \vec{\phi}_j \cdot \vec{\phi}_i \, d\Omega, \\ K_{ij} &= \nu \int_{\Omega} \nabla \vec{\phi}_j : \nabla \vec{\phi}_i \, d\Omega, \\ D_{ik} &= - \int_{\Omega} \psi_k (\nabla \cdot \vec{\phi}_i) \, d\Omega \end{aligned}$$

for $1 \leq i, j \leq \beta_v$ and $1 \leq k \leq \beta_p$.

The matrix $\mathbf{N}(\mathbf{v})$ is defined with entries

$$N(\mathbf{v})_{ij} = \sum_{r=1}^{\beta_v} \int_{\Omega} (\vec{v}_r \vec{\phi}_r \cdot \nabla) \vec{\phi}_j \cdot \vec{\phi}_i \, d\Omega, \quad 1 \leq i, j \leq \beta_v \quad (3.10)$$

in order to manage the nonlinear term in (3.8). The algebraic matrix-vector form of the discrete non-linear problem reads as

$$\begin{bmatrix} \mathbf{K} + \mathbf{N}(\mathbf{v}) & \mathbf{D} \\ \mathbf{D}^T & \mathbf{0} \end{bmatrix} \begin{bmatrix} \mathbf{v} \\ \mathbf{p} \end{bmatrix} = \begin{bmatrix} \mathbf{Mf} \\ \mathbf{0} \end{bmatrix}. \quad (3.11)$$

However, no boundary condition is specified for the pressure. Instead, the condition on p is given as $\int_{\Omega} p \, d\Omega = 0$, which can be imposed by introducing a new variable, so-called Lagrange multiplier, such that

$$\int_{\Omega} p \, d\Omega + \int_{\Omega} c \, q \, d\Omega = 0, \quad c, d \in \mathbb{R}.$$

Here, c is the unknown Lagrange multiplier represented in a real finite element space R_h having only one degree of freedom and d is the corresponding test function from the same finite element space. Thus, the non-linear system in (3.11) turns into the following system

$$\begin{bmatrix} \mathbf{K} + \mathbf{N}(\mathbf{v}) & \mathbf{D} & \mathbf{0} \\ \mathbf{D}^T & \mathbf{0} & \mathbf{r}^T \\ \mathbf{0} & \mathbf{r} & 0 \end{bmatrix} \begin{bmatrix} \mathbf{v} \\ \mathbf{p} \\ \mathbf{c} \end{bmatrix} = \begin{bmatrix} \mathbf{Mf} \\ \mathbf{0} \\ 0 \end{bmatrix}, \quad (3.12)$$

where $\mathbf{r} = (r_k) = \int_{\Omega} d\psi_k d\Omega$ for $1 \leq k \leq \beta_p$. To be clear, the dimensional structure of the block matrices in (3.12) is

$$\begin{bmatrix} \beta_v \times \beta_v & \beta_v \times \beta_p & \beta_v \times 1 \\ \beta_p \times \beta_v & \beta_p \times \beta_p & \beta_p \times 1 \\ 1 \times \beta_v & 1 \times \beta_p & 1 \times 1 \end{bmatrix} \begin{bmatrix} \beta_v \times 1 \\ \beta_p \times 1 \\ 1 \times 1 \end{bmatrix} = \begin{bmatrix} \beta_v \times 1 \\ \beta_p \times 1 \\ 1 \times 1 \end{bmatrix},$$

which has $(\beta_v + \beta_p + 1) \times (\beta_v + \beta_p + 1)$ dimension. Shortly, the problem in (3.12) reads:

$$\text{solve } \mathbf{C}(\mathbf{z}) = 0 \quad \text{for } \mathbf{z} = (\mathbf{v}, \mathbf{p}, \mathbf{c})^T, \quad (3.13)$$

where

$$\mathbf{C}(\mathbf{z}) = \begin{bmatrix} \mathbf{C}_1(\mathbf{z}) \\ \mathbf{C}_2(\mathbf{z}) \\ \mathbf{C}_3(\mathbf{z}) \end{bmatrix} = \begin{bmatrix} \mathbf{K} + \mathbf{N}(\mathbf{v}) & \mathbf{D} & \mathbf{0} \\ \mathbf{D}^T & \mathbf{0} & \mathbf{r}^T \\ \mathbf{0} & \mathbf{r} & 0 \end{bmatrix} \begin{bmatrix} \mathbf{v} \\ \mathbf{p} \\ \mathbf{c} \end{bmatrix} - \begin{bmatrix} \mathbf{M}\mathbf{f} \\ \mathbf{0} \\ 0 \end{bmatrix} = \mathbf{0}. \quad (3.14)$$

Considering a Galerkin type discretization (projection) of a PDE, Newton's system for the solution of non-linear equations can be equally well interpreted either as a discretization of the linearized operator or as a linearization of the discrete non-linear system [101]. Thus, a *discretize-then-linearize* approach is followed to handle the non-linear problem. This can be summarized briefly as

$$\mathcal{J}(\mathbf{z}^k)(\mathbf{z}^{k+1} - \mathbf{z}^k) = -\mathbf{C}(\mathbf{z}^k), \quad (3.15)$$

where $\mathcal{J}(\mathbf{z}^k)$ is the Jacobian with the entries

$$\mathcal{J}_{ij}(\mathbf{z}^k) = \frac{\partial \mathbf{C}_i}{\partial z_j}(\mathbf{z}^k).$$

Since the contribution to Jacobian from the linear parts is trivial, the non-linearity arising from only the convective term is examined in detail

$$\mathbf{N}(\mathbf{v})_i = \sum_{j,r}^{\beta_v} \int_{\Omega} \vec{v}_r (\vec{\phi}_r \cdot \nabla) \vec{v}_j \vec{\phi}_j \cdot \vec{\phi}_i d\Omega \quad \text{for } i = 1, \dots, \beta_v$$

so that

$$\begin{aligned} \frac{\partial \mathbf{N}(\mathbf{v})_i}{\partial v_l}(\mathbf{v}) &= \sum_r^{\beta_v} \int_{\Omega} \vec{v}_r (\vec{\phi}_r \cdot \nabla) \vec{v}_l \vec{\phi}_l \cdot \vec{\phi}_i d\Omega \\ &\quad + \sum_j^{\beta_v} \int_{\Omega} \vec{v}_l (\vec{\phi}_l \cdot \nabla) \vec{v}_j \vec{\phi}_j \cdot \vec{\phi}_i d\Omega. \end{aligned}$$

This contribution can be also written as

$$\mathcal{J}_{NL}(\mathbf{v}) = \mathbf{N}(\mathbf{v}) + \mathbf{N}^*(\mathbf{v}),$$

where $\mathcal{J}_{NL}(\mathbf{v})$ denotes the Jacobian corresponding to the non-linear term, which depends only on \mathbf{v} . The components of $\mathbf{N}(\mathbf{v})$ are given in (3.10) and the components of $\mathbf{N}^*(\mathbf{v})$ are defined as

$$N^*(\mathbf{v})_{ij} = \sum_{r=1}^{\beta_v} \int_{\Omega} (\vec{\phi}_j \cdot \nabla) \vec{v}_r \vec{\phi}_r \cdot \vec{\phi}_i, \quad 1 \leq i, j \leq \beta_v \, d\Omega.$$

Thus, each Newton iteration becomes

$$\begin{bmatrix} \mathbf{K} + \mathbf{N}(\mathbf{v}^k) + \mathbf{N}^*(\mathbf{v}^k) & \mathbf{D} & \mathbf{0} \\ \mathbf{D}^T & \mathbf{0} & \mathbf{r}^T \\ \mathbf{0} & \mathbf{r} & 0 \end{bmatrix} \begin{bmatrix} \mathbf{v}^{k+1} - \mathbf{v}^k \\ \mathbf{p}^{k+1} - \mathbf{p}^k \\ \mathbf{c}^{k+1} - \mathbf{c}^k \end{bmatrix} = \begin{bmatrix} \mathbf{M}\mathbf{f} \\ \mathbf{0} \\ 0 \end{bmatrix} - \begin{bmatrix} \mathbf{K} + \mathbf{N}(\mathbf{v}^k) & \mathbf{D} & \mathbf{0} \\ \mathbf{D}^T & \mathbf{0} & \mathbf{r}^T \\ \mathbf{0} & \mathbf{r} & 0 \end{bmatrix} \begin{bmatrix} \mathbf{v}^k \\ \mathbf{p}^k \\ \mathbf{c}^k \end{bmatrix}.$$

Using the fact that $\mathbf{N}(\mathbf{v}^k)\mathbf{v}^k = \mathbf{N}^*(\mathbf{v}^k)\mathbf{v}^k$, the simplified system of equations is obtained as follows

$$\begin{bmatrix} \mathbf{K} + \mathbf{N}(\mathbf{v}^k) + \mathbf{N}^*(\mathbf{v}^k) & \mathbf{D} & \mathbf{0} \\ \mathbf{D}^T & \mathbf{0} & \mathbf{r}^T \\ \mathbf{0} & \mathbf{r} & 0 \end{bmatrix} \begin{bmatrix} \mathbf{v}^{k+1} \\ \mathbf{p}^{k+1} \\ \mathbf{c}^{k+1} \end{bmatrix} = \begin{bmatrix} \mathbf{M}\mathbf{f} + \mathbf{N}^*(\mathbf{v}^k)\mathbf{v}^k \\ \mathbf{0} \\ 0 \end{bmatrix},$$

which is to be solved iteratively until the absolute and relative errors between two consecutive solutions are less than the given tolerance.

3.3 FEM Applications to MHD Flows and Heat Transfer with Temperature Dependent Viscosity

The FEM approximations of the MHD flow and heat transfer equations in terms of the velocity magnitude and the temperature introduced in Section 2.2:

$$\frac{\partial}{\partial x} \left(\bar{\mu} \frac{\partial \omega}{\partial x} \right) + \frac{\partial}{\partial y} \left(\bar{\mu} \frac{\partial \omega}{\partial y} \right) = -1 + \frac{\text{Ha}^2}{1 + m^2} \omega \quad (3.16)$$

and

$$\nabla^2 T + \text{Br} \bar{\mu} \left[\left(\frac{\partial \omega}{\partial x} \right)^2 + \left(\frac{\partial \omega}{\partial y} \right)^2 \right] + \frac{\text{Ha}^2 \text{Br}}{1 + m^2} \omega^2 = \frac{\omega}{\omega_m} \quad (3.17)$$

are examined in a square duct with no-slip and zero-temperature walls, where ω_m is defined as $\omega_m = \frac{1}{L} \int_{\Omega} \omega \, d\Omega$, L being the aspect ratio. It is also assumed that the

flow has a temperature dependent viscosity, $\bar{\mu} = e^{-BT}$, where B is the viscosity parameter. In order to derive a finite element method, the dimensionless system of equations (3.16)–(3.17) is reformulated in the weak form. Multiplying (3.16) and (3.17) by the test functions $(v, q) \in H_0^1(\Omega)^2$ and integrating over the domain Ω , it is obtained that

$$\int_{\Omega} \bar{\mu} \nabla \omega \cdot \nabla v \, d\Omega - \int_{\partial\Omega} (\bar{\mu} \nabla \omega \cdot \hat{n}) v \, dS - \int_{\Omega} \left(1 - \frac{\text{Ha}^2}{1+m^2} \omega \right) v \, d\Omega = 0$$

and

$$\begin{aligned} \int_{\Omega} \nabla T \cdot \nabla q \, d\Omega - \int_{\partial\Omega} (\nabla T \cdot \hat{n}) q \, dS - \int_{\Omega} \text{Br} \bar{\mu} \left[\left(\frac{\partial \omega}{\partial x} \right)^2 + \left(\frac{\partial \omega}{\partial y} \right)^2 \right] q \, d\Omega \\ - \int_{\Omega} \left(\frac{\text{Ha}^2 \text{Br}}{1+m^2} \right) \omega^2 q \, d\Omega + \int_{\Omega} \frac{\omega}{\omega_m} q \, d\Omega = 0. \end{aligned}$$

Here, $\hat{n} = (n_1, n_2)$ is the unit normal vector pointing out of $\partial\Omega$. Integrating by parts, the variational formulation of the problem (3.16)–(3.17) yields: find $(\omega, T) \in H_0^1(\Omega)^2$ such that

$$\langle \bar{\mu} \nabla \omega, \nabla v \rangle_{\Omega} - \left\langle 1 - \frac{\text{Ha}^2}{1+m^2} \omega, v \right\rangle_{\Omega} = 0, \quad v \in H_0^1(\Omega), \quad (3.18)$$

$$\begin{aligned} \langle \nabla T, \nabla q \rangle_{\Omega} - \left\langle \text{Br} \bar{\mu} \left[\left(\frac{\partial \omega}{\partial x} \right)^2 + \left(\frac{\partial \omega}{\partial y} \right)^2 \right], q \right\rangle_{\Omega} - \left(\frac{\text{Ha}^2 \text{Br}}{1+m^2} \right) \langle \omega^2, q \rangle_{\Omega} \\ + \left\langle \frac{\omega}{\omega_m}, q \right\rangle_{\Omega} = 0, \quad q \in H_0^1(\Omega). \end{aligned} \quad (3.19)$$

Now, the finite-dimensional approximations for the governing equations are introduced by employing quadratic finite elements for both variables, velocity and temperature. Let \mathcal{K}_h be a triangulation of Ω with size $h > 0$ and let $V_{h,0}$ and $Q_{h,0}$ be the space of quadratic polynomials on \mathcal{K}_h such that $V_{h,0} \subset H_0^1(\Omega)$ and $Q_{h,0} \subset H_0^1(\Omega)$. Replacing $H_0^1(\Omega)$ with $V_{h,0}$ and $Q_{h,0}$ in the variational formulation, the following finite element problem is attained: find $(\omega, T) \in V_{h,0} \times Q_{h,0}$ such that

$$\langle \bar{\mu} \nabla \omega, \nabla v \rangle_{\Omega} - \left\langle 1 - \frac{\text{Ha}^2}{1+m^2} \omega, v \right\rangle_{\Omega} = 0, \quad v \in V_{h,0} \quad (3.20)$$

$$\begin{aligned} \langle \nabla T, \nabla q \rangle_{\Omega} - \left\langle \text{Br} \bar{\mu} \left[\left(\frac{\partial \omega}{\partial x} \right)^2 + \left(\frac{\partial \omega}{\partial y} \right)^2 \right], q \right\rangle_{\Omega} - \left(\frac{\text{Ha}^2 \text{Br}}{1+m^2} \right) \langle \omega^2, q \rangle_{\Omega} \\ + \left\langle \frac{\omega}{\omega_m}, q \right\rangle_{\Omega} = 0, \quad q \in Q_{h,0}. \end{aligned} \quad (3.21)$$

Therefore, letting $\{\phi_i\}_{i=1}^{\beta_\omega}$ and $\{\psi_k\}_{k=1}^{\beta_T}$ being the bases for $V_{h,0}$ and $Q_{h,0}$, respectively, we have

$$\omega = \sum_{j=1}^{\beta_\omega} \omega_j \phi_j \quad \text{and} \quad T = \sum_{l=1}^{\beta_T} T_l \psi_l,$$

where ω_j and T_l are the components of the vectors ω and T , respectively. Accordingly, the approximations are introduced in the following forms:

$$\begin{aligned} \bar{\mu} &= e^{-BT} \approx \sum_{l=1}^{\beta_T} e^{-BT_l} \psi_l, \\ \omega^2 &\approx \sum_{j=1}^{\beta_\omega} \omega_j^2 \phi_j, \\ \frac{\partial \omega}{\partial x} &\approx \sum_{j=1}^{\beta_\omega} \omega_j (\phi_j)_x, \quad \text{and} \quad \frac{\partial \omega}{\partial y} \approx \sum_{j=1}^{\beta_\omega} \omega_j (\phi_j)_y, \\ \left(\frac{\partial \omega}{\partial x} \right)^2 &\approx \sum_{j=1}^{\beta_\omega} \omega_j^2 (\phi_j)_x, \quad \text{and} \quad \left(\frac{\partial \omega}{\partial y} \right)^2 \approx \sum_{j=1}^{\beta_\omega} \omega_j^2 (\phi_j)_y, \\ \left(\frac{\partial \omega}{\partial x} \right)^2 + \left(\frac{\partial \omega}{\partial y} \right)^2 &\approx \sum_{j=1}^{\beta_\omega} \omega_j^2 [(\phi_j)_x + (\phi_j)_y]. \end{aligned}$$

Furthermore, entries of the vector $\mathbf{d} = (d_i)$ and the matrices $\mathbf{M} = (M_{ij})$ and $\mathbf{S} = (S_{kl})$ are

$$\begin{aligned} d_i &= \int_{\Omega} \phi_i \, d\Omega, \quad 1 \leq i \leq \beta_\omega, \\ M_{ij} &= \int_{\Omega} \phi_j \phi_i \, d\Omega \quad 1 \leq i, j \leq \beta_\omega, \\ S_{kl} &= \int_{\Omega} \nabla \psi_l \nabla \psi_k \, d\Omega \quad 1 \leq k, l \leq \beta_T. \end{aligned}$$

In order to manage the non-linear terms, the matrices $\mathbf{K}(\mathbf{T})$, $\mathbf{D}(\omega, \mathbf{T})$, $\mathbf{N}(\omega)$ and $\mathbf{P}(\omega)$ are proposed with the following entries

$$\begin{aligned} K(\mathbf{T})_{ij} &= \sum_{r=1}^{\beta_T} e^{-BT_r} \int_{\Omega} \psi_r \nabla \phi_j \nabla \phi_i \, d\Omega, \\ D(\omega, \mathbf{T})_{kj} &= \sum_{r=1}^{\beta_T} e^{-BT_r} \omega_j \int_{\Omega} \psi_r \left(\frac{\partial \phi_j}{\partial x} + \frac{\partial \phi_j}{\partial y} \right) \psi_k \, d\Omega, \\ N(\omega)_{kj} &= \int_{\Omega} \omega_j \phi_j \psi_k \, d\Omega, \\ P(\omega)_{kj} &= \frac{\int_{\Omega} \phi_j \psi_k \, d\Omega}{\frac{1}{L} \int_{\Omega} \left(\sum_{l=1}^{\beta_\omega} \omega_l \phi_l \right) \, d\Omega}, \end{aligned}$$

where $1 \leq i, j \leq \beta_\omega$, and $1 \leq k \leq \beta_T$. The algebraic form of the discrete problem reads:

$$\begin{bmatrix} c_1 \mathbf{M} & \mathbf{0} \\ \mathbf{0} & \mathbf{S} \end{bmatrix} \begin{bmatrix} \boldsymbol{\omega} \\ \mathbf{T} \end{bmatrix} + \begin{bmatrix} \mathbf{K}(\mathbf{T})\boldsymbol{\omega} - \mathbf{d} \\ c_2 \mathbf{N}(\boldsymbol{\omega}) - \text{Br} \mathbf{D}(\boldsymbol{\omega}, \mathbf{T})\boldsymbol{\omega} + \mathbf{P}(\boldsymbol{\omega})\boldsymbol{\omega} \end{bmatrix} = \mathbf{0},$$

where constants c_1 and c_2 are defined as

$$c_1 = \frac{\text{Ha}^2}{1 + m^2} \quad \text{and} \quad c_2 = \frac{\text{Ha}^2 \text{Br}}{1 + m^2}.$$

Then discrete non-linear system of equations can be reformulated for finding $\mathbf{z} = (\boldsymbol{\omega}, \mathbf{T})$ such that

$$\mathbf{C}(\mathbf{z}) := \begin{bmatrix} c_1 \mathbf{M} & \mathbf{0} \\ \mathbf{0} & \mathbf{S} \end{bmatrix} \begin{bmatrix} \boldsymbol{\omega} \\ \mathbf{T} \end{bmatrix} + \begin{bmatrix} \mathbf{K}(\mathbf{T})\boldsymbol{\omega} - \mathbf{d} \\ c_2 \mathbf{N}(\boldsymbol{\omega})\boldsymbol{\omega} - \text{Br} \mathbf{D}(\boldsymbol{\omega}, \mathbf{T})\boldsymbol{\omega} + \mathbf{P}(\boldsymbol{\omega})\boldsymbol{\omega} \end{bmatrix} = \mathbf{0}. \quad (3.22)$$

Because of the same reasoning given in Section 3.2, a *discretize-then-linearize* approach is followed. The Newton formula for the mixed problem given in (3.15) is used with the Jacobian

$$\mathcal{J}(\mathbf{z}) = \begin{bmatrix} c_1 \mathbf{M} & \mathbf{0} \\ \mathbf{0} & \mathbf{S} \end{bmatrix} + \begin{bmatrix} \mathbf{K}(\mathbf{T}) & \frac{\partial \mathbf{K}(\mathbf{T})}{\partial \mathbf{T}} \boldsymbol{\omega} \\ \mathbf{G}(\mathbf{z}) & -\text{Br} \frac{\partial \mathbf{D}(\boldsymbol{\omega}, \mathbf{T})}{\partial \mathbf{T}} \boldsymbol{\omega} \end{bmatrix}, \quad (3.23)$$

where

$$\mathbf{G}(\mathbf{z}) = c_2 \left[\frac{\partial \mathbf{N}(\boldsymbol{\omega})}{\partial \boldsymbol{\omega}} \boldsymbol{\omega} + \mathbf{N}(\boldsymbol{\omega}) \right] - \text{Br} \left[\frac{\partial \mathbf{D}(\boldsymbol{\omega}, \mathbf{T})}{\partial \boldsymbol{\omega}} \boldsymbol{\omega} + \mathbf{D}(\boldsymbol{\omega}, \mathbf{T}) \right] + \frac{\partial \mathbf{P}(\boldsymbol{\omega})}{\partial \boldsymbol{\omega}} \boldsymbol{\omega} + \mathbf{P}(\boldsymbol{\omega}).$$

Due to the local convergence of Newton's method, an appropriate initial guess is obtained by solving the problem with zero initials for both velocity and temperature, which corresponds to a constant viscosity and accordingly a linear problem. Then the resulting approximation is used as an initial guess for Newton's method.

Below are some important physical constants and notations used in the sequel. The product of the friction factor f and the Reynolds number Re is given as

$$f\text{Re} = \frac{2L^2}{(1 + L)^2 \omega_m}$$

and the average Nusselt number Nu is

$$\text{Nu} = -\frac{L^2}{(1 + L)^2 T_m},$$

where

$$T_m = \frac{1}{L \omega_m} \int_{\Omega} \omega T d\Omega$$

is the mean fluid temperature and L is the aspect ratio.

3.4 FEM Applications to Power-Law Fluid Flow and Heat Transfer

The solutions of the power-law fluid flow and heat transfer equations are investigated by the FEM for the velocity magnitude and the temperature, previously introduced in Section 2.3, as follows:

$$\frac{\partial}{\partial x} \left(\bar{\mu} \frac{\partial \omega}{\partial x} \right) + \frac{\partial}{\partial y} \left(\bar{\mu} \frac{\partial \omega}{\partial y} \right) = -1 + \text{Ha}^2 \omega \quad (3.24)$$

and

$$\nabla^2 T + \text{Br} \bar{\mu} \left[\left(\frac{\partial \omega}{\partial x} \right)^2 + \left(\frac{\partial \omega}{\partial y} \right)^2 \right] + \text{Ha}^2 \text{Br} \omega^2 = \frac{4\omega}{\omega_m} \quad (3.25)$$

with the boundary conditions

$$\omega = 0 \quad \text{on} \quad \partial\Omega$$

and

$$\frac{\partial T}{\partial y} \Big|_{(x,b/a)} = \frac{\partial T}{\partial x} \Big|_{(1,y)} = 1, \quad \frac{\partial T}{\partial y} \Big|_{(x,0)} = \frac{\partial T}{\partial x} \Big|_{(0,y)} = -1$$

where

$$\bar{\mu} = \left(\sqrt{\left(\frac{\partial \omega}{\partial x} \right)^2 + \left(\frac{\partial \omega}{\partial y} \right)^2} \right)^{n-1}.$$

As a first attempt for deriving finite element equations, the weak form of the dimensionless system of equations (3.24)–(3.25) is reconstructed. Multiplying (3.24) and (3.25) by the test functions v and q , respectively, and integrating over the domain Ω , it is obtained that

$$\int_{\Omega} \bar{\mu} \nabla \omega \cdot \nabla v \, d\Omega - \int_{\partial\Omega} (\bar{\mu} \nabla \omega \cdot \hat{n}) v \, dS + \int_{\Omega} (-1 + \text{Ha}^2 \omega) v \, d\Omega = 0,$$

and

$$\begin{aligned} \int_{\Omega} \nabla T \cdot \nabla q \, d\Omega - \int_{\partial\Omega} (\nabla T \cdot \hat{n}) q \, dS - \int_{\Omega} \text{Br} \bar{\mu} \left[\left(\frac{\partial \omega}{\partial x} \right)^2 + \left(\frac{\partial \omega}{\partial y} \right)^2 \right] q \, d\Omega \\ - \int_{\Omega} (\text{Ha}^2 \text{Br}) \omega^2 q \, d\Omega + \int_{\Omega} \frac{4\omega}{\omega_m} q \, d\Omega = 0, \end{aligned}$$

where $\hat{n} = (n_1, n_2)$ is the unit normal vector pointing out of $\partial\Omega$. Hence, the variational formulation of the problem (3.24)–(3.25) yields: find $(\omega, T) \in H_0^1(\Omega) \times H^1(\Omega)$

such that

$$\langle \bar{\mu} \nabla \omega, \nabla v \rangle_{\Omega} + \langle -1 + \text{Ha}^2 \omega, v \rangle_{\Omega} = 0, \quad v \in H_0^1(\Omega), \quad (3.26)$$

$$\begin{aligned} & \langle \nabla T, \nabla q \rangle_{\Omega} - \langle 1, q \rangle_{\partial\Omega} - \left\langle \text{Br} \bar{\mu} \left[\left(\frac{\partial \omega}{\partial x} \right)^2 + \left(\frac{\partial \omega}{\partial y} \right)^2 \right], q \right\rangle_{\Omega} \\ & - (\text{Ha}^2 \text{Br}) \langle \omega^2, q \rangle_{\Omega} + \left\langle \frac{4\omega}{\omega_m}, q \right\rangle_{\Omega} = 0, \quad q \in H^1(\Omega). \end{aligned} \quad (3.27)$$

Here, the Neumann boundary condition of the temperature is weakly imposed. Next, the finite-dimensional approximations for the governing equations are introduced by employing the quadratic and linear finite elements for velocity and temperature, respectively. Let \mathcal{K}_h be a triangulation of Ω with size $h > 0$ and let $V_{h,0}$ and Q_h be the space of quadratic and linear polynomials on \mathcal{K}_h and $V_{h,0} \subset H_0^1(\Omega)$, $Q_h \subset H^1(\Omega)$. Replacing $H_0^1(\Omega)$ with β_{ω} -dimensional $V_{h,0}$ and $H^1(\Omega)$ with β_T -dimensional Q_h in the variational formulation, respectively, we obtain the following finite element formulation: find $(\omega, T) \in V_{h,0} \times Q_h$ such that

$$\begin{aligned} & \langle \bar{\mu} \nabla \omega, \nabla v \rangle_{\Omega} + \langle -1 + \text{Ha}^2 \omega, v \rangle_{\Omega} = 0, \quad v \in V_{h,0}(\Omega), \\ & \langle \nabla T, \nabla q \rangle_{\Omega} - \langle 1, q \rangle_{\partial\Omega} - \left\langle \text{Br} \bar{\mu} \left[\left(\frac{\partial \omega}{\partial x} \right)^2 + \left(\frac{\partial \omega}{\partial y} \right)^2 \right], q \right\rangle_{\Omega} \\ & - (\text{Ha}^2 \text{Br}) \langle \omega^2, q \rangle_{\Omega} + \left\langle \frac{4\omega}{\omega_m}, q \right\rangle_{\Omega} = 0, \quad q \in Q_h(\Omega). \end{aligned}$$

Within this formulation, given the bases $\{\phi_i\}_{i=1}^{\beta_{\omega}}$ and $\{\psi_k\}_{k=1}^{\beta_T}$ for $V_{h,0}$ and Q_h , respectively, we can express ω and T as

$$\omega = \sum_{j=1}^{\beta_{\omega}} \omega_j \phi_j \quad \text{and} \quad T = \sum_{l=1}^{\beta_T} T_l \psi_l,$$

where ω_j and T_l are the components of the vectors $\boldsymbol{\omega}$ and \mathbf{T} . The similar approximations in Section 3.3 are not repeated here; however, it should be noted that the basis functions ϕ_i and ψ_k are quadratic and linear, respectively, in this problem. Accordingly, the approximation of the variable viscosity is introduced as

$$\bar{\mu} = \left[\left(\frac{\partial \omega}{\partial x} \right)^2 + \left(\frac{\partial \omega}{\partial y} \right)^2 \right]^{\frac{n-1}{2}} \approx \left(\sum_{j=1}^{\beta_{\omega}} \omega_j^2 [(\phi_j)_x + (\phi_j)_y] \right)^{\frac{n-1}{2}}.$$

Besides, the vector $\mathbf{e} = (e_k)$ and the entries of the non-linear stiffness matrix

$\mathbf{K}(\omega)$ are proposed as

$$e_k = \int_{\partial\Omega} \psi_k dS, \quad 1 \leq k \leq \beta_T,$$

$$\mathbf{K}(\omega)_{ij} = \int_{\Omega} \left(\sum_{k=1}^{\beta_{\omega}} \omega_k^2 [(\phi_k)_x + (\phi_k)_y] \right)^{\frac{n-1}{2}} \nabla \phi_j \nabla \phi_i d\Omega.$$

Due to the form of (3.24), the velocity solution can be obtained separately from the temperature since it is not coupled with (3.25). Thus, the algebraic form of the discrete problem for the velocity reads:

$$\mathbf{K}(\omega)\omega + \text{Ha}^2 \mathbf{M}\omega = \mathbf{d};$$

and the resulting non-linear system of equations can then be represented as

$$\mathbf{F}(\omega) = \mathbf{K}(\omega)\omega + \text{Ha}^2 \mathbf{M}\omega - \mathbf{d} = 0.$$

This can be solved using Newton's method by following a *discretize-then-linearize* approach. Same as before, we solve a linear problem considering a constant viscosity to obtain a proper suitable initial guess. The Newton formula given in (3.15) is implemented with the Jacobian

$$\mathcal{J}(\omega) = \frac{\partial \mathbf{F}}{\partial \omega} = \frac{\partial \mathbf{K}(\omega)}{\partial \omega} \omega + \mathbf{K}(\omega) + \text{Ha}^2 \mathbf{M}$$

of the non-linear velocity equation. Accordingly, with the known velocity profile, temperature equation folds into a linear one:

$$\mathbf{S}\mathbf{T} = \mathbf{f} + \mathbf{e},$$

or, equivalently,

$$\mathbf{G}(\mathbf{T}) = \mathbf{S}\mathbf{T} - (\mathbf{f} + \mathbf{e}) = 0,$$

where the vector $\mathbf{f} = (f_k)$ has the components

$$f_k = \int_{\Omega} \text{Br} \bar{\mu} \left[\left(\frac{\partial \omega}{\partial x} \right)^2 + \left(\frac{\partial \omega}{\partial y} \right)^2 \right] \psi_k d\Omega + \int_{\Omega} (\text{Ha}^2 \text{Br}) \omega^2 \psi_k d\Omega - \int_{\Omega} \frac{4\omega}{\omega_m} \psi_k d\Omega,$$

for $1 \leq k \leq \beta_T$. Although equations are solved in a decoupled way, the discrete problem can be reformulated as a system of equations in the form of $\mathbf{C}(\mathbf{z}) = 0$, where

$\mathbf{z} = (\boldsymbol{\omega}, \mathbf{T})$ to be used as the discretized PDE constraints in the control problem as follows:

$$\mathbf{C}(\mathbf{z}) := \begin{bmatrix} \mathbf{F}(\boldsymbol{\omega}) \\ \mathbf{G}(\mathbf{T}) \end{bmatrix} = 0.$$

Below are some important physical constants and notations to be used in the sequel. The term $f\text{Re}$ defines the product of the fanning friction factor f and the Reynolds number Re [89],

$$f\text{Re} = \frac{(2L)^n}{(1+L)^{n+1}\omega_m^n},$$

which depends also on the flow index parameter n in this case, unlike the case before. Likewise, the average Nusselt number is defined to be

$$\text{Nu} = \frac{2L}{(1+L)(T_{\omega_m} - T_m)},$$

where T_m is the mean fluid temperature given in (2.35) and T_{ω_m} is

$$T_{\omega_m} = \frac{2}{1+L} \int_0^1 T(x, 0) dx + \frac{1}{2} \int_0^L T(0, y) dy.$$

3.5 Numerical Results

In this section, FEM solutions to steady, two-dimensional, laminar flow problems of incompressible Newtonian and non-Newtonian fluids in a square duct are presented. Firstly, simulations are performed for a benchmark problem, Navier-Stokes equations, with an exact solution given in Section 3.5.1 to ensure the efficiency of approaches in this study. Secondly, in Section 3.5.2 the solution of the MHD flow and heat transfer equations with temperature dependent viscosity is presented. The MHD flow contains the viscous and Joule dissipations; and the Hall effect is taken into consideration as well. The coupled non-linear equations are solved by Newton's method using quadratic elements. Finally, the solution of the power-law fluid flow and heat transfer, where the fluid may become non-Newtonian according to the value of the flow index, is presented in Section 3.5.3. Since the non-linear momentum equation does not depend on the temperature in this problem, its solution is obtained by the Newton method using quadratic elements, and thereby, the resulting velocity magnitude is used for the solution of the linear temperature equation with the help of linear elements.

Besides, the linear system of equations in each iteration is solved, particularly, by standard LU decomposition. Computer simulations are executed on a platform with Intel Core i7-4770 processor and 15.6 GB RAM using Python programming language with a computing platform FEniCS [66] for solving PDEs. Python codes used for all simulations in this thesis are basically sampled in Appendix A.2.

3.5.1 Navier-Stokes Equation with Exact Solutions

The Navier-Stokes equations which consist of the momentum and the continuity equation are solved by Newton's method using a mixed FEM. The velocity and the pressure are obtained on a unit square $[0, 1] \times [0, 1]$ for an incompressible flow. In order to ensure the stability and convergence, Ladyzhenskaja-Babuska-Brezzi (LBB) condition [76], or also known as compatibility condition, is satisfied by choosing the Taylor-Hood element pair (P2-P1) for the velocity and the pressure, respectively. In order to verify the accuracy of the FEM procedure, a test problem is studied with the following functions

$$\begin{aligned}\vec{v} &= \exp(-0.5\nu) \begin{pmatrix} \sin^2(\pi x) \sin(\pi y) \cos(\pi y) \\ -\sin^2(\pi y) \sin(\pi x) \cos(\pi x) \end{pmatrix} \\ p &= \exp(-0.5\nu) \cos(\pi x) \sin(\pi y)\end{aligned}$$

from which the homogeneous Dirichlet type boundary condition of the velocity is obtained and the force function f is derived by substitution this exact solution into (3.6). The convergence of solutions is tested for decreasing maximum cell diameter (h_{\max}) as given in Table 3.1. The results in Table 3.1 show that the difference between the exact and FEM solution is decreasing as h decreases, which validates the accuracy of the method. The convergence rates for the FEM solutions of the velocity and the pressure are also attained at optimal orders, namely, they are three and two for P2 and P1 elements, respectively. Numerical solutions for various values of ν are depicted in Figure 3.3, where we consider a uniform mesh consisting of 1089 vertices and 2048 triangular elements with 8450 and 1089 nodes respectively for quadratic and linear finite element spaces for velocity and pressure.

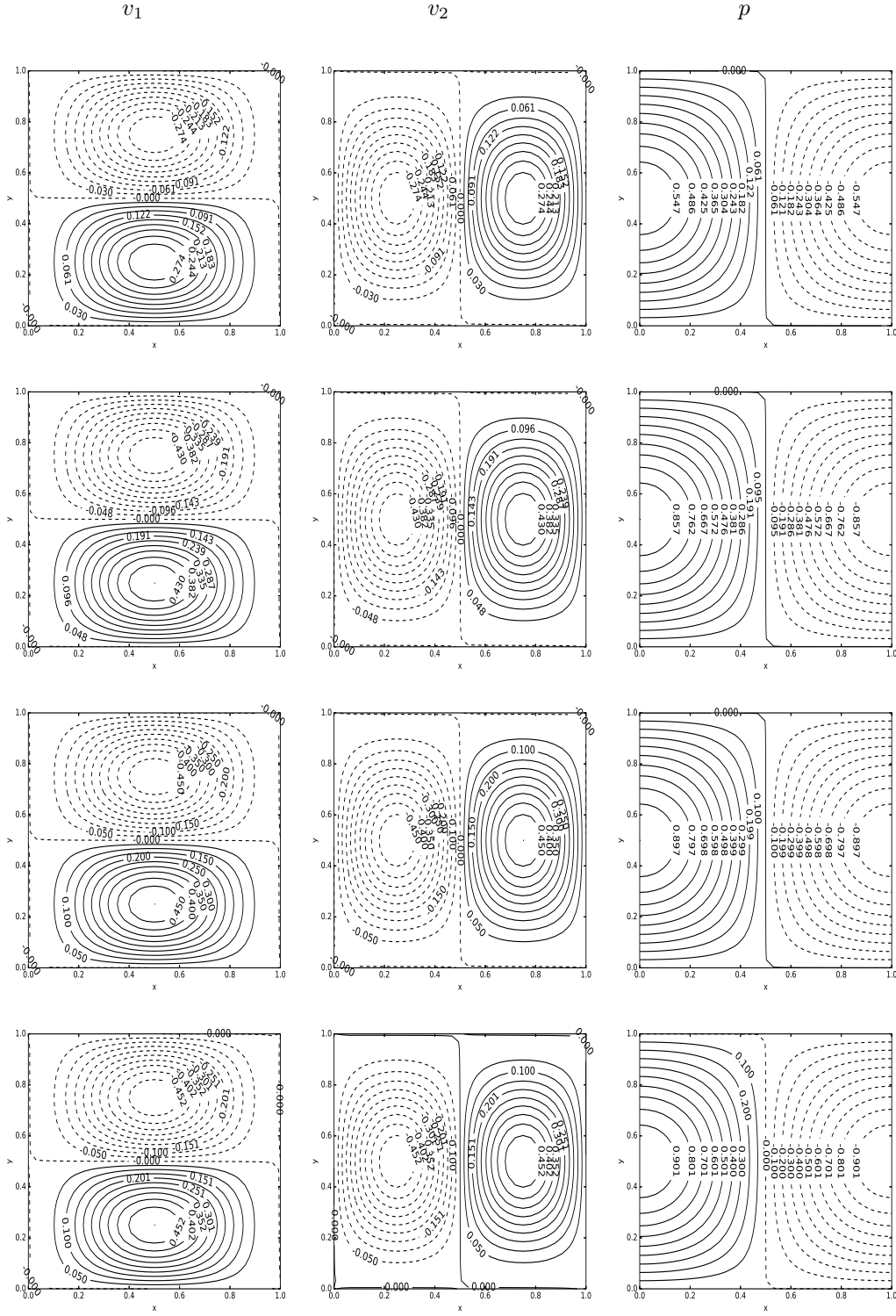


Figure 3.3: Solutions v_1, v_2 and p of the Navier-Stokes equation, row 1: $\nu = 1$, row 2: $\nu = 10^{-1}$, row 3: $\nu = 10^{-2}$, row 4: $\nu = 10^{-3}$.

Table 3.1: L^2 Errors and convergence rates for $\nu = 0.1$

h_{\max}	v_1	rate	v_2	rate	p	rate
7.0710×10^{-1}	7.1345×10^{-2}	-	7.1994×10^{-2}	-	1.2367×10^{-1}	-
3.5355×10^{-1}	1.1739×10^{-2}	2.6035	1.1532×10^{-2}	2.6423	2.8548×10^{-2}	2.1151
1.7678×10^{-1}	1.2644×10^{-3}	3.2148	1.2597×10^{-3}	3.1945	6.3510×10^{-3}	2.1683
8.8388×10^{-2}	1.4741×10^{-4}	3.1006	1.4727×10^{-4}	3.0965	1.5421×10^{-3}	2.0421
4.4194×10^{-2}	1.8055×10^{-5}	3.0293	1.8051×10^{-5}	3.0283	3.8288×10^{-4}	2.0100
2.2097×10^{-2}	2.2451×10^{-6}	3.0075	2.2450×10^{-6}	3.0073	9.5557×10^{-5}	2.0025
1.1049×10^{-2}	2.8028×10^{-7}	3.0019	2.8028×10^{-7}	3.0018	2.3879×10^{-5}	2.0006

3.5.2 The MHD Flows and Heat Transfer with Temperature Dependent Viscosity and Hall Effect

The MHD flow equations containing viscous and Joule dissipations in which the Hall effect is taken into account are solved together with the energy equation by using a mixed FEM. The pipe axis velocity and the temperature are obtained in the square cross-section of the pipe $[0, 1] \times [0, 1]$ for the hydrodynamically and thermally fully developed flow. At each simulation, Newton's method for the solution of the coupled non-linear equations (3.16)–(3.17) is initialized by solving the problem for a constant viscosity with zero initials for both velocity and temperature. Considering the small velocity magnitude in the problem, Newton's iterations are performed until not only the absolute error becomes below 10^{-10} but also the relative error falls below 10^{-9} .

A quadratic finite element method on a uniform mesh, consisting of 2601 vertices and 5000 triangular elements, is used with the 10201 nodes for each subspace of the mixed finite element space. The number of unknowns is pre-determined according to the mesh dependence convergence test results given in Figure 3.4(a) providing an accuracy about 10^{-6} . The time costs for the finite element solutions are tested for increasing degrees of freedom (Dofs) and depicted Figure 3.4(b).

The following results are obtained for various values of the Hartmann number, $0 \leq \text{Ha} \leq 10$; viscosity parameter, $B = 0, 1, 2$; Brinkman number $\text{Br} = 0, 1$; and the Hall parameter, $m = 0, 3, 8$.

Figure 3.5 shows the velocity behavior for increasing values of Ha . It can be seen that as Ha increases the velocity magnitude drops, verifying the well-known flattening

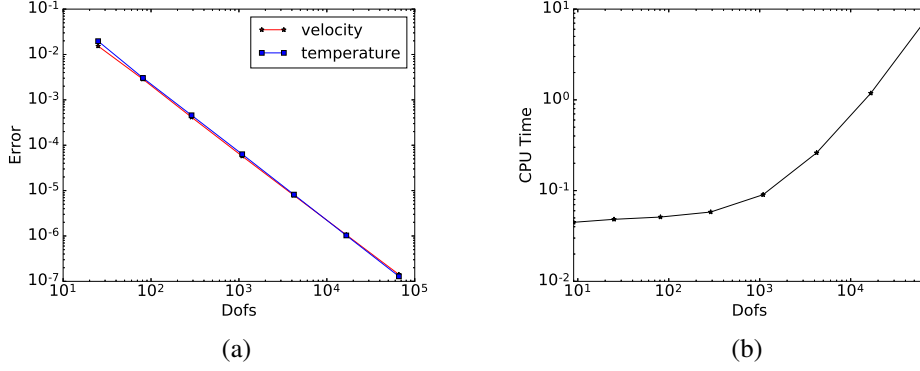
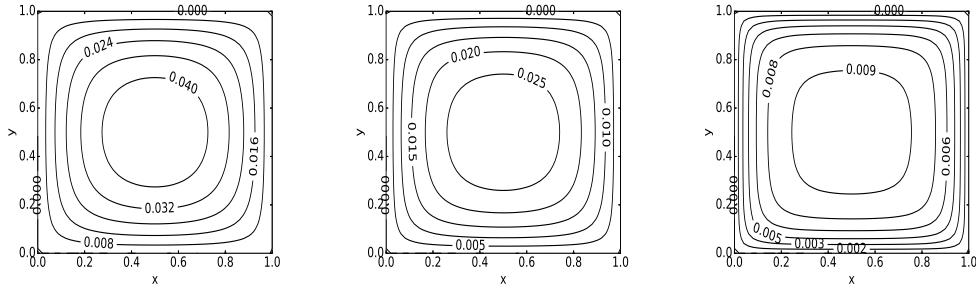


Figure 3.4: Error and CPU time analysis of FEM solutions with increasing number of degrees of freedom (Dofs) for $Ha = 1.0$, $m = 1.0$, $Br = 1.0$, $B = 1.0$.

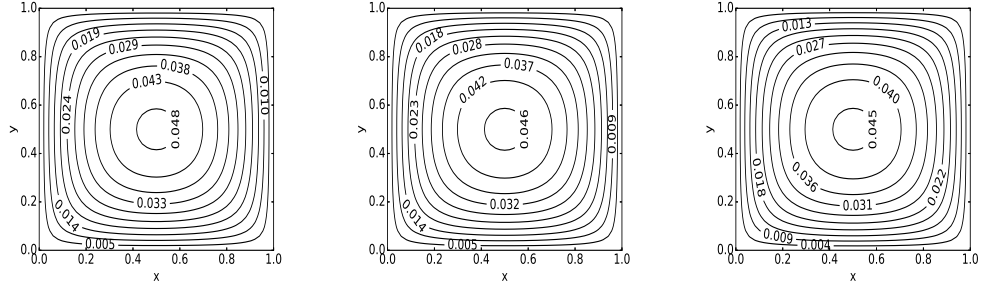


$Ha = 3, \max \omega = 0.04715$ $Ha = 5, \max \omega = 0.02913$ $Ha = 10, \max \omega = 0.00971$

Figure 3.5: Velocity contours for $m = 0$, $Br = 0$, $B = 1$ and for increasing values of Ha .

tendency of the MHD flow or the damping effect of external magnetic field with increasing intensity [22]. Same behavior for the velocity is also observed when the viscosity parameter B is increased, since the viscosity of the fluid is incremented due to the exponential variation of $-BT$ (see Figure 3.6).

One can deduce that increasing the Hall parameter m increases the magnitude of the axis velocity ω : Figure 3.7 and Figure 3.8 show such an increase for $Br = 0$ and for $Br = 1$, respectively. This is due to the fact that an increase in the Hall parameter reduces the effective conductivity $\frac{\sigma}{1+m^2}$ of the fluid and decreases the damping effect of the magnetic force. As can be seen from the temperature equation (2.19), nonzero values of the Brinkman number Br introduce the non-linear terms of the axis velocity due to the constant variation dT_m/dz . Thus, the inclusion of these effects with $Br = 1$ slightly increases the velocity magnitude for all values of m , shown as $\max \omega = 0.04715$ in Figure 3.7 and $\max \omega = 0.04718$ in Figure 3.8 for $m = 0$.

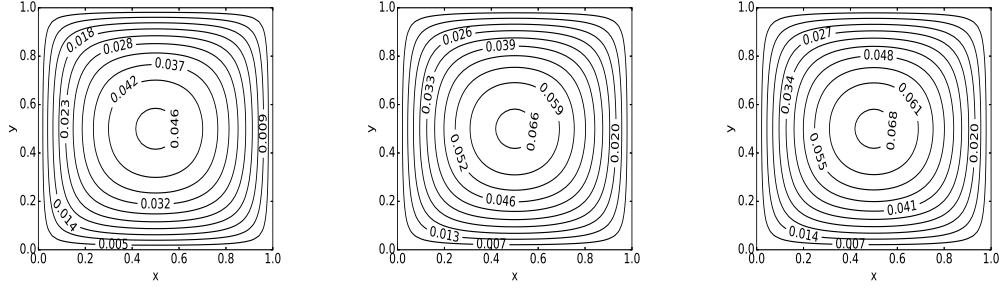


$B = 0, \max \omega = 0.04875$

$B = 1, \max \omega = 0.04715$

$B = 2, \max \omega = 0.04568$

Figure 3.6: Velocity contours for $\text{Ha} = 3$, $\text{Br} = 0$, $m = 0$ and for increasing values of B .

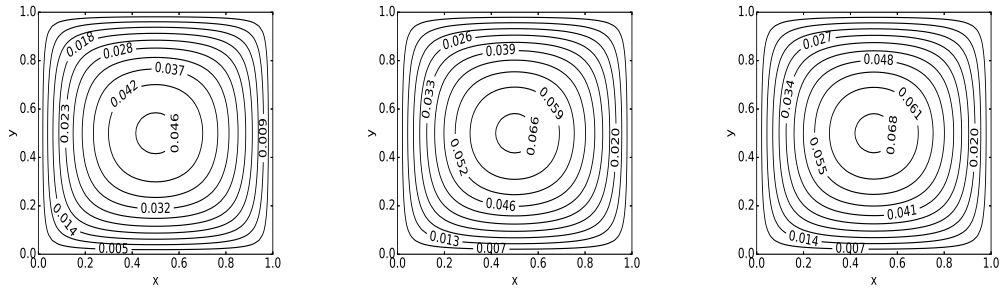


$m = 0, \max \omega = 0.04715$

$m = 3, \max \omega = 0.06696$

$m = 8, \max \omega = 0.06964$

Figure 3.7: Velocity contours for $\text{Ha} = 3$, $\text{Br} = 0$, $B = 1$ and for increasing values of m .

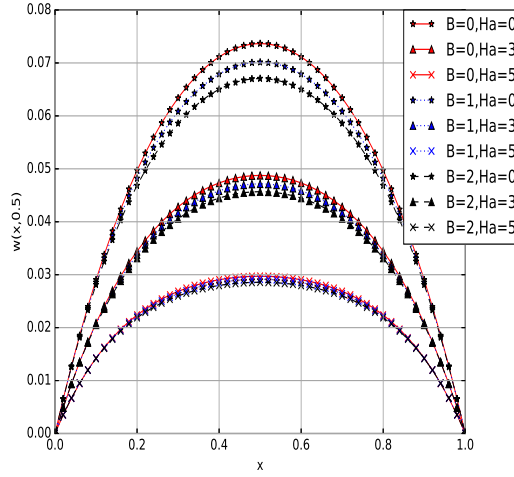


$m = 0, \max \omega = 0.04718$

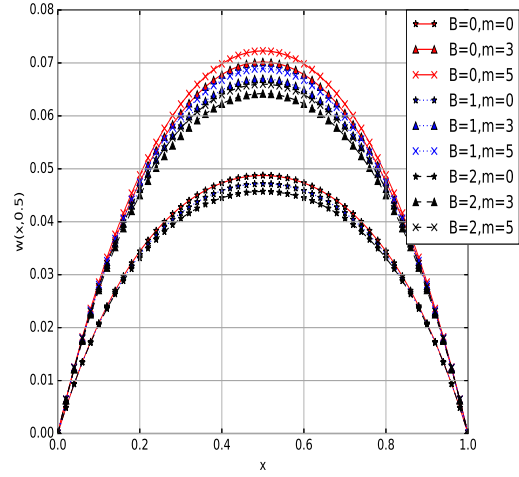
$m = 3, \max \omega = 0.06701$

$m = 8, \max \omega = 0.06969$

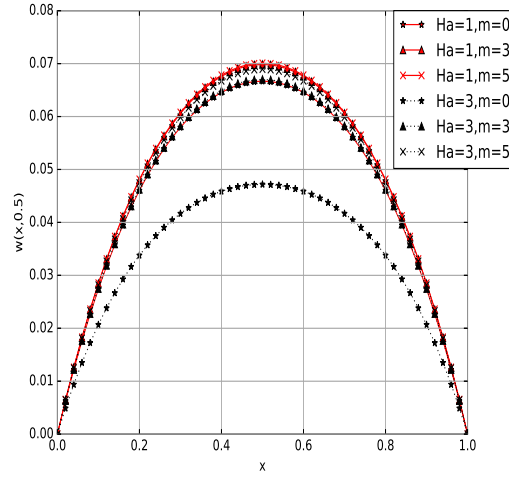
Figure 3.8: Velocity contours for $\text{Ha} = 3$, $\text{Br} = 1$, $B = 1$ and for increasing values of m .



(a) $m = 0$ and $Br = 0$



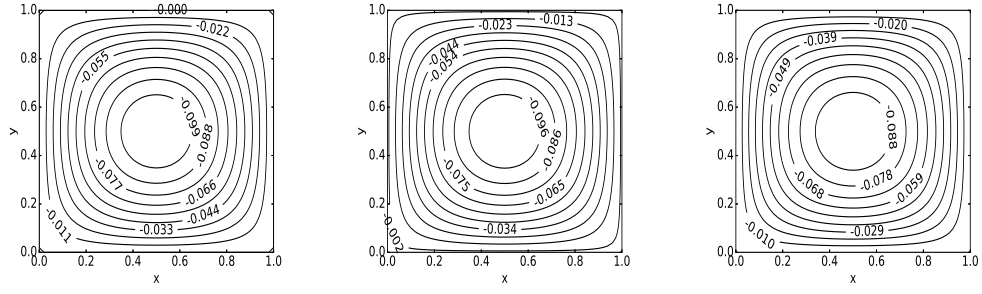
(b) $Ha = 3$ and $Br = 1$



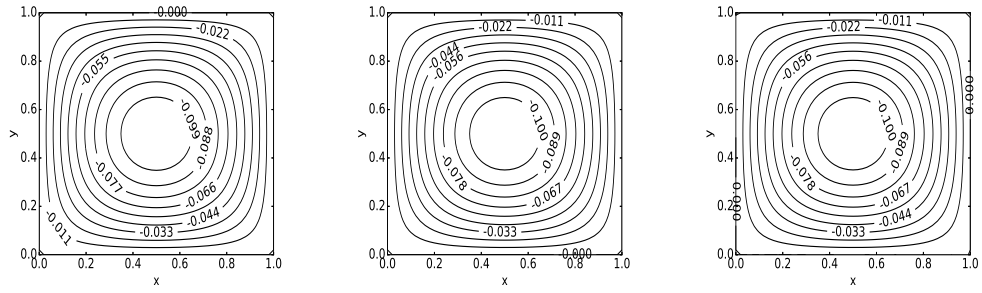
(c) $B = 1$ and $Br = 1$

Figure 3.9: Velocity profiles along the midline of the square duct.

Figure 3.9(a) depicts the variation of midline velocity $\omega(x, 0.5)$ for increasing B and Ha values when $m = 0$ and $Br = 0$. It is clearly seen that the increase in Ha or B drops the midline velocity magnitude as it was observed in the whole contour behaviors of ω in Figure 3.9(a). This increase of B decreases ω for all values of m ; and the influence of B on ω is more seen for larger values of m . Figure 3.9(b) and Figure 3.9(c) show again the midline velocity $\omega(x, 0.5)$ for increasing B and m when $Ha = 3$ and $Br = 1$ while increasing Ha and m when $B = Br = 1$. In both cases, the increase of m overwhelms the drop of the velocity with the increase in Ha or B .



Ha = 3, $\min T = -0.10976$ Ha = 5, $\min T = -0.10682$ Ha = 10, $\min T = -0.0978$
Figure 3.10: Isolines for $m = 0$, $Br = 0$, $B = 1$ and for increasing values of Ha .

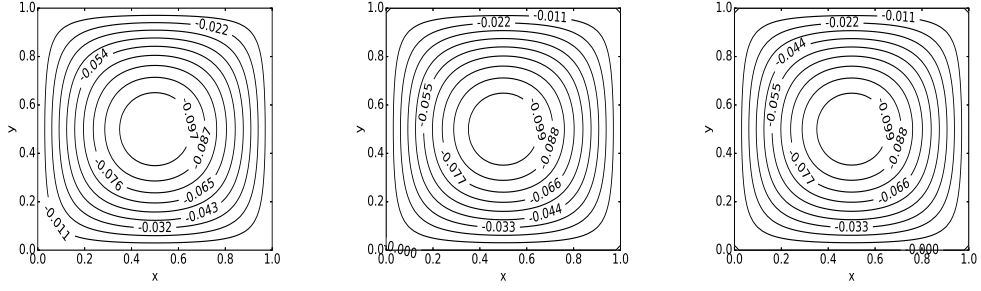


$m = 0$, $\min T = -0.10976$ $m = 3$, $\min T = -0.11111$ $m = 8$, $\min T = -0.11121$
Figure 3.11: Isolines for $Ha = 3$, $Br = 0$, $B = 1$ and for increasing values of m .

Meanwhile, the temperature attains negative values inside the cavity, dropping to zero on the insulated walls. As Ha increases temperature increases through the center of the cavity, since the fluid tends to be stagnate at the center. This can be seen from equal temperature contours (isolines) in Figure 3.10 for various values of Ha . Increasing m decreases isoline values due to the reduction in the effective conductivity, which reduces the Joule dissipation when both $Br = 0$ and $Br = 1$ in Figure 3.11 and Figure 3.12. When the viscosity parameter B increases, temperature increases as a result of increasing the viscosity; and consequently, the viscous dissipation increases as depicted in Figure 3.13. Furthermore, in Figure 3.14 and Figure 3.15, a slight increase is observed in temperature for all values of m when $Br = 0$ is changed to $Br = 1$ as is in the pipe-axis velocity.

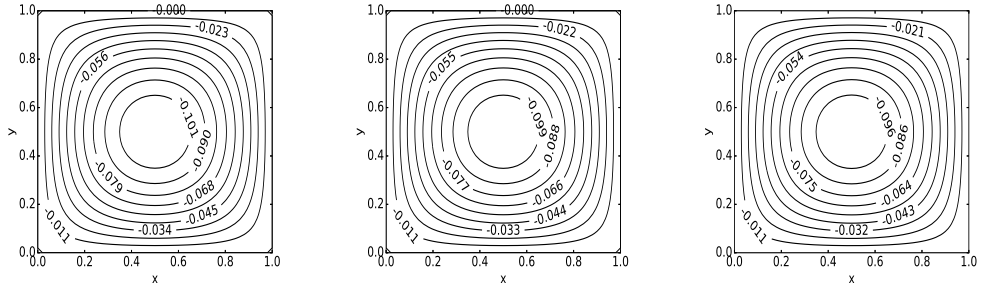
Table 3.2 and Table 3.6 show the effects of both viscosity parameter B and Hartman number Ha on fRe and the average Nusselt number Nu when $m = 0$ and $Br = 0$. Both fRe and Nu increase as B increases; and also, as Ha increases due to the increase in viscous dissipation and strong magnetic field, respectively.

On the other hand, Table 3.4 and Table 3.5 demonstrate the effect of increase in m on



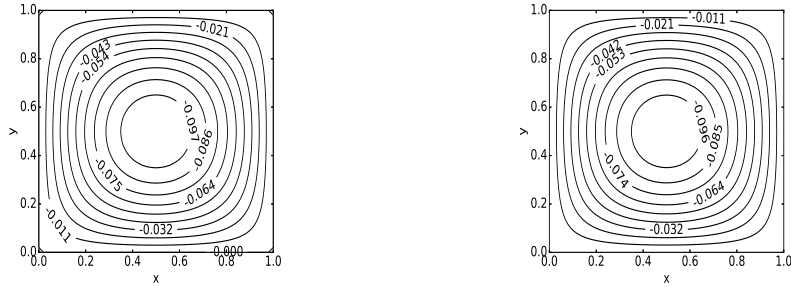
$m = 0, \min T = -0.10829$ $m = 3, \min T = -0.10984$ $m = 8, \min T = -0.11000$

Figure 3.12: Isolines for $Ha = 3$, $Br = 1$, $B = 1$ and for increasing values of m .



$B = 0, \min T = -0.11259$ $B = 1, \min T = -0.10976$ $B = 2, \min T = -0.10713$

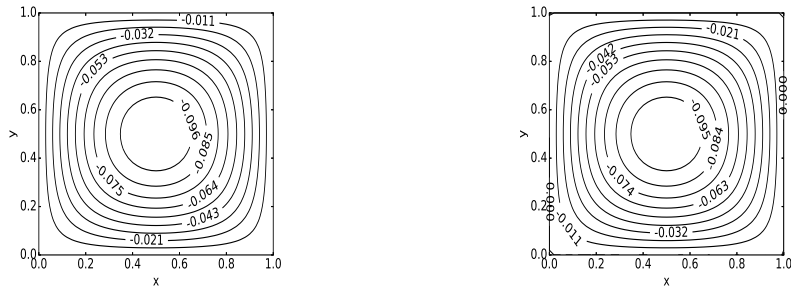
Figure 3.13: Isolines for $Ha = 3$, $Br = 0$, $m = 0$ and for increasing values of B .



$Br = 0, \min T = -0.10744$

$Br = 1, \min T = -0.10620$

Figure 3.14: Isolines for $Ha = 5$, $B = 2$, $m = 3$.



$Br = 0, \min T = -0.10679$

$Br = 1, \min T = -0.10543$

Figure 3.15: Isolines for $Ha = 5$, $B = 2$, $m = 1$.

Table 3.2: The effect of the viscosity parameter B and Ha on Nu ($m = 0$, $Br = 0$).

B / Ha	0.0	1.0	2.0	3.0	4.0	5.0
0.0	3.6079	3.6232	3.6678	3.7375	3.8269	3.9297
1.0	3.7582	3.7665	3.7932	3.8411	3.9095	3.9946
2.0	3.9042	3.9042	3.9149	3.9427	3.9915	4.0597

Table 3.3: The effect of the viscosity parameter B and Ha on fRe ($m = 0$, $Br = 0$)

B / Ha	0.0	1.0	2.0	3.0	4.0	5.0
0.0	14.2270	14.9150	16.9646	20.3368	24.9783	30.8325
1.0	14.6620	15.3442	17.3773	20.7253	25.3387	31.1643
2.0	15.0748	15.7531	17.7747	21.1042	25.6944	31.4952

Nu and fRe , respectively, for increasing values of Hartmann number when $Br = 0$ and $B = 1$. As m increases, fRe decreases; Nusselt number Nu also decreases due to the reduction in the effective conductivity, which reduces the Joule dissipation.

While Ahmed and Attia [81] investigated this problem by using finite difference method for solving temperature and velocity equations iteratively, here in this thesis, finite element solutions are provided, which are more reliable and fast, within a mixed formulation of the velocity and temperature equations. Furthermore, the physical quantities such as fRe and Nu obtained in the thesis show similar behaviors with the ones given in [81]. Also, although their numerical results are limited to some range of parameters such as $0 \leq Ha \leq 3$, the results are extended to $0 \leq Ha \leq 10$. However, even for larger Hartman values solutions by FEM are easily attainable; they are not reported here due to small velocity magnitude. Therefore, this thesis extends the results of [81] in terms of both the underlying method and the ranges of the considered parameters besides the accuracy obtained.

Table 3.4: The effect of the Hall parameter m and Ha on Nu ($Br = 0$, $B = 1$)

m / Ha	0.0	1.0	2.0	3.0	4.0	5.0
0.0	3.7582	3.7665	3.7932	3.8411	3.9095	3.9946
3.0	3.7582	3.7590	3.7615	3.7656	3.7716	3.7796
5.0	3.7582	3.7585	3.7594	3.7610	3.7633	3.7662
8.0	3.7582	3.7583	3.7587	3.7593	3.7602	3.7613

Table 3.5: The effect of the Hall parameter m and Ha on fRe ($Br = 0$, $B = 1$)

m / Ha	0.0	1.0	2.0	3.0	4.0	5.0
0.0	14.6620	15.3642	17.3773	20.7253	25.3387	31.1643
3.0	14.6620	14.7303	14.9351	15.2760	15.7524	16.3632
5.0	14.6620	14.6883	14.7611	14.8984	15.0821	15.3180
8.0	14.6620	14.6725	14.7040	14.7566	14.8301	14.9246

3.5.3 Power-Law Fluid Flow and Heat Transfer

In this part of the section, solutions of the power-law fluid flow and heat transfer equations are obtained numerically by using FEM. Different from the previous methodology, velocity and energy equations are treated in a decoupled form. At each simulation, Newton's method for the solution of the non-linear momentum equation is initialized with a constant viscosity. Then, substituting this velocity, the temperature is found by solving the linear equation. Same as before, the pipe axis velocity and the temperature are obtained in the square cross-section $[0, 1] \times [0, 1]$ of the pipe and stopping tolerance is 10^{-10} for absolute error and 10^{-9} for the relative error.

In this problem, considering the non-linearity in the momentum equation and the linearity in the energy equation, P2-P1 (quadratic-linear) finite element pair is used for the velocity and temperature. A uniform mesh, consisting 4225 vertices and 8192 triangular elements, is used with 16641 and 4225 nodes for quadratic and linear finite element spaces, respectively. These are determined according to the mesh dependence convergence test results given in Figure 3.16(a) in order to provide an accuracy about 10^{-6} . Since the number of degrees of freedom is different for each finite element space, tests for the convergence and time costs are conducted for the maximum cell diameter (h), which is same for both spaces. Accordingly, the time costs for the finite element solutions are depicted in Figure 3.16(b). The results are obtained for various values of the Hartmann number ($0 \leq Ha \leq 10$), Brinkman number ($0 \leq Br \leq 2$), and the flow index ($\frac{1}{2} \leq n \leq 2$).

Figure 3.17 shows the velocity behavior for increasing values of the Hartmann number Ha for a fixed value of $n = 0.5$. As Ha increases boundary layers are formed: flow concentrates near the walls and the fluid becomes stagnant at the center of the duct. Flow behavior is also simulated for increasing values of Ha when $n = 1.5$ and

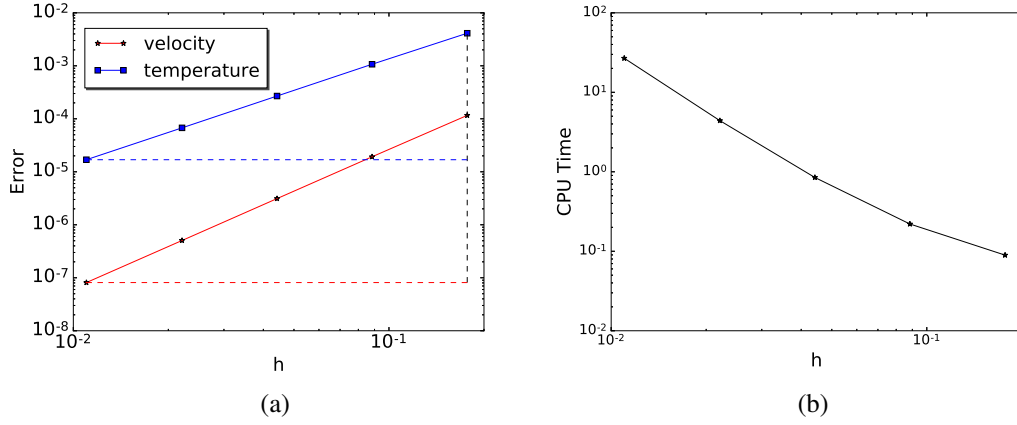


Figure 3.16: Error and CPU time of FEM solutions for $Ha = 1.0$, $n = 1.5$, $Br = 1.0$.

$n = 2.0$; see Figure 3.18 and Figure 3.19, respectively.

As the flow index n increases, in Figure 3.18, boundary layer formation occurs when Ha is increased, but for much smaller Ha when compared with the formation when $n = 0.5$. For $Ha \geq 30$ the duct is almost stagnant except a thin boundary layer with very small velocity magnitude there ($n = 1.5$). The increase in n causes an increase in the magnitude of the velocity; however, this is lost when Ha is also increased as it can be seen in Figure 3.19 for $n = 2.0$.

Meanwhile, Figure 3.20 depicts the variation of the midline velocity $\omega(x, 0.5)$ for increasing values of Ha for each fixed n . It is clear that as Ha increases the velocity magnitude drops for all values of n , verifying the well-known flattening tendency of the MHD flow in Figure 3.20. On the contrary, an increase in the flow index n results in an increase in the velocity and consequently, a peak at the center $x = 0.5$ occurs.

Furthermore, in Figure 3.21, velocity drop continues with an increase in Ha for all values of n . However, increase in the velocity is compensated by an increase in n for values of $Ha \geq 30$ and $n \geq 1$. The reason is that MHD equations become reaction dominated and this fact diminishes the effect of variable viscosity coefficient.

We also present the effects of the flow index and the Hartmann number on fRe in Table 3.6. It is clearly seen that as Ha increases fRe increases for any values of n ; however, the change of fRe is very small for $n = 0.5$. One can also deduce that as n decreases, fRe decreases for any values of Ha because of the fact that the viscosity decreases faster than the increase in the wall shear rate.

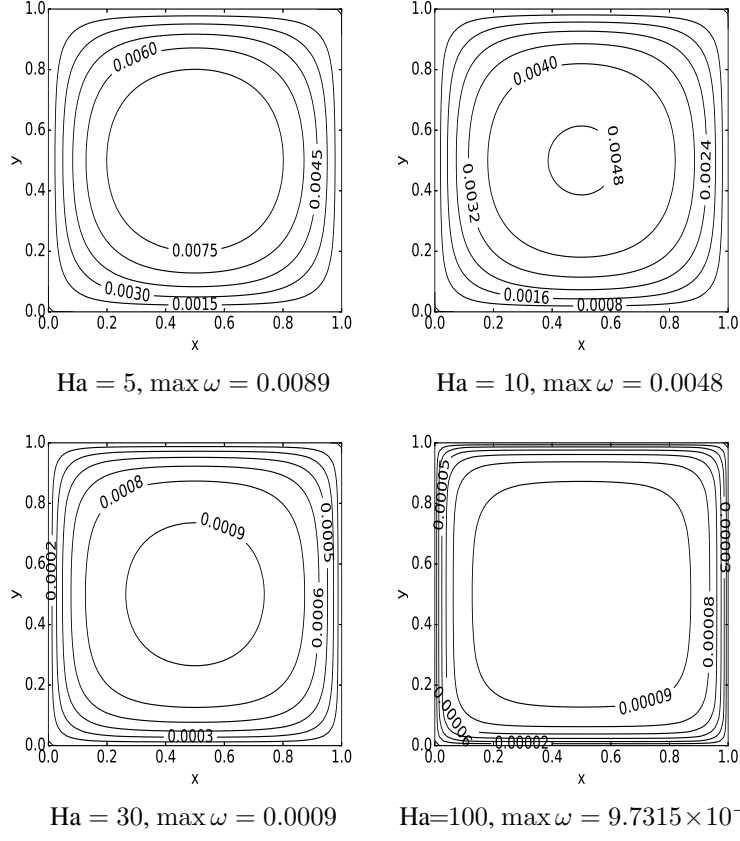


Figure 3.17: Velocity contours for $n = 0.5$ and increasing values of Ha .

Table 3.6: The effect of the parameter n and Ha on $f\text{Re}$

n / Ha	0.0	1.0	2.0	3.0	4.0	5.0	7.5	10.0
0.5	5.7214	5.7775	5.9394	6.1909	6.5126	6.8866	7.9672	9.1623
1.0	14.2270	14.9150	16.9646	20.3368	24.9783	30.8324	50.4572	76.8114
1.5	34.8609	37.8540	47.7100	66.8303	98.4061	145.5560	349.5695	711.2614
2.0	85.1464	95.0650	131.5440	217.5824	393.7651	709.7827	2522.4330	6846.6395

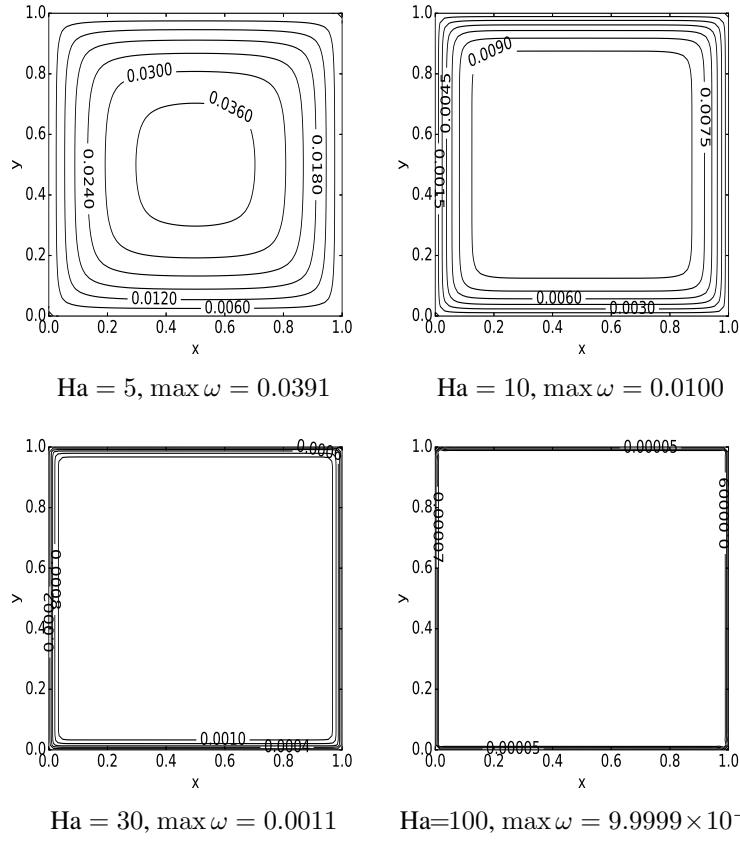


Figure 3.18: Velocity contours for $n = 1.5$ and increasing values of Ha .

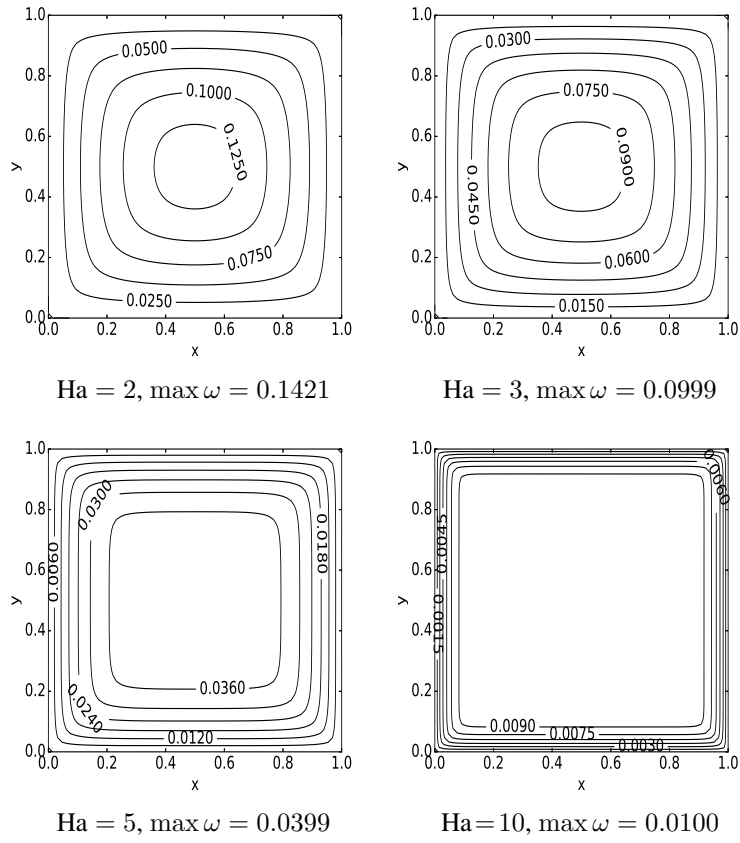


Figure 3.19: Velocity contours for $n = 2.0$ and increasing values of Ha .

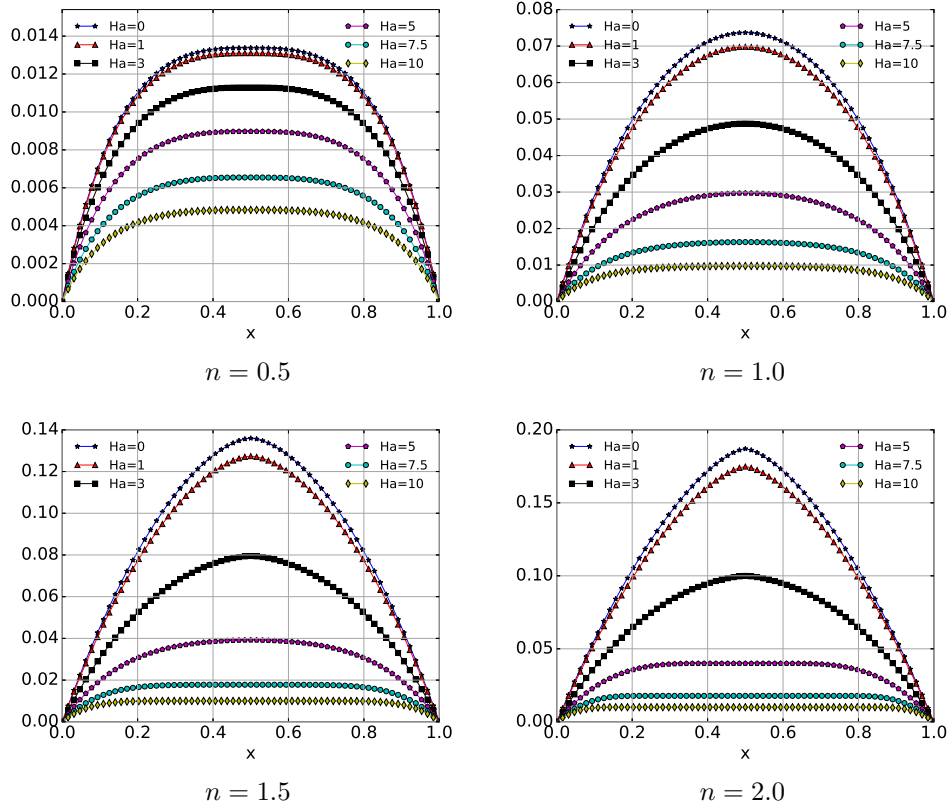


Figure 3.20: Midline velocity profiles for $Ha \leq 10$.

On the other hand, temperature attains positive values on the walls where we have assumed constant heat flux. As Ha increases temperature increases through the center of the cavity; this can be seen from the temperature contours (isolines) in Figure 3.22 for $Br = 1.0$. Increasing n also increases the values on the isolines as presented in Figure 3.23 for $n = 1.5$.

We also note that the constant heat flux condition $\frac{\partial T}{\partial \hat{n}} = 1$ on the duct walls yields symmetrical temperature isolines about the central lines $x = 0.5$ and $y = 0.5$. Heat circulates through the corner symmetrically with increasing values. Temperature variation can be visualized better when the vertical walls are changed to the insulated walls condition $\frac{\partial T}{\partial \hat{n}} = 0$. This time heat reaches positive maximum values on the upper and bottom walls symmetrically with respect to $y = 0.5$ line. Furthermore, if one of the walls, for instance $x = 1$, has the constant heat flux condition $\frac{\partial T}{\partial \hat{n}} = 1$ and the rest of the walls are insulated, then isolines become perpendicular to these insulated walls and temperature achieves its maximum near $x = 1$. These conditions as well as the behaviors of the isolines are depicted in Figure 3.24.

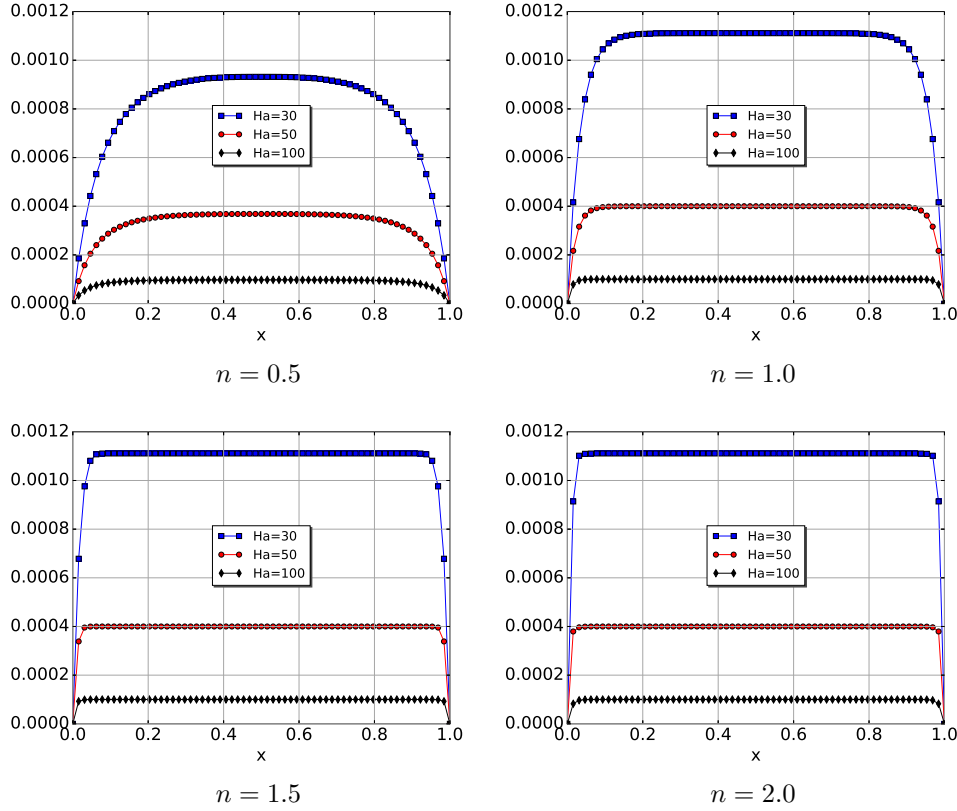


Figure 3.21: Midline velocity profiles for $Ha = 30, 50, 100$.

Meanwhile, another physical quantity Nu , which represents the dynamic on the temperature is investigated. Figure 3.25 presents the variation of the Nusselt number Nu with the Hartmann number Ha for $Br = 0$ and $Br = 2$. It indicates that as the flow index increases the average Nusselt number decreases for small values of Ha ($Ha \lesssim 3$). On the other hand, the effect is reversed for larger values of Ha ($Ha \gtrsim 5$) so that increasing n increases Nu . For Ha such that $3 \lesssim Ha \lesssim 5$ a transition is observed.

In Tables 3.7, 3.8 and 3.9, respectively for $n = 0.5$, $n = 1.0$, and $n = 1.5$, it is also observed that the effect of Brinkman number Br on Nu is non-uniform. The increment in the Brinkman number Br decreases the value of Nu for $n = 0.5$ for all values of Ha ; however, for $n = 1.0$ and $n = 1.5$ it increases the values of Nu for $Ha > 3$ and $Ha > 1$, respectively. It should also be noted that the effect of Br on Nu is almost invisible, when compared to the effects of other parameters on Nu .

Inspiring the work of Ahmed in [80], where he employed finite difference method for the numerical solution of this problem, solutions are enlarged with the finite element method in this study. In addition, the parameter ranges of the flow index as well as

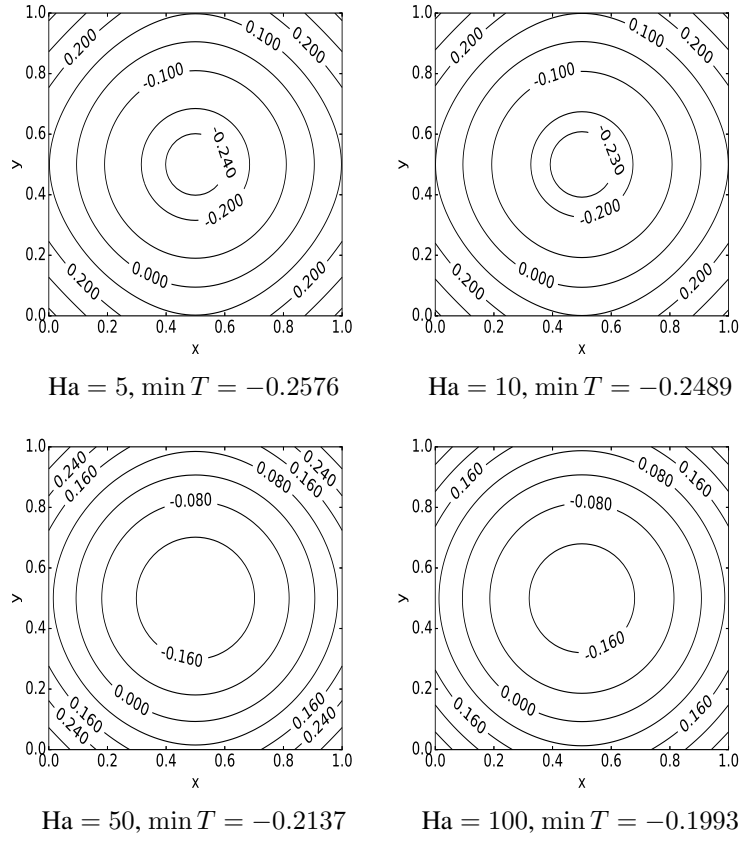


Figure 3.22: Isolines for $n = 0.5$ and increasing values of Ha .

Table 3.7: The effect of the parameter Br and Ha on Nu (when $n = 0.5$)

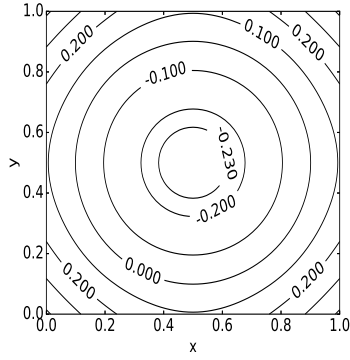
Br / Ha	0.0	1.0	2.0	3.0	4.0	5.0	7.5	10.0
0.0	3.3023	3.3060	3.3166	3.3329	3.3533	3.3765	3.4401	3.5054
1.0	3.3009	3.3047	3.3154	3.3319	3.3525	3.3759	3.4398	3.5053
2.0	3.2995	3.3033	3.3143	3.3309	3.3517	3.3752	3.4395	3.5052

Table 3.8: The effect of the parameter Br and Ha on Nu (when $n = 1.0$)

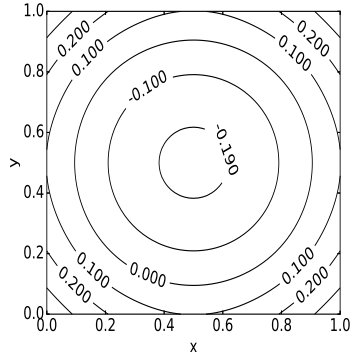
Br / Ha	0.0	1.0	2.0	3.0	4.0	5.0	7.5	10.0
0.0	3.0880	3.1006	3.1370	3.1941	3.2673	3.3515	3.5824	3.8080
1.0	3.0839	3.0972	3.1353	3.1939	3.2680	3.3527	3.5837	3.8090
2.0	3.0799	3.0939	3.1336	3.1937	3.2687	3.3538	3.5850	3.8100

Table 3.9: The effect of the parameter Br and Ha on Nu (when $n = 1.5$)

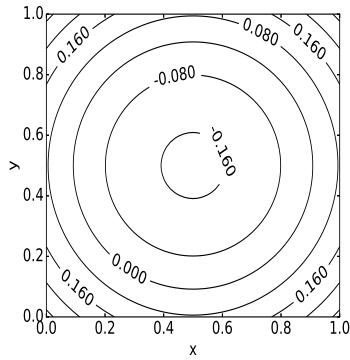
Br / Ha	0.0	1.0	2.0	3.0	4.0	5.0	7.5	10.0
0.0	3.0067	3.0239	3.0786	3.1766	3.3177	3.4894	3.9320	4.2905
1.0	3.0013	3.0204	3.0788	3.1794	3.3214	3.4929	3.9343	4.2919
2.0	2.9960	3.0169	3.0789	3.1822	3.3250	3.4964	3.9365	4.2933



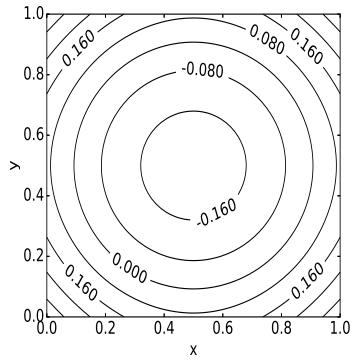
Ha = 5, $\min T = -0.2536$



Ha = 10, $\min T = -0.2075$

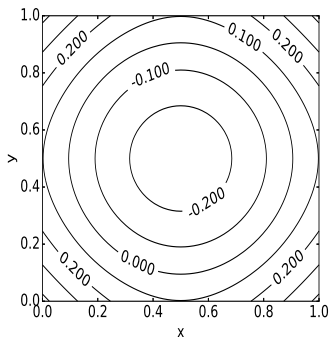


Ha = 50, $\min T = -0.1723$

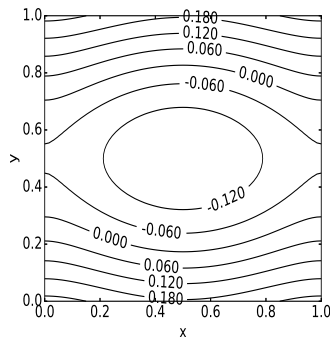


Ha = 100, $\min T = -0.1692$

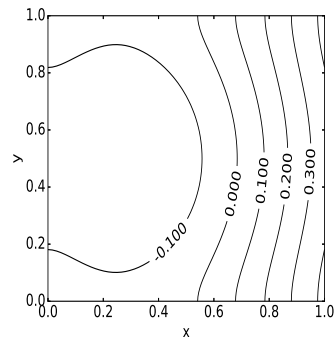
Figure 3.23: Isolines for $n = 1.5$ and increasing values of Ha.



$\frac{\partial T}{\partial \mathbf{n}} = 1$ on $\partial\Omega$



$\frac{\partial T}{\partial \mathbf{n}} = 1$ on $y = 0, 1$
 $\frac{\partial T}{\partial \mathbf{n}} = 0$ on $x = 0, 1$



$\frac{\partial T}{\partial \mathbf{n}} = 1$ on $x = 1$
 $\frac{\partial T}{\partial \mathbf{n}} = 0$ on $x = 0, y = 0, 1$

Figure 3.24: Isolines for $n = 0.5$, Ha = 5.0, Br = 1.0.

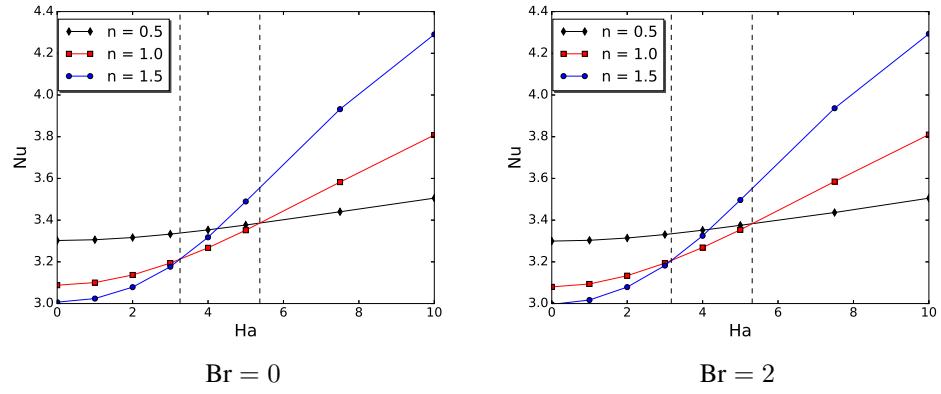


Figure 3.25: Variation of the average Nusselt number with Ha for various values of Br .

the Hartman number are expanded to larger intervals with respect to the ones in [80].

CHAPTER 4

OPTIMAL CONTROL IN FLUID FLOW PROBLEMS

In this chapter optimal control problems for two-dimensional flows of laminar, incompressible viscous Newtonian and non-Newtonian fluids are introduced. The aim of this part in the thesis is to contribute the application of powerful methods from mathematical optimization to the control of fluid flow problems. For this purpose methods under investigation are introduced firstly. Then, applications to the N-S equations, MHD flow and heat transfer equations and also the power-law fluid flows are presented.

4.1 Introduction to Optimal Control with PDE Constraints

Optimal control problems are formulated for many purposes in science and engineering such as tracking a velocity field, designing an aircraft or reduction of turbulence. Defining a cost functional for tracking the difference between the current state and the desired state, an optimization problem is constructed. Controlling idea is achieved by minimizing or maximizing the cost functional based on the needs of the underlying systems. The constraints arising from the dynamics of these systems can be governed by the ordinary differential equations (ODEs), PDEs or some other types. In this study, we consider the control of fluid flow problems constrained by the PDEs.

In general, the PDE-constrained optimization problem can be stated as

$$\underset{u}{\text{minimize}} J(z, u) \tag{4.1}$$

$$\text{subject to } C(z, u) = 0 \text{ on } \Omega, \tag{4.2}$$

where J is the cost functional, C is the set of partial differential equations, z is the state and u is the control variable. There might be additional constraints on the control and the state variables. Here, u can be embedded in a boundary condition, or be a source term or a parameter appearing in the PDE. The functional J and the constraint PDE operator are assumed to be Fréchet differentiable, which is a generalization of differentiability for functions from \mathbb{R}^n to Banach spaces:

Definition 1. Let $g : B \subset B_x \rightarrow B_y$ be an operator with Banach spaces B_x, B_y and $B \neq 0$ open. g is called Fréchet differentiable if for all $x \in B$ there exist a bounded linear operator $g'(x) : B_x \rightarrow B_y$ such that:

$$\lim_{\|h\|_{B_x} \rightarrow 0} \frac{\|g(x+h) - g(x) - g'(x)h\|_{B_y}}{\|h\|_{B_x}} = 0.$$

g is continuously Fréchet differentiable if the function $x \mapsto g'(x)$ is continuous.

Also, the state equation in (4.2) is assumed to have a unique solution z and $C_z(z, u)$ is invertible for all $u \in U$ where U is a Banach space. Then, a solution operator $z(u)$ can be defined as $u \mapsto z(u)$, which is continuously differentiable. Thus, embedding the PDE constraints into the cost functional in (4.1) gives rise to

$$\tilde{J}(u) := J(z(u), u), \quad (4.3)$$

which is generally referred to as the *reduced cost functional*. A more detailed information about the mathematical foundations of the control theory is provided in [47] and [95].

The solution process of an optimization problem begins with invoking the first derivative of the cost functional to derive the optimality conditions that have to be satisfied. These ensure that the numerically obtained controls are optimal. In this respect the derivative of \tilde{J} is derived as follows

$$\begin{aligned} \left\langle \tilde{J}'(u), s \right\rangle_{U^*, U} &= \left\langle J_z(z(u), u), z'(u)s \right\rangle_{Z^*, Z} + \left\langle J_u(z(u), u), s \right\rangle_{U^*, U} \\ &= \left\langle z'(u)^* J_z(z(u), u), s \right\rangle_{U^*, U} + \left\langle J_u(z(u), u), s \right\rangle_{U^*, U} \end{aligned}$$

so that

$$\tilde{J}'(u) = z'(u)^* J_z(z(u), u) + J_u(z(u), u),$$

where we refer to [47] for the definition of an adjoint operator and dual space. However, $z'(u)$ cannot be obtained directly. Instead, (4.2) is used to obtain the following relation

$$C_z(z(u), u)z'(u) + C_u(z(u), u) = 0,$$

which yields to

$$z'(u) = -C_z(z(u), u)^{-1}C_u(z(u), u),$$

and

$$z'(u)^* = -C_u(z(u), u)^* (C_z(z(u), u)^{-1})^*.$$

Rather calculating inverse in the last equation, a new variable, so-called the *adjoint variable* is defined as

$$\Lambda = - (C_z(z(u), u)^{-1})^* J_z(z(u), u),$$

which can be solved by the *adjoint equation*

$$C_z(z(u), u)^* \Lambda = -J_z(z(u), u). \quad (4.4)$$

This yields:

$$\tilde{J}'(u) = J_u(z(u), u) + C_u(z(u), u)^* \Lambda(u). \quad (4.5)$$

Therefore, the adjoint approach computes the derivative $\tilde{J}'(u)$ by solving the adjoint equation.

This approach can also be constructed on a *Lagrangian* formulation: let the Lagrange function $\mathcal{L} : Z \times U \times Y^* \rightarrow \mathbb{R}$ be such that

$$\mathcal{L}(z, u, \Lambda) = J(z, u) + \langle \Lambda, C(z, u) \rangle_{Y^*, Y} \quad (4.6)$$

for $\Lambda \in Y^*$, where $Z, Y^* = H^1(\Omega)$ and $U = L^2(\Omega)$. Then, substituting $z = z(u)$ into (4.6) yields to

$$\mathcal{L}(z(u), u, \Lambda) = J(z(u), u) + \langle \Lambda, C(z, u) \rangle_{Y^*, Y}, \quad (4.7)$$

and the corresponding optimization problem becomes an unconstrained one:

$$\underset{u}{\text{minimize}} \mathcal{L}(z, u, \Lambda).$$

For the optimality, the derivatives of \mathcal{L} with respect to z , u and λ are expected to vanish. Thus, the derivation of them are obtained as follows

$$\begin{aligned}\langle \mathcal{L}_z(z, u, \Lambda), d \rangle_{Z^*, Z} &= \langle J_z(z, u), d \rangle_{Z^*, Z} + \langle \Lambda, C_z(z, u)d \rangle_{Y^*, Y} \\ &= \langle J_z(z, u) + C_z(z, u)^* \Lambda, d \rangle_{Z^*, Z}\end{aligned}$$

so that

$$\mathcal{L}_z(z, u, \Lambda) = J_z(z, u) + C_z(z, u)^* \Lambda.$$

By imposing $\mathcal{L}_z = 0$, the adjoint equation (4.4) is obtained

$$C_z(z, u)^* \Lambda = -J_z(z, u).$$

Similarly, $\mathcal{L}_u(z, u, \Lambda)$ is derived:

$$\begin{aligned}\langle \mathcal{L}_u(z, u, \Lambda), e \rangle_{U^*, U} &= \langle J_u(z, u), e \rangle_{U^*, U} + \langle \Lambda, C_u(z, u)e \rangle_{Y^*, Y} \\ &= \langle J_u(z, u) + C_u(z, u)^* \Lambda, e \rangle_{U^*, U}\end{aligned}$$

so that

$$\mathcal{L}_u(z, u, \Lambda) = J_u(z, u) + C_u(z, u)^* \Lambda,$$

which represents the same equation in (4.5).

Both approaches are well applicable and generate the same adjoint equations to be solved in the optimization. Picking up an optimization algorithm, problem is solved after the discretization of the PDE constraints and the adjoint equations. In the literature, this procedure is called as *optimize-then-discretize*, where all derivatives are attained in the PDE-level and then discretization is performed to get a finite-dimensional problem. This procedure can improve the numerical accuracy when independent discretization schemes are necessary for the primal and adjoint problem. However, manual derivation of the continuous adjoint system can be tough for complex PDEs and this leads to additional complexity for the implementation [27]. Instead, first the state equation can be discretized then the adjoint equation can be derived from the discrete first-order optimality conditions. This is called as *discretize-then-optimize*. Once the forward model has been discretized, the procedure to obtain the corresponding adjoint model becomes conventional in *discretize-then-optimize*

approach. It is also attractive in practice since discrete adjoints can be generated with low effort using automatic differentiation, which we followed in this thesis. Readers can also refer to [27] for more information and pros-and-cons of the two approaches.

After all, whichever approach is chosen, an optimization algorithm has to be selected; below we present the general steps in a gradient-based optimization algorithm.

4.2 Optimization Algorithm

For the implementations in this thesis a gradient-based algorithm is used. It is a type of quasi-Newton method with a limited memory usage, called as L-BFGS (Limited-Memory Broyden-Fletcher-Goldfarb-Shanno) method, which is introduced by Liu and Nocedal in [64].

In the quasi-Newton type methods only the gradient of the cost function is required. Unlike Newton's method, the second derivative is not addressed, thus they become more efficient computational tools. The most popular one is the BFGS method whose derivation starts with forming a quadratic model of the cost function at the iterate u_k : for the reduced cost functional \tilde{J} in (4.3) we have

$$\tilde{J}_k(p) \approx q_k(p) = \tilde{J}_k + \nabla \tilde{J}_k^T p + \frac{1}{2} p^T B_k p,$$

where B_k is an $n \times n$ symmetric positive definite matrix so that if $p = 0$ then

$$q_k(0) = \tilde{J}_k \quad \text{and} \quad \nabla q_k(0) = \nabla \tilde{J}_k.$$

This quadratic model is minimized for the search direction p_k by imposing $\nabla q_k(p_k) = 0$ so that

$$p_k = -B_k^{-1} \nabla \tilde{J}_k,$$

and new iterate becomes

$$u_{k+1} = u_k + \gamma_k p_k.$$

This update is very close to the line search Newton method except that the exact Hessian is replaced with the approximate B_k .

Updating of the approximate Hessian B_k has many versions in the literature [71]. An alternative is to update the inverse of B_k , denoted by H_k , so that the search direction can be computed by a matrix-vector multiplication. The inverse Hessian approximation H_k can be updated by the following formula:

$$H_{k+1} = (I - \rho_k s_k y_k^T) H_k (I - \rho_k y_k s_k^T) + \rho_k s_k s_k^T, \quad (4.8)$$

where $s_k = u_{k+1} - u_k$, $y_k = \nabla \tilde{J}_{k+1} - \nabla \tilde{J}_k$ and $\rho_k = \frac{1}{y_k^T s_k}$. The use of this approximation, so-called the BFGS update, can be invoked in an optimization as presented in Algorithm 1. As mentioned in Algorithm 1, a step length γ_k has to be determined from a line search, where sufficient decrease and curvature conditions are satisfied. They are called as Wolfe conditions and stated as

$$\begin{aligned} J(u_k + \gamma_k p_k) &\leq J(u_k) + d_1 \gamma_k \nabla J_k^T p_k, \\ \nabla J(u_k + \gamma_k p_k)^T p_k &\geq d_2 \nabla J_k^T p_k, \end{aligned}$$

with $0 < d_1 < d_2 < 1$.

Algorithm 1 BFGS Method

```

1: procedure BFGS( $\tilde{J}$ ,  $u_0$ ,  $H_0$ ,  $\epsilon$ )
2:    $k \leftarrow 1$ 
3:   while  $\|\nabla \tilde{J}_k\| > \epsilon$ ; do
4:     Compute search direction  $p_k = -H_k \nabla \tilde{J}_k$ ;
5:     Set  $u_{k+1} + \gamma_k p_k$  where  $\gamma_k$  is computed from a line search procedure to
       satisfy the Wolfe condition;
6:     Define  $s_k = u_{k+1} - u_k$  and  $y_k = \nabla \tilde{J}_{k+1} - \nabla \tilde{J}_k$ ;
7:     Compute  $H_{k+1}$  by (4.8);
8:      $k \leftarrow k + 1$ ;
9:   end while
10: end procedure

```

Although the convergence rate of this algorithm is super-linear, that is slower than Newton's method, its cost per iteration is much smaller due to the absence of the second order derivatives. Yet, one drawback is the requirement for a storage of the inverse Hessian approximation H_k . Fortunately, this is overcome by a memory saving

strategy, yielding the so-called limited-memory BFGS method (L-BFGS) [64]. In this version of BFGS method, $H_k \nabla \tilde{J}_k$ is computed by carrying out a sequence of vector summations and inner products by storing a certain number, say m , of the vector pairs (s_i, y_i) . By the computation of the new iterate, the new pair $\{s_k, y_k\}$ of the current step is substituted into the set of pairs $\{s_i, y_i\}$, which includes information from the m most recent iterations, and the oldest vector pair is removed from the set. Therefore, the storage requirement for fully dense approximations of H_k is resolved by saving only a few vectors.

In order to give a more detailed description, the BFGS update formulas are rewritten in the following form:

$$H_{k+1} = V_k^T H_k V_k + \rho_k s_k s_k^T, \quad (4.9)$$

where

$$\rho_k = \frac{1}{y_k^T s_k} \quad \text{and} \quad V_k = I - \rho_k y_k s_k^T. \quad (4.10)$$

If the update formula (4.9) is recursively substituted into itself, then it yields to the following formula

$$\begin{aligned} H_k &= (V_{k-1}^T \cdots V_{k-m}^T) H_k^0 \\ &+ \rho_{k-m} (V_{k-1}^T \cdots V_{k-m+1}^T) s_{k-m} s_{k-m}^T (V_{k-m+1} \cdots V_{k-1}) \\ &+ \rho_{k-m+1} (V_{k-1}^T \cdots V_{k-m+2}^T) s_{k-m+1} s_{k-m+1}^T (V_{k-m+2} \cdots V_{k-1}) \\ &+ \cdots + \rho_{k-1} s_{k-1} s_{k-1}^T. \end{aligned}$$

This expression enables us to perform a recursive computation of $H_k \nabla \tilde{J}_k$, which can be simply stated by the case of two-loop recursion in Algorithm 4 in Appendix A.1. The full version of the limited-memory BFGS method is summarized in Algorithm 2.

In the following, first, the optimal control of the Navier-Stokes equations is studied using a distributed control function based on a Lagrangian view. Second, control of the MHD flow and heat transfer with variable viscosity and Hall effect is investigated by considering the parameters of the problem as control variables. Third, the optimal control of the power-law fluid flow and heat transfer is examined by determining the optimal parameters of the problem. Optimization structure is constructed directly based on the reduced cost functional for the last two problems in order to exemplify both approaches introduced in Section 4.1.

Algorithm 2 L-BFGS method

```
1: procedure L-BFGS( $\tilde{J}, u_0, m$ )
2:    $k \leftarrow 0$ ;
3:   repeat
4:     Choose  $H_k^0$ ;
5:     Compute  $p_k \leftarrow -H_k \nabla \tilde{J}_k$  from Algorithm 4;
6:     Compute  $u_{k+1} \leftarrow u_k + \gamma_k p_k$  where  $\gamma_k$  is chosen to satisfy the Wolfe
       condition;
7:     if  $k > m$  then
8:       Discard the vector pair  $[s_{k-m}, y_{k-m}]$  from storage;
9:     end if
10:    Compute and save  $s_k \leftarrow u_{k+1} - u_k$  and  $y_k = \nabla \tilde{J}_{k+1} - \nabla \tilde{J}_k$ ;
11:     $k \leftarrow k + 1$ ;
12:  until convergence
13: end procedure
```

4.3 Distributed Control of Navier-Stokes Equations with Exact Solution

The optimal control problem of the Navier-Stokes equations is investigated by invoking a control function distributed over whole domain, which is introduced in Section 2.1 as follows

$$\underset{\vec{u}}{\text{minimize}} \quad J(\vec{v}, \vec{u}) = \frac{\alpha_v}{2} \int_{\Omega} (\vec{v} - \vec{v}_d)^T (\vec{v} - \vec{v}_d) d\Omega + \frac{\alpha_u}{2} \int_{\Omega} \vec{u}^T \vec{u} d\Omega \quad (4.11)$$

$$\text{subject to} \quad -\nu \Delta \vec{v} + (\vec{v} \cdot \nabla) \vec{v} + \nabla p = \vec{f} + \vec{u} \quad \text{in } \Omega \quad (4.12)$$

$$\nabla \cdot \vec{v} = 0 \quad \text{in } \Omega \quad (4.13)$$

$$\vec{v} = 0 \quad \text{on } \partial\Omega. \quad (4.14)$$

As stated in Section 4.1, optimization is to be performed by the DO approach. Thus, the procedure begins with finding finite-dimensional approximation of the problem. Since we implement approximations to velocity \vec{v} and pressure p by using FEM with

$$\vec{v} \approx \sum_{j=1}^{\beta_v} \mathbf{v}_j \vec{\phi}_j \quad \text{and} \quad p \approx \sum_{l=1}^{\beta_p} p_l \psi_l,$$

where β_v and β_p denote the number of basis functions in finite element spaces of velocity and temperature; and the control function \vec{u} is also approximated within the

same setting

$$\vec{u} \approx \sum_{i=1}^{\beta_v} \mathbf{u}_i \vec{\phi}_i.$$

So that adding the term corresponding to the control function to the discrete non-linear system of N-S equations in (3.12) yields to

$$\begin{bmatrix} \mathbf{K} + \mathbf{N}(\mathbf{v}) & \mathbf{D} & \mathbf{0} \\ \mathbf{D}^T & \mathbf{0} & \mathbf{r}^T \\ \mathbf{0} & \mathbf{r} & 0 \end{bmatrix} \begin{bmatrix} \mathbf{v} \\ \mathbf{p} \\ \mathbf{c} \end{bmatrix} = \begin{bmatrix} \mathbf{M}(\mathbf{f} + \mathbf{u}) \\ \mathbf{0} \\ 0 \end{bmatrix}. \quad (4.15)$$

Then, constraint equation (3.13) turns into $\mathbf{C}(\mathbf{z}, \mathbf{u}) = 0$. In order to get the discretized form of the control problem, we substitute the finite element approximations into the cost function $J = J(\vec{v}, p, \vec{u})$ in (4.11). Hence, the discretized optimal control problem takes the form

$$\begin{aligned} & \underset{\mathbf{u}}{\text{minimize}} \quad \mathbf{J}(\mathbf{z}, \mathbf{u}) \\ & \text{subject to} \quad \mathbf{C}(\mathbf{z}, \mathbf{u}) = 0, \end{aligned}$$

where \mathbf{J} is the discrete objective function computed as

$$\mathbf{J}(\mathbf{z}, \mathbf{u}) = \frac{\alpha_v}{2} (\mathbf{v} - \mathbf{v}_d)^T \mathbf{M}(\mathbf{v} - \mathbf{v}_d) + \frac{\alpha_u}{2} \mathbf{u}^T \mathbf{M} \mathbf{u}.$$

Now, the procedure based on a Lagrange function, introduced in Section 4.1, is going to be used in the discrete concept. Thus, discretized Lagrange function in the derivation of first-order optimality condition is formulated as follows

$$\mathcal{L}(\mathbf{z}, \mathbf{\Lambda}, \mathbf{u}) = \mathbf{J}(\mathbf{z}, \mathbf{u}) + \mathbf{\Lambda}^T \mathbf{C}(\mathbf{z}, \mathbf{u}),$$

where $\mathbf{\Lambda} = (\boldsymbol{\lambda}, \boldsymbol{\eta}, \mathbf{e})$ is the discrete adjoint variable corresponding to primal variable $\mathbf{z} = (\mathbf{v}, \mathbf{p}, \mathbf{c})$. As stated earlier, the first-order optimality condition requires that the partial derivatives of the Lagrangian function are zero at the optimality. That is, the formulations in Section 4.1 are stated once again but now for the discrete case:

$$\frac{\partial \mathcal{L}(\mathbf{z}, \mathbf{\Lambda}, \mathbf{u})}{\partial \mathbf{\Lambda}} = \mathbf{C}(\mathbf{z}, \mathbf{u}) = 0, \quad (4.16)$$

$$\frac{\partial \mathcal{L}(\mathbf{z}, \mathbf{\Lambda}, \mathbf{u})}{\partial \mathbf{z}} = \frac{\partial \mathbf{J}(\mathbf{z}, \mathbf{u})}{\partial \mathbf{z}} + \left(\frac{\partial \mathbf{C}(\mathbf{z}, \mathbf{u})}{\partial \mathbf{z}} \right)^* \mathbf{\Lambda} = 0, \quad (4.17)$$

$$\frac{\partial \mathcal{L}(\mathbf{z}, \mathbf{\Lambda}, \mathbf{u})}{\partial \mathbf{u}} = \frac{\partial \mathbf{J}(\mathbf{z}, \mathbf{u})}{\partial \mathbf{u}} + \left(\frac{\partial \mathbf{C}(\mathbf{z}, \mathbf{u})}{\partial \mathbf{u}} \right)^* \mathbf{\Lambda} = 0, \quad (4.18)$$

which are satisfied at an optimal point $(\mathbf{z}^*, \mathbf{\Lambda}^*, \mathbf{u}^*)$.

First, from (4.16) the constraint equation of the problem is obtained, which is already have to be satisfied. Second, from (4.17) the adjoint equation

$$\mathbf{C}_z(\mathbf{z}, \mathbf{u})^* \mathbf{\Lambda} = -\mathbf{J}_z(\mathbf{z}, \mathbf{u}),$$

leads to a linear system of equations

$$\begin{bmatrix} \mathbf{K}^T + \mathbf{N}^T(\mathbf{v}) & \mathbf{D} & \mathbf{0} \\ \mathbf{D}^T & \mathbf{0} & \mathbf{r}^T \\ \mathbf{0} & \mathbf{r} & \mathbf{0} \end{bmatrix} \begin{bmatrix} \boldsymbol{\lambda} \\ \boldsymbol{\eta} \\ \mathbf{e} \end{bmatrix} = \begin{bmatrix} -\alpha_v \mathbf{M}(\mathbf{v} - \mathbf{v}_d) \\ \mathbf{0} \\ 0 \end{bmatrix} \quad (4.19)$$

that is to be solved for $\mathbf{\Lambda}$. Third, from (4.18) the equation for the control function is derived,

$$\mathbf{C}_u(\mathbf{z}, \mathbf{u})^* \mathbf{\Lambda} = -\mathbf{J}_u,$$

which, in turn, gives

$$(-\mathbf{M}) \mathbf{\Lambda} = -\alpha_u \mathbf{M} \mathbf{u},$$

or equivalently,

$$\mathbf{M}(\boldsymbol{\lambda} - \alpha_u \mathbf{u}) = \mathbf{0}.$$

The discrete formulation of the derivative of reduced cost functional in (4.5) is obtained by (4.18). Therein, the optimization is conducted for the equation (4.18), by using the L-BFGS algorithm given in Section 4.2. This procedure requires solutions of the state and adjoint equations iteratively. In other words, at each optimization step, a new control candidate u_k is generated, so that this new \mathbf{u}_k is used to obtain a new \mathbf{z}_k and correspondingly a new $\mathbf{\Lambda}_k$.

4.4 Parameter Control of MHD Flows with Temperature Dependent Viscosity

This section is devoted to the problem of controlling the MHD flows and heat transfer equations with temperature dependent viscosity and Hall effect by using the parameters of problem as control variables. The mathematical statement is formulated as in

Section 2.2 for $\mathcal{U} = \{\text{Ha}, m, \text{Br}, B\}$,

$$\begin{aligned} \underset{\mathbf{u} \in \mathcal{U}}{\text{minimize}} \quad J(\omega, T, \mathbf{u}) &= \frac{\alpha_\omega}{2} \int_{\Omega} (\omega - \omega_d)^2 d\Omega + \frac{\alpha_T}{2} \int_{\Omega} (T - T_d)^2 d\Omega \\ &\quad + \frac{\alpha_{\mathbf{u}}}{2} \int_{\Omega} \|\mathbf{u}\|^2 d\Omega \end{aligned} \quad (4.20)$$

$$\text{subject to} \quad \frac{\partial}{\partial x} \left(\bar{\mu} \frac{\partial \omega}{\partial x} \right) + \frac{\partial}{\partial y} \left(\bar{\mu} \frac{\partial \omega}{\partial y} \right) = -1 + \frac{\text{Ha}^2}{1 + m^2} \omega \quad \text{in } \Omega \quad (4.21)$$

$$\nabla^2 T + \text{Br} \bar{\mu} \left[\left(\frac{\partial \omega}{\partial x} \right)^2 + \left(\frac{\partial \omega}{\partial y} \right)^2 \right] + \frac{\text{Ha}^2 \text{Br}}{1 + m^2} \omega^2 = \frac{\omega}{\omega_m} \quad \text{in } \Omega \quad (4.22)$$

$$\omega = 0, \quad T = 0 \quad \text{on } \partial\Omega. \quad (4.23)$$

Again, pursuing the similar structure with the DO approach, implementation is started with the discretization of the problem. Having implemented a finite element approximation to the velocity ω , the temperature T and the control variable \mathbf{u} , their discretized forms are substituted to the cost functional $J = J(\omega, T, \mathbf{u})$ in order to get the discretized form \mathbf{J} in (4.20). Hence, the discretized optimal control problem takes the form

$$\underset{\mathbf{u} \in \mathcal{U}}{\text{minimize}} \quad \mathbf{J}(\mathbf{z}, \mathbf{u}) \quad (4.24)$$

$$\text{subject to} \quad \mathbf{C}(\mathbf{z}, \mathbf{u}) = 0, \quad (4.25)$$

where $\mathbf{z} = (\boldsymbol{\omega}, \mathbf{T})$, and \mathbf{J} is the discrete objective function computed as

$$\mathbf{J}(\mathbf{z}, \mathbf{u}) = \frac{\alpha_\omega}{2} (\boldsymbol{\omega} - \boldsymbol{\omega}_d)^T \mathbf{M} (\boldsymbol{\omega} - \boldsymbol{\omega}_d) + \frac{\alpha_T}{2} (\mathbf{T} - \mathbf{T}_d)^T \mathbf{M} (\mathbf{T} - \mathbf{T}_d) + \frac{\alpha_u}{2} \|\mathbf{u}\|^2 |\Omega|,$$

where $|\Omega|$ represents the area of the domain in two-dimensional space. Here, it is assumed that \mathbf{C} and \mathbf{J} are continuously differentiable, and for all control \mathbf{u} the state equation $\mathbf{C}(\mathbf{z}, \mathbf{u}) = 0$ has a unique solution $\mathbf{z} = \mathbf{z}(\mathbf{u})$, and the derivative $\mathbf{C}_{\mathbf{z}}(\mathbf{z}, \mathbf{u})$ is invertible. By the implicit function theorem, $\mathbf{u} \mapsto \mathbf{z}(\mathbf{u})$ is continuously differentiable, and hence, the cost function can be considered as

$$\tilde{\mathbf{J}}(\mathbf{u}) = \mathbf{J}(\mathbf{z}(\mathbf{u}), \mathbf{u}), \quad (4.26)$$

where the PDE constraints are embedded to this cost function. Generally, such form $\tilde{\mathbf{J}}(\mathbf{u})$ is referred to as discrete reduced cost function.

Again, the first-order optimality conditions are derived as in Section 4.1, but for the discretized problem. This implies that the discrete form of the adjoint equation in

(4.4) becomes

$$\mathbf{C}_z(\mathbf{z}(\mathbf{u}), \mathbf{u})^* \boldsymbol{\Lambda} = -\mathbf{J}_z(\mathbf{z}(\mathbf{u}), \mathbf{u}), \quad (4.27)$$

which is to be solved for $\boldsymbol{\Lambda} = (\boldsymbol{\lambda}, \boldsymbol{\eta})$. Hence, it is substituted into the discrete form of (4.5) is obtained as

$$\tilde{\mathbf{J}}'(\mathbf{u}) = \mathbf{J}_u(\mathbf{z}, \mathbf{u}) + \mathbf{C}_u(\mathbf{z}, \mathbf{u})^* \boldsymbol{\Lambda}. \quad (4.28)$$

Consequently, $\mathbf{C}_z(\mathbf{z}(\mathbf{u}), \mathbf{u})$ has to be computed for the discretized non-linear system of equations of PDEs in (4.21) and (4.22) with (4.23) as follows

$$\mathbf{C}_z(\mathbf{z}(\mathbf{u}), \mathbf{u}) = \begin{bmatrix} c_1 \mathbf{M} & \mathbf{0} \\ \mathbf{0} & \mathbf{S} \end{bmatrix} + \begin{bmatrix} \mathbf{K}(\mathbf{T}) & \mathbf{K}_T(\mathbf{T})\boldsymbol{\omega} \\ \mathbf{G}(\mathbf{z}) & -\text{Br}\mathbf{D}_T(\boldsymbol{\omega}, \mathbf{T})\boldsymbol{\omega} \end{bmatrix},$$

where

$$\mathbf{G}(\mathbf{z}) = c_2 \left[\frac{\partial \mathbf{N}(\boldsymbol{\omega})}{\partial \boldsymbol{\omega}} \boldsymbol{\omega} + \mathbf{N}(\boldsymbol{\omega}) \right] - \text{Br} \left[\frac{\partial \mathbf{D}(\boldsymbol{\omega}, \mathbf{T})}{\partial \boldsymbol{\omega}} \boldsymbol{\omega} + \mathbf{D}(\boldsymbol{\omega}, \mathbf{T}) \right] + \frac{\partial \mathbf{P}(\boldsymbol{\omega})}{\partial \boldsymbol{\omega}} \boldsymbol{\omega} + \mathbf{P}(\boldsymbol{\omega}).$$

Then, the adjoint system to be solved becomes

$$\mathbf{C}_z(\mathbf{z}(\mathbf{u}), \mathbf{u})^* \begin{bmatrix} \boldsymbol{\lambda} \\ \boldsymbol{\eta} \end{bmatrix} = - \begin{bmatrix} \alpha_\omega \mathbf{M}(\boldsymbol{\omega} - \boldsymbol{\omega}_d) \\ \alpha_T \mathbf{M}(\mathbf{T} - \mathbf{T}_d) \end{bmatrix}. \quad (4.29)$$

Having derived the system (4.29), the adjoint-based reduced gradient equation in (4.28) is used to find the optimal parameter(s) by the L-BFGS algorithm, described in Section 4.2.

4.5 Parameter Control of Power-Law Fluid Flow and Heat Transfer

Now, we will investigate the problem of controlling the power-law fluid flow and heat transfer equations considering the parameters as control variables. The formulation

in Section 2.3 for $\mathcal{U} = \{\text{Ha}, n\}$ reads:

$$\begin{aligned} \underset{\mathbf{u} \in \mathcal{U}}{\text{minimize}} \quad J(\omega, T, \mathbf{u}) &= \frac{\alpha_\omega}{2} \int_{\Omega} (\omega - \omega_d)^2 d\Omega + \frac{\alpha_T}{2} \int_{\Omega} (T - T_d)^2 d\Omega \\ &\quad + \frac{\alpha_u}{2} \int_{\Omega} \|\mathbf{u}\|^2 d\Omega \end{aligned} \quad (4.30)$$

$$\text{subject to} \quad \frac{\partial}{\partial x} \left(\bar{\mu} \frac{\partial \omega}{\partial x} \right) + \frac{\partial}{\partial y} \left(\bar{\mu} \frac{\partial \omega}{\partial y} \right) = -1 + \text{Ha}^2 \omega \quad \text{in } \Omega \quad (4.31)$$

$$\nabla^2 T + \text{Br} \bar{\mu} \left[\left(\frac{\partial \omega}{\partial x} \right)^2 + \left(\frac{\partial \omega}{\partial y} \right)^2 \right] + \text{Ha}^2 \text{Br} \omega^2 = \frac{4\omega}{\omega_m} \quad \text{in } \Omega \quad (4.32)$$

$$\omega = 0 \quad \text{on } \partial\Omega \quad (4.33)$$

$$\frac{\partial T}{\partial y} \Big|_{(x,b/a)} = \frac{\partial T}{\partial x} \Big|_{(1,y)} = 1, \quad \frac{\partial T}{\partial y} \Big|_{(x,0)} = \frac{\partial T}{\partial x} \Big|_{(0,y)} = -1. \quad (4.34)$$

Using the DO approach, firstly, the discretized form \mathbf{J} of the cost function in (4.30) is obtained by substituting the discrete solutions into $J(\omega, T, u)$. As a result, the discretized control problem is stated as

$$\begin{aligned} \underset{\mathbf{u} \in \mathcal{U}}{\text{minimize}} \quad & \mathbf{J}(\mathbf{z}, \mathbf{u}) \\ \text{subject to} \quad & \mathbf{C}(\mathbf{z}, \mathbf{u}) = 0, \end{aligned}$$

where $\mathbf{z} = (\boldsymbol{\omega}, \mathbf{T})$, and \mathbf{J} is the discrete objective function constructed as

$$\mathbf{J}(\mathbf{z}, \mathbf{u}) = \frac{\alpha_\omega}{2} (\boldsymbol{\omega} - \boldsymbol{\omega}_d)^T \mathbf{M}_\omega (\boldsymbol{\omega} - \boldsymbol{\omega}_d) + \frac{\alpha_T}{2} (\mathbf{T} - \mathbf{T}_d)^T \mathbf{M}_T (\mathbf{T} - \mathbf{T}_d) \quad (4.35)$$

$$+ \frac{\alpha_u}{2} \|\mathbf{u}\|^2 |\Omega|. \quad (4.36)$$

Here, \mathbf{M}_ω and \mathbf{M}_T are mass matrices of the quadratic and linear finite element spaces for ω and T , respectively. The adjoint equation has to be formulated as

$$\mathbf{C}_z^*(\mathbf{z}(\mathbf{u}), \mathbf{u}) \boldsymbol{\Lambda} = -\mathbf{J}_z(\mathbf{z}(\mathbf{u}), \mathbf{u}), \quad (4.37)$$

where

$$\mathbf{C}_z(\mathbf{z}(\mathbf{u}), \mathbf{u}) = \begin{bmatrix} \mathbf{F}_z \\ \mathbf{G}_z \end{bmatrix} = \begin{bmatrix} \frac{\partial \mathbf{F}(\boldsymbol{\omega})}{\partial \boldsymbol{\omega}} & 0 \\ 0 & \frac{\partial \mathbf{G}(\mathbf{T})}{\partial \mathbf{T}} \end{bmatrix}.$$

Hence, the adjoint problem in (4.37) for $\boldsymbol{\Lambda} = (\boldsymbol{\lambda}, \boldsymbol{\eta})$ becomes

$$\mathbf{C}_z(\mathbf{z}(\mathbf{u}), \mathbf{u})^* \begin{bmatrix} \boldsymbol{\lambda} \\ \boldsymbol{\eta} \end{bmatrix} = - \begin{bmatrix} \alpha_\omega \mathbf{M}_\omega (\boldsymbol{\omega} - \boldsymbol{\omega}_d) \\ \alpha_T \mathbf{M}_T (\mathbf{T} - \mathbf{T}_d) \end{bmatrix},$$

which has to be solved at each optimization step for the gradient of the reduced cost function:

$$\frac{\partial \tilde{\mathbf{J}}(\mathbf{u})}{\partial \mathbf{u}} = \Lambda^* \mathbf{C}_u(\mathbf{z}(\mathbf{u}), \mathbf{u}) + \mathbf{J}_u(\mathbf{z}(\mathbf{u}), \mathbf{u}) = 0. \quad (4.38)$$

The optimization algorithm is, used here, again L-BFGS algorithm, described in Section 4.2.

4.6 Numerical Results

This section presents solutions to the optimal control of steady, two-dimensional, laminar flow problems of incompressible, Newtonian and non-Newtonian fluids. First simulations are conducted for the distributed control of Navier-Stokes equations with an exact solution to confirm the performance of control approaches in this study. Second, numerical tests are performed for the parameter control of the MHD flow and heat transfer with temperature dependent viscosity. Third, simulations are implemented for the control of power-law fluid flow and heat transfer with parameter control.

Controls are studied as single and as well as pairwise parameters for both problems. The numerical results with parameter control indicate the efficiency of the controlling idea not only for regaining the flow and temperature profiles but also the characterization of them, specifically for the classification as Newtonian or non-Newtonian of a power-law fluid.

Computer simulations of the optimal control problem are executed using *dolfin-adjoint* [24] which is implemented in Python and works with FEniCS platform. *dolfin-adjoint* provides algorithmic differentiation routines acting on the discrete equation of the primal problem to derive the discrete adjoint equations. The gradients obtained are used in the optimization process of the L-BFGS algorithm. Starting with an initial estimate the optimization loop to calculate new estimates for optimal solution is repeated until the norm of the gradient of the reduced cost function $\tilde{\mathbf{J}}$ is less than the value of a tolerance 10^{-10} .

Table 4.1: Distributed control for regaining the desired states given below with the uncontrolled initial state of $\nu = 1.0$

ν_d	$\ v_1^{\text{opt}} - v_1^d\ _{L2}$	$\ v_2^{\text{opt}} - v_2^d\ _{L2}$	J	Tit
0.1	2.2452×10^{-3}	2.2452×10^{-3}	1.512×10^{-4}	11
0.05	2.2401×10^{-3}	2.2401×10^{-3}	1.731×10^{-4}	12
0.01	2.5297×10^{-3}	2.5297×10^{-3}	1.921×10^{-4}	12
0.005	2.5427×10^{-3}	2.5427×10^{-3}	1.946×10^{-4}	13
0.001	2.5557×10^{-3}	2.5557×10^{-3}	1.966×10^{-4}	13

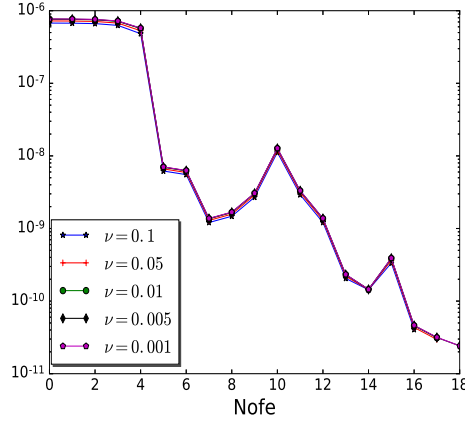


Figure 4.1: Norm of the gradient values versus number of function evaluations (Nofe) during optimization.

4.6.1 Control for Navier-Stokes Equations

Control of the steady Navier-Stokes flow in (4.11)-(4.14) is simulated by using an additional source function as a distributed control. The uncontrolled initial state of the velocity is produced by simulating the flow for $\nu = 1.0$ with the given exact solution in Section 3.5.1. The aim is to find the required force function to move the velocity profile to the desired velocity, which has various values as given in Table 4.1. It also indicates that the number of iterations is increasing for smaller initial values of ν as the difference between the desired and initial states increases.

Test results indicate that the optimization algorithm is successful for attaining the desired profiles even if the desired states are chosen far from the initial ones, where the regularization parameters are chosen as $(\alpha_v, \alpha_u) = (10^3, 10^{-3})$, which are successful in the penalization of corresponding variables. In order to see the convergence of the optimization to the optimal states, the norm of the gradient values versus number of function evaluations during the optimization are presented in Figure 4.1.

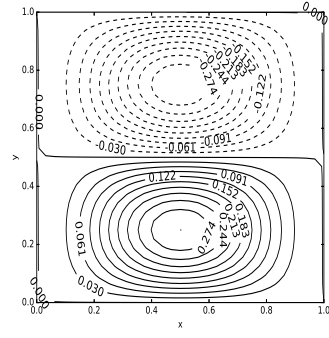
Figure 4.2 is depicted for monitoring the difference between the uncontrolled initial states and desired states corresponding to $\nu_d = 0.005$, and also the closeness of the controlled and desired profiles. Profiles are also presented in Figure 4.3 as vector fields.

4.6.2 Control for MHD Flow and Heat Transfer with Temperature Dependent Viscosity and Hall Effect

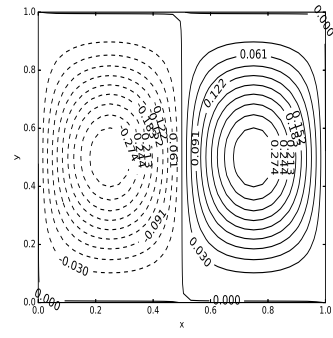
The MHD flow is constructed as an optimal control problem by using the parameters of the system as the control variables. These parameters include Hartmann number, Brinkman number, viscosity parameter and Hall parameter. The control of each of these parameters has a significant importance in achieving the desired state of hydrodynamically and thermally fully developed flow and the fluid temperature in the duct. For example, the control of Hartmann number determines how strong the magnetic field should be applied for reaching a desired velocity profile, and hence, isolines in the duct.

Since the magnitude of the velocity is small, regularization parameters are chosen large enough in this respect to prevent the objective function from being close to zero because of the cancellation without converging to optimal state.

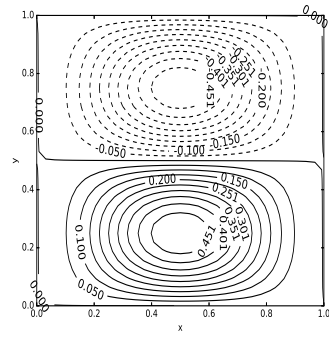
First, the Hartmann number Ha is introduced as the control variable \mathbf{u} , since its control provides information about the optimal electromagnetic force to reach a desired flow. As illustrated in Figure 3.5 and Figure 3.10, the increase in Hartmann number has more significant effect on the velocity than on the temperature of the flow in the duct. In order to reach the desired states for both velocity ω_d and temperature T_d , the regularization parameters are chosen as $\alpha_\omega = 10^3$, $\alpha_T = 10^0$, $\alpha_{Ha} = 10^{-5}$. Here, the desired states ω_d and T_d are (pre-)computed FEM solutions (as in Section 3.5.2) given the parameters in Table 4.2, particularly the values of Ha_d . At optimality, the states ω_{opt} , T_{opt} , and the optimal control variable Ha_{opt} in Table 4.2 indicate that the choice of regularization parameters is not only sufficient to control the states, but it also ensures that the optimal Ha_{opt} is close to the Hartmann number Ha_d of the desired flow even if the initial Ha^0 is chosen far away from Ha_{opt} in BFGS algorithm. It is also noted that the total number of iterations required in the optimization is remarkably



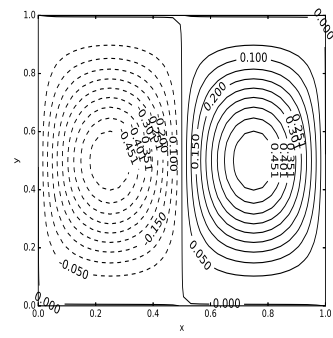
uncontrolled v_1



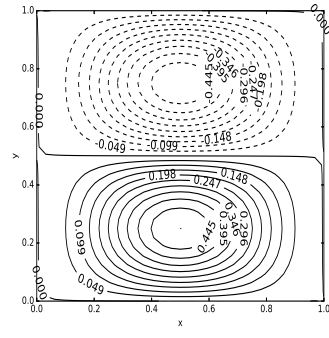
uncontrolled v_2



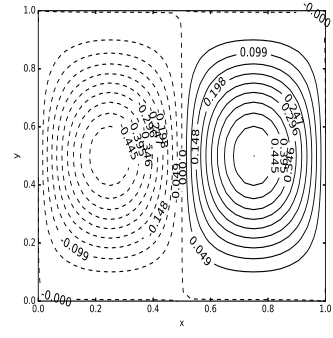
desired v_1



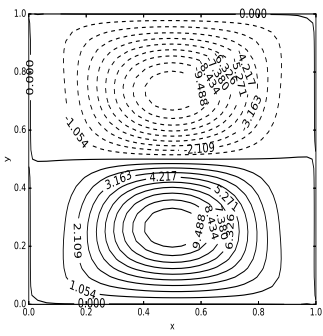
desired v_2



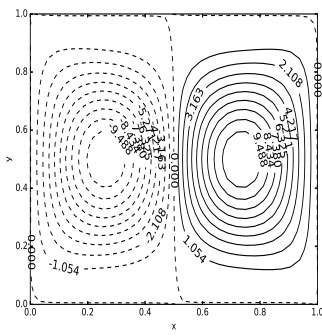
controlled v_1



controlled v_2

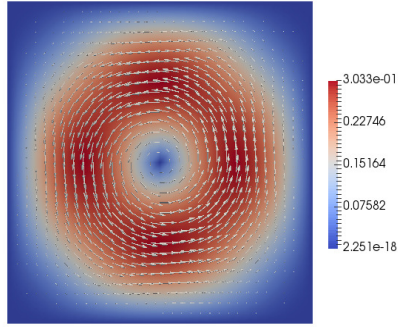


control u_1

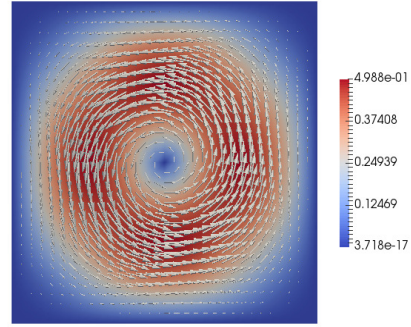


control u_2

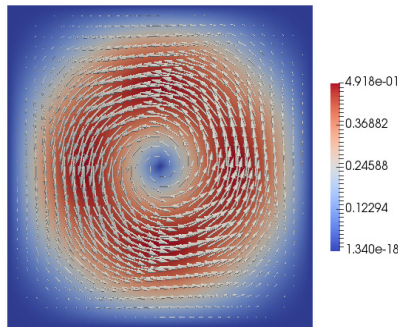
Figure 4.2: Uncontrolled ($\nu_0 = 1.0$), desired ($\nu_d = 0.005$) and controlled velocity profiles and control profile.



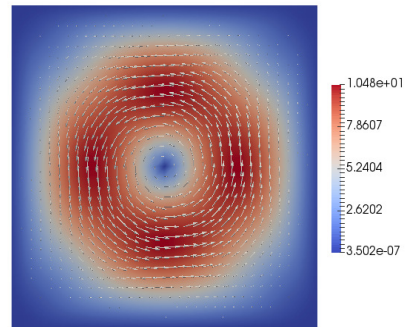
(a) uncontrolled \vec{v}



(b) desired \vec{v}



(c) controlled \vec{v}



(d) control \vec{u}

Figure 4.3: Velocity field and control field for the desired state of $\nu_d = 0.005$ and uncontrolled state $\nu_0 = 1.0$.

Table 4.2: Control with Hartman number Ha , $m = 1$, $Br = 1$, $B = 1$, $\alpha_\omega = 10^3$, $\alpha_T = 10^0$, $\alpha_{Ha} = 10^{-5}$, $Ha^0 = 0.1$.

Ha_d	Ha_{opt}	$\ \omega_{opt} - \omega_d\ _\infty$	$\ T_{opt} - T_d\ _\infty$	J	Tit
1.0	1.0125	4.4417×10^{-5}	2.6390×10^{-6}	6.059×10^{-6}	3
3.0	3.0353	2.6263×10^{-4}	2.0360×10^{-5}	9.816×10^{-5}	4
5.0	5.0374	2.6129×10^{-4}	3.3324×10^{-5}	3.500×10^{-4}	4
10.0	9.9696	8.7007×10^{-5}	3.7295×10^{-5}	1.214×10^{-3}	3

Table 4.3: Control with Hall parameter m , $Ha = 1$, $Br = 1$, $B = 1$, $\alpha_\omega = 10^3$, $\alpha_T = 10^0$, $\alpha_m = 0.0$, $m^0 = 10.0$

m_d	m_{opt}	$\ \omega_{opt} - \omega_d\ _\infty$	$\ T_{opt} - T_d\ _\infty$	J	Tit
1.0	0.9693	5.4917×10^{-5}	3.2632×10^{-6}	8.997×10^{-7}	5
3.0	2.9521	1.0771×10^{-5}	6.2470×10^{-7}	3.170×10^{-8}	3
5.0	4.9379	3.4532×10^{-6}	1.9957×10^{-7}	3.206×10^{-9}	3
8.0	8.0076	1.0692×10^{-9}	6.1708×10^{-9}	1.943×10^{-10}	3

few, denoted by Tit.

Second, the Hall parameter m is introduced as the control variable \mathbf{u} because it is also significant to gain information about, for instance, the material from which the conductor should be made of. The increase of the Hall parameter has an effect that is contrary to the effect of Ha , but the magnitude of the effect on the velocity is larger than that on the temperature, again. Thus, regularization parameters α_ω , α_T are selected the same as in the case of Ha ; however, α_m is taken zero so that optimal m is obtained close to the Hall parameter of the desired state. At optimality, Table 4.3 shows that the state of the flow is perfectly controlled. In fact, no matter what value of α_m is given, the optimization algorithm converges and the desired state of the flow are achieved. However, due to the significance of the penalization effect of α_m , no matter how small, at the optimal solution, m_{opt} may not be close to m_d ; this is illustrated in Table 4.4.

Table 4.4: Control with Hall parameter m , $Ha = 1$, $Br = 1$, $B = 1$, $\alpha_\omega = 10^3$, $\alpha_T = 10^0$, $\alpha_m = 10^{-5}$, $m^0 = 10.0$

m_d	m_{opt}	$\ \omega_{opt} - \omega_d\ _\infty$	$\ T_{opt} - T_d\ _\infty$	J	Tit
1.0	0.9581	7.5264×10^{-5}	4.4729×10^{-6}	5.543×10^{-6}	5
3.0	2.2898	2.2016×10^{-4}	1.2791×10^{-5}	3.184×10^{-5}	6
5.0	2.6081	3.2969×10^{-4}	1.9103×10^{-5}	4.758×10^{-5}	7
8.0	2.7242	3.8048×10^{-4}	2.2024×10^{-5}	5.549×10^{-5}	5

Table 4.5: Control with Brinkman number Br, $Ha = 1$, $m = 1$, $B = 1$, $\alpha_\omega = 10^0$, $\alpha_T = 10^3$, $\alpha_{Br} = 10^{-5}$, $Br^0 = 0.0$

Br_d	Br_{opt}	$\ \omega_{opt} - \omega_d\ _\infty$	$\ T_{opt} - T_d\ _\infty$	J	Tit
1.0	0.9870	7.0049×10^{-7}	1.6050×10^{-5}	4.935×10^{-6}	3
2.0	1.9742	1.3999×10^{-6}	3.2051×10^{-5}	1.974×10^{-5}	4
3.0	2.9615	2.0984×10^{-6}	4.8004×10^{-5}	4.442×10^{-5}	4

Table 4.6: Control with B , $Ha = 1$, $m = 1$, $Br = 1$, $\alpha_\omega = 10^3$, $\alpha_T = 10^3$, $\alpha_B = 10^{-5}$, $B^0 = 0.0$

B_d	B_{opt}	$\ \omega_{opt} - \omega_d\ _\infty$	$\ T_{opt} - T_d\ _\infty$	J	Tit
1.0	0.9980	6.1371×10^{-6}	7.6739×10^{-6}	4.990×10^{-6}	4
2.0	1.9951	1.3414×10^{-5}	1.6993×10^{-5}	1.995×10^{-5}	6
3.0	2.9911	2.1835×10^{-5}	2.7997×10^{-5}	4.487×10^{-5}	7

Third, the Brinkman number Br is used as the control variable \mathbf{u} . Being one of the important parameters, it specifies the speed of the conduction of the heat produced by the viscous dissipation. Since its presence in the system of PDEs mostly dominates the temperature, the regularization parameters are chosen as $\alpha_\omega = 10^0$, $\alpha_T = 10^3$, $\alpha_{Br} = 10^{-5}$; and this selection is again rather sufficient to reach the desired states within a few iterations shown in Table 4.5.

Fourth, the control of the viscosity parameter B is considered. The control of the viscosity provides another essential information of the fluid so that flow can be manipulated by changing its viscosity to reach a desired flow behavior. The different test values of regularization terms show that B has almost the similar dominance on both velocity and temperature, thus they are selected as $\alpha_\omega = 10^3$, $\alpha_T = 10^3$, $\alpha_B = 10^{-5}$. As shown in Table 4.6, the algorithm is successful to control the states of the flow for various values of B_d .

In the light of the above discussions and the results obtained for the control problem using only one significant parameter of the MHD flow, the optimal control parameters are studied, now in this case, pairwise so that the velocity and isolines are controlled at the desired states.

To begin with, pairwise control is performed by Ha and B , that is, $\mathbf{u} = (Ha, B)$. As it is clear from Figure 3.5, Figure 3.10, Figure 3.6 and Figure 3.13, these parameters highly effect the velocity and isolines. In any case, the control of the problem

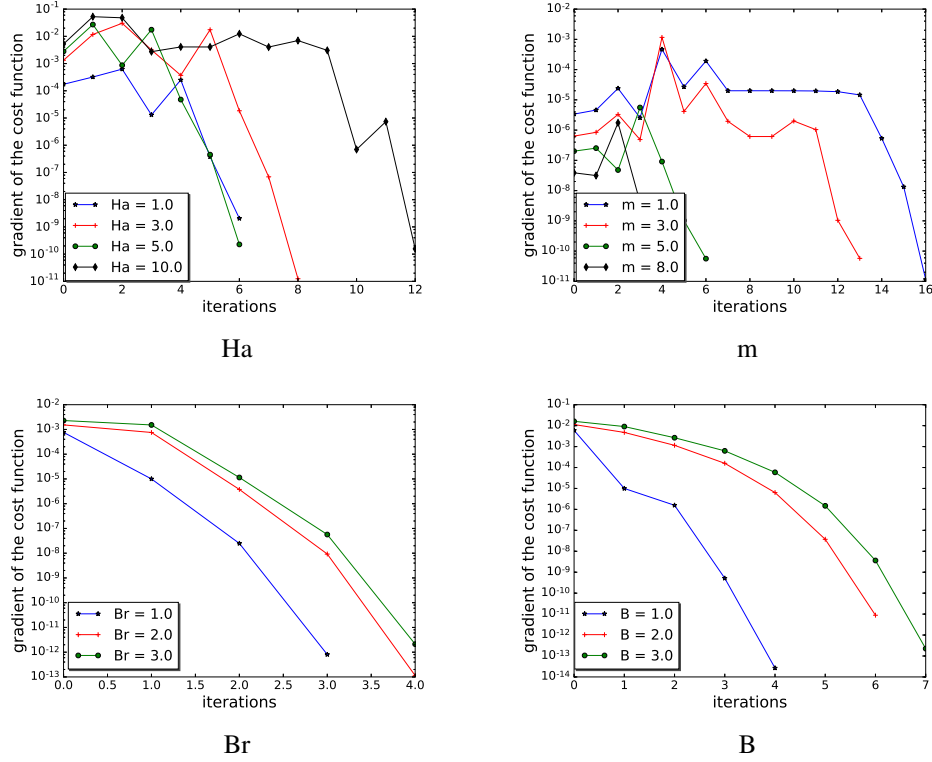


Figure 4.4: Norm of the gradient versus the number of evaluations of the cost function (Nofe) for the control with single parameter.

Table 4.7: Control with Hartmann number Ha and B , $m = 1$, $Br = 1$, $\alpha_\omega = 10^3$, $\alpha_T = 10^0$, $\alpha_{(Ha,B)} = 10^{-5}$, $(Ha^0, B^0) = (0.1, 0.0)$

Ha_d	B_d	Ha_{opt}	B_{opt}	$\ \omega_{opt} - \omega_d\ _\infty$	$\ T_{opt} - T_d\ _\infty$	J	Tit
1.0	0.0	0.9494	0.0654	3.9802×10^{-5}	2.6174×10^{-4}	5.702×10^{-6}	12
1.0	1.0	1.0201	0.9888	3.7112×10^{-5}	3.8666×10^{-5}	1.105×10^{-5}	12
3.0	2.0	3.0804	1.9691	4.9921×10^{-4}	7.4232×10^{-5}	1.188×10^{-4}	10
5.0	1.0	5.0446	0.9103	2.0662×10^{-4}	1.6474×10^{-4}	3.550×10^{-4}	10

is achieved, shown in Table 4.7; and even, the optimal values of (Ha, B) are close to those of the desired states. Another pairwise control is conducted by taking the control variable as $\mathbf{u} = (Br, B)$. At optimality, the controlled parameters are again close enough to the ones of the desired states, even they do not have to be close, along with successfully controlling the desired velocity profiles and isolines. See Table 4.8.

The pairwise control is also considered with $\mathbf{u} = (m, Br)$. However, the effects of these parameters on the change of the magnitude of velocity and temperature are too small as indicated in Section 3.5.2. Fortunately, as is shown in Table 4.9, the optimal

Table 4.8: Control with Brinkman number Br and B , $m = 1$, $\text{Ha} = 1$, $\alpha_\omega = 10^3$, $\alpha_T = 10^3$, $\alpha_{(\text{Br}, B)} = 10^{-5}$, $(\text{Br}^0, B^0) = (0.0, 0.0)$

Br_d	B_d	Br_{opt}	B_{opt}	$\ \omega_{\text{opt}} - \omega_d\ _\infty$	$\ T_{\text{opt}} - T_d\ _\infty$	J	Tit
1.0	1.0	0.9784	1.0045	1.4931×10^{-5}	1.5024×10^{-5}	9.914×10^{-6}	10
2.0	1.0	1.9493	1.0134	4.3470×10^{-5}	3.1279×10^{-5}	2.456×10^{-5}	10
1.0	2.0	0.9865	1.9991	1.1013×10^{-6}	1.8125×10^{-5}	2.492×10^{-5}	11
2.0	2.0	1.9547	2.0087	2.7642×10^{-5}	3.1640×10^{-5}	3.963×10^{-5}	11

Table 4.9: Control with the Hall parameter m and Br , $B = 1$, $\text{Ha} = 1$, $\alpha_\omega = 10^0$, $\alpha_T = 10^3$, $\alpha_{(m, \text{Br})} = 10^{-5}$, $(m^0, \text{Br}^0) = (10.0, 0.0)$

m_d	Br_d	m_{opt}	Br_{opt}	$\ \omega_{\text{opt}} - \omega_d\ _\infty$	$\ T_{\text{opt}} - T_d\ _\infty$	J	Tit
1.0	1.0	1.6959	0.2678	8.2345×10^{-4}	9.4556×10^{-4}	2.354×10^{-5}	13
1.0	2.0	1.5727	1.1708	7.1134×10^{-4}	1.0789×10^{-3}	2.997×10^{-5}	14
3.0	1.0	1.7736	0.3098	5.5295×10^{-4}	8.2053×10^{-4}	2.717×10^{-5}	14
3.0	2.0	1.6818	1.2376	6.3009×10^{-4}	9.0018×10^{-4}	3.554×10^{-5}	13

states of the flow is successfully recovered; but the optimal solution $\mathbf{u} = (m_{\text{opt}}, \text{Br}_{\text{opt}})$ differs from the parameters m_d and Br_d used to describe the desired velocity profiles and isolines.

Although using pairwise controls requires relatively more number of iterations than the single ones as expected, the most costly one may be considered as the case when the pair $\mathbf{u} = (m, B)$ is used. Indeed, this is due to their counter-effects on the velocity and temperature: see Figure 3.7, Figure 3.6, Figure 3.11 and Figure 3.13. As a result, the total number of iterations is reported up to 22 given in Table 4.10. Although at optimality $\mathbf{u} = (m_{\text{opt}}, B_{\text{opt}})$ are relatively far from the parameters m_d and B_d used in the desired velocity and isolines, the major aim of the implementation of the controlling idea is successfully achieved by attaining the desired profiles.

Gradient values, which are the crucial quantities in the first-order optimality conditions, are given in Figure 4.4 and Figure 4.5. These figures also confirm the convergence to the optimal controls of corresponding simulations.

4.6.3 Control for Power-Law Fluid Flow and Heat Transfer

In the sequel, the power-law fluid flow and heat transfer is investigated as a control problem considering the problem parameters, such as Hartmann number and the flow

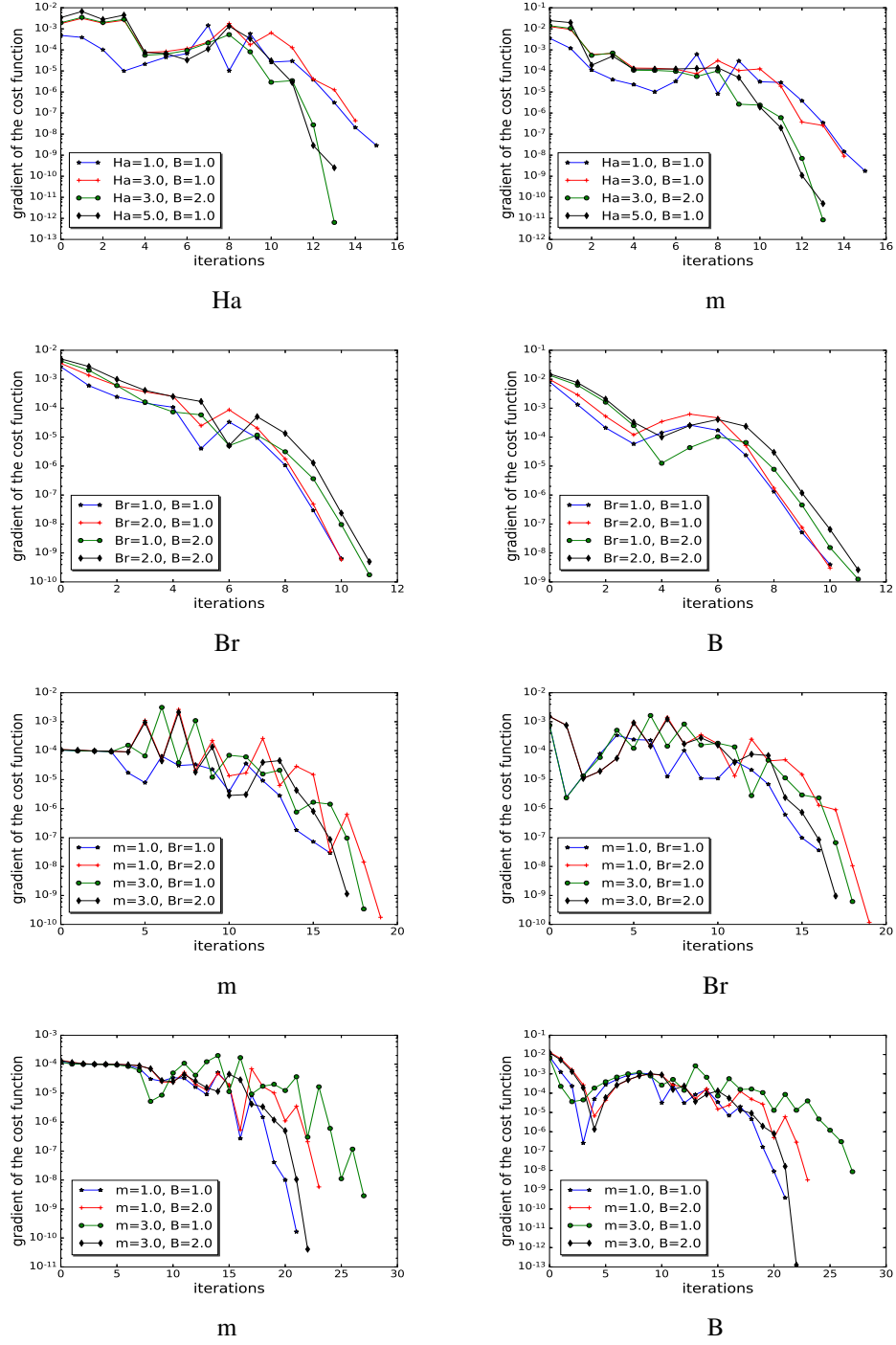


Figure 4.5: Gradient of the objective function during the optimization iterations for the control with pairwise parameters.

Table 4.10: Control with the Hall parameter m and B , $\text{Br} = 1$, $\text{Ha} = 1$, $\alpha_\omega = 10^3$, $\alpha_T = 10^3$, $\alpha_{(m,B)} = 10^{-5}$, $(m^0, B^0) = (10.0, 0.0)$

m_d	B_d	m_{opt}	B_{opt}	$\ \omega_{\text{opt}} - \omega_d\ _\infty$	$\ T_{\text{opt}} - T_d\ _\infty$	J	Tit
1.0	1.0	1.5012	0.8148	1.2745×10^{-3}	7.6907×10^{-4}	3.034×10^{-4}	16
3.0	1.0	1.4884	0.6167	4.6715×10^{-4}	1.4806×10^{-3}	3.180×10^{-5}	22
1.0	2.0	1.2871	1.7006	1.2463×10^{-3}	1.0617×10^{-3}	2.976×10^{-4}	22
3.0	2.0	1.3442	1.5438	4.4036×10^{-4}	1.6208×10^{-3}	4.075×10^{-3}	22

index n as control variables. Apart from the discussion on the parameter control given in the previous problem, idea of optimal control has more crucial effect on power-law fluid flow. Having the flow index n as control variable, it is not only possible to derive the flow to the desired state but it is also possible to identify the flow type: Newtonian or non-Newtonian. Moreover, it enables the classification of the non-Newtonian fluid as shear-thinning or shear-thickening as well.

Firstly, the control variable \mathbf{u} is introduced as the flow index n . Here, the desired states ω_d and T_d are (pre-)computed FEM solutions given the parameters in Table 4.11; particularly the values of n_d are given for the forward problem. In order to reach the desired states for both velocity ω_d and temperature T_d , corresponding regularization parameters $(\alpha_\omega, \alpha_T, \alpha_n)$ in (4.35) have to be chosen. The effect of n is more significant on the velocity magnitude than on the temperature; therefore, the corresponding regularization parameter to regain the desired velocity has to be more pronounced. This is achieved when the regularization parameters are chosen as $(\alpha_\omega, \alpha_T, \alpha_n) = (10^5, 10^0, 10^{-5})$, for instance.

At optimality, the states ω_{opt} , T_{opt} , and the optimal control variable n_{opt} in Table 4.11 indicate that the choice of the regularization parameters is sufficiently suitable so that it successfully controls the states and even ensures that the optimal n_{opt} is close to n_d of the desired flow.

Secondly, the control variable \mathbf{u} is introduced as the Hartmann number Ha , whose control enables to find the optimal electromagnetic force in order to yield a desired fluid flow. As demonstrated in Figure 3.22 and Figure 3.23, heat transfer is too slow with respect to the increment of Ha compared to the change in the magnitude of the velocity. Thus, the regularization parameters are chosen as $(\alpha_\omega, \alpha_T, \alpha_n) = (10^3, 10^0, 10^{-5})$ to impose a large penalization effect on the velocity. As reported in

Table 4.11: Control with n , $\text{Ha} = 1.0$, $\text{Br} = 1.0$, $\alpha_\omega = 10^5$, $\alpha_T = 10^0$, $\alpha_n = 10^{-5}$, and $n_0 = 0.5$

n_d	n_{opt}	$\ \omega_{\text{opt}} - \omega_d\ _\infty$	$\ T_{\text{opt}} - T_d\ _\infty$	J	Tit
0.6	0.5999	3.6768×10^{-6}	2.0850×10^{-6}	5.520×10^{-4}	6
0.8	0.7998	1.4206×10^{-5}	4.6814×10^{-6}	6.370×10^{-3}	5
1.0	0.9997	2.7075×10^{-5}	6.3191×10^{-6}	1.933×10^{-2}	7
1.2	1.1997	4.0722×10^{-5}	7.4407×10^{-6}	3.823×10^{-2}	7
1.5	1.4994	6.0865×10^{-5}	8.5349×10^{-6}	7.365×10^{-2}	5
1.8	1.7991	7.9540×10^{-5}	9.1834×10^{-6}	1.130×10^{-1}	8
2.0	1.9989	9.0956×10^{-5}	9.4505×10^{-6}	1.398×10^{-1}	10

Table 4.12: Control with Ha , $n = 1.5$, $\text{Br} = 1.0$, $\alpha_\omega = 10^3$, $\alpha_T = 10^0$, $\alpha_{\text{Ha}} = 10^{-5}$, and $\text{Ha}_0 = 0.1$

Ha_d	Ha_{opt}	$\ \omega_{\text{opt}} - \omega_d\ _\infty$	$\ T_{\text{opt}} - T_d\ _\infty$	J	Tit
1.0	0.9994	9.6677×10^{-6}	2.4025×10^{-6}	9.931×10^{-6}	3
3.0	2.9982	4.5044×10^{-5}	2.0047×10^{-5}	2.245×10^{-4}	5
5.0	4.9956	6.1726×10^{-5}	6.1227×10^{-5}	4.845×10^{-4}	5
8.0	7.9824	6.9147×10^{-5}	1.3982×10^{-4}	6.027×10^{-4}	7
10.0	9.9491	1.0267×10^{-4}	2.5725×10^{-4}	7.026×10^{-4}	6

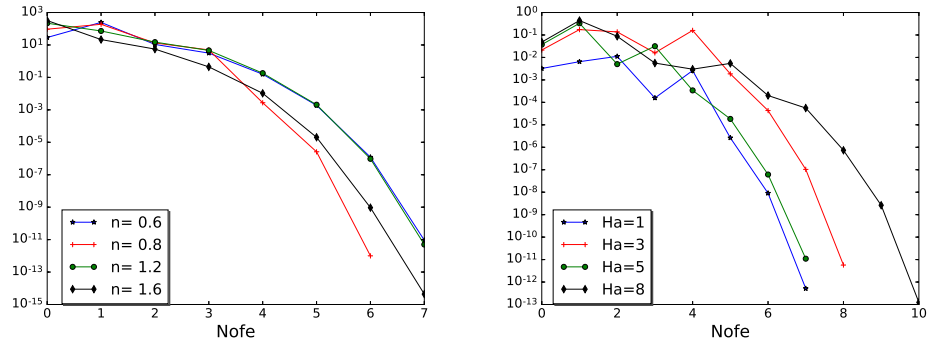
Table 4.12, the desired states of the flow are achieved and the optimal Ha_{opt} is found close to Ha_d even if the initial Ha_0 is chosen far away from Ha_d .

Thirdly, rather than using only one significant parameter, we also seek the optimal control parameters in pairs: a pairwise control is performed by n and Ha , $\mathbf{u} = (n, \text{Ha})$, whose effects counteract on the dynamics of the system. Different scenarios are studied as given in Tables 4.13 for various n and Ha values. In all cases, the controlled optimal states are perfectly matched with the desired states; even the optimal values of $\mathbf{u}_{\text{opt}} = (n_{\text{opt}}, \text{Ha}_{\text{opt}})$ are close to those of the desired states $\mathbf{u}_d = (n_d, \text{Ha}_d)$. However, the cost of achieving optimal control parameters is paid with an increasing number of iterations (Tit) in the optimization (see Table 4.13).

Verification of the controls are provided by the history of the norm of the gradient values versus the number of function evaluations depicted in Figure 4.6 for each of the simulations.

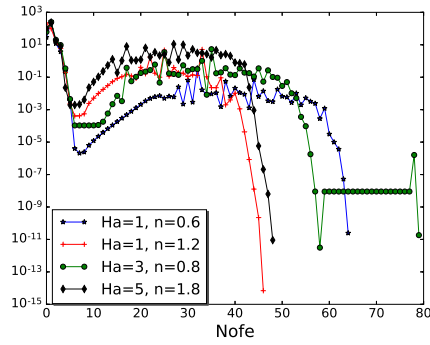
Table 4.13: Control with n and Ha, Br = 1.0, $\alpha_\omega = 10^5$, $\alpha_T = 10^0$, $\alpha_{\text{Ha}} = 10^{-5}$, $\alpha_n = 10^{-5}$, Ha₀ = 0.1 and $n_0 = 0.5$

Ha _d	n_d	n_{opt}	Ha _{opt}	$\ \omega_{\text{opt}} - \omega_d\ _\infty$	$\ T_{\text{opt}} - T_d\ _\infty$	J	Tit
1.0	0.6	0.5988	0.9119	6.1196×10^{-6}	2.6280×10^{-5}	5.043×10^{-4}	53
	0.8	0.8032	1.0961	1.8956×10^{-5}	6.2564×10^{-5}	6.016×10^{-3}	47
	1.0	1.0057	1.0917	3.8514×10^{-5}	8.8894×10^{-5}	1.837×10^{-2}	43
	1.2	1.2078	1.0807	5.6036×10^{-5}	1.0274×10^{-4}	3.646×10^{-2}	40
	1.5	1.5107	1.0679	7.8726×10^{-5}	1.3050×10^{-4}	7.039×10^{-2}	38
	1.8	1.8134	1.0591	9.8521×10^{-5}	1.5060×10^{-4}	1.081×10^{-1}	33
	2.0	2.0151	1.0547	1.1227×10^{-4}	1.6105×10^{-4}	1.338×10^{-1}	30
3.0	0.6	0.5974	2.9251	1.1670×10^{-5}	7.0598×10^{-5}	1.896×10^{-4}	45
	0.8	0.8022	3.0277	1.2439×10^{-5}	5.4969×10^{-5}	2.423×10^{-3}	36
	1.0	1.0039	3.0259	2.6034×10^{-5}	9.7203×10^{-5}	7.040×10^{-3}	36
	1.2	1.2046	3.0196	3.8319×10^{-5}	1.2127×10^{-4}	1.315×10^{-2}	40
	1.5	1.5050	3.0125	6.4596×10^{-5}	1.3772×10^{-4}	2.339×10^{-2}	42
	1.8	1.8049	3.0080	9.2681×10^{-5}	1.4171×10^{-4}	3.338×10^{-2}	39
	2.0	2.0047	3.0060	1.1115×10^{-4}	1.4040×10^{-4}	3.941×10^{-2}	32
5.0	0.6	0.5949	4.8878	2.0484×10^{-5}	1.7541×10^{-4}	1.245×10^{-4}	51
	0.8	0.8005	5.0052	4.0751×10^{-6}	2.1532×10^{-5}	5.901×10^{-4}	45
	1.0	1.0016	5.0081	1.2639×10^{-5}	6.9971×10^{-5}	1.590×10^{-3}	37
	1.2	1.2018	5.0056	2.0973×10^{-5}	8.7427×10^{-5}	2.670×10^{-3}	40
	1.5	1.5017	5.0030	3.0269×10^{-5}	9.2425×10^{-5}	3.879×10^{-3}	36
	1.8	1.8016	5.0019	2.9640×10^{-5}	8.6835×10^{-5}	4.385×10^{-3}	32
	2.0	2.0017	5.0015	2.3644×10^{-5}	7.8796×10^{-5}	4.421×10^{-3}	32



(a)

(b)



(c)

Figure 4.6: Norm of the gradient versus the number of evaluations of the cost function (Nofe): (a) when n is the control parameter and $Ha = 1$; (b) when Ha is the control parameter and $n = 1.5$; (c) when both n and Ha are control parameters. For all cases $Br = 1$.

CHAPTER 5

MODEL ORDER REDUCTION OF OPTIMAL CONTROL PROBLEMS IN FLUID FLOWS

This chapter presents the model order reduction of finite element solutions for the optimal control problems of two-dimensional incompressible viscous Newtonian and non-Newtonian fluid flows. The main goal of this chapter is to contribute to the control of fluid flow problems by the application of the proper orthogonal decomposition (POD) method with a Galerkin projection based on a continuous formulation. Thus, the model reduction technique to be used in the sequel is introduced, firstly. Then, reduced models for the control problems, given in Chapter 4, are investigated.

5.1 Introduction

Numerical solutions of the PDE-constrained optimal control problems require the repeated evaluations of high-fidelity solutions of the state and adjoint equations. These fine-scaled solutions are attained from the discretization of the PDE constraints by some numerical schemes such as finite difference, finite volume or finite elements. They require long computational times due to the large size of the resulting algebraic systems. For example, typical finite element simulations may appeal for hundred of thousands of degrees of freedom. Moreover, computational cost grows extensively within the simulation of the solution at several instants of time of a transient PDE or several values of parameter of a parametrized PDE or combination of both. In order to decrease the cost of such simulations, reduced order modeling has been devised as an efficient way of reducing required computational resources. This approach relies

on the assumption that the characteristics of the system can be described by a small number of dominant modes (global functions) which encode the information of the system in detail.

One of the most powerful and probably the mostly used reduced modeling technique is the proper orthogonal decomposition (POD), which is also named as Karhunen-Loeve expansion or principal component analysis. POD produces a global basis by using the samples of system's trajectories, the so-called 'snapshots' which take pictures of the underlying system's dynamics. These snapshots can be collected from the sample instants of time, parameters or both depending on the problem. However, the possibility of exhibiting linear dependency of the snapshots requires an orthogonalization procedure. This is achieved by applying a singular value decomposition (SVD) and selecting left singular vectors corresponding to the leading singular values as POD basis functions. Then, this 'intelligent basis' is used to establish an approximate solution by applying a projection. Due to this projection, high-dimensional system of equations are replaced with a very low-dimensional one, which enables the repetitive evaluation of the solution of reduced PDEs with a relatively small computational cost.

The discretization stage of the model order reduction is an important subject in terms of obtaining ROM. Usually, studies follow the *discretize-then-reduce* approach, where the full order model (FOM) is discretized first then the Galerkin-projection is performed on the discrete setting. In contrast, it is also possible to carry out projection in continuous formulation, in other words, projection is attained on the weak form of the problem using the POD basis first, then the discretization is followed. This approach can be called as the *reduce-then-discretize*. Although both approaches lead to the same reduced order model (ROM), the latter provides a user-friendly setting for the implementation in the automated framework used in this thesis.

When the PDE solver environment works on the variational form of the PDEs, development of the ROM in the weak form is also applicable and does not require the user-defined discretization of the FOM. Hence, the automated optimization framework (dolfin-adjoint), which uses algorithmic differentiation to derive adjoint models, also becomes adaptable to work with the ROM without requiring any extra cost

of user's discretization. Consequently, the reduced optimal control problem can be represented in a continuous environment and solved automatically. By this approach, a user-friendly solution of the reduced optimal control problem is proposed. Even if it does not provide a computational efficiency or advantages over the former approach, it proposes a simpler and more trivial way of construction for the ROM.

The literature of the MOR with POD for reducing computing resources are summarized as follows.

The idea of low dimensional approximations for coherent structures of turbulent flows have been introduced by Lumley [67, 68]. Lumley has stated that the velocity correlations can be orthogonally decomposed and called as the proper orthogonal expansion. It has been also called as the Karhunen-Loeve expansion by Fukunaga [26] in pattern recognition or the principal component analysis by Nasir [2] in statistics. Later, Sirovich has also discussed the methodology in detail for supporting its usefulness in a series of studies [82, 83, 84]. The subject has attracted the attention of many scientists and illustrative results have been proposed. The analysis of a large eddy simulation of axisymmetric jet flow by the snapshots has conducted by Kirby [55]. Christensen et al [17] has used the POD based on snapshots generated from a finite-difference algorithm for the axisymmetric Navier-Stokes equations. More recently, error estimates for Galerkin POD methods for linear and certain non-linear parabolic systems have been proved by Kunisch and Volkwein [59, 60]. They have also proposed a strategy for the application of POD on the optimality systems, so-called OS-POD in [61]. Specifically, applications of MOR on problems of fluid dynamics have been reviewed in [63].

In terms of the parameter dependent systems, a reduced basis method has been proposed by Ito and Ravindran [52] for simulation and control of viscous flows. Christensen et al. [18] have derived the residual functions to measure the quality of the reduced systems by allowing to weight the snapshots according to the effects of the parameters. Reduced basis approximation for affinely parametrized elliptic PDEs have been studied by Rozza et al. [79]. Certified rapid solution for real-time parameter estimation has been given by Grepl et al. [33]. Dede has given the posteriori error estimates for parametrized linear-quadratic optimal control problems in [20].

Moreover, Chappelle et al. have addressed the issue of parameter variations in POD approximations of time-dependent problems in [14].

Since the POD does not fully reduce the dimension of the problems having nonlinearities, some other variants of applications for the POD are developed such as empirical interpolation method (EIM) [9] or the discrete empirical interpolation method (DEIM) [15]. These methods determine some interpolation points on the domain, where the dynamics of the system is mostly carried, either before the projection (EIM) or after the projection (DEIM). After all, they have to deal with the grid points of the domain for the evaluation of the interpolation.

However, in this study, since we do not aim to work on the discrete settings of the problems, the main concern is to implement the POD method in a user-friendly setting. We will discuss the main steps of POD as well as its properties and applications later in the next section.

5.2 Proper Orthogonal Decomposition (POD)

In this section, the detailed procedure of the POD based model reduction is presented by focusing on the general form of the steady parametrized PDEs with the parameter vector $\nu \in \mathcal{D} \subset \mathbb{R}^p$ which describes the physical properties of the system. Thus, the system of equations given in (3.1) takes the following form

$$C(z(\vec{x}, \nu)) = 0, \quad \vec{x} \in \Omega \subset \mathbb{R}^n, \quad \nu \in \mathcal{D} \subset \mathbb{R}^p. \quad (5.1)$$

Main stages of the POD application consist of the collection of snapshots, generation of the POD basis and the projection. Collection of snapshots is composed from the high-fidelity FEM solutions of (5.1) obtained in Chapter 3 and constitutes the snapshot matrix with columns representing solutions for several values of the parameter(s). In order to motivate second stage, some basic definitions are introduced for clarification.

Let $\mathbf{Z} = [\mathbf{z}_1, \dots, \mathbf{z}_\mu]$ be a real valued $\beta \times \mu$ dimensional snapshot matrix of rank e ,

where each column represents coefficients in the FEM approximations so that

$$z_i = \sum_{k=1}^{\beta} z_i^k \phi_k \text{ with } z_i^k = \langle z_i, \phi_k \rangle, \mathbf{z}_i = (z_i^k).$$

The inner product for the space of square integrable functions leads to the definition of a weighted inner product for FEM approximations as follows:

$$\begin{aligned} \langle z_i, z_j \rangle_{L^2(\Omega)} &= \int_{\Omega} z_i z_j d\Omega \\ &= \int_{\Omega} \left(\sum_{k=1}^{\beta} z_i^k \phi_k \right) \left(\sum_{l=1}^{\beta} z_j^l \phi_l \right) d\Omega \\ &= \mathbf{z}_i^T \mathbf{W} \mathbf{z}_j \\ &= \langle \mathbf{z}_i, \mathbf{z}_j \rangle_W, \end{aligned}$$

where $\mathbf{W} = (W_{kl})$ is the weight matrix with components $W_{kl} = \int_{\Omega} \phi_l \phi_k d\Omega$ representing the symmetric positive definite mass matrix of the corresponding finite element basis functions. Then, considering the matrix $\bar{\mathbf{Z}} = \mathbf{W}^{1/2} \mathbf{Z}$, the Singular Value Decomposition (SVD) of $\bar{\mathbf{Z}}$ guarantees the existence of real numbers $\sigma_1 \geq \sigma_2 \geq \dots \geq \sigma_e > 0$ and orthogonal matrices $\bar{\mathbf{\Upsilon}} \in \mathbb{R}^{\beta \times \beta}$ with columns $\{\bar{\mathbf{v}}_i\}_{i=1}^{\beta}$ and $\bar{\mathbf{\Pi}} \in \mathbb{R}^{\mu \times \mu}$ with columns $\{\bar{\boldsymbol{\pi}}_i\}_{i=1}^{\mu}$ such that

$$\bar{\mathbf{\Upsilon}}^T \bar{\mathbf{Z}} \bar{\mathbf{\Pi}} = \begin{pmatrix} \mathbf{D} & \mathbf{0} \\ \mathbf{0} & \mathbf{0} \end{pmatrix} =: \boldsymbol{\Sigma} \in \mathbb{R}^{\beta \times \mu},$$

where $\mathbf{D} = \text{diag}(\sigma_1, \dots, \sigma_e) \in \mathbb{R}^{e \times e}$. Moreover, the set of vectors $\{\bar{\mathbf{v}}_i\}_{i=1}^e$ and $\{\bar{\boldsymbol{\pi}}_i\}_{i=1}^e$ are left and right singular vectors of $\bar{\mathbf{Z}}$ corresponding to its non-zero singular values and they are also eigenvectors of $\bar{\mathbf{Z}} \bar{\mathbf{Z}}^T$ and $\bar{\mathbf{Z}}^T \bar{\mathbf{Z}}$, respectively, satisfying

$$\bar{\mathbf{Z}} \bar{\boldsymbol{\pi}}_i = \sigma_i \bar{\mathbf{v}}_i \quad \text{and} \quad \bar{\mathbf{Z}}^T \bar{\mathbf{v}}_i = \sigma_i \bar{\boldsymbol{\pi}}_i$$

for $i = 1, \dots, e$. So that, the reduced SVD of $\bar{\mathbf{Z}}$ is given as

$$\bar{\mathbf{Z}} = \bar{\mathbf{\Upsilon}}^e \mathbf{D} (\bar{\mathbf{\Pi}}^e)^T,$$

where $\bar{\mathbf{\Upsilon}}^e = (\bar{\mathbf{v}}_i)_{i=1}^e$ and $\bar{\mathbf{\Pi}}^e = (\bar{\boldsymbol{\pi}}_i)_{i=1}^e$. Alternatively, it can also be written as $\bar{\mathbf{Z}} = \bar{\mathbf{\Upsilon}}^e \bar{\mathbf{B}}^e$ with $\bar{\mathbf{B}}^e = \mathbf{D} (\bar{\mathbf{\Pi}}^e)^T \in \mathbb{R}^{e \times \mu}$ so that the column space of $\bar{\mathbf{Z}}$ can be

represented in terms of $\bar{\Upsilon}^e$. Moreover, orthogonality of $\bar{\Upsilon}$ indicates that

$$\begin{aligned}
\bar{\mathbf{z}}_j &= \sum_{i=1}^e \bar{\mathbf{B}}_{ij}^e \bar{\Upsilon}_i = \sum_{i=1}^e \left(\mathbf{D} (\bar{\Pi}^e)^T \right)_{ij} \bar{\Upsilon}_i \\
&= \sum_{i=1}^e \left((\bar{\Upsilon}^e)^T \bar{\Upsilon}^e \mathbf{D} (\bar{\Pi}^e)^T \right)_{ij} \bar{\Upsilon}_i \\
&= \sum_{i=1}^e \left((\bar{\Upsilon}^e)^T \bar{\mathbf{Z}} \right)_{ij} \bar{\Upsilon}_i \\
&= \sum_{i=1}^e \left(\sum_{k=1}^{\beta} \bar{\Upsilon}_{ki}^e \bar{\mathbf{z}}_{kj} \right) \bar{\Upsilon}_i = \sum_{i=1}^e \langle \bar{\Upsilon}_i, \bar{\mathbf{z}}_j \rangle_{\mathbb{R}^{\beta}} \bar{\Upsilon}_i.
\end{aligned}$$

Knowing $\bar{\mathbf{z}}_j = \mathbf{W}^{1/2} \mathbf{z}_j$ and $\bar{\Upsilon}_i = \mathbf{W}^{1/2} \Upsilon_i$, the following relation is obtained

$$\mathbf{z}_j = \sum_{i=1}^e \langle \mathbf{z}_j, \Upsilon_i \rangle_{\mathbf{W}} \Upsilon_i,$$

which asserts that the high-fidelity solutions collected as the columns \mathbf{z}_j of the matrix \mathbf{Z} can be written as linear combination of the left singular vectors of the matrix $\bar{\mathbf{Z}}$. This result states the importance of SVD as an orthogonal basis selection and can be summarized in the following theorem.

Theorem 1 (Theorem 1.3.2 [99]). *Let $\mathbf{Z} \in \mathbb{R}^{\beta \times \mu}$ be a given matrix with rank $e \leq \min\{\beta, \mu\}$, \mathbf{W} be a symmetric, positive definite matrix, $\bar{\mathbf{Z}} = \mathbf{W}^{1/2} \mathbf{Z}$ and $l \in \{1, \dots, e\}$. Further, let $\bar{\mathbf{Z}} = \bar{\Upsilon}^T \Sigma \bar{\Pi}$ be the singular value decomposition of $\bar{\mathbf{Z}}$, where $\bar{\Upsilon} = [\bar{\mathbf{v}}_1, \dots, \bar{\mathbf{v}}_{\beta}] \in \mathbb{R}^{\beta \times \beta}$, $\bar{\Pi} = [\bar{\pi}_1, \dots, \bar{\pi}_{\mu}] \in \mathbb{R}^{\mu \times \mu}$ are orthogonal matrices and the matrix Σ has the form*

$$\bar{\Upsilon}^T \bar{\mathbf{Z}} \bar{\Pi} = \begin{pmatrix} \mathbf{D} & \mathbf{0} \\ \mathbf{0} & \mathbf{0} \end{pmatrix} =: \Sigma \in \mathbb{R}^{\beta \times \mu}.$$

Then the solution to

$$(\mathbf{P}_{\mathbf{W}}^l) \quad \max_{\tilde{\mathbf{v}}_1, \dots, \tilde{\mathbf{v}}_l \in \mathbb{R}^{\beta}} \sum_{i=1}^l \sum_{j=1}^{\mu} \left\| \langle \mathbf{z}_j, \tilde{\mathbf{v}}_i \rangle_{\mathbf{W}} \right\|_{\mathbb{R}^{\beta}}^2 \quad \text{s.t.} \quad \langle \tilde{\mathbf{v}}_i, \tilde{\mathbf{v}}_j \rangle = \delta_{ij} \quad \text{for } 1 \leq i, j \leq l$$

is given by the vectors $\mathbf{v}_i = \mathbf{W}^{-1/2} \bar{\mathbf{v}}_i$, $i = 1, \dots, l$. Moreover,

$$\text{argmax}(\mathbf{P}_{\mathbf{W}}^l) = \sum_{i=1}^l \sigma_i^2 = \sum_{i=1}^l \tau_i.$$

The detailed proof can be found in [99].

In the light of above theorem, it becomes clear that the vectors $\{\mathbf{v}_i\}_{i=1}^\gamma$ for $\gamma \in \{1, \dots, \mu\}$ are named as POD basis of rank γ . Also, the theorem reveals the optimality of this basis in the mean among all rank γ approximations to the columns of \mathbf{Z} . For the choice of γ following remark becomes crucial.

Remark 1. *The determination of the size of the reduced basis is also crucial part in POD. This selection is performed according to an energy criterion given as*

$$\varepsilon_{POD}(\gamma) = \frac{\sum_{i=1}^\gamma \tau_i}{\sum_{i=1}^n \tau_i}.$$

Hence, γ is chosen to be the minimum integer satisfying

$$\varepsilon_{POD}(\gamma) \geq \varepsilon_{tol},$$

for a given tolerance, $0 < \varepsilon_{tol} \leq 1$.

The procedure for the generation of the POD basis is summarized in Algorithm 3, which constitutes the second stage of the process of reducing model order.

Algorithm 3 POD basis of rank e with a weighted inner product

- 1: **procedure** POD($\{\mathbf{z}_i\}_{i=1}^\mu \subset \mathbb{R}^\beta$, $\mathbf{W} \in \mathbb{R}^{\beta \times \beta}$)
 - 2: Set $\mathbf{Z} = [\mathbf{z}_1, \dots, \mathbf{z}_\mu] \in \mathbb{R}^{\beta \times \mu}$;
 - 3: Determine $\bar{\mathbf{Z}} = \mathbf{W}^{1/2} \mathbf{Z}$;
 - 4: Compute singular value decomposition $[\bar{\mathbf{\Upsilon}}, \mathbf{\Sigma}, \bar{\mathbf{\Pi}}] = \text{svd}(\bar{\mathbf{Z}})$;
 - 5: Set $v_i = \mathbf{W}^{-1/2} \bar{\mathbf{\Upsilon}}_{:,i} \in \mathbb{R}^\beta$ and $\tau_i = \mathbf{\Sigma}_{ii}^2$ for $i = 1, \dots, e$;
 - 6: Compute the energy criterion $\varepsilon(e)_{POD} = \frac{\sum_{i=1}^e \tau_i}{\sum_{i=1}^d \tau_i}$;
 - 7: **return** POD basis $\{v_i\}_{i=1}^e$, eigenvalues $\{\tau_i\}_{i=1}^e$ and ratio $\varepsilon(e)_{POD}$.
 - 8: **end procedure**
-

Finally, at the last stage, the solution of the PDE system is projected in a low-dimensional space spanned by the set of POD basis functions. Recalling the Galerkin projection, method of weighted residual form in (3.5) is reproduced by the POD basis $\{v_i\}_{i=1}^\gamma$ to find the reduced solution vector $\tilde{\mathbf{z}} = (\tilde{z}_i)$:

$$\left\langle v_j, C \left(\sum_{i=1}^\gamma \tilde{z}_i v_i \right) \right\rangle = 0, \quad (5.2)$$

which results in the reduced system of equations.

In the next section, Section 5.3, reduced order modeling is applied for the FEM solutions of the distributed control of Navier-Stokes equations using POD method. Then, the same approach is used for the FEM solutions of the parameter control of the MHD flow and the heat transfer equations with temperature-dependent viscosity and also power-law fluid flow in Section 5.4 and in Section 5.5, respectively. Results of the numerical simulations and analyses are presented in Section 5.6 for the comparison of FOM and ROM solutions of three problems.

5.3 Reduced Model for Distributed Control of Navier-Stokes Equations

The reduced model of the FEM solutions of the Navier-Stokes equations is established as a steady parametrized PDEs in terms of both velocity and pressure variables. Having obtained the high-fidelity solutions in Section 3.2, POD bases are generated by the help of Algorithm 3. Then, projection onto the low-dimensional space is conducted for the control problem as wells as the PDEs.

Let $\{\vec{\xi}_j\}_{j=1}^{\gamma_v}$ and $\{\theta_l\}_{l=1}^{\gamma_p}$ be the POD basis functions for the velocity and pressure functions so that

$$\vec{v} \approx \sum_{j=1}^{\gamma_v} \tilde{v}_j \vec{\xi}_j \quad \text{and} \quad \tilde{p} \approx \sum_{l=1}^{\gamma_p} \tilde{p}_l \theta_l, \quad (5.3)$$

where \tilde{v}_j and \tilde{p}_l are the components of the vectors $\tilde{\mathbf{v}}$ and $\tilde{\mathbf{p}}$. It is also noted that the function \vec{f} and \vec{u} have to be approximated in the reduced space, which is spanned by the POD basis. These approximations can be written as follows:

$$\vec{f} \approx \sum_{j=1}^{\gamma_v} \tilde{f}_j \vec{\xi}_j \quad \text{with} \quad \tilde{f}_j = \int_{\Omega} \vec{f} \cdot \vec{\xi}_j d\Omega, \quad (5.4)$$

and

$$\vec{u} \approx \sum_{j=1}^{\gamma_v} \tilde{u}_j \vec{\xi}_j \quad \text{with} \quad \tilde{u}_j = \int_{\Omega} \vec{u} \cdot \vec{\xi}_j d\Omega.$$

Then, following the idea of Galerkin, test functions $(\vec{\vartheta}, \rho)$ are chosen the same as the POD basis functions and the weak formulation of the equations in (4.12)–(4.14)

becomes

$$\begin{aligned} \left\langle \nu \nabla \tilde{\vec{v}}, \nabla \tilde{\vec{v}} \right\rangle_{\Omega} + \left\langle \left(\tilde{\vec{v}} \cdot \nabla \right) \tilde{\vec{v}}, \tilde{\vec{v}} \right\rangle_{\Omega} - \left\langle \tilde{p}, \nabla \cdot \tilde{\vec{v}} \right\rangle_{\Omega} \\ - \left\langle \tilde{\vec{f}}, \tilde{\vec{v}} \right\rangle_{\Omega} - \left\langle \tilde{\vec{u}}, \tilde{\vec{v}} \right\rangle_{\Omega} = 0, \end{aligned} \quad (5.5)$$

$$\left\langle \nabla \cdot \tilde{\vec{v}}, \rho \right\rangle_{\Omega} = 0, \quad (5.6)$$

where the boundary integrals vanish. This is due to the fact that POD basis generated from the solutions vanishing on the boundary.

Thus, substitution of the reduced approximations in (5.3) and (5.4) into the equations (5.5) and (5.6) leads to

$$\begin{aligned} \left\langle \nu \nabla \sum_{j=1}^{\gamma_v} \tilde{\vec{v}}_j \vec{\xi}_j, \nabla \vec{\xi}_i \right\rangle_{\Omega} + \left\langle \left(\sum_{j=1}^{\gamma_v} \tilde{\vec{v}}_j \vec{\xi}_j \cdot \nabla \right) \sum_{j=1}^{\gamma_v} \tilde{\vec{v}}_j \vec{\xi}_j, \vec{\xi}_i \right\rangle_{\Omega} \\ - \left\langle \sum_{l=1}^{\gamma_p} \tilde{p}_l \theta_l, \nabla \cdot \vec{\xi}_i \right\rangle_{\Omega} - \left\langle \sum_{j=1}^{\gamma_v} \tilde{\vec{f}}_j \vec{\xi}_j, \vec{\xi}_i \right\rangle_{\Omega} = 0, \\ \left\langle \nabla \cdot \sum_{j=1}^{\gamma_v} \tilde{\vec{v}}_j \vec{\xi}_j, \theta_k \right\rangle_{\Omega} = 0 \end{aligned}$$

for any integers i and j in $\{1, 2, \dots, \gamma_v\}$ and k and l in $\{1, 2, \dots, \gamma_p\}$. In order to obtain the reduced algebraic form of the problem, introducing the components of the reduced matrices and the vectors is necessary: Let $\tilde{\mathbf{M}} = (\tilde{M}_{ij})$, $\tilde{\mathbf{K}} = (\tilde{K}_{ij})$, $\tilde{\mathbf{D}} = (\tilde{D}_{ik})$, and $\tilde{\mathbf{N}}(\tilde{\mathbf{v}})$ denote the reduced matrices whose entries are

$$\begin{aligned} \tilde{M}_{ij} &= \int_{\Omega} \vec{\xi}_j \cdot \vec{\xi}_i \, d\Omega, \\ \tilde{K}_{ij} &= \nu \int_{\Omega} \nabla \vec{\xi}_j : \nabla \vec{\xi}_i \, d\Omega, \\ \tilde{D}_{ik} &= - \int_{\Omega} \theta_k \left(\nabla \cdot \vec{\xi}_i \right) \, d\Omega, \\ \tilde{N}(\tilde{\mathbf{v}})_{ij} &= \sum_{r=1}^{\gamma_v} \int_{\Omega} (\tilde{v}_r \vec{\xi}_r \cdot \nabla) \vec{\xi}_j \cdot \vec{\xi}_i \, d\Omega \end{aligned}$$

for i and j in $\{1, 2, \dots, \gamma_v\}$ and k and l in $\{1, 2, \dots, \gamma_p\}$. In fact, these matrices can also be derived from the discretized full order model in the *discretize-then-reduce* approach via the use of

$$\tilde{\mathbf{M}} = \Upsilon_v^T \mathbf{M} \Upsilon_v,$$

where columns of the matrix Υ_v are the POD basis vectors of the velocity and \mathbf{M} is the corresponding mass matrix of the full order model.

Nevertheless, the algebraic form of the discrete reduced non-linear problem reads:

$$\begin{bmatrix} \tilde{\mathbf{K}} + \tilde{\mathbf{N}}(\tilde{\mathbf{v}}) & \tilde{\mathbf{D}} \\ \tilde{\mathbf{D}}^T & \mathbf{0} \end{bmatrix} \begin{bmatrix} \tilde{\mathbf{v}} \\ \tilde{\mathbf{p}} \end{bmatrix} = \begin{bmatrix} \tilde{\mathbf{M}}(\tilde{\mathbf{f}} + \tilde{\mathbf{u}}) \\ \mathbf{0} \end{bmatrix}, \quad (5.7)$$

which stands for the reduced formulation of (3.11). The treatment for the boundary evaluation of the pressure follows the idea in Section 3.2 and POD basis generation is maintained for the Lagrange multiplier c as well. Thus, the reduced non-linear system in (5.7) turns into

$$\begin{bmatrix} \tilde{\mathbf{K}} + \tilde{\mathbf{N}}(\tilde{\mathbf{v}}) & \tilde{\mathbf{D}} & \mathbf{0} \\ \tilde{\mathbf{D}}^T & \mathbf{0} & \tilde{\mathbf{r}}^T \\ \mathbf{0} & \tilde{\mathbf{r}} & 0 \end{bmatrix} \begin{bmatrix} \tilde{\mathbf{v}} \\ \tilde{\mathbf{p}} \\ \tilde{\mathbf{c}} \end{bmatrix} = \begin{bmatrix} \tilde{\mathbf{M}}(\tilde{\mathbf{f}} + \tilde{\mathbf{u}}) \\ \mathbf{0} \\ 0 \end{bmatrix}, \quad (5.8)$$

where $\tilde{r}_k = \int_{\Omega} \tilde{d} \theta_k d\Omega$ for $1 \leq k \leq \gamma_p$ are the components of $\tilde{\mathbf{r}}$, and \tilde{d} is the POD basis for the Lagrange multiplier. Hence, the reduced problem simply becomes:

$$\text{solve } \tilde{\mathbf{C}}(\tilde{\mathbf{z}}, \tilde{\mathbf{u}}) = 0 \quad \text{for } \tilde{\mathbf{z}} = (\tilde{\mathbf{v}}, \tilde{\mathbf{p}}, \tilde{\mathbf{c}})^T, \quad (5.9)$$

where $\tilde{\mathbf{C}}(\tilde{\mathbf{z}}, \tilde{\mathbf{u}})$ is the reduced discrete non-linear system of N-S equations. Solution of (5.9) is carried out using Newton's method and this procedure may be named as *reduce-then-discretize-then-linearize*.

Meanwhile, the reduced objective function formulated with the POD basis leads to the discrete form

$$\mathbf{J}^R(\tilde{\mathbf{z}}, \tilde{\mathbf{u}}) = \frac{\alpha_v}{2} (\tilde{\mathbf{v}} - \tilde{\mathbf{v}}_d)^T \tilde{\mathbf{M}} (\tilde{\mathbf{v}} - \tilde{\mathbf{v}}_d) + \frac{\alpha_u}{2} \tilde{\mathbf{u}}^T \tilde{\mathbf{M}} \tilde{\mathbf{u}}$$

so that the reduced discretized optimal control problem takes the form

$$\begin{aligned} & \underset{\tilde{\mathbf{u}}}{\text{minimize}} \quad \mathbf{J}^R(\tilde{\mathbf{z}}, \tilde{\mathbf{u}}) \\ & \text{subject to} \quad \tilde{\mathbf{C}}(\tilde{\mathbf{z}}, \tilde{\mathbf{u}}) = 0. \end{aligned}$$

Furthermore, the same procedure with the FOM is carried out for the ROM of control problem as well and the discrete adjoint equations are derived as follows

$$\tilde{\mathbf{C}}_{\tilde{\mathbf{z}}}^*(\tilde{\mathbf{z}}(\tilde{\mathbf{u}}), \mathbf{u}) \tilde{\boldsymbol{\Lambda}} = -\mathbf{J}_{\tilde{\mathbf{z}}}^R(\tilde{\mathbf{z}}(\mathbf{u}), \mathbf{u}), \quad (5.10)$$

where

$$\begin{bmatrix} \tilde{\mathbf{K}}^T + \tilde{\mathbf{N}}^T(\tilde{\mathbf{v}}) & \tilde{\mathbf{D}} & \mathbf{0} \\ \tilde{\mathbf{D}}^T & \mathbf{0} & \tilde{\mathbf{r}}^T \\ \mathbf{0} & \tilde{\mathbf{r}} & 0 \end{bmatrix} \begin{bmatrix} \tilde{\boldsymbol{\lambda}} \\ \tilde{\boldsymbol{\eta}} \\ \tilde{\mathbf{e}} \end{bmatrix} = \begin{bmatrix} -\alpha_v \tilde{\mathbf{M}}(\tilde{\mathbf{v}} - \tilde{\mathbf{v}}_d) \\ \mathbf{0} \\ 0 \end{bmatrix}, \quad (5.11)$$

has to be solved for the reduced adjoint variable $\tilde{\Lambda} = (\tilde{\lambda}, \tilde{\eta}, \tilde{e})$. Herewith, the optimization algorithm, L-BFGS, given in Section 4.2 is carried out again, but now for a very low-dimensional system of equations.

5.4 Reduced Model for Parameter Control of MHD Flow and Heat Transfer with Temperature Dependent Viscosity

Here in this section we analyze the reduced order modeling of the FEM solutions of the MHD flow and heat transfer with temperature dependent viscosity as a steady parametrized PDEs. Pursuing Algorithm 3 and using the fine-scaled solutions obtained in Section 3.3, POD bases of the velocity and temperature variables are constructed. Then, control problem as well as the PDE constraints are projected to the space spanned by these POD basis functions.

The ROM approximation $\tilde{z} = (\tilde{\omega}, \tilde{T})$ of the solution (ω, T) can be written as

$$\tilde{\omega} = \sum_{j=1}^{\gamma_{\omega}} \tilde{\omega}_j \xi_j \quad \text{and} \quad \tilde{T} = \sum_{l=1}^{\gamma_T} \tilde{T}_l \theta_l, \quad (5.12)$$

where $\{\xi_j\}_{j=1}^{\gamma_{\omega}}$ and $\{\theta_l\}_{l=1}^{\gamma_T}$ are the POD basis functions for ω and T , respectively. Reduced variational formulation is found by writing the forms in (3.18)–(3.19) by using the POD basis functions as test functions, namely ϑ and ρ ; this yields

$$\langle \tilde{\mu} \nabla \tilde{\omega}, \nabla \vartheta \rangle_{\Omega} - \left\langle 1 - \frac{\text{Ha}^2}{1 + m^2} \tilde{\omega}, \vartheta \right\rangle_{\Omega} = 0, \quad (5.13)$$

$$\begin{aligned} \langle \nabla \tilde{T}, \nabla \rho \rangle_{\Omega} - \left\langle \text{Br} \tilde{\mu} \left[\left(\frac{\partial \tilde{\omega}}{\partial x} \right)^2 + \left(\frac{\partial \tilde{\omega}}{\partial y} \right)^2 \right], \rho \right\rangle_{\Omega} \\ - \left(\frac{\text{Ha}^2 \text{Br}}{1 + m^2} \right) \langle \tilde{\omega}^2, \rho \rangle_{\Omega} + \left\langle \frac{\tilde{\omega}}{\tilde{\omega}_m}, \rho \right\rangle_{\Omega} = 0, \end{aligned} \quad (5.14)$$

where $\tilde{\mu}$ is the reduced variable viscosity, and

$$\tilde{\mu} = e^{-B\tilde{T}} \approx \sum_{l=1}^{\gamma_T} e^{-B\tilde{T}_l} \theta_l.$$

Since it is temperature dependent viscosity, it is approximated by the POD basis of temperature.

It is notable that POD basis generated from the snapshots having homogeneous Dirichlet boundary condition vanishes on the boundary; and hence, the boundary integrals become zero as in the FOM model by FEM basis.

Substituting the low-dimensional approximations in (5.12) into the equations (5.13)-(5.14) results in

$$\begin{aligned} & \left\langle \tilde{\mu} \sum_{j=1}^{\gamma_\omega} \tilde{\omega}_j \nabla \xi_j, \nabla \xi_i \right\rangle_\Omega - \left\langle 1 - \frac{\text{Ha}^2}{1+m^2} \sum_{j=1}^{\gamma_\omega} \tilde{\omega}_j \xi_j, \xi_i \right\rangle_\Omega = 0, \\ & \left\langle \sum_{l=1}^{\gamma_T} \tilde{T}_l \nabla \theta_l, \nabla \theta_k \right\rangle_\Omega - \left\langle \text{Br} \tilde{\mu} \left[\left(\sum_{j=1}^{\gamma_\omega} \tilde{\omega}_j \nabla \xi_j \right) \cdot \left(\sum_{j=1}^{\gamma_\omega} \tilde{\omega}_j \nabla \xi_j \right) \right], \theta_k \right\rangle_\Omega \\ & - \left(\frac{\text{Ha}^2 \text{Br}}{1+m^2} \right) \left\langle \left(\sum_{j=1}^{\gamma_\omega} \tilde{\omega}_j \xi_j \right)^2, \theta_k \right\rangle_\Omega + \left\langle \frac{1}{\tilde{\omega}_m} \sum_{j=1}^{\gamma_\omega} \tilde{\omega}_j \xi_j, \theta_k \right\rangle_\Omega = 0 \end{aligned}$$

for i and j in $\{1, 2, \dots, \gamma_\omega\}$ and k and l in $\{1, 2, \dots, \gamma_T\}$. Before giving the reduced form of the discrete algebraic problem, components of the reduced vector and matrices, namely, $\tilde{\mathbf{d}} = (\tilde{d}_i)$, $\tilde{\mathbf{M}} = (\tilde{M}_{ij})$ and $\tilde{\mathbf{S}} = (\tilde{S}_{kl})$ are introduced as follows:

$$\begin{aligned} \tilde{d}_i &= \int_\Omega \xi_i d\Omega, \quad 1 \leq i \leq \gamma_\omega, \\ \tilde{M}_{ij} &= \int_\Omega \xi_j \xi_i d\Omega \quad 1 \leq i, j \leq \gamma_\omega, \\ \tilde{S}_{kl} &= \int_\Omega \nabla \theta_l \nabla \theta_k d\Omega \quad 1 \leq k, l \leq \gamma_T. \end{aligned}$$

Furthermore, the non-linear terms $\tilde{\mathbf{K}}(\tilde{\mathbf{T}})$, $\tilde{\mathbf{D}}(\tilde{\omega}, \tilde{\mathbf{T}})$, $\tilde{\mathbf{N}}(\tilde{\omega})$ and $\tilde{\mathbf{P}}(\tilde{\omega})$ have the entries defined by

$$\begin{aligned} \tilde{K}(\tilde{\mathbf{T}})_{ij} &= \sum_{r=1}^{\gamma_T} e^{-B\tilde{T}_r} \int_\Omega \theta_r \nabla \xi_j \nabla \xi_i d\Omega, \\ \tilde{D}(\tilde{\omega}, \tilde{\mathbf{T}})_{kj} &= \sum_{r=1}^{\gamma_T} e^{-B\tilde{T}_r} \omega_j \int_\Omega \theta_r \left(\frac{\partial \xi_j}{\partial x} + \frac{\partial \xi_j}{\partial y} \right) \theta_k d\Omega, \\ \tilde{N}(\tilde{\omega})_{kj} &= \int_\Omega \tilde{\omega}_j \xi_j \theta_k d\Omega, \\ \tilde{P}(\tilde{\omega})_{kj} &= \frac{\int_\Omega \xi_j \theta_k d\Omega}{\frac{1}{L} \int_\Omega (\sum_{l=1}^{\gamma_\omega} \tilde{\omega}_l \xi_l) d\Omega}, \end{aligned}$$

for i and j in $\{1, 2, \dots, \gamma_\omega\}$ and k in $\{1, 2, \dots, \gamma_T\}$.

Alternatively, projection can be performed on the discretized FOM by the substitution of the discrete approximation formulas,

$$\omega = \Upsilon_\omega \tilde{\omega} \quad \text{and} \quad \mathbf{T} = \Upsilon_T \tilde{\mathbf{T}}, \quad (5.15)$$

where Υ_ω and Υ_T are the POD basis matrices having columns as basis coefficients of the velocity and the temperature, respectively. Therefore, the algebraic form of the discrete problem in reduced form is then formulated as

$$\begin{bmatrix} c_1 \tilde{\mathbf{M}} & \mathbf{0} \\ \mathbf{0} & \tilde{\mathbf{S}} \end{bmatrix} \begin{bmatrix} \tilde{\boldsymbol{\omega}} \\ \tilde{\mathbf{T}} \end{bmatrix} + \begin{bmatrix} \tilde{\mathbf{K}}(\tilde{\mathbf{T}})\tilde{\boldsymbol{\omega}} - \tilde{\mathbf{d}} \\ c_2 \tilde{\mathbf{N}}(\tilde{\boldsymbol{\omega}})\tilde{\boldsymbol{\omega}} - \text{Br}\tilde{\mathbf{D}}(\tilde{\boldsymbol{\omega}}, \tilde{\mathbf{T}})\tilde{\boldsymbol{\omega}} + \tilde{\mathbf{P}}(\tilde{\boldsymbol{\omega}})\tilde{\boldsymbol{\omega}} \end{bmatrix} = \mathbf{0}.$$

As a result, the reduced problem given by discrete non-linear system of equations reads:

$$\text{solve } \tilde{\mathbf{C}}(\tilde{\mathbf{z}}) = \mathbf{0} \quad \text{for } \tilde{\mathbf{z}} = (\tilde{\boldsymbol{\omega}}, \tilde{\mathbf{T}}). \quad (5.16)$$

Pursuing the structure in Section 5.3, *reduce-then-discretize-then-linearize* approach is used by applying the Newton method. Apart from the previous application of MOR on the control problem of Navier-Stokes equations, where the control is a vector field function, the current MHD problem considers the control as a constant variable. Thus, the control does not need to be approximated in the low-dimensional space.

Having reduced the constraint PDEs, dimension reduction is also applied to the objective function of the optimal control problem. Hence, substituting the POD approximations into (4.20) leads to the following discrete reduced cost function:

$$\begin{aligned} \mathbf{J}^R(\tilde{\mathbf{z}}, \mathbf{u}) = & \frac{\alpha_\omega}{2} (\tilde{\boldsymbol{\omega}} - \tilde{\boldsymbol{\omega}}_d)^T \tilde{\mathbf{M}} (\tilde{\boldsymbol{\omega}} - \tilde{\boldsymbol{\omega}}_d) + \frac{\alpha_T}{2} (\tilde{\mathbf{T}} - \tilde{\mathbf{T}}_d)^T \tilde{\mathbf{M}} (\tilde{\mathbf{T}} - \tilde{\mathbf{T}}_d) \\ & + \frac{\alpha_u}{2} \|\mathbf{u}\|^2 |\Omega|. \end{aligned} \quad (5.17)$$

Therefore, the problem in (4.24)–(4.25) turns into the discrete constrained optimization problem

$$\underset{\mathbf{u} \in \mathcal{U}}{\text{minimize}} \quad \mathbf{J}^R(\tilde{\mathbf{z}}, \mathbf{u}) \quad (5.18)$$

$$\text{subject to } \tilde{\mathbf{C}}(\tilde{\mathbf{z}}, \mathbf{u}) = \mathbf{0}. \quad (5.19)$$

Similarly, the discrete adjoint equations of the reduced model can be written in the form

$$\tilde{\mathbf{C}}_{\tilde{\mathbf{z}}}^*(\tilde{\mathbf{z}}(\tilde{\mathbf{u}}), \mathbf{u}) \tilde{\boldsymbol{\Lambda}} = -\mathbf{J}_{\tilde{\mathbf{z}}}^R(\tilde{\mathbf{z}}(\mathbf{u}), \mathbf{u}), \quad (5.20)$$

where

$$\tilde{\mathbf{C}}_{\tilde{\mathbf{z}}}(\tilde{\mathbf{z}}(\mathbf{u}), \mathbf{u}) = \begin{bmatrix} c_1 \tilde{\mathbf{M}} & \mathbf{0} \\ \mathbf{0} & \tilde{\mathbf{S}} \end{bmatrix} + \begin{bmatrix} \tilde{\mathbf{K}}(\tilde{\mathbf{T}}) & \tilde{\mathbf{K}}_{\tilde{\mathbf{T}}}(\tilde{\mathbf{T}})\tilde{\boldsymbol{\omega}} \\ \tilde{\mathbf{G}}(\tilde{\mathbf{z}}) & -\text{Br}\tilde{\mathbf{D}}_{\tilde{\mathbf{T}}}(\tilde{\boldsymbol{\omega}}, \tilde{\mathbf{T}})\tilde{\boldsymbol{\omega}} \end{bmatrix}$$

with

$$\tilde{\mathbf{G}}(\tilde{\mathbf{z}}) = c_2 \left[\frac{\partial \tilde{\mathbf{N}}(\tilde{\omega})}{\partial \tilde{\omega}} \tilde{\omega} + \tilde{\mathbf{N}}(\tilde{\omega}) \right] - \text{Br} \left[\frac{\partial \tilde{\mathbf{D}}(\tilde{\omega}, \tilde{\mathbf{T}})}{\partial \tilde{\omega}} \tilde{\omega} + \tilde{\mathbf{D}}(\tilde{\omega}, \tilde{\mathbf{T}}) \right] + \frac{\partial \tilde{\mathbf{P}}(\tilde{\omega})}{\partial \tilde{\omega}} \tilde{\omega} + \tilde{\mathbf{P}}(\tilde{\omega}),$$

which is to be solved for the reduced adjoint $\tilde{\mathbf{\Lambda}} = (\tilde{\boldsymbol{\lambda}}, \tilde{\eta})$.

Finally, the reduced optimal control is achieved by the implementation of the optimization algorithm given in Section 4.2.

5.5 Reduced Model for Parameter Control of Power-Law Fluid Flow and Heat Transfer

This section of the thesis constructs the reduced order model for the power-law fluid flow and heat transfer equations which constitute a steady parametrized problem. As in Section 5.4, POD bases of the velocity and temperature variables are generated by following Algorithm 3 and using high-fidelity solutions obtained in Section 3.4. Afterwards, reduced control problem and reduced constraint equations are obtained by projection to the low-dimensional space spanned by the POD basis functions.

Similarly, the reduced approximation $\tilde{z} = (\tilde{\omega}, \tilde{T})$ of the solution (ω, T) can be formed as

$$\tilde{\omega} = \sum_{j=1}^{\gamma_{\omega}} \tilde{\omega}_j \xi_j \quad \text{and} \quad \tilde{T} = \sum_{l=1}^{\gamma_T} \tilde{T}_l \theta_l, \quad (5.21)$$

where $\{\xi_j\}_{j=1}^{\gamma_{\omega}}$ and $\{\theta_l\}_{l=1}^{\gamma_T}$ are the POD basis functions for ω and T , respectively. By choosing the test functions, namely ϑ and ρ , as POD basis functions, reduced variational forms are derived for the forms in (3.26)–(3.27) as follows:

$$\langle \tilde{\mu} \nabla \tilde{\omega}, \nabla \vartheta \rangle_{\Omega} + \langle -1 + \text{Ha}^2 \tilde{\omega}, \vartheta \rangle_{\Omega} = 0, \quad (5.22)$$

$$\begin{aligned} \langle \nabla \tilde{T}, \nabla \rho \rangle_{\Omega} - \langle 1, \rho \rangle_{\partial \Omega} - \left\langle \text{Br} \tilde{\mu} \left[\left(\frac{\partial \tilde{\omega}}{\partial x} \right)^2 + \left(\frac{\partial \tilde{\omega}}{\partial y} \right)^2 \right], \rho \right\rangle_{\Omega} \\ - (\text{Ha}^2 \text{Br}) \langle \tilde{\omega}^2, \rho \rangle_{\Omega} + \left\langle \frac{4 \tilde{\omega}}{\tilde{\omega}_m}, \rho \right\rangle_{\Omega} = 0, \end{aligned} \quad (5.23)$$

where $\tilde{\mu}$ is the reduced variable viscosity, and

$$\tilde{\mu} = \left[\left(\frac{\partial \tilde{\omega}}{\partial x} \right)^2 + \left(\frac{\partial \tilde{\omega}}{\partial y} \right)^2 \right]^{\frac{n-1}{2}} \approx \left(\sum_{j=1}^{\gamma_{\omega}} \tilde{\omega}_j^2 [(\xi_j)_x + (\xi_j)_y] \right)^{\frac{n-1}{2}}.$$

Now, since it is a velocity dependent viscosity, its approximation is obtained by the POD basis functions of the velocity.

The low-dimensional approximations in (5.21) are substituted into the equations (5.22)–(5.23); this yields

$$\begin{aligned} & \left\langle \tilde{\mu} \sum_{j=1}^{\gamma_\omega} \tilde{\omega}_j \nabla \xi_j, \nabla \xi_i \right\rangle_\Omega + \left\langle -1 + \text{Ha}^2 \sum_{j=1}^{\gamma_\omega} \tilde{\omega}_j \xi_j, \xi_i \right\rangle_\Omega = 0, \\ & \left\langle \sum_{l=1}^{\gamma_T} \tilde{T}_l \nabla \theta_l, \nabla \theta_k \right\rangle_\Omega - \langle 1, \theta_k \rangle_{\partial\Omega} - \left\langle \text{Br} \tilde{\mu} \left[\left(\sum_{j=1}^{\gamma_\omega} \tilde{\omega}_j \nabla \xi_j \right) \cdot \left(\sum_{j=1}^{\gamma_\omega} \tilde{\omega}_j \nabla \xi_j \right) \right], \theta_k \right\rangle_\Omega \\ & - (\text{Ha}^2 \text{Br}) \left\langle \left(\sum_{j=1}^{\gamma_\omega} \tilde{\omega}_j \xi_j \right)^2, \theta_k \right\rangle_\Omega + \left\langle \frac{4}{\tilde{\omega}_m} \sum_{j=1}^{\gamma_\omega} \tilde{\omega}_j \xi_j, \theta_k \right\rangle_\Omega = 0 \end{aligned}$$

for i and j in $\{1, 2, \dots, \gamma_\omega\}$ and k and l in $\{1, 2, \dots, \gamma_T\}$. We refer to Section 5.4 for components of the reduced vectors and matrices except the vector $\tilde{\mathbf{e}} = (\tilde{e}_k)$ and the entries of the reduced non-linear stiffness matrix $\tilde{\mathbf{K}}(\tilde{\omega})$, which are given as

$$\begin{aligned} \tilde{e}_k &= \int_{\partial\Omega} \theta_k dS, \\ \tilde{\mathbf{K}}(\tilde{\omega})_{ij} &= \int_{\Omega} \left(\sum_{k=1}^{\gamma_\omega} \tilde{\omega}_k^2 [(\xi_k)_x + (\xi_k)_y] \right)^{\frac{n-1}{2}} \nabla \xi_j \nabla \xi_i d\Omega. \end{aligned}$$

The reduced form of the discrete algebraic problem can also be obtained by the projection in the discretized FOM by defining discrete approximations given in (5.15) so that the discrete form of the ROM is derived as

$$\tilde{\mathbf{C}}(\tilde{\mathbf{z}}) = \begin{bmatrix} \tilde{\mathbf{F}}(\tilde{\omega}) \\ \tilde{\mathbf{G}}(\tilde{\mathbf{T}}) \end{bmatrix} = \begin{bmatrix} \tilde{\mathbf{K}}(\tilde{\omega})\tilde{\omega} + \text{Ha}^2 \tilde{\mathbf{M}}\tilde{\omega} - \tilde{\mathbf{d}} \\ \tilde{\mathbf{S}}\tilde{\mathbf{T}} - (\tilde{\mathbf{f}} + \tilde{\mathbf{e}}) \end{bmatrix} = 0$$

for $\tilde{\mathbf{z}} = (\tilde{\omega}, \tilde{\mathbf{T}})$, where the vector $\tilde{\mathbf{f}} = (\tilde{f}_k)$ has the components

$$\tilde{f}_k = \int_{\Omega} \text{Br} \tilde{\mu} \left[\left(\frac{\partial \tilde{\omega}}{\partial x} \right)^2 + \left(\frac{\partial \tilde{\omega}}{\partial y} \right)^2 \right] \theta_k d\Omega + \int_{\Omega} (\text{Ha}^2 \text{Br}) \tilde{\omega}^2 \theta_k d\Omega - \int_{\Omega} \frac{4 \tilde{\omega}}{\tilde{\omega}_m} \theta_k d\Omega,$$

for $1 \leq k \leq \gamma_T$. Then, solution procedure in the FOM is followed by the ROM as well, again in a decoupled way.

After obtaining the discretized reduced constraint equations, reduced cost function $\mathbf{J}^R(\tilde{\mathbf{z}}, \mathbf{u})$ is formulated as in (5.17) for controlling the power-law fluid flow as well.

Thus, the reduced control problem has the same structure in (5.18),

$$\begin{aligned} & \underset{\mathbf{u} \in \mathcal{U}}{\text{minimize}} && \mathbf{J}^R(\tilde{\mathbf{z}}, \mathbf{u}) \\ & \text{subject to} && \tilde{\mathbf{C}}(\tilde{\mathbf{z}}, \mathbf{u}) = 0. \end{aligned}$$

Accordingly, the reduced adjoint equation has to be formulated as

$$\tilde{\mathbf{C}}_{\tilde{\mathbf{z}}}^*(\tilde{\mathbf{z}}(\mathbf{u}), \mathbf{u}) \tilde{\boldsymbol{\Lambda}} = -\mathbf{J}_{\tilde{\mathbf{z}}}^R(\tilde{\mathbf{z}}(\mathbf{u}), \mathbf{u}), \quad (5.24)$$

where

$$\tilde{\mathbf{C}}_{\tilde{\mathbf{z}}}(\tilde{\mathbf{z}}(\mathbf{u}), \mathbf{u}) = \begin{bmatrix} \tilde{\mathbf{F}}_{\tilde{\mathbf{z}}} \\ \tilde{\mathbf{G}}_{\tilde{\mathbf{z}}} \end{bmatrix} = \begin{bmatrix} \frac{\partial \tilde{\mathbf{F}}(\tilde{\boldsymbol{\omega}})}{\partial \tilde{\boldsymbol{\omega}}} & 0 \\ 0 & \frac{\partial \tilde{\mathbf{G}}(\tilde{\mathbf{T}})}{\partial \tilde{\mathbf{T}}} \end{bmatrix}.$$

Thus, the reduced adjoint problem in (5.24) for $\tilde{\boldsymbol{\Lambda}} = (\tilde{\boldsymbol{\lambda}}, \tilde{\boldsymbol{\eta}})$ becomes

$$\tilde{\mathbf{C}}_{\tilde{\mathbf{z}}}(\tilde{\mathbf{z}}(\mathbf{u}), \mathbf{u})^* \begin{bmatrix} \tilde{\boldsymbol{\lambda}} \\ \tilde{\boldsymbol{\eta}} \end{bmatrix} = - \begin{bmatrix} \alpha_{\tilde{\boldsymbol{\omega}}} \tilde{\mathbf{M}}_{\tilde{\boldsymbol{\omega}}}(\tilde{\boldsymbol{\omega}} - \tilde{\boldsymbol{\omega}}_d) \\ \alpha_T \tilde{\mathbf{M}}_{\tilde{\mathbf{T}}}(\tilde{\mathbf{T}} - \tilde{\mathbf{T}}_d) \end{bmatrix},$$

which is to be solved for the reduced adjoint $\tilde{\boldsymbol{\Lambda}} = (\tilde{\boldsymbol{\lambda}}, \tilde{\boldsymbol{\eta}})$.

After all, solution of the reduced optimal control problem is attained by the performing the optimization algorithm given in Section 4.2. In the next part, the simulation results for the reduced modeling of the FEM solutions of the control problems investigated so far are presented.

5.6 Numerical Results

This section presents numerical results obtained via the ROM solutions of the control problem of steady, parametrized, two-dimensional and laminar flow of incompressible Newtonian and non-Newtonian fluids applying the method of POD. Firstly, numerical results of the MOR application to the FEM solutions of the Navier-Stokes equations are presented in Section 5.6.1. Next, results of the analyses of the reduced models for the control of MHD flow and heat transfer with temperature dependent viscosity and for the power-law fluid flows are given in Section 5.6.2 and in Section 5.6.3, respectively. As being steady parametrized problems, POD bases of three problems are generated over the snapshots obtained for various values of the problem parameters. Singular values and as well as the resulting POD bases are depicted.

Simulations performed for the FOM in Section 4.6 are implemented for the ROM under the same conditions and stopping criteria. Comparisons between the FOM and the ROM are also provided to see the effectiveness of the MOR.

5.6.1 POD Application to Navier-Stokes Equations

The reduced modeling of the distributed control of the Navier-Stokes equations is implemented with the POD application. Simulations are performed for the parameter $\nu \in [1/300, 1]$, that is, snapshots are saved for several values of ν ,

$$s(\nu) = \left\{ 1, \frac{1}{10}, \frac{1}{20}, \frac{1}{30}, \frac{1}{40}, \dots, \frac{1}{300} \right\},$$

where $s(\cdot)$ denotes the set of values of the given parameter. Hence, $\text{card}(s(\nu)) = 31$ shows the number of FEM solutions in the snapshot matrices. Singular values obtained for the POD generation are shown in Figure 5.1, where the sharp decrease can be seen clearly. The energy of the system can be well approximated with the first two singular values and its corresponding left singular vectors included in the POD basis. POD basis of the velocity as vector fields are depicted in Figure 5.2. Since the

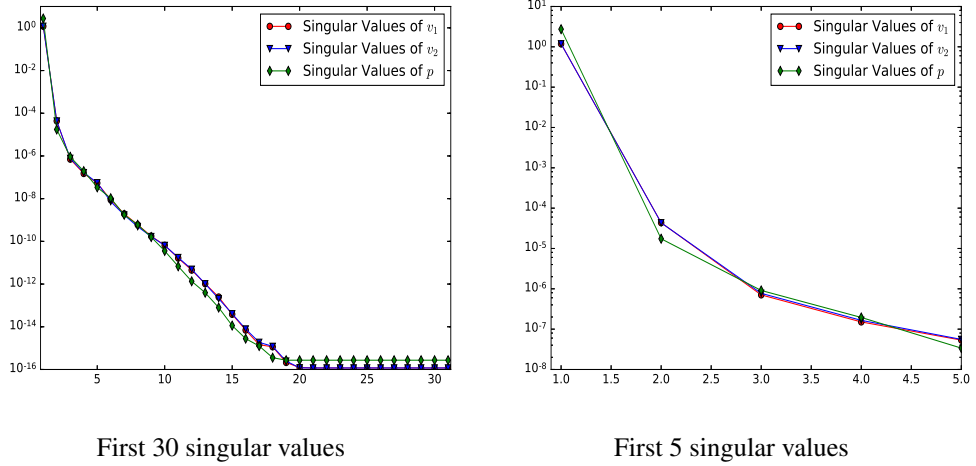
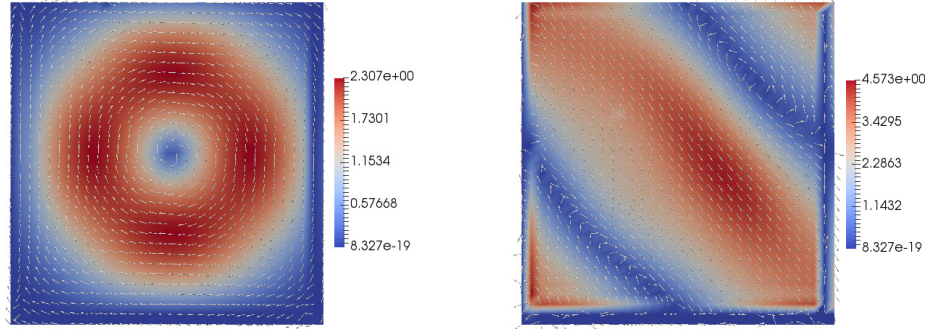


Figure 5.1: Singular values of velocity and pressure.

leading singular values are expected to be responsible for the leading basis elements in the approximation, first POD basis function reflects the main characteristic of the velocity. As expected, second basis provides a bit more detailed information about the dynamics. Other remaining singular values do not contribute significant improvement

on the characterization of the problem. More descriptive figures are given by contours of the basis functions of velocity components in Figure 5.3.



First POD basis function of velocity Second POD basis function of velocity

Figure 5.2: POD basis functions of velocity vector field.

In Figure 5.4, POD basis functions for pressure are also shown indicating that first basis function can almost catch the overall dynamics alone. Noting the first singular values of pressure, it can be inferred that the second basis function corresponding to the singular value $\sigma = 1.7396 \times 10^{-5}$ carries very small information about the dynamics of the pressure. Meanwhile, contours corresponding to the POD basis functions of pressure given in Figure 5.5 provide more interpretive data about this basis.

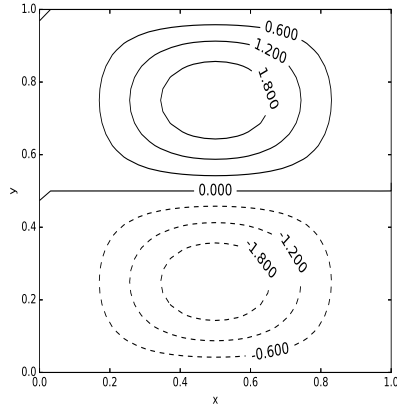
In Table 5.1, CPU times are given for FOM and ROM solutions in order to interpret the efficiency of the POD, where the speed-up with the POD is calculated according to the ratio

$$\text{Speed-up} = \frac{\text{CPU time for FOM}}{\text{CPU time for ROM}}.$$

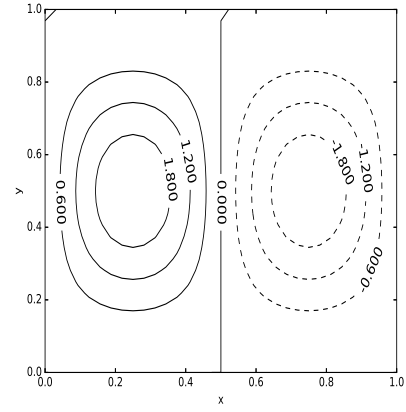
The results in Table 5.1 also show that as ν decreases computing time increases. However, this cost is minimized by the ROM with POD indicated by the given speed-up values.

Test controls are conducted for regaining desired velocity profiles corresponding to ν values, $\nu_d = 0.1, 0.05, 0.01, 0.005, 0.001$, given in Table 5.2. It is clear that ROM is capable of finding optimal states with relatively small number of iterations compared to the FOM results given in Table 4.1 of Chapter 4.

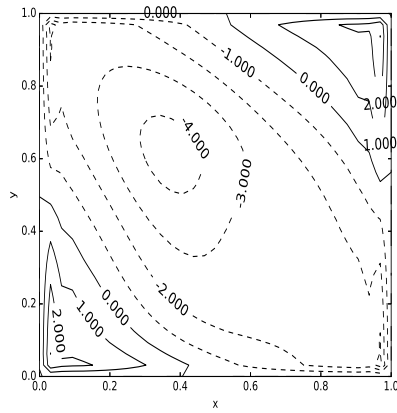
For a comprehensive understanding of the test results, the case for the desired state



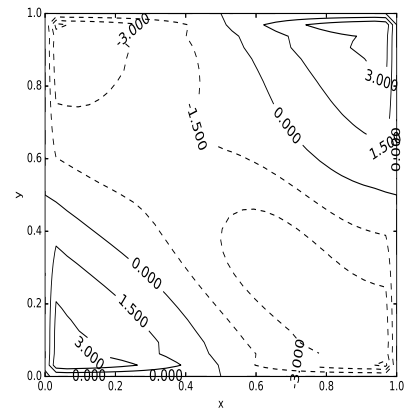
First POD basis function of v_1



First POD basis function of v_2



Second POD basis function of v_1



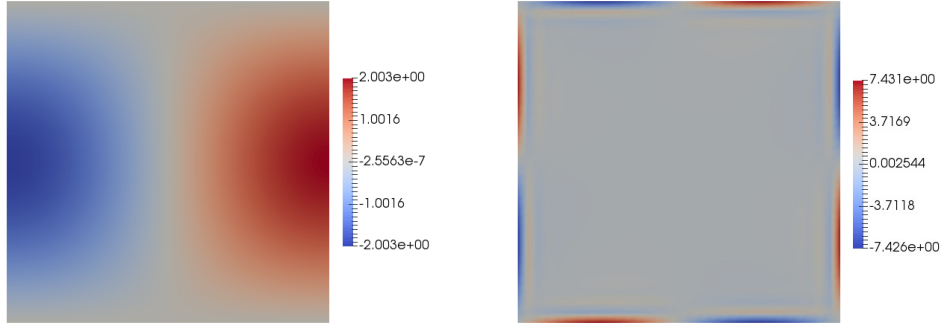
Second POD basis function of v_2

Figure 5.3: Contours of POD basis functions of velocity vector components.

when $\nu = \nu_d = 0.005$ is analyzed in detail. The contours of the components of the controlled velocity in ROM are presented in Figure 5.6 which depicts almost the same results with Figure 4.2 in the FOM. Moreover, observations are maintained with the required control field and its components given in Figure 5.7 and Figure 5.8, which demonstrate that the optimal control in ROM is achieved with the same optimal states and control function given in Figure 4.3(c) and Figure 4.3(d).

5.6.2 POD Application to Control of MHD Flow and Heat Transfer with Temperature Dependent Viscosity

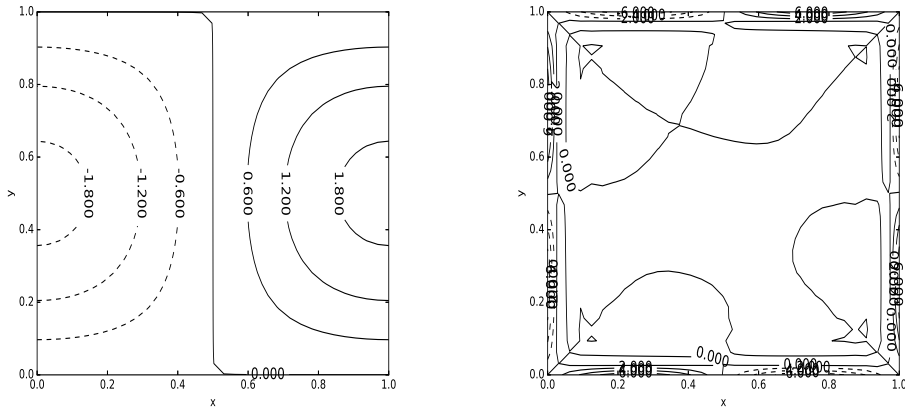
In this section, the control problem of MHD flow and heat transfer with temperature dependent viscosity is subjected to the model reduction with POD application. Con-



First POD basis of pressure

Second POD basis of pressure

Figure 5.4: POD basis functions of pressure.



First POD basis function of pressure

Second POD basis function of pressure

Figure 5.5: Contours of POD basis functions of pressure.

sidering the equations in (3.16)–(3.17) as steady parametrized PDEs, the high-fidelity solutions obtained in Section 3.5.2 are replicated for various values of the parameters for the generation of the snapshots. Comparisons for the optimal control as well as the FEM solutions are provided.

Snapshot matrices of velocity and temperature are sampled based on the solutions for the following values of the parameters:

$$s(\text{Ha}) = \{0, 1, \dots, 10\},$$

$$s(\text{Br}) = \{0, 1, 2\},$$

$$s(B) = \{0, 1, 2\},$$

$$s(m) = \{0, 1\}.$$

Table 5.1: FOM-ROM Errors and CPU times for the solutions of N-S equations and speed-up with POD

ν	L^2 -Error v_1	L^2 -Error v_2	L^2 -Error p	CPU-FOM	CPU-ROM	Speed-up
1.0	2.9499×10^{-6}	2.9521×10^{-6}	2.5867×10^{-3}	2.4228	3.2201×10^{-1}	7.52
0.05	5.0746×10^{-6}	5.0169×10^{-6}	1.4015×10^{-3}	2.3523	2.1646×10^{-1}	10.86
0.01	1.0266×10^{-5}	1.0142×10^{-5}	4.7506×10^{-5}	3.1392	3.4542×10^{-1}	9.09
0.005	1.8720×10^{-5}	1.9718×10^{-5}	8.0802×10^{-5}	3.1532	2.5522×10^{-1}	12.35
0.001	9.7841×10^{-5}	9.7345×10^{-5}	2.1895×10^{-4}	5.6834	1.7702×10^{-1}	32.10

Table 5.2: Distributed control for regaining the desired states given below with the uncontrolled initial state of $\nu = 1.0$ in ROM

ν_d	$\ v_1^{\text{opt}} - v_1^d\ _{L2}$	$\ v_2^{\text{opt}} - v_2^d\ _{L2}$	J	Tit
0.1	2.0121×10^{-3}	2.0120×10^{-3}	1.502×10^{-4}	2
0.05	2.1526×10^{-3}	2.1526×10^{-3}	1.719×10^{-4}	2
0.01	2.2676×10^{-3}	2.2676×10^{-3}	1.907×10^{-4}	2
0.005	2.2822×10^{-3}	2.2822×10^{-3}	1.932×10^{-4}	2
0.001	2.2938×10^{-3}	2.2938×10^{-3}	1.952×10^{-4}	2

The cartesian product

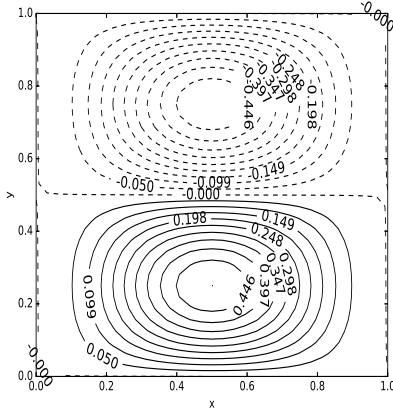
$$s(\text{Ha}, \text{Br}, B, m) = s(\text{Ha}) \times s(\text{Br}) \times s(B) \times s(m),$$

which corresponds to the set of values for the parameters in the snapshot matrices. Thus,

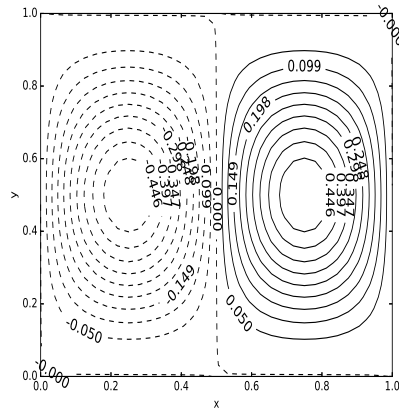
$$\begin{aligned} \text{card}(s(\text{Ha}, \text{Br}, B, m)) &= \text{card}(s(\text{Ha})) \times \text{card}(s(\text{Br})) \times \text{card}(s(B)) \times \text{card}(s(m)) \\ &= 11 \times 3 \times 3 \times 2 = 198 \end{aligned}$$

shows the number of solutions that are generated for the snapshot matrices. It is noticeable that the sample values of the Hall parameter m is less than the others. This is because of the fact that m and Ha dominate the same terms in the system, thus it is not necessary to extend the samples in both parameters.

The SVD is applied to the velocity and temperature snapshots separately and the corresponding singular values are given in the Figure 5.9. Therein, it reports the first 80 singular values to see the rapid decay and stagnation for both functions. The first 5 singular values are presented to see clearly how many singular values are sufficient for satisfying the energy criterion for velocity and temperature. Moreover, since the singular values of the temperature decreasing more rapidly than the velocity, POD algorithm (see Algorithm 3) generates four basis functions for the velocity and three basis functions for the temperature for a given tolerance of the energy criterion.

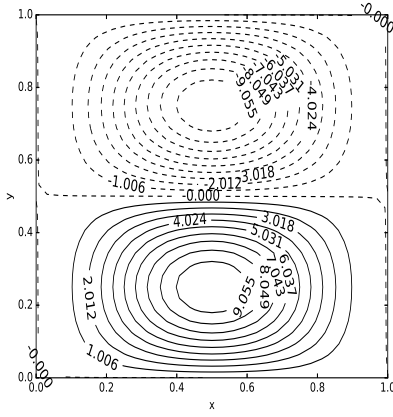


Reduced controlled velocity v_1

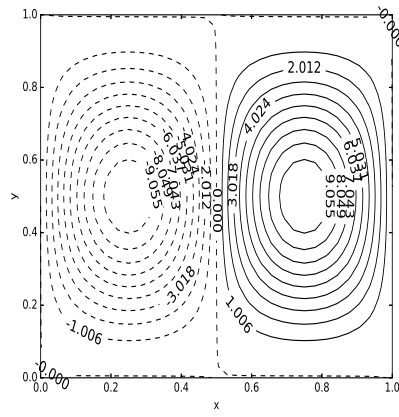


Reduced controlled velocity v_2

Figure 5.6: Reduced controlled velocity



Reduced control u_1

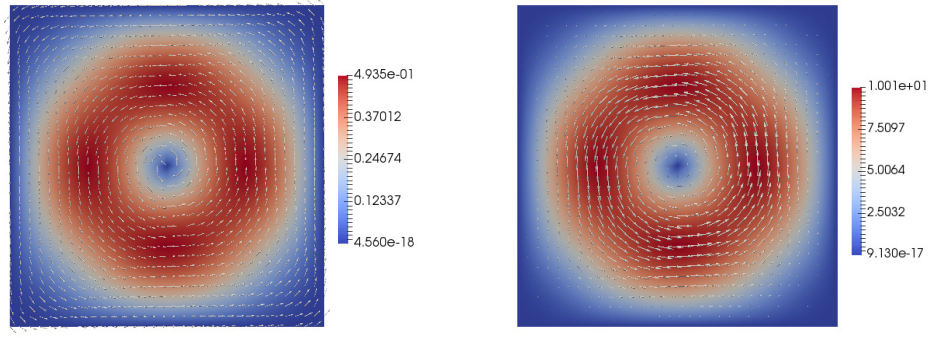


Reduced control u_2

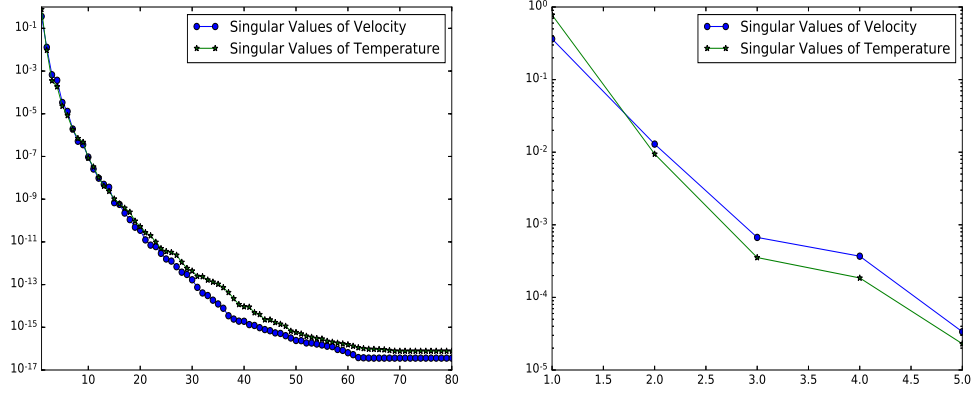
Figure 5.7: Components of the reduced control.

The four POD basis functions of the velocity are given in Figure 5.10. As expected, first basis function reflects the main behavior about the velocity. The more the number of basis increases the more they include the detailed information for the velocity. Also, the contours of the velocity POD basis functions are reported in Figure 5.11 to see the behavior clearly.

Next, the three POD basis functions for temperature and the corresponding isolines are presented in Figure 5.12 and in Figure 5.13, respectively. Similar behavior as in the case for the velocity is obtained for the temperature as well. That is, by the increase in the number of basis functions, POD basis starts to include more detailed information of the solution.

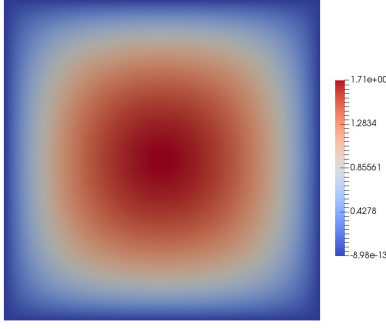


Reduced controlled velocity vector field Reduced control vector field
Figure 5.8: Reduced controlled velocity vector field and control vector field.

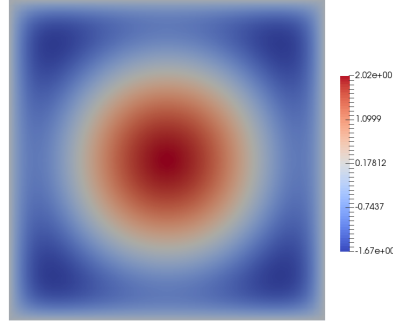


First 80 singular values First 5 singular values
Figure 5.9: Singular values of velocity and temperature.

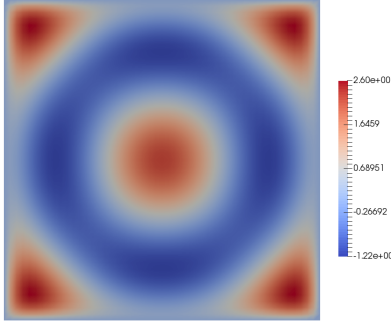
Error plots of the reduced order model with the increasing number of basis functions are given in Figure 5.14, which indicates that the POD reduced model can approximate the solution even if small number of basis functions are used. Similar results supporting the accuracy of the reduced order solution are obtained for all values of the parameters in the snapshot matrix. In addition, the efficiency of the application of ROM with POD is verified in Table 5.3 which provides the CPU times and the speed-ups of the solutions for various values of the parameters of the problem. Moreover, the largest speed-up is obtained for the case when the viscosity parameter B is large, $B = 2.0$, which is the coefficient of the exponential non-linearity. However, the overall speed-up for the MHD problem compared to the N-S equations is small; but this is due to the high non-linearity of the problem.



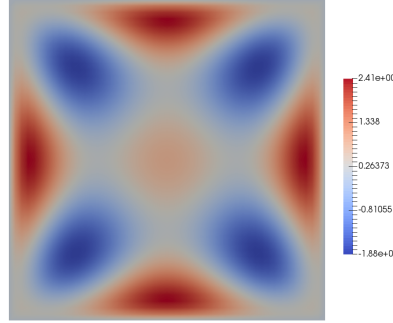
First POD basis function of velocity



Second POD basis function of velocity



Third POD basis function of velocity

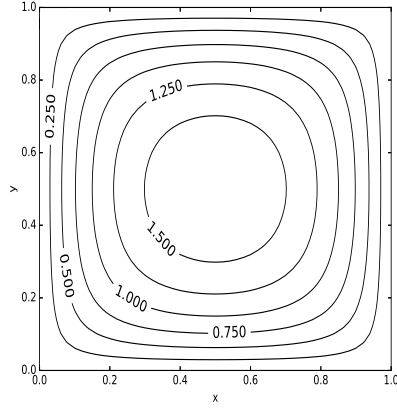


Fourth POD basis function of velocity

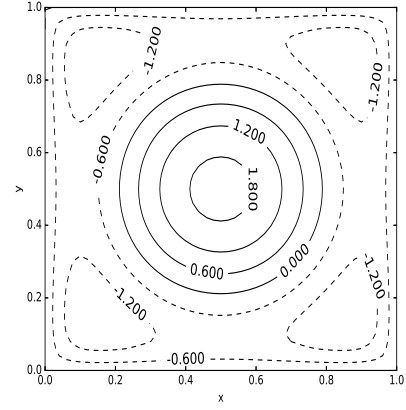
Figure 5.10: POD basis functions of velocity.

Numerical simulations performed for the FOM of the optimal control problem are reconducted for the ROM in order to make comparison. Same regularization parameters are chosen as in the FOM. The ROM solutions satisfactorily reconstruct the high-fidelity solutions for the control problem by using a small number of basis functions.

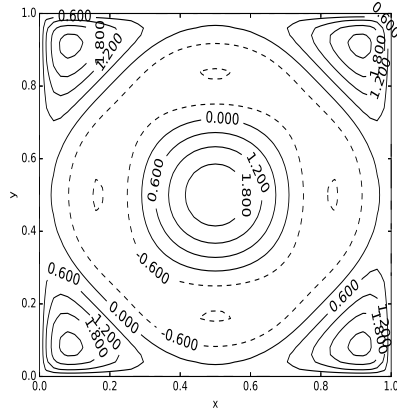
Among all the results corresponding to the reduced control problem, most important ones are reported. For example, the total number of iterations (Tit), the optimal parameter values and the cost function value are exactly the same as the full order model for one single parameter control. The differences occur only in $\|\tilde{\omega}_{\text{opt}} - \tilde{\omega}_d\|_{\infty}$ and $\|\tilde{T}_{\text{opt}} - \tilde{T}_d\|_{\infty}$. This is surely expected due to the projection error inherently included from the beginning of the optimization. Moreover, results given for $\|\tilde{\omega}_{\text{opt}} - \tilde{\omega}_d\|_{\infty}$ and $\|\tilde{T}_{\text{opt}} - \tilde{T}_d\|_{\infty}$ state the convergence of the optimization algorithm up to a given toler-



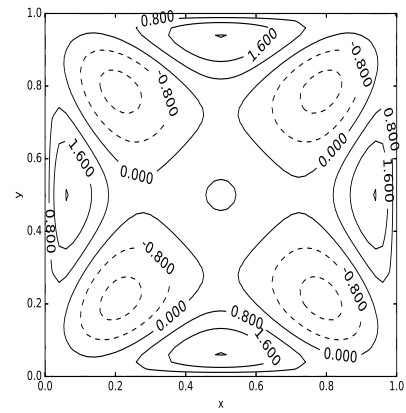
First POD basis function of velocity



Second POD basis function of velocity



Third POD basis function of velocity

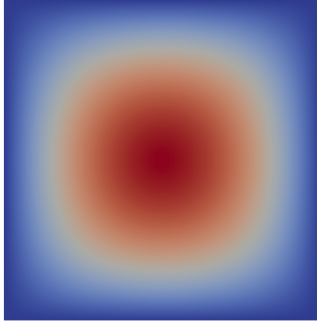


Fourth POD basis function of velocity

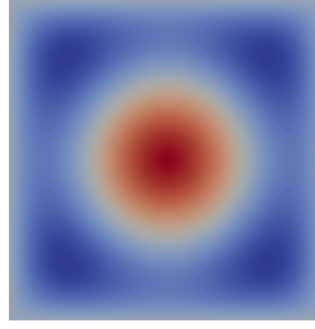
Figure 5.11: Contours of POD basis functions of velocity.

ance to the reduced desired state. Hence, it will not be appropriate to compare these values with full order model since they have desired states having different accuracy (representation). Below, results are summarized in two parts: single and pairwise control.

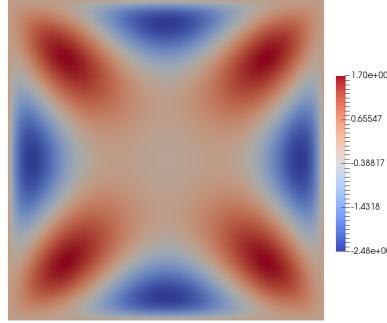
Using a single control, first, simulations for the ROM of the control problem with the Hartmann number as the control variable are summarized in Table 5.4. Optimal values indicate that the POD basis exactly reflects the dynamics of the problem and solutions attain optimal states at the desired (designed) values of the parameters. Second, reduced model is tested for the control with the Brinkman number in Table 5.5 and they are all compatible with the FOM results obtained in Table 4.5. Third, similar satisfactory results are obtained for the ROM of the control problem with the viscosity parameter B as the control in Table 5.6. Final simulation of the single parameter



First POD basis function of temperature



Second POD basis function of temperature

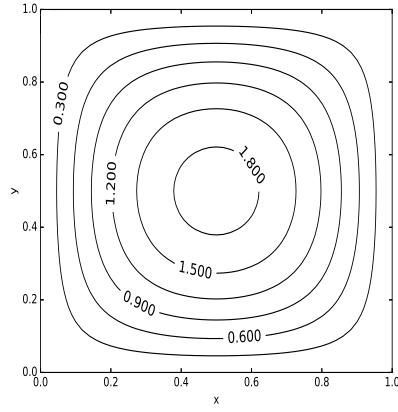


Third POD basis function of temperature

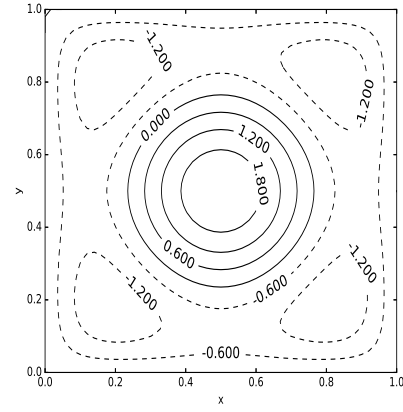
Figure 5.12: POD basis functions of temperature.

control is implemented for the Hall parameter m , which is sensitive to the value of the corresponding regularization parameter. Thus, tests are conducted twice, one for $\alpha_m = 0$ and the other for $\alpha_m = 10^{-5}$ in Table 5.7 and in Table 5.8. These results are very close to the ones in Table 4.3 and Table 4.4, respectively, which shows that solutions of the ROM have also same sensitivities as in the FOM.

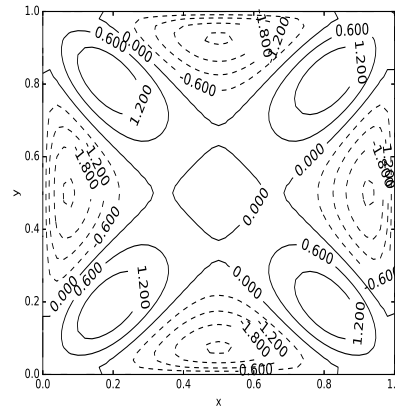
Simulations are also performed for the pairwise control of the parameters. First, the pairwise control in ROM is executed for the control problem with Hartmann number and viscosity parameter as the control variables. The results are shown in Table 5.9 and verify that optimal states are significantly close to desired states. The difference between the optimal values of the FOM in Table 4.7 and ROM in Table 5.9 just appears at least after the third decimal digit. For instance, in order to obtain the desired state for the case in which $Ha = 1.0$ and $B = 0.0$, optimal state in ROM



First POD basis function of temperature



Second POD basis function of temperature



Third POD basis function of temperature

Figure 5.13: Isolines of POD basis functions of temperature.

is attained at $Ha = 0.9491$ and $B = 0.0658$ while the optimality is achieved $Ha = 0.9494$ and $B = 0.0654$ in FOM.

Second, pairing of Brinkman number and the viscosity parameter is reported in Table 5.10. The optimal values of ROM are almost exactly same as the FOM given in Table 4.8.

Third, optimal control in ROM is examined with the pairwise control of Hall parameter and Brinkman number as the control variables; and results are reported in Table 5.11. Although optimal values start to change after the second decimal digit, the desired states are achieved at the optimal states. It is worth noting that although Hall parameter values m for $m > 1$ are not covered in the snapshot set, the generated POD bases are capable to reflect the solutions for those as well.

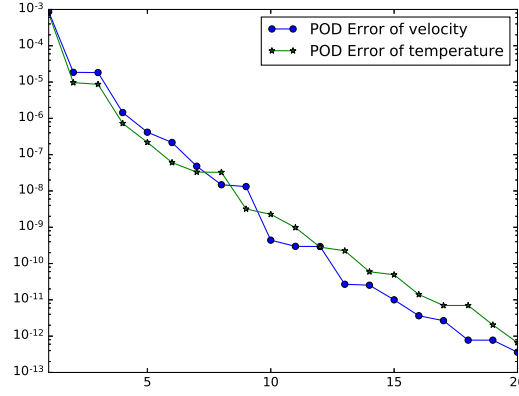


Figure 5.14: POD Errors of Velocity and Temperature corresponding to the solution for $Ha = 1, Br = 1, B = 1, m = 1$.

Table 5.3: FOM-ROM Errors and CPU times for solutions of the MHD equations and heat transfer with temperature dependent viscosity and speed-up with POD

(Ha, m, Br, B)	$\ \omega - \tilde{\omega}\ _{L^2}$	$\ T - \tilde{T}\ _{L^2}$	CPU-FOM	CPU-ROM	Speed-up
(1.0, 1.0, 1.0, 1.0)	1.6218×10^{-6}	9.0379×10^{-6}	2.4506×10^{-1}	8.6063×10^{-2}	2.84
(3.0, 1.0, 1.0, 1.0)	1.1036×10^{-6}	8.6997×10^{-7}	2.2383×10^{-1}	8.6133×10^{-2}	2.61
(5.0, 1.0, 1.0, 1.0)	9.0775×10^{-7}	8.4900×10^{-6}	2.1916×10^{-1}	7.0967×10^{-2}	2.97
(10.0, 1.0, 1.0, 1.0)	1.2821×10^{-6}	4.6399×10^{-6}	1.6395×10^{-1}	6.6184×10^{-2}	2.43
(1.0, 3.0, 1.0, 1.0)	1.7540×10^{-6}	1.0209×10^{-5}	2.4358×10^{-1}	8.8826×10^{-2}	2.74
(1.0, 5.0, 1.0, 1.0)	1.7761×10^{-6}	1.0395×10^{-5}	2.4415×10^{-1}	8.8721×10^{-2}	2.75
(1.0, 8.0, 1.0, 1.0)	1.7846×10^{-6}	1.0465×10^{-5}	2.4381×10^{-1}	8.9996×10^{-2}	2.70
(1.0, 1.0, 2.0, 1.0)	2.0096×10^{-6}	5.7881×10^{-6}	2.4495×10^{-1}	8.5833×10^{-2}	2.85
(1.0, 1.0, 1.0, 2.0)	2.5921×10^{-6}	5.5032×10^{-6}	3.2410×10^{-1}	9.9516×10^{-2}	3.25

Fourth, control in the ROM is implemented with the Hall parameter and the viscosity parameter; and the results are summarized in Table 5.12. Since these parameters have opposite effects on the fluid, optimization becomes more challenging, especially in the ROM. So, desired states are successfully achieved at the optimal values, which are differ only after the first decimal digit from the optimal values attained by the FOM. However, it does not imply a failure in ROM, since the opposite effects of the parameters just leads to another optimal state to meet for the desired state.

To sum up, the results obtained for the pairwise control in ROM are identical to the FOM's in a general perspective. First of all, some optimal parameter values are attained with the differences between FOM and ROM at fourth or fifth digit. However, this does not effect the total number of iterations in the cases when controlling using Ha and B , or Br and B . On the other hand, in the case of controlling with m and Br , first test case requires 12 Tit instead of 13; similarly, in the case of controlling m and B , first test case requires 21 Tit instead of 16.

Table 5.4: Control with Hartman number Ha , $m = 1$, $\text{Br} = 1$, $B = 1$, $\alpha_\omega = 10^3$, $\alpha_T = 10^0$, $\alpha_{\text{Ha}} = 10^{-5}$, $\text{Ha}^0 = 0.1$

Ha_d	Ha_{opt}	$\ \tilde{\omega}_{\text{opt}} - \tilde{\omega}_d\ _\infty$	$\ \tilde{T}_{\text{opt}} - \tilde{T}_d\ _\infty$	J	Tit
1.0	1.0125	4.4411×10^{-5}	2.5290×10^{-6}	6.059×10^{-6}	3
3.0	3.0353	2.6265×10^{-4}	1.9812×10^{-5}	9.816×10^{-5}	4
5.0	5.0374	2.6137×10^{-4}	3.2947×10^{-5}	3.500×10^{-4}	4
10.0	9.9696	8.6965×10^{-5}	3.7786×10^{-5}	1.214×10^{-3}	3

Table 5.5: Control with Brinkman number Br , $m = 1$, $\text{Ha} = 1$, $B = 1$, $\alpha_\omega = 10^0$, $\alpha_T = 10^3$, $\alpha_{\text{Br}} = 10^{-5}$, $\text{Br}^0 = 0.0$

Br_d	Br_{opt}	$\ \tilde{\omega}_{\text{opt}} - \tilde{\omega}_d\ _\infty$	$\ \tilde{T}_{\text{opt}} - \tilde{T}_d\ _\infty$	J	Tit
1.0	0.9870	7.1252×10^{-7}	1.5914×10^{-5}	4.935×10^{-6}	3
2.0	1.9743	1.4240×10^{-6}	3.1781×10^{-5}	1.974×10^{-5}	4
3.0	2.9615	2.1345×10^{-6}	4.7602×10^{-5}	4.442×10^{-5}	4

5.6.3 POD Application to Control of Power-Law Fluid Flow and Heat Transfer

In this part, the MOR with POD method is applied to the control problem of power-law fluid flow and heat transfer. The snapshots are generated for the fine-scaled solutions of the equations in (3.24)–(3.25) given in Section 3.5.3. The results for the FOM and the ROM are compared regarding CPU times and accuracy.

Sample solutions of the velocity and temperature are collected for the snapshot matrices for various values of the parameters:

$$\begin{aligned}
 s(\text{Ha}) &= \{1, \dots, 5\}, \\
 s(n) &= \{0.5, 0.6, \dots, 2.0\}, \\
 s(\text{Br}) &= \{1, 2\}
 \end{aligned}$$

so that the set of values for the parameters to form snapshot matrices are constructed by the following cartesian product:

$$s(\text{Ha}, n, \text{Br}) = s(\text{Ha}) \times s(n) \times s(\text{Br}).$$

Table 5.6: Control with B , $\text{Ha} = 1$, $m = 1$, $\text{Br} = 1$, $\alpha_\omega = 10^3$, $\alpha_T = 10^3$, $\alpha_B = 10^{-5}$, $B^0 = 0.0$

B_d	B_{opt}	$\ \tilde{\omega}_{\text{opt}} - \tilde{\omega}_d\ _\infty$	$\ \tilde{T}_{\text{opt}} - \tilde{T}_d\ _\infty$	J	Tit
1.0	0.9980	6.1231×10^{-6}	7.5840×10^{-6}	4.990×10^{-6}	4
2.0	1.9951	1.3428×10^{-5}	1.6815×10^{-5}	1.995×10^{-5}	6
3.0	2.9911	2.1916×10^{-5}	2.7733×10^{-5}	4.487×10^{-5}	7

Table 5.7: Control with Hall parameter m , $\text{Ha} = 1$, $\text{Br} = 1$, $B = 1$, $\alpha_\omega = 10^3$, $\alpha_T = 10^0$, $\alpha_m = 0.0$, $m^0 = 10.0$

m_d	m_{opt}	$\ \tilde{\omega}_{\text{opt}} - \tilde{\omega}_d\ _\infty$	$\ \tilde{T}_{\text{opt}} - \tilde{T}_d\ _\infty$	J	Tit
1.0	0.9693	5.4910×10^{-5}	3.1272×10^{-6}	8.997×10^{-7}	5
3.0	2.9521	1.0770×10^{-5}	5.9757×10^{-7}	3.170×10^{-8}	3
5.0	4.9379	3.4527×10^{-6}	1.9082×10^{-7}	3.206×10^{-9}	3
8.0	8.0076	1.0690×10^{-7}	5.8996×10^{-9}	1.943×10^{-10}	3

Table 5.8: Control with Hall parameter m , $\text{Ha} = 1$, $\text{Br} = 1$, $B = 1$, $\alpha_\omega = 10^3$, $\alpha_T = 10^0$, $\alpha_m = 10^{-5}$, $m^0 = 10.0$

m_d	m_{opt}	$\ \tilde{\omega}_{\text{opt}} - \tilde{\omega}_d\ _\infty$	$\ \tilde{T}_{\text{opt}} - \tilde{T}_d\ _\infty$	J	Tit
1.0	0.9581	7.5255×10^{-5}	4.2866×10^{-6}	5.543×10^{-6}	5
3.0	2.2898	2.2013×10^{-4}	1.2236×10^{-5}	3.184×10^{-5}	6
5.0	2.6081	3.2965×10^{-4}	1.8270×10^{-5}	4.758×10^{-5}	7
8.0	2.7242	3.8043×10^{-4}	2.1063×10^{-5}	5.549×10^{-5}	5

Table 5.9: Control with Hartmann number Ha and B , $m = 1$, $\text{Br} = 1$, $\alpha_\omega = 10^3$, $\alpha_T = 10^0$, $\alpha_{(\text{Ha}, B)} = 10^{-5}$, $(\text{Ha}^0, B^0) = (0.1, 0.0)$

Ha_d	B_d	Ha_{opt}	B_{opt}	$\ \tilde{\omega}_{\text{opt}} - \tilde{\omega}_d\ _\infty$	$\ \tilde{T}_{\text{opt}} - \tilde{T}_d\ _\infty$	J	Tit
1.0	0.0	0.9491	0.0658	3.8818×10^{-5}	2.6019×10^{-4}	5.700×10^{-6}	12
1.0	1.0	1.0201	0.9887	3.7135×10^{-5}	3.8663×10^{-5}	1.105×10^{-5}	12
3.0	2.0	3.0804	1.9693	4.9949×10^{-4}	7.3384×10^{-5}	1.188×10^{-4}	10
5.0	1.0	5.0445	0.9119	2.0677×10^{-4}	1.5976×10^{-4}	3.550×10^{-4}	10

Table 5.10: Control with Brinkman number Br and B , $m = 1$, $\text{Ha} = 1$, $\alpha_\omega = 10^3$, $\alpha_T = 10^3$, $\alpha_{(\text{Br}, B)} = 10^{-5}$, $(\text{Br}^0, B^0) = (0.0, 0.0)$

Br_d	B_d	Br_{opt}	B_{opt}	$\ \tilde{\omega}_{\text{opt}} - \tilde{\omega}_d\ _\infty$	$\ \tilde{T}_{\text{opt}} - \tilde{T}_d\ _\infty$	J	Tit
1.0	1.0	0.9784	1.0045	1.4933×10^{-5}	1.4960×10^{-5}	9.914×10^{-6}	10
2.0	1.0	1.9493	1.0134	4.3465×10^{-5}	3.1019×10^{-5}	2.456×10^{-5}	10
1.0	2.0	0.9865	1.9991	1.0906×10^{-6}	1.7890×10^{-5}	2.492×10^{-5}	11
2.0	2.0	1.9547	2.0087	2.7740×10^{-5}	3.1628×10^{-5}	3.963×10^{-5}	11

Table 5.11: Control with the Hall parameter m and Br , $B = 1$, $\text{Ha} = 1$, $\alpha_\omega = 10^3$, $\alpha_T = 10^0$, $\alpha_{(m, \text{Br})} = 10^{-5}$, $(m^0, \text{Br}^0) = (10.0, 0.0)$

m_d	Br_d	m_{opt}	Br_{opt}	$\ \tilde{\omega}_{\text{opt}} - \tilde{\omega}_d\ _\infty$	$\ \tilde{T}_{\text{opt}} - \tilde{T}_d\ _\infty$	J	Tit
1.0	1.0	1.6986	0.2699	8.2493×10^{-4}	9.3333×10^{-4}	2.363×10^{-5}	12
1.0	2.0	1.5757	1.1733	7.1337×10^{-4}	1.0648×10^{-3}	3.009×10^{-5}	14
3.0	1.0	1.7754	0.3111	5.5214×10^{-4}	8.1828×10^{-4}	2.722×10^{-5}	14
3.0	2.0	1.6834	1.2389	6.2940×10^{-4}	8.9842×10^{-4}	3.559×10^{-5}	13

Table 5.12: Control with the Hall parameter m and B , $\text{Br} = 1$, $\text{Ha} = 1$, $\alpha_\omega = 10^3$, $\alpha_T = 10^3$, $\alpha_{(m, B)} = 10^{-5}$, $(m^0, B^0) = (10.0, 0.0)$

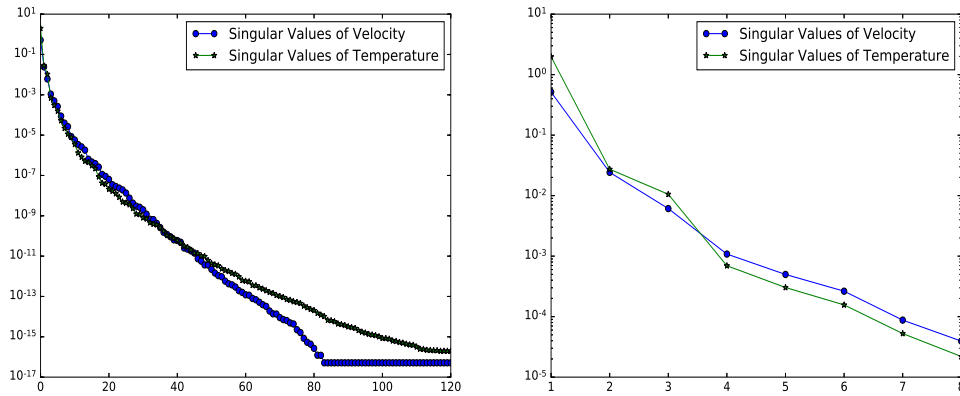
m_d	B_d	m_{opt}	B_{opt}	$\ \tilde{\omega}_{\text{opt}} - \tilde{\omega}_d\ _\infty$	$\ \tilde{T}_{\text{opt}} - \tilde{T}_d\ _\infty$	J	Tit
1.0	1.0	1.4309	0.7838	1.2961×10^{-3}	8.7522×10^{-4}	3.033×10^{-4}	21
3.0	1.0	1.4851	0.6152	4.6409×10^{-4}	1.4693×10^{-3}	3.173×10^{-5}	22
1.0	2.0	1.2854	1.6996	1.2474×10^{-3}	1.0527×10^{-3}	2.976×10^{-4}	22
3.0	2.0	1.3414	1.5423	4.4070×10^{-4}	1.6096×10^{-3}	4.068×10^{-5}	22

Accordingly, the number of solutions is determined as

$$\begin{aligned}\text{card}(s(\text{Ha}, n, \text{Br})) &= \text{card}(s(\text{Ha})) \times \text{card}(s(n)) \times \text{card}(s(\text{Br})) \\ &= 5 \times 16 \times 2 = 160.\end{aligned}$$

Considering the effect of the parameters on the dynamics of the problem, the number of sample values of the flow index parameter n is chosen larger than the other parameters. The other significant parameter Ha is also considered on the interval $[1, 5]$ regarding the previous simulations on the problem.

As the main part of the POD method, SVD is applied to the snapshot matrices of the velocity and temperature. As a result, Figure 5.15 interprets the first 120 singular values decaying for both functions. Further, the first 8 singular values are shown closely here to clarify the sufficient number of singular values satisfying the energy criterion. Accordingly, POD algorithm (see Algorithm 3) determines six basis functions for the velocity and four basis functions for the temperature for a given tolerance of the energy criterion.



First 120 singular values

First 8 singular values

Figure 5.15: Singular values of velocity and temperature.

The POD basis functions of the velocity are depicted in Figure 5.16, where the similar expected behavior is observed as in the POD basis functions of the previous problems. First basis functions govern the fundamental part of the system's dynamics and the remaining basis functions assist to reflect the detailed information about the system. The more quantitative information about the POD basis of the velocity is also given in Figure 5.17 by the contours.

Table 5.13: FOM-ROM Errors and CPU times for solutions of the power-law fluid flow and heat transfer and speed-up with POD

(Ha, n, Br)	$\ \omega - \tilde{\omega}\ _{L^2}$	$\ T - \tilde{T}\ _{L^2}$	CPU-FOM	CPU-ROM	Speed-up
(1.0, 0.8, 1.0)	8.0021×10^{-6}	7.5868×10^{-5}	9.6441×10^{-1}	3.6147×10^{-1}	2.66
(3.0, 0.8, 1.0)	2.7490×10^{-6}	1.4703×10^{-5}	9.6647×10^{-1}	3.5914×10^{-1}	2.69
(5.0, 0.8, 1.0)	9.0134×10^{-6}	1.3042×10^{-4}	8.3896×10^{-1}	3.6117×10^{-1}	2.32
(1.0, 1.2, 1.0)	8.3909×10^{-6}	5.1176×10^{-5}	7.2048×10^{-1}	3.7084×10^{-1}	1.94
(3.0, 1.2, 1.0)	8.9679×10^{-6}	1.0644×10^{-4}	7.8558×10^{-1}	3.6716×10^{-1}	2.14
(5.0, 1.2, 1.0)	5.7618×10^{-6}	2.2080×10^{-4}	7.8447×10^{-1}	3.6939×10^{-1}	2.12
(1.0, 1.8, 1.0)	4.2095×10^{-6}	2.1822×10^{-4}	1.0997×10^0	5.7737×10^{-1}	1.90
(3.0, 1.8, 1.0)	9.3888×10^{-6}	1.8972×10^{-4}	1.0840×10^0	5.0642×10^{-1}	2.14
(5.0, 1.8, 1.0)	1.8120×10^{-5}	1.7314×10^{-4}	1.0808×10^0	4.3894×10^{-1}	2.46

Next, POD basis functions of the temperature and the isolines are interpreted in Figure 5.18 and in Figure 5.19, respectively. Similarly, POD basis reflects more detailed information by the increase in the number of basis functions.

Figure 5.20 plots the projection errors by the increasing number of POD basis functions for velocity and temperature. As it can be seen clearly from this graph, the increase in the number of POD basis functions decreases the error up to a certain number of basis functions. That is, whereas the error of the velocity becomes constant after 17 basis functions, the error of the temperature do not decrease after 11 basis functions. This result also clarifies the reason why the required number of basis functions for the velocity is greater than the number of basis functions for the temperature determined by the same tolerance for the energy criterion. Moreover, Table 5.13 reports the errors and CPU times for various cases of the parameters to demonstrate the accuracy and efficiency attained by the POD method. However, when compared to the results of the problem with temperature dependent viscosity given in Table 5.3, required computational times increase for both FOM and ROM due to highly non-linear structure of the power-law model.

The performance of the ROM is investigated by the simulation of the optimal control problem for various cases. The conditions of the numerical implementation are arranged in the same manner of the FOM for an ideal comparison. Thus, the same regularization parameters and stopping criteria are considered. The ROM with a low dimension is able to approximate the solutions of the FOM sufficiently.

In the following, most significant results of the reduced optimal control problem are

Table 5.14: Control with n , $Ha = 1.0$, $Br = 1.0$, $\alpha_\omega = 10^5$, $\alpha_T = 10^0$, $\alpha_n = 10^{-5}$, and $n_0 = 0.5$

n_d	n_{opt}	$\ \tilde{\omega}_{opt} - \tilde{\omega}_d\ _\infty$	$\ \tilde{T}_{opt} - \tilde{T}_d\ _\infty$	J	Tit
0.6	0.6	1.7354×10^{-9}	9.9681×10^{-10}	4.577×10^{-6}	6
0.8	0.8	2.3388×10^{-9}	7.5598×10^{-10}	1.950×10^{-5}	5
1.0	1.0	3.2764×10^{-9}	7.3168×10^{-10}	3.665×10^{-5}	7
1.2	1.2	4.5396×10^{-9}	7.7922×10^{-10}	5.285×10^{-5}	7
1.5	1.5	5.3226×10^{-9}	6.8661×10^{-10}	7.428×10^{-5}	2
1.8	1.8	1.0568×10^{-8}	1.1043×10^{-9}	9.273×10^{-5}	7
2.0	2.0	1.3444×10^{-8}	1.2527×10^{-9}	1.038×10^{-4}	8

summarized. First of all, it is noted that the total number of iterations (Tit) in the optimization of ROM are very close FOM's; the difference in Tit is at most 3 and 4 for single and pairwise controls, respectively. Moreover, the optimal states attained in the ROM are closer the desired states of the ROM with respect to the results in the FOM. These are clearly observed in the Table 5.14, Table 5.15 and Table 5.16 with the values $\|\tilde{\omega}_{opt} - \tilde{\omega}_d\|_\infty$ and $\|\tilde{T}_{opt} - \tilde{T}_d\|_\infty$ of the velocity and temperature, respectively. This also indicates the convergence of the optimization in the ROM satisfactorily. Further, the values of the cost functional J attained at the optimal states of the ROM are smaller than the FOM's, which also assures the efficiency of the underlying POD basis. Below, the detailed analysis of the reduced control problems are given for both single and pairwise controls.

First, simulations of the ROM are conducted for the single parameter control with the flow index n as given in Table 5.14. Although the aim of the control is to achieve the desired states of the velocity and temperature, the optimal parameter values are also attained exactly at the same parameter values of the desired states in the ROM, which is a different result than the one obtained for the FOM in Table 4.11. Second, the Hartmann number is used to control the ROM as summarized in Table 5.15. As in the previous case, in addition to being close the desired states, optimal parameter values are closer to the parameter values of the desired states with respect to the values obtained for the FOM in Table 4.12.

Third, control in the ROM is simulated with pairwise control of the parameters Ha and n . Besides reaching the desired states successfully, the optimal parameter values given in Table 5.16 are close to the parameters of the desired states similar to the

Table 5.15: Control with Ha , $n = 1.5$, $\text{Br} = 1.0$, $\alpha_\omega = 10^3$, $\alpha_T = 10^0$, $\alpha_{\text{Ha}} = 10^{-5}$, and $\text{Ha}_0 = 0.1$

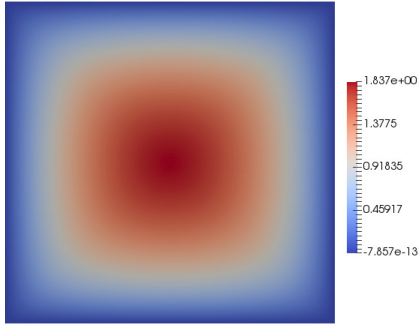
Ha_d	Ha_{opt}	$\ \tilde{\omega}_{\text{opt}} - \tilde{\omega}_d\ _\infty$	$\ \tilde{T}_{\text{opt}} - \tilde{T}_d\ _\infty$	J	Tit
1.0	0.9998	2.8809×10^{-6}	7.1494×10^{-7}	5.300×10^{-6}	3
3.0	2.9998	5.4765×10^{-6}	2.4386×10^{-6}	6.803×10^{-5}	5
5.0	4.9990	1.3708×10^{-5}	1.4147×10^{-5}	2.734×10^{-4}	5
8.0	7.9886	4.5965×10^{-5}	1.0293×10^{-4}	8.162×10^{-4}	6
10.0	9.9564	9.1193×10^{-5}	2.5134×10^{-4}	1.204×10^{-3}	6

results obtained for the FOM in Table 4.13 except the first simulation. The most apparent difference is observed for the case in which the desired states are generated for $\text{Ha} = 1.0$ and $n = 0.6$. However, the optimal states are obtained sufficiently closed to the desired states.

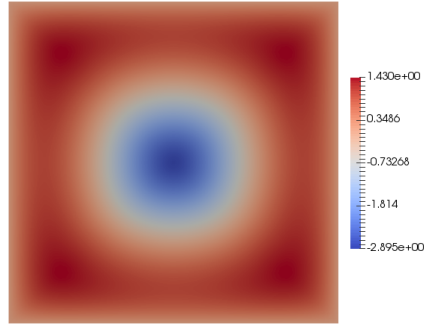
To conclude, the POD bases generated for the three problems in this thesis are not only capable of inheriting the dynamics of the problem but they can also be used to identify the characteristics of the problems in the optimal control. Moreover, the low-dimensional systems obtained by these bases reduce the cost of computational time in the optimization algorithm.

Table 5.16: Control with n and Ha , $\text{Br} = 1.0$, $\alpha_\omega = 10^5$, $\alpha_T = 10^0$, $\alpha_{\text{Ha}} = 10^{-5}$, $\alpha_n = 10^{-5}$, $\text{Ha}_0 = 0.1$ and $n_0 = 0.5$

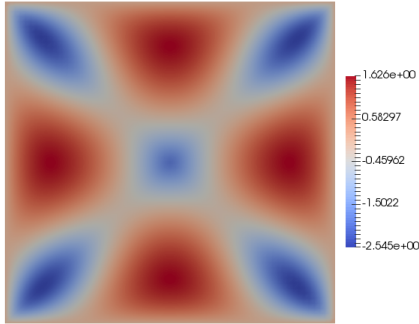
Ha_d	n_d	n_{opt}	Ha_{opt}	$\ \tilde{\omega}_{\text{opt}} - \tilde{\omega}_d\ _\infty$	$\ \tilde{T}_{\text{opt}} - \tilde{T}_d\ _\infty$	J	Tit
1.0	0.6	0.5973	0.7689	1.2019×10^{-5}	7.2518×10^{-5}	8.283×10^{-6}	52
	0.8	0.7994	0.9826	3.6069×10^{-6}	1.1797×10^{-5}	2.375×10^{-5}	45
	1.0	0.9997	0.9960	1.7844×10^{-6}	4.0165×10^{-6}	4.071×10^{-5}	39
	1.2	1.1999	0.9985	1.1316×10^{-6}	1.9730×10^{-6}	5.675×10^{-5}	39
	1.5	1.4999	0.9994	7.3910×10^{-7}	1.0955×10^{-6}	7.800×10^{-5}	38
	1.8	1.7999	0.9996	5.8852×10^{-7}	7.9352×10^{-7}	9.633×10^{-5}	32
	2.0	1.9999	0.9997	5.4209×10^{-7}	6.9688×10^{-7}	1.074×10^{-4}	30
3.0	0.6	0.5964	2.8928	1.5120×10^{-5}	1.1119×10^{-4}	4.570×10^{-5}	48
	0.8	0.7992	2.9914	4.3351×10^{-6}	1.8373×10^{-5}	5.347×10^{-5}	36
	1.0	0.9997	2.9984	1.8717×10^{-6}	6.4208×10^{-6}	6.035×10^{-5}	37
	1.2	1.1999	2.9995	9.8641×10^{-7}	3.0299×10^{-6}	6.587×10^{-5}	43
	1.5	1.4999	2.9999	4.7879×10^{-7}	1.3101×10^{-6}	7.195×10^{-5}	42
	1.8	1.8000	3.0000	3.0722×10^{-7}	7.1170×10^{-7}	7.653×10^{-5}	39
	2.0	2.0000	3.0000	2.7835×10^{-7}	5.1798×10^{-7}	7.930×10^{-5}	38
5.0	0.6	0.5949	4.8874	1.9584×10^{-5}	1.9185×10^{-4}	1.251×10^{-4}	53
	0.8	0.7991	4.9920	4.9366×10^{-6}	3.5157×10^{-5}	1.294×10^{-4}	46
	1.0	0.9997	4.9988	1.8002×10^{-6}	1.1502×10^{-5}	1.333×10^{-4}	36
	1.2	1.1999	4.9997	8.3467×10^{-7}	4.8658×10^{-6}	1.395×10^{-4}	40
	1.5	1.5000	4.9999	5.0940×10^{-7}	1.8675×10^{-6}	1.585×10^{-4}	36
	1.8	1.8000	5.0000	3.4405×10^{-7}	1.0440×10^{-6}	1.945×10^{-4}	30
	2.0	2.0000	5.0000	2.6720×10^{-7}	8.8031×10^{-7}	2.276×10^{-4}	30



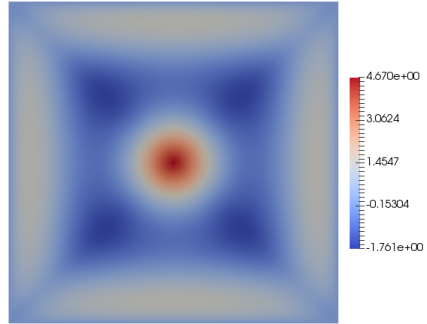
First POD basis function of velocity



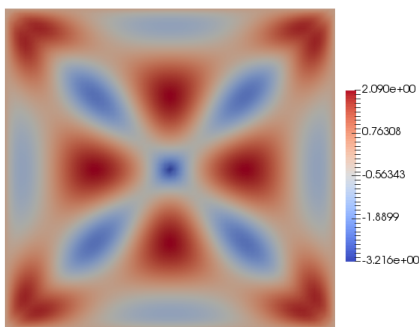
Second POD basis function of velocity



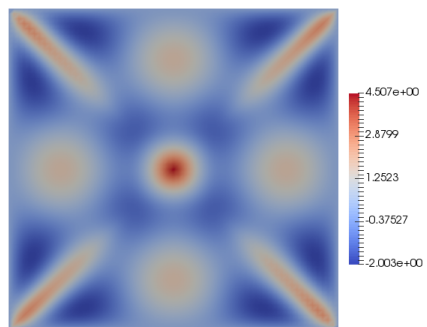
Third POD basis function of velocity



Fourth POD basis function of velocity

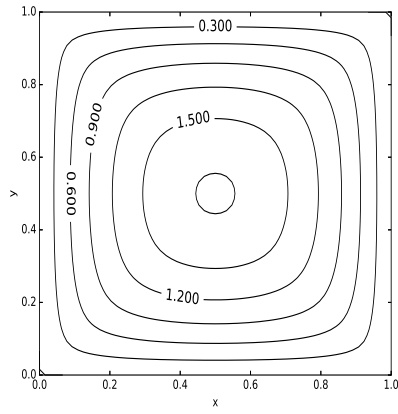


Fifth POD basis function of velocity

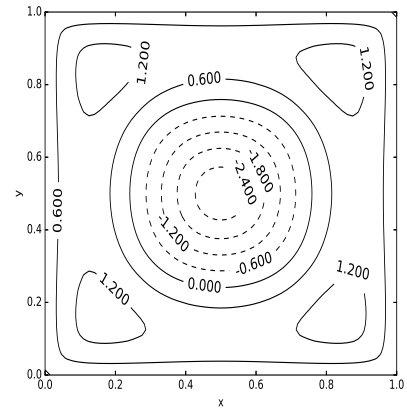


Sixth POD basis function of velocity

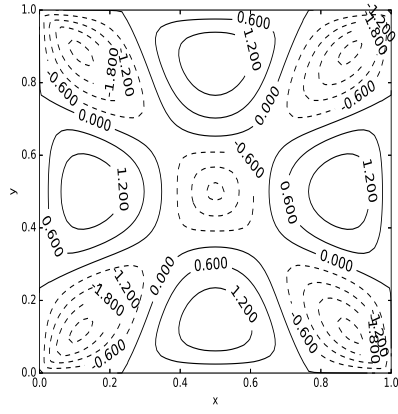
Figure 5.16: POD basis functions of velocity.



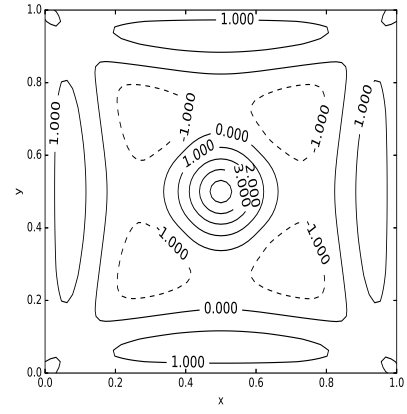
First POD basis function of velocity



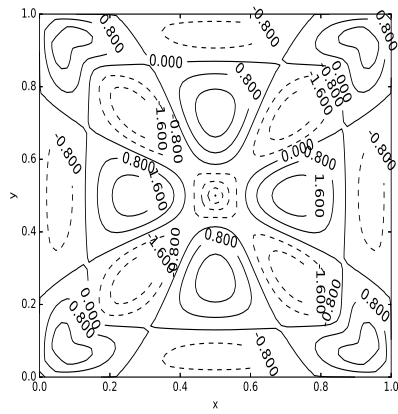
Second POD basis function of velocity



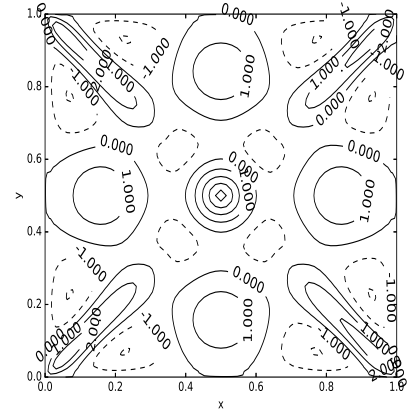
Third POD basis function of velocity



Fourth POD basis function of velocity

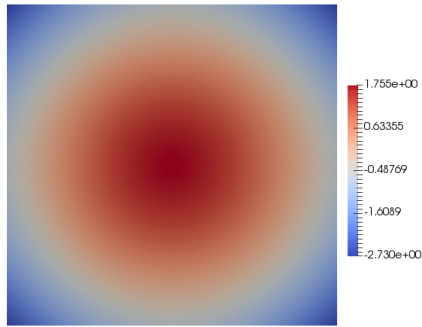


Fifth POD basis function of velocity

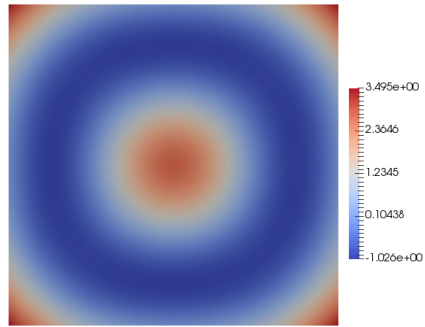


Sixth POD basis function of velocity

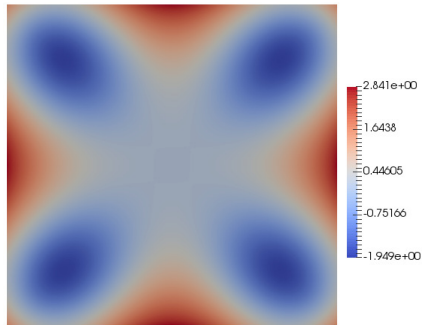
Figure 5.17: Contours of POD basis functions of velocity.



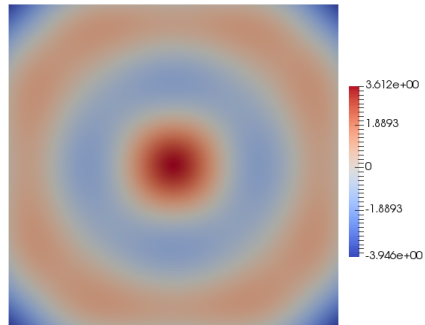
First POD basis function of temperature



Second POD basis function of temperature

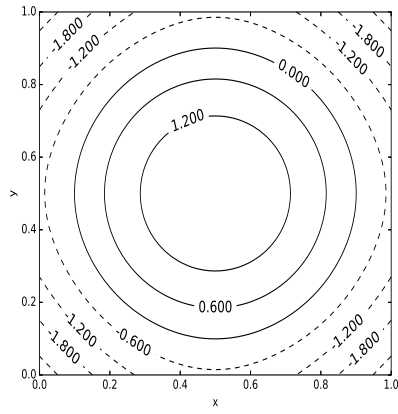


Third POD basis function of temperature

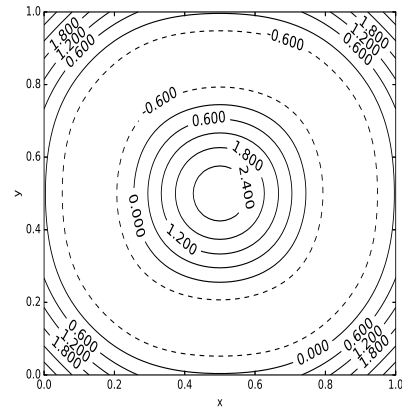


Fourth POD basis function of temperature

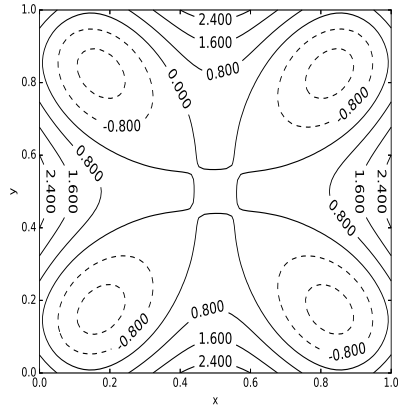
Figure 5.18: POD basis functions of temperature.



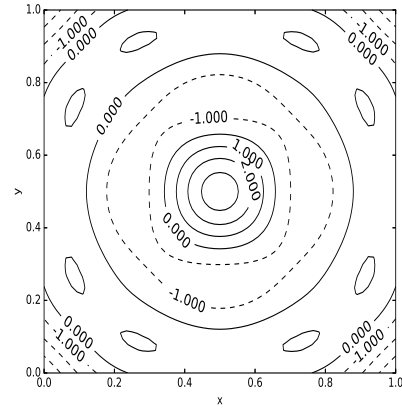
First POD basis function of temperature



Second POD basis function of temperature



Third POD basis function of temperature



Third POD basis function of temperature

Figure 5.19: Isolines of POD basis functions of temperature.

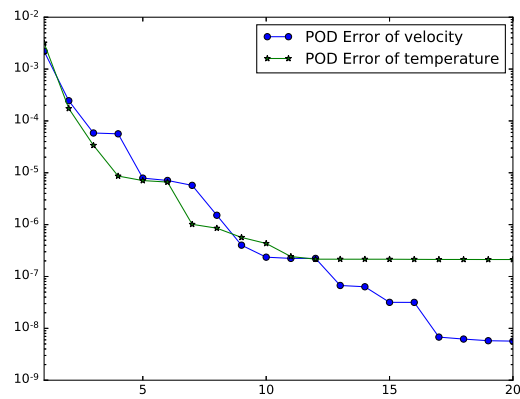


Figure 5.20: POD Errors of Velocity and Temperature corresponding to the solution for $Ha = 1$, $n = 1.5$, $Br = 1$,

CHAPTER 6

CONCLUSION

In this study, numerical solutions of the optimal control problems constrained by the governing PDEs for laminar, steady flows of incompressible viscous fluids are presented. By the implementation of the model order reduction with the proper orthogonal decomposition method, solutions are obtained with the reduced order models.

The problems under investigation are the Navier-Stokes equations, MHD flow and heat transfer equations with temperature dependent viscosity, and power-law fluid flows. As being the fundamental tool for interpreting the flow behavior, N-S equations constitute the basis for applications on fluid flows. Moreover, consideration of MHD flow and heat transfer with temperature dependent viscosity as well as the non-Newtonian fluids enables to explain advanced physical phenomena. However, the high non-linearity in these equations poses new challenges in terms of providing solutions and controls. Thus, this study implements numerical methods and apply optimization for the optimal control of these problems.

Specifically, the considered problems are treated from the three aspects: numerical solutions by FEM, optimal control solutions by the adjoint method following the *discretize-then-optimize* approach, and the reduced order modeling solutions by the POD method with the projection on a continuous form.

While the efficiency of the methods are proved by studying the steady state N-S equations, where the exact solution is available, implementations for the other two problems, where the closed form solutions are not available, are carried out. These studies constitute the extensions of the literature and may be regarded as the main contribu-

tions of the thesis.

First, N-S equations are considered in a velocity-pressure formulation with the mixed finite element method using the Taylor-Hood elements in order to ensure the stability and convergence. Meanwhile, the control problem is designed for a force function distributed over the whole domain. The efficiency of the methods are validated for various values of the parameter ν within the exact solution.

Second, the FEM solutions of MHD flow and heat transfer equations with temperature dependent viscosity and also the case for the power-law fluids are obtained extending the results in literature, where other easy to implement numerical methods such as finite difference have been used.

Third, the main contribution of the thesis is attained by investigating the optimal control for these problems by using the parameters as the control variables. This approach has not been considered before in the literature for such problems and is addressed here for the first time. Furthermore, the control is not only applied for a single parameter but also for pairwise parameters of the underlying systems. Attained controls are successful in achieving the desired states and as well as characterization of the fluids in the case of the power-law fluids. Particularly, since the non-Newtonian fluids are classified as shear-thinning or shear-thickening according to the flow index parameter, the determination of the optimal values of the parameters for a given state is of great importance when the power-law fluids are considered.

Fourth, the computational costs due to the repeated evaluation of the constraint and adjoint equations in the optimal control problems are reduced by the model order reduction. Particularly in this study, POD method is used to obtain a set of basis functions with a low-dimension by using the snapshots taken over the various values of the parameters. The resulting POD basis functions are capable to reflect the dynamics of the fluids for all parameter values covered by the snapshots. Furthermore, these basis functions also enable to obtain controls with pairwise parameters, which is a more challenging optimization problem.

Besides those mentioned above, in this thesis, computer programming of the model order reduction is performed with the projection on a continuous level using a com-

bined automated framework, which is also applicable directly to the optimal control problems by supplying a user-friendly approach of the implementation of the POD in reduced control problems.

To sum up, the outcomes of this study provide a new understanding of the fluid dynamics problems in terms of the optimal control applications and offer a user-friendly computing approach for achieving reduced order models in order to fast computation of the solutions.

Studies can be extended to the time-dependent dynamical systems where the model order reduction has to be conducted on the snapshots having the time information as well. Also, in terms of the physical applications, consideration of the more complex geometries and boundary conditions are also of vital importance. Moreover, controls can be supplied on the boundary of the domain for the heat transfer problems. Therefore, the next step to move this study forward is to work on the boundary controls on the more complex geometries and time-dependent systems for optimal control of the fluid dynamics problems in real-world, industrial applications.

REFERENCES

- [1] F. Abergel and R. Temam, On some control problems in fluid mechanics, *Theoretical and Computational Fluid Dynamics*, 1, pp. 303–325, 1990.
- [2] N. U. Ahmed and K. R. Rao, *Orthogonal Transforms for Digital Signal Processing*, Springer-Verlag New York, Inc., 1975.
- [3] N. Ali and T. Hayat, Peristaltic motion of a Carreau fluid in an asymmetric channel, *Applied Mathematics and Computation*, 193(2), pp. 535–552, 2007.
- [4] N. Alsoy-Akgün and M. Tezer-Sezgin, DRBEM and DQM solutions of natural convection flow in a cavity under a magnetic field, *Progress in Computational Fluid Dynamics*, 13(5), pp. 270–284, 2013.
- [5] J. D. Anderson and J. Wendt, *Computational Fluid Dynamics*, Springer, 1995.
- [6] N. Arada, Optimal control of shear-thinning fluids, *SIAM Journal on Control and Optimization*, 50(4), pp. 2515–2542, 2012.
- [7] H. A. Attia, Influence of temperature dependent viscosity on the MHD–channel flow of dusty fluid with heat transfer, *Acta Mechanica*, 151, pp. 89–101, 2001.
- [8] H. A. Attia, Influence of temperature dependent viscosity on the MHD Couette flow of dusty fluid with heat transfer, *Differential Equations and Nonlinear Mechanics*, 2006, pp. 1–14, 2006.
- [9] M. Barrault, Y. Maday, N. C. Nguyen, and A. T. Patera, An ‘empirical interpolation method’: application to efficient reduced-basis discretization of partial differential equations, *Comptes Rendus Mathematique Academie des Sciences*, Paris, 2004.
- [10] C. E. Baumann and J. T. Oden, A discontinuous hp finite element method for the Euler and Navier–Stokes equations, *International Journal for Numerical Methods in Fluids*, 31(1), pp. 79–95, 1999.
- [11] C. O. Bennett and J. E. Myers, *Momentum, Heat and Mass Transfer*, McGraw-Hill New York, 1982.
- [12] G. Bornia, *Analysis of Optimal Control Problems for the Incompressible MHD Equations and Implementation in a Finite Element Multiphysics Code*, Ph.D. thesis, Alma Mater Studiorum - University of Bologna, 2012.

- [13] R. M. Bryce and M. R. Freeman, Extensional instability in electro-osmotic microflows of polymer solutions, *Physical Review E*, 81(3), p. 036328, 2010.
- [14] D. Chapelle, A. Gariah, P. Moireau, and J. Sainte-Marie, A Galerkin strategy with proper orthogonal decomposition for parameter-dependent problems—analysis, assessments and applications to parameter estimation, *ESAIM: Mathematical Modeling and Numerical Analysis*, 47(6), pp. 1821–1843, 2013.
- [15] S. Chaturantabut and D. C. Sorenson, Nonlinear model reduction via discrete empirical interpolation, *SIAM Journal on Scientific Computing*, 32(5), 2010.
- [16] A. J. Chorin, Numerical solution of the Navier-Stokes equations, *Mathematics of Computation*, 22(104), pp. 745–762, 1968.
- [17] E. Christensen, J. Sørensen, M. Brøns, and P. Christiansen, Low-dimensional representations of early transition in rotating fluid flow, *Theoretical and Computational Fluid Dynamics*, 5(6), pp. 259–267, 1993.
- [18] E. A. Christensen, M. Brøns, and J. N. Sørensen, Evaluation of proper orthogonal decomposition–based decomposition techniques applied to parameter-dependent nonturbulent flows, *SIAM Journal on Scientific Computing*, 21(4), pp. 1419–1434, 1999.
- [19] C. L. Cox, H. Lee, and D. C. Szurley, Optimal control of non-isothermal viscous fluid flow, *Mathematical and Computer Modeling*, 50, pp. 1142–1153, 2009.
- [20] L. Dedè, Reduced basis method and a posteriori error estimation for parametrized linear–quadratic optimal control problems, *SIAM Journal on Scientific Computing*, 32(2), pp. 997–1019, 2010.
- [21] M. Desai and K. Ito, Optimal controls of Navier–Stokes equations, *SIAM Journal on Control and Optimization*, 32(5), pp. 1428–1446, 1994.
- [22] L. Dragos, *Magnetofluid Dynamics*, Abacus Press, 1975.
- [23] H. C. Elman, Preconditioning for the steady-state Navier–Stokes equations with low viscosity, *SIAM Journal on Scientific Computing*, 20(4), pp. 1299–1316, 1999.
- [24] P. E. Farrell, D. A. Ham, S. W. Funke, and M. E. Rognes, Automated derivation of the adjoint of high-level transient finite element programs, *SIAM Journal on Scientific Computing*, 35(4), pp. 369–393, 2013.
- [25] B. A. Finlayson, *The Method of Weighted Residuals and Variational Principles*, volume 87, Elsevier, 1972.
- [26] K. Fukunaga, *Instruction to Statistical Pattern Recognition*, Elsevier, 1972.

- [27] S. W. Funke, *The Automation of PDE-Constrained Optimisation and Its Applications*, Ph.D. thesis, Department of Earth Science and Engineering, Imperial College London, 2012.
- [28] T. Gänzler, S. Volkwein, and M. Weiser, SQP methods for parameter identification problems arising in hyperthermia, *Optimization Methods and Software*, 21(6), pp. 869–887, 2006.
- [29] M. R. Garvie and C. Trenchea, Identification of space-time distributed parameters in the Gierer–Meinhardt reaction-diffusion system, *SIAM Journal on Applied Mathematics*, 74(1), pp. 147–166, 2014.
- [30] A. Gavrus, E. Massoni, and J. L. Chenot, An inverse analysis using a finite element model for identification of rheological parameters, *Journal of Materials Processing Technology*, 60, pp. 447–454, 1996.
- [31] O. Ghattas and J.-H. Bark, Optimal control of two-and three-dimensional incompressible Navier–Stokes flows, *Journal of Computational Physics*, 136(2), pp. 231–244, 1997.
- [32] V. Girault and P.-A. Raviart, *Finite Element Methods for Navier–Stokes Equations: Theory and Algorithms*, volume 5, Springer Science & Business Media, 1986.
- [33] M. A. Grepl, N. C. Nguyen, K. Veroy, A. T. Patera, and G. R. Liu, Certified rapid solution of partial differential equations for real-time parameter estimation and optimization, in *Real-time PDE-constrained optimization*, pp. 199–216, SIAM, 2007.
- [34] R. Griesse and K. Kunisch, Optimal control for a stationary MHD system in velocity-current formulation, *SIAM Journal on Control and Optimization*, 45, pp. 1822–1845, 2006.
- [35] T. Guerra, Distributed control for shear–thinning non–Newtonian fluids, *Journal of Mathematical Fluid Mechanics*, 14, pp. 771–789, 2012.
- [36] T. Guerra, C. Catarino, T. Mestre, S. Santos, J. Tiago, and A. Sequeira, A data assimilation approach for non–Newtonian blood flow simulations in 3d geometries, *Applied Mathematics and Computation*, 321, pp. 176–194, 2018.
- [37] T. Guerra, J. Tiago, and A. Sequeira, Optimal control in blood flow simulations, *International Journal of Non–Linear Mechanics*, 64, pp. 57–69, 2014.
- [38] M. Gunzburger, L. Hou, and T. P. Svobodny, Analysis and finite element approximation of optimal control problems for the stationary Navier-Stokes equations with Dirichlet controls, *ESAIM: Mathematical Modeling and Numerical Analysis*, 25(6), pp. 711–748, 1991.

- [39] M. D. Gunzburger, *Flow Control*, Springer Science & Business Media, 2012.
- [40] M. D. Gunzburger, L. Hou, and T. P. Svobodny, Analysis and finite element approximation of optimal control problems for the stationary Navier–Stokes equations with distributed and Neumann controls, *Mathematics of Computation*, 57(195), pp. 123–151, 1991.
- [41] M. D. Gunzburger and C. Trencha, Analysis and discretization of an optimal control problem for the time-periodic MHD equations, *Mathematical Analysis and Applications*, 308, pp. 440–446, 2005.
- [42] M. Hadigol, R. Nosrati, A. Nourbakhsh, and M. Raisee, Numerical study of electroosmotic micromixing of non-Newtonian fluids, *Journal of Non-Newtonian Fluid Mechanics*, 166(17-18), pp. 965–971, 2011.
- [43] T. M. Harms, M. A. Jog, and R. M. Manglik, Effects of temperature-dependent viscosity variations and boundary conditions on fully developed laminar forced convection in a semicircular duct, *Journal of Heat Transfer*, 120(3), pp. 600–605, 1998.
- [44] P. J. Hartnett and M. Kostic, Heat transfer to Newtonian and non-Newtonian fluids in rectangular ducts, *Advances in Heat Transfer*, 19, pp. 247–356, 1989.
- [45] M. Heinkenschloss, Formulation and analysis of a sequential quadratic programming method for the optimal Dirichlet boundary control of Navier–Stokes flow, in *Optimal Control*, pp. 178–203, Springer, 1998.
- [46] J. Heinrich, P. Huyakorn, O. Zienkiewicz, and A. Mitchell, An ‘upwind’ finite element scheme for two-dimensional convective transport equation, *International Journal for Numerical Methods in Engineering*, 11(1), pp. 131–143, 1977.
- [47] M. Hinze, R. Pinnau, M. Ulbrich, and S. Ulbrich, *Optimization with PDE Constraints*, Springer, 2009.
- [48] L. S. Hou and A. J. Meir, Boundary optimal control of MHD flows, *Applied Mathematics and Optimization*, 32, pp. 143–162, 1995.
- [49] K. Ito, M. Kroller, and K. Kunisch, A numerical study of an augmented lagrangian method for the estimation of parameters in elliptic systems, *SIAM journal on scientific and statistical computing*, 12(4), pp. 884–910, 1991.
- [50] K. Ito and K. Kunisch, Augmented Lagrangian-SQP-methods in Hilbert spaces and application to control in the coefficients problems, *SIAM Journal on Optimization*, 6(1), pp. 96–125, 1996.
- [51] K. Ito and S. S. Ravindran, Optimal control of thermally convected fluid flows, *SIAM Journal on Scientific Computing*, 19, pp. 1847–1869, 1998.

- [52] K. Ito and S. S. Ravindran, A reduced-order method for simulation and control of fluid flows, *Journal of computational physics*, 143(2), pp. 403–425, 1998.
- [53] H. Jasak, *Error analysis and estimation for the finite volume method with applications to fluid flows*, Ph.D. thesis, Imperial College London (University of London), 1996.
- [54] C. Kahle and K. F. Lam, Parameter identification via optimal control for a Cahn–Hilliard-chemotaxis system with a variable mobility, *Applied Mathematics & Optimization*, pp. 1–42, 2017.
- [55] M. Kirby, J. Boris, and L. Sirovich, An eigenfunction analysis of axisymmetric jet flow, *Journal of Computational Physics*, 90(1), pp. 98–122, 1990.
- [56] N. Kishan and B. C. Shekar, Finite element analysis of fully developed unsteady MHD convection flow in a vertical rectangular duct with viscous dissipation and heat source/sink, *Journal of Applied Science and Engineering*, 18(2), pp. 143–152, 2015.
- [57] K. Kunisch and X. Marduel, Optimal control of non-isothermal viscoelastic fluid flow, *Journal of Non-Newtonian Fluid Mechanics*, 88(3), pp. 261–301, 2000.
- [58] K. Kunisch and E. W. Sachs, Reduced SQP methods for parameter identification problems, *SIAM Journal on Numerical Analysis*, 29(6), pp. 1793–1820, 1992.
- [59] K. Kunisch and S. Volkwein, Galerkin proper orthogonal decomposition methods for parabolic problems, *Numerische Mathematik*, 90(1), pp. 117–148, 2001.
- [60] K. Kunisch and S. Volkwein, Galerkin proper orthogonal decomposition methods for a general equation in fluid dynamics, *SIAM Journal on Numerical Analysis*, 40(2), pp. 492–515, 2002.
- [61] K. Kunisch and S. Volkwein, Proper orthogonal decomposition for optimality systems, *ESAIM: Mathematical Modeling and Numerical Analysis*, 42(1), pp. 1–23, 2008.
- [62] M. G. Larson and F. Bengzon, *The Finite Element Method: Theory, Implementation and Applications*, volume 10, Springer Science & Business Media, 2013.
- [63] T. Lassila, A. Manzoni, A. Quarteroni, and G. Rozza, Model order reduction in fluid dynamics: Challenges and perspectives, in *Reduced Order Methods for Modeling and Computational Reduction*, pp. 235–273, Springer, 2014.
- [64] D. C. Liu and J. Nocedal, On the limited memory BFGS method for large scale optimization, *Mathematical Programming*, 45(1-3), pp. 503–528, 1989.

- [65] D. Logashenko, B. Maar, and V. Schulz, Optimal geometrical design of Bingham parameter measurement devices, in *Fast Solution of Discretized Optimization Problems: Workshop held at the Weierstrass Institute for Applied Analysis and Stochastics, Berlin, May 8–12, 2000*, volume 138, p. 167, Birkhäuser, 2012.
- [66] A. Logg, K. A. Mardal, and G. Wells, *Automated Solution of Differential Equations by the Finite Element Method*, Springer, 2012.
- [67] J. Lumley, A. Yaglom, and V. Tatarski, Atmospheric turbulence and wave propagation, *The Structure of Inhomogeneous Turbulence*, pp. 166–178, 1967.
- [68] J. L. Lumley, Coherent structures in turbulence, in *Transition and Turbulence*, pp. 215–242, Elsevier, 1981.
- [69] J. Málek and T. Roubíček, Optimization of steady flows for incompressible viscous fluids, in *Applied Nonlinear Analysis*, pp. 355–372, Springer, 2002.
- [70] G. L. Morini, Analytical determination of the temperature distribution and Nusselt numbers in rectangular ducts with constant axial heat flux, *International Journal of Heat and Mass Transfer*, 43(5), pp. 741–755, 2000.
- [71] J. Nocedal and S. J. Wright, *Numerical Optimization*, Springer Series in Operations Research, 2006.
- [72] H. M. Park, S. M. Hong, and J. Y. Lim, Estimation of rheological parameters using velocity measurements, *Chemical Engineering Science*, 62, pp. 6806–6815, 2007.
- [73] M. Patel and M. G. Timol, Numerical treatment of Powell–Eyring fluid flow using method of satisfaction of asymptotic boundary conditions (MSABC), *Applied Numerical Mathematics*, 59(10), pp. 2584–2592, 2009.
- [74] B. Pekmen and M. Tezer-Sezgin, DRBEM solution of MHD flow with magnetic induction and heat transfer, *Computer Modeling in Engineering & Sciences*, 1(1), pp. 1–26, 2014.
- [75] J. M. Pereira, M. Kobayashi, and J. C. Pereira, A fourth-order-accurate finite volume compact method for the incompressible Navier–Stokes solutions, *Journal of Computational Physics*, 167(1), pp. 217–243, 2001.
- [76] A. Quarteroni and A. Valli, *Numerical Approximation of Partial Differential Equations*, Springer, 2008.
- [77] Z. Ren, X. Liu, C. Xu, T. Chen, and Z. Wu, Optimal control for realizing target flow velocity in 1D MHD flow, in *Proceedings of the 36th Chinese Control Conference*, pp. 1591–1596, IEEE, 2017.

- [78] T. Richter and T. Wick, Optimal control and parameter estimation for stationary fluid-structure interaction problems, *SIAM Journal on Scientific Computing*, 35(5), pp. B1085–B1104, 2013.
- [79] G. Rozza, D. B. P. Huynh, and A. T. Patera, Reduced basis approximation and a posteriori error estimation for affinely parametrized elliptic coercive partial differential equations, *Archives of Computational Methods in Engineering*, 15(3), p. 1, 2007.
- [80] M. E. Sayed-Ahmed, Numerical solution of power law fluids flow and heat transfer with a magnetic field in a rectangular duct, *International Communications in Heat and Mass Transfer*, 33, pp. 1165–1176, 2006.
- [81] M. E. Sayed-Ahmed and H. A. Attia, MHD flow and heat transfer in a rectangular duct with temperature dependent viscosity and Hall effect, *International Communications in Heat and Mass Transfer*, 27(8), pp. 1177–1187, 2000.
- [82] L. Sirovich, Turbulence and the dynamics of coherent structures. Part I: Coherent structures, *Quarterly of Applied Mathematics*, 45(1), pp. 561–571, 1987.
- [83] L. Sirovich, Turbulence and the dynamics of coherent structures. Part II: Symmetries and transformations, *Quarterly of Applied Mathematics*, 45(2), pp. 571–583, 1987.
- [84] L. Sirovich, Turbulence and the dynamics of coherent structures. Part III: Dynamics and scaling, *Quarterly of Applied Mathematics*, 45(3), pp. 583–590, 1987.
- [85] T. Slawig, Distributed control for a class of non-Newtonian fluids, *Journal of Differential Equations*, 219, pp. 116–143, 2005.
- [86] S. S. Sritharan, *Optimal Control of Viscous Flow*, SIAM, 1998.
- [87] M. Stoll, J. W. Pearson, and P. K. Maini, Fast solvers for optimal control problems from pattern formation, *Journal of Computational Physics*, 304, pp. 27–45, 2016.
- [88] V. L. Streeter, *Handbook of Fluid Dynamics*, McGraw-Hill Book Company, 1961.
- [89] S. Syrjala, Finite element analysis of fully developed laminar flow of power-law non-Newtonian fluid in a rectangular duct, *International Communications in Heat and Mass Transfer*, 22(4), pp. 549–557, 1995.
- [90] S. Syrjala, Further finite element analysis of fully developed laminar flow of power-law non-Newtonian fluid in rectangular ducts: Heat transfer predictions, *International Communications in Heat and Mass Transfer*, 23(6), pp. 799–807, 1996.

- [91] C. Taylor and P. Hood, A numerical solution of the Navier–Stokes equations using the finite element technique, *Computers & Fluids*, 1(1), pp. 73–100, 1973.
- [92] R. Temam, *Navier-Stokes Equations: Theory and Numerical Analysis*, volume 343, American Mathematical Society, 1977.
- [93] F. Thomasset, *Implementation of Finite Element Methods for Navier–Stokes Equations*, Springer Science & Business Media, 1981.
- [94] T. Tonn, K. Urban, and S. Volkwein, Optimal control of parameter-dependent convection-diffusion problems around rigid bodies, *SIAM Journal on Scientific Computing*, 32(3), pp. 1237–1260, 2010.
- [95] F. Tröltzsch, *Optimal Control of Partial Differential Equations: Theory, Methods and Applications*, American Mathematical Society, 2010.
- [96] Ö. Türk and M. Tezer-Sezgin, Chebyshev spectral collocation method for unsteady MHD flow and heat transfer of a dusty fluid between parallel plates, *Numerical Heat Transfer, Part A: Applications*, 64(7), pp. 597–610, 2013.
- [97] Ö. Türk and M. Tezer-Sezgin, FEM solution of natural convection flow in square enclosures under magnetic field, *International Journal of Numerical Methods for Heat & Fluid Flow*, 23(5), pp. 844–866, 2013.
- [98] J. C. Umavathi, I. C. Liu, J. P. Kumar, and I. Pop, Fully developed magneto convection flow in a vertical rectangular duct, *Heat and Mass Transfer*, 47, pp. 1–11, 2011.
- [99] S. Volkwein, *Proper Orthogonal Decomposition: Theory and Reduced-Order Modelling*, University of Konstanz, Department of Mathematics and Statistics, <http://www.math.uni-konstanz.de/numerik/personen/volkwein/teaching/POD-Book.pdf>, 2013.
- [100] D. Wachsmuth and T. Roubicek, Optimal control of planar flow of incompressible non–Newtonian fluids, *Journal for Analysis and Its Applications*, 29, pp. 351–376, 2010.
- [101] M. Weiser, A. Schiela, and P. Deuffhard, Asymptotic mesh independence of Newton’s method revisited, *SIAM Journal on Numerical Analysis*, 42(5), pp. 1830–1845, 2005.

APPENDIX A

ALGORITHMS, COMPUTER CODES AND OPTIMALITY CONDITIONS

A.1 L-BFGS two loop recursion

Algorithm 4 L-BFGS two-loop recursion

```
1: procedure L-BFGS2LOOP( $\tilde{J}$ ,  $m$ ,  $S_k^m$ ,  $Y_k^m$ ,  $\rho_k^m$ )
2:    $S_k^m = s_{k-1}, \dots, s_{k-m}$ ,  $Y_k^m = y_{k-1}, \dots, y_{k-m}$  and  $\rho_k^m = \rho_{k-1}, \dots, \rho_{k-m}$ ;
3:    $r \leftarrow \nabla \tilde{J}_k$ ;
4:   for  $i = k-1, k-2, \dots, k-m$  do
5:      $\gamma_i \leftarrow \rho_i s_i^T r$ ;
6:      $r \leftarrow r - \gamma_i y_i$ ;
7:   end for
8:    $d \leftarrow H_k^0 r$ ;
9:   for  $i = k-m, k-m+1, \dots, k-1$  do
10:     $\beta \leftarrow \rho_i y_i^T d$ ;
11:     $d \leftarrow d + s_i(\gamma_i - \beta)$ ;
12:   end for
13:   Stop with  $H_k \nabla \tilde{J} = d$ 
14: end procedure
```

A.2 Python Codes

```

1 mesh      = UnitSquareMesh(nx,ny)
2 V_element = VectorElement('CG', triangle, 2)
3 Q_element = FiniteElement('CG', triangle, 1)
4 R_element = FiniteElement('R', triangle, 0)
5 W_element = MixedElement([V_element, Q_element, R_element])
6 W         = FunctionSpace(mesh, W_element)
7 v, q, d   = TestFunctions(W)
8 w         = Function(W)
9 y, p, c   = split(w)

```

Listing A.1: Mesh, elements and function spaces of the Navier-Stokes equations

```

1 def main():
2     F = nu*inner(grad(y), grad(v))*dx\
3         + inner(dot(y, nabla_grad(y)), v)*dx\
4         - q*div(y)*dx\
5         - p*div(v)*dx\
6         + c*q*dx\
7         + p*d*dx\
8         - inner(f, v)*dx
9     solve(F==0, w, bc)

```

Listing A.2: Variational formulation of the Navier-Stokes equations

A.3 First-order optimality conditions for the control of the MHD Flow and heat transfer equations with variable viscosity

For deriving the first order optimality conditions in case when *optimize-then-discretize* approach is used, we introduce the Lagrange multiplier $\Lambda = (\lambda, \eta)$ and construct the Lagrange function as

$$\begin{aligned}
\mathcal{L}(\omega, T, \mathbf{u}, \lambda, \eta) = & J(\omega(\mathbf{u}), T(\mathbf{u})) + \langle \bar{\mu} \nabla \omega, \nabla \lambda \rangle_{\Omega} - \left\langle 1 - \frac{\text{Ha}^2}{1 + m^2} \omega, \lambda \right\rangle_{\Omega} \\
& + \langle \nabla T, \nabla \eta \rangle_{\Omega} - \left\langle \text{Br} \bar{\mu} \left[\left(\frac{\partial \omega}{\partial x} \right)^2 + \left(\frac{\partial \omega}{\partial y} \right)^2 \right], \eta \right\rangle_{\Omega} \\
& - \left(\frac{\text{Ha}^2 \text{Br}}{1 + m^2} \right) \langle \omega^2, \eta \rangle_{\Omega} + \left\langle \frac{\omega}{\omega_m}, \eta \right\rangle_{\Omega}, \quad \Lambda = (\lambda, \eta) \in H_0^1(\Omega)^2.
\end{aligned}$$

```

1 J      = Functional( 0.5 * alphav * inner(y - yd, y - yd) * dx \
2                + 0.5 * alphau * inner(u, u) * dx )
3 rf      = ReducedFunctional(J, Control(u))
4 u_opt   = minimize(rf, options = {"gtol": 1e-10, "ftol": 1e-10})

```

Listing A.3: Optimization of the Navier-Stokes equations

```

1 yPHI, k_y = load_PODbasis(yPhi,V)
2 pPHI, k_p = load_PODbasis(pPhi,Q)
3 cPHI, k_c = load_PODbasis(cPhi,R)
4 Rv_element = VectorElement('R', triangle,0, dim=k_y)
5 Rq_element = VectorElement('R', triangle,0, dim=k_p)
6 Rr_element = VectorElement('R', triangle,0, dim=k_c)
7 Rw_element = MixedElement([Rv_element,Rq_element,Rr_element])
8 Rw         = FunctionSpace(mesh, Rw_element)
9 Rv         = FunctionSpace(mesh, Rv_element)
10 vdofs,qdofs,ddofs = TestFunctions(Rw)
11 wdofs       = Function(Rw)
12 ydofs,pdofs,cdofs = split(wdofs)
13 yr = sum([ydofs[i]*yPHI[i] for i in range(k_y)])
14 pr = sum([pdofs[i]*pPHI[i] for i in range(k_p)])
15 cr = sum([cdofs[i]*cPHI[i] for i in range(k_c)])
16 vr = sum([vdofs[i]*yPHI[i] for i in range(k_y)])
17 qr = sum([qdofs[i]*pPHI[i] for i in range(k_p)])
18 dr = sum([ddofs[i]*cPHI[i] for i in range(k_c)])

```

Listing A.4: Elements and function spaces for the ROM of the Navier-Stokes equations

In order to satisfy the first-order necessary optimality conditions, the derivatives of \mathcal{L} with respect to ω and T have to vanish at the optimal solution; that is,

$$\begin{aligned}
\mathcal{L}_\omega(\omega, T, \mathbf{u}, \lambda, \eta)h_\omega &= J_\omega(h_\omega) + \langle \bar{\mu} \nabla h_\omega, \nabla \lambda \rangle_\Omega + \left\langle \frac{\text{Ha}^2}{1+m^2} h_\omega, \lambda \right\rangle_\Omega \\
&\quad - 2 \langle \text{Br} \bar{\mu} (\nabla \omega \cdot \nabla h_\omega), \eta \rangle_\Omega - 2 \left(\frac{\text{Ha}^2 \text{Br}}{1+m^2} \right) \langle h_\omega, \eta \rangle_\Omega \\
&\quad + \left\langle \frac{h_\omega \cdot \omega_m - (h_\omega)_m \omega}{\omega_m^2}, \eta \right\rangle_\Omega = 0
\end{aligned} \tag{A.1}$$

for $h_\omega \in H^1(\Omega)$, and

$$\begin{aligned}
\mathcal{L}_T(\omega, T, \mathbf{u}, \lambda, \eta)h_T &= J_T(h_T) - B h_T \langle \bar{\mu} \nabla \omega, \nabla \lambda \rangle_\Omega + \langle (\nabla h_T, \nabla \eta) \rangle_\Omega \\
&\quad - B \left\langle \text{Br} \bar{\mu} \left[\left(\frac{\partial \omega}{\partial x} \right)^2 + \left(\frac{\partial \omega}{\partial y} \right)^2 \right], \eta h_T \right\rangle_\Omega = 0
\end{aligned} \tag{A.2}$$

```

1 def main():
2     Fr = nu*inner(grad(yr), grad(vr))*dx\
3         + inner(dot(yr, nabla_grad(yr)), vr)*dx\
4         - qr*div(yr)*dx\
5         - pr*div(vr)*dx\
6         + cr*qr*dx\
7         + pr*dr*dx\
8         - inner(fr, vr)*dx
9     solve(Fr==0, wdots)

```

Listing A.5: Variational formulation of the Navier-Stokes equations

```

1 udofs = Function(Rv, name="Control")
2 ur = sum([udofs[i]*yPHI[i] for i in range(k_y)])
3 J = Functional(0.5 * alphav * inner(yr - ydes, yr - ydes) * dx(mesh)
4     + 0.5 * alpha * inner(ur, ur) * dx(mesh))
5 rf = ReducedFunctional(J, Control(udofs))
6 u_opt = minimize(rf, options = {"gtol": 1e-10, "ftol": 1e-10})

```

Listing A.6: Optimization with the ROM of the Navier-Stokes equations

for $h_T \in H^1(\Omega)$. Hence, (A.1) and (A.2) determine the adjoint problem to be in the form

$$\begin{aligned}
 & -\frac{\partial}{\partial x} \left(\bar{\mu} \frac{\partial \lambda}{\partial x} \right) - \frac{\partial}{\partial y} \left(\bar{\mu} \frac{\partial \lambda}{\partial y} \right) + \frac{\text{Ha}^2}{1+m^2} \lambda - 2\text{Br} \bar{\mu} \nabla \omega \cdot \nabla \eta - 2 \frac{\text{Ha}^2 \text{Br}}{1+m^2} \omega \eta \\
 & \quad + \frac{\eta \omega_m - \omega \eta_m}{\omega_m^2} = -\alpha_\omega (\omega - \omega_d) \\
 & -\Delta \eta + B \text{Br} \bar{\mu} \left[\left(\frac{\partial \omega}{\partial x} \right)^2 + \left(\frac{\partial \omega}{\partial y} \right)^2 \right] \eta + B \frac{\partial}{\partial x} \left(\bar{\mu} \frac{\partial \omega}{\partial x} \right) + \frac{\partial}{\partial y} \left(\bar{\mu} \frac{\partial \omega}{\partial y} \right) \lambda = -\alpha_T (T - T_d) \\
 & \quad \lambda = 0 \quad \text{and} \quad \eta = 0 \quad \text{on} \quad \partial \Omega.
 \end{aligned}$$

Optimality condition on the derivative with respect to the control vector \mathbf{u} should be considered similarly. If, for instance, $\mathbf{u} = \text{Ha}$ is assumed to be the control variable, then

$$\mathcal{L}_{\mathbf{u}}(\omega, T, \mathbf{u}, \lambda, \eta) = 0$$

is simplified into

$$\left\langle \frac{2\text{Ha}\omega}{1+m^2}, \lambda \right\rangle_\Omega - \left\langle \frac{2\text{HaBr}}{1+m^2} \omega^2, \eta \right\rangle_\Omega + \frac{\partial J}{\partial \text{Ha}} = 0.$$


```

1 mesh      = RectangleMesh(Point(0.0,0.0), Point(a,b), nx, ny)
2 V_element = FiniteElement('CG', triangle, 2)
3 P_element = FiniteElement('CG', triangle, 2)
4 W_element = MixedElement([V_element, V_element])
5 P         = FunctionSpace(mesh, P_element)
6 W         = FunctionSpace(mesh, W_element)
7 V         = FunctionSpace(mesh, V_element)
8 q, r      = TestFunctions(W)
9 u         = Function(W)
10 w, theta  = split(u)

```

Listing A.7: Mesh, elements and function spaces of the MHD flow and heat transfer with temperature dependent viscosity

```

1 def main():
2     F1 = inner(-mu(B, theta)*grad(w), grad(q))*dx\
3         - Ha*Ha/(1+m*m)*w*q*dx\
4         + one*q*dx
5     F2 = inner(grad(theta), grad(r))*dx\
6         + (b/a)/(w_m(w))*w*r*dx(mesh)\
7         - Br*mu(B, theta)*inner(grad(w), grad(w))*r*dx\
8         - Ha*Ha*Br/(1+m*m)*w*w*r*dx
9     F = F1+F2
10    solve(F==0, u, bc)

```

Listing A.8: Variational formulation of the MHD flow and heat transfer with temperature dependent viscosity

```

1 def w_m(w):
2     return assemble(w*dx)
3 def mu(B, theta):
4     return exp(-B*theta)

```

Listing A.9: Nonlinear terms of the MHD flow and heat transfer with temperature dependent viscosity

```

1 J = Functional( 0.5 * alfaw * ( w - w_d ) * ( w - w_d ) * dx(mesh)\
2               + 0.5 * alfatheta*(theta - theta_d)*(theta - theta_d) * dx(mesh)\
3               + 0.5 * alfau * Ha * Ha * dx(mesh))
4 rf = ReducedFunctional(J, Control(Ha))
5 par_opt = minimize(rf, options = {"gtol": 1e-10, "ftol": 1e-10})

```

Listing A.10: Optimization of the MHD flow and heat transfer with temperature dependent viscosity

```

1 wPHI, k_w      = load_PODbasis(wPhi,V)
2 thetaPHI, k_theta = load_PODbasis(thetaPhi,V)
3 mesh          = RectangleMesh(Point(0.0,0.0), Point(a,b), nx, ny)
4 Rw_element    = VectorElement('R', triangle,0, dim=k_w)
5 Rtheta_element = VectorElement('R', triangle,0, dim=k_theta)
6 Ru_element    = MixedElement([Rw_element,Rtheta_element])
7 Ru            = FunctionSpace(mesh, Ru_element)
8 vdofs,qdofs   = TestFunctions(Ru)
9 udofs         = Function(Ru)
10 wdofs,thetadofs = split(udofs)
11 wr           = sum([wdofs[i]*wPHI[i] for i in range(k_w)])
12 thetar       = sum([thetadofs[i]*thetaPHI[i] for i in range(k_theta)])
13 vr           = sum([vdofs[i]*wPHI[i] for i in range(k_w)])
14 qr           = sum([qdofs[i]*thetaPHI[i] for i in range(k_theta)])

```

Listing A.11: Elements and function spaces for ROM of the MHD flow and heat transfer with temperature dependent viscosity

```

1 def main():
2     Fr1 = inner(-mu(B,thetar)*grad(wr),grad(vr))*dx\
3           - Ha*Ha/(1+m*m)*wr*vr*dx\
4           + one*vr*dx
5     Fr2 = inner(grad(thetar),grad(qr))*dx\
6           + (b/a)/(w_m(wr))*wr*qr*dx(mesh)\
7           - Br*mu(B,thetar)*inner(grad(wr),grad(wr))*qr*dx\
8           - Ha*Ha*Br/(1+m*m)*wr*wr*qr*dx
9     Fr = Fr1+Fr2
10    solve(Fr==0, udofs)

```

Listing A.12: Reduced variational formulation of the MHD flow and heat transfer with temperature dependent viscosity

```

1 J = Functional( 0.5 * alfaw * ( wr - wr_d ) * ( wr - wr_d ) * dx(mesh)\
2               + 0.5 * alfatheta*(thetar - thetar_d)*(thetar - thetar_d)*dx(mesh)\
3               + 0.5 * alfau * Ha * Ha *dx(mesh))
4 rf = ReducedFunctional(J,Control(Ha))
5 par_opt = minimize(rf,options = {"gtol": 1e-10, "ftol": 1e-10})

```

Listing A.13: Optimization with the ROM of the MHD flow and heat transfer with temperature dependent viscosity

```

1 mesh      = RectangleMesh(Point(0.0,0.0), Point(a,b), nx, ny)
2 V_element = FiniteElement('CG', triangle, 2)
3 Q_element = FiniteElement('P', triangle, 1)
4 R_element = FiniteElement('R', triangle, 0)
5 W_element = MixedElement([Q_element, R_element])
6 V          = FunctionSpace(mesh, V_element)
7 Q          = FunctionSpace(mesh, Q_element)
8 R          = FunctionSpace(mesh, R_element)
9 W          = FunctionSpace(mesh, W_element)
10 normal     = FacetNormal(mesh)
11 boundary_markers = FacetFunction('size_t', mesh)
12 ds = Measure('ds', domain=mesh, subdomain_data=boundary_markers)
13 q          = TestFunction(V)
14 w          = Function(V)
15 q1, d1     = TestFunctions(W)
16 th         = TrialFunction(W)
17 theta, c   = split(t)

```

Listing A.14: Mesh, elements and function spaces of the power-law fluid flow and heat transfer

```

1 def main():
2     F1 = inner(-mu(w, (n-1.0)/2.0)*grad(w), grad(q))*dx\
3         - Ha*Ha*w*q*dx\
4         + one*q*dx
5     solve(F1==0, w, bc)
6     F2 = inner(grad(theta), grad(q1))*dx\
7         + (4.0*(b/a)/w_m(w))*w*q1*dx\
8         - Br*mu(w, (n+1.0)/2.0)*q1*dx\
9         - Ha*Ha*Br*w*w*q1*dx\
10        - one*q1*ds\
11        + c*q1*dx\
12        + d1*theta*dx
13    a2, L2 = lhs(F2), rhs(F2)
14    th     = Function(W)
15    solve(a2==L2, th)
16    theta, c = th.split()

```

Listing A.15: Variational formulation of the power-law fluid flow and heat transfer

```

1 def w_m(w):
2     return assemble(w*dx)
3 def mu(w, n):
4     return (inner(grad(w), grad(w)))*n

```

Listing A.16: Nonlinear terms of the power-law fluid flow and heat transfer

```

1 J = Functional( 0.5 * alfaw * ( w - w_d ) * ( w - w_d ) * dx(mesh)\
2   + 0.5 * alfatheta*(theta - theta_d)*(theta - theta_d) * dx(mesh)\
3   + 0.5 * alfau * n * n * dx(mesh))
4 rf      = ReducedFunctional(J, Control(n))
5 par_opt = minimize(rf,options = {"gtol": 1e-10, "ftol": 1e-10})

```

Listing A.17: Optimization of the power-law fluid flow and heat transfer

```

1 vPHI, k_v      = load_PODbasis(vPhi,V)
2 thetaPHI, k_theta = load_PODbasis(thetaPhi,Q)
3 cPHI, k_c      = load_PODbasis(cPhi,R)
4 Rv_element    = VectorElement('R', triangle,0, dim=k_v)
5 Rtheta_element = VectorElement('R', triangle,0, dim=k_theta)
6 Rc_element    = VectorElement('R', triangle,0, dim=k_c)
7 Rw_element    = MixedElement([Rtheta_element,Rc_element])
8 Rv            = FunctionSpace(mesh, Rv_element)
9 Rtheta       = FunctionSpace(mesh, Rtheta_element)
10 Rc          = FunctionSpace(mesh, Rc_element)
11 Rw          = FunctionSpace(mesh, Rw_element)
12 vdofs       = Function(Rv)
13 qdofs       = TestFunction(Rv)
14 qtdofs, ddofs = TestFunctions(Rw)
15 wdofs       = TrialFunction(Rw)
16 thetadofs, cdofs = split(wdofs)
17 vr         = sum([vdofs[i]*vPHI[i] for i in range(k_v)])
18 qr         = sum([qdofs[i]*vPHI[i] for i in range(k_v)])
19 thetar     = sum([thetadofs[i]*thetaPHI[i] for i in range(k_theta)])
20 qtr        = sum([qtdofs[i]*thetaPHI[i] for i in range(k_theta)])
21 dr         = sum([ddofs[i]*cPHI[i] for i in range(k_c)])
22 cr         = sum([cdofs[i]*cPHI[i] for i in range(k_c)])

```

Listing A.18: Elements and function spaces for ROM of the power-law fluid flow and heat transfer

```

1 def main():
2     Fr1 = inner(-mu(vr, (n-1.0)/2.0)*grad(vr), grad(qr))*dx\
3         - Ha*Ha*vr*qr*dx\
4         + one*qr*dx
5     bc = None
6     solve(Fr1==0, vdofs, bc)
7     vr = sum([vdofs[i]*vPHI[i] for i in range(k_v)])
8     Fr2 = inner(grad(thetar), grad(qtr))*dx\
9         + (4.0*(b/a)/w_m(vr))*vr*qtr*dx\
10        - Br*mu(vr, (n+1.0)/2.0)*qtr*dx\
11        - Ha*Ha*Br*vr*vr*qtr*dx\
12        - one*qtr*ds\
13        + cr*qtr*dx\
14        + dr*thetar*dx
15    a2, L2 = lhs(F2), rhs(F2)
16    wdofs = Function(Rw)
17    solve(a2==L2, wdofs)
18    thetadofs, cdofs = wdofs.split()

```

Listing A.19: Reduced variational formulation of the power-law fluid flow and heat transfer

```

1 J = Functional( 0.5 * alfaw * ( wr - wr_d ) * ( wr - wr_d ) * dx(mesh)\
2     + 0.5 * alfatheta*(thetar - thetar_d)*(thetar - thetar_d)*dx(mesh)\
3     + 0.5 * alfau * n * n *dx(mesh))
4 rf = ReducedFunctional(J, Control(n))
5 par_opt = minimize(rf, options = {"gtol": 1e-10, "ftol": 1e-10})

```

Listing A.20: Optimization with the ROM of the power-law fluid flow and heat transfer

```

1  from dolfin import *
2  import numpy as np
3  def pod_basis(percentage,Mass,U,snapshots):
4      """ pod_basis generates the pod basis of a given snapshots set.
5      Parameters
6      percentage : percentage of the information content in POD bases.
7      Mass : Mass matrix of the related function (u).
8      U : function space of the related function (u).
9      snapshots : it is .numpy object which has the snapshots.
10     Returns
11     k : number of selected pod basis
12     Phi : coefficient matrix of the pod basis.
13     PHI : function matrix of the pod basis.
14     Svel : singular values of the snapshot matrix.
15     """
16     snaps = snapshots
17     massL = np.linalg.cholesky(Mass)
18     massLT = massL.T
19     snaps_tilde = np.dot(massLT, snaps)
20     Uvel, Svel, Vhvel = np.linalg.svd(snaps_tilde)
21     sum_full = sum(Svel[:]**2)
22     sum_partial = 0.0
23     information = 0.0
24     while information<(percentage/100):
25         sum_partial +=Svel[k]**2
26         k += 1
27         information = sum_partial/sum_full
28     print k, "number of POD basis is selected."
29     Ulvel = Uvel[:,0:k]
30     massLT_inv = np.linalg.inv(massLT)
31     Phi = np.dot(massLT_inv, Ulvel)
32     PHI = []
33     for i in range(k):
34         ph = Function(U)
35         ph_array = ph.vector().array()
36         ph_array[:] = Phi[:,i]
37         ph.vector()[:]= ph_array
38         PHI.append(ph)
39     return k, Phi, PHI, Svel

```

Listing A.21: Generation of the POD basis

```

1  def load_PODbasis(Phi,U):
2      PHI = []
3      k = Phi.shape[1]
4      for i in range(k):
5          ph = Function(U)
6          ph_array = ph.vector().array()
7          ph_array[:] = Phi[:,i]
8          ph.vector()[:] = ph_array
9          PHI.append(ph)
10     return PHI, k

```

Listing A.22: Assignment of the POD basis

CURRICULUM VITAE

PERSONAL INFORMATION

Surname, Name: Evcin, Cansu

Nationality: Turkish (TC)

Date and Place of Birth: 27.11.1986, İzmir

Marital Status: Married

Phone: +90 312 2105610

Fax: +90 312 2102985

EDUCATION

Degree	Institution	Year of Graduation
Ph.D.	Institute of Applied Mathematics, METU	2018
M.S.	Institute of Applied Mathematics, METU	2013
B.S.	Department of Mathematics, Ege University	2009
High School	İzmir Kız Lisesi	2004

PROFESSIONAL EXPERIENCE

Year	Place	Enrolment
2010-2018	Institute of Applied Mathematics, METU	Research Assistant
2009-2010	Department of Mathematics, NKU	Research Assistant

PUBLICATIONS

Journal Publications

1. Cansu Evcin, Ömür Uğur, Münevver Tezer-Sezgin, Determining the Optimal Parameters for MHD Flow and Heat Transfer with Variable Viscosity and Hall Effect, Computers and Mathematics with Applications, 2018, DOI: 10.1016/j.camwa.2018.06.027.
2. Cansu Evcin, Ömür Uğur, Münevver Tezer-Sezgin, Controlling the Power Law Fluid Flow and Heat Transfer Under the External Magnetic Field Using the Flow Index and the Hartmann Number, International Journal of Computational Methods, 2018, DOI: 10.1142/S0219876218501438.

Abstracts in International Conference Publications

1. Cansu Evcin, Ömür Uğur, Münevver Tezer-Sezgin, "Optimal Control for the MHD Flow and Heat Transfer with Variable Viscosity in a Square Duct", 6th European Seminar on Computing (ESCO), Pilsen, Czech Republic, 3-8 June 2018.
2. Cansu Evcin, Ömür Uğur, "Model Order Reduction on Control Problems of Navier-Stokes Equations", 7th International Conference on Advanced Computational Methods in Engineering (ACOMEN), Ghent, Belgium, 18-22 September 2017.
3. Cansu Evcin, Ömür Uğur, "Nonlinear Model Order Reduction in PDE Constrained Optimal Control Problems", European Conference on Numerical Mathematics and Advanced Applications (ENUMATH), Ankara, Turkey, 14-18 September 2015.
4. Cansu Evcin, Ömür Uğur, "Threshold Dynamics of Avian-Human Influenza in a Periodic Environment", 12th International Workshop on Dynamical Systems and Applications, Ankara, Turkey, 12-15 August 2013.

5. Cansu Evcin, Ömür Uğur, "Analysis of Threshold Dynamics of Epidemic Models in a Periodic Environment", 26th European Conference on Operational Research (EURO), Rome, Italy, 1-4 June 2013.

Participation in Scientific Meetings

1. 4th Workshop of Association for Turkish Women in Maths, Ankara, Turkey, 28-29 April 2017.
2. FEniCS'15, London, United Kingdom, 29 June-1 July 2015.
3. 1. Ulusal Karmaşık Dinamik Sistemler ve Uygulamaları Çalıştayı, Ankara, Türkiye, 12-13 Ekim 2012.

PROJECTS

1. Derivative Pricing by Monte Carlo Methods Under Lévy Models (BAP-07-05-2017-006), 2017.
2. Control Problems and Applications for Navier-Stokes Equations (BAP-07-05-2016-004), 2016.
3. Optimal Control and Parameter Estimation Methods for Advection- and Reaction-Diffusion Systems (BAP-07-05-2015-009), 2015.